Electrodeposition of Copper using Additive-containing Low Metal Ion concentration Electrolytes for EnFACE Applications

Eden May B. Dela Pena

Thesis submitted to the University of Strathclyde for the degree of Doctor of Philosophy

Department of Chemical and Process Engineering

University of Strathclyde

2017

Declaration of Authenticity and Author's Rights

This thesis is the result of the author's original research. It has been composed by the author and has not been previously submitted for examination, which has led to the award of a degree.

The copyright of this thesis belongs to the author under the terms of the United Kingdom Copyright Acts as qualified by University of Strathclyde Regulation 3.50. Due acknowledgement must always be made of the use of any material contained in, or derived from, this thesis.

Signed: *[signature]*

Date: January 10, 2017

ABSTRACT

In the past decade a new electrodeposition process called Electrochemical nano and micro Fabrication by flow and Chemistry (EnFACE) was developed which enabled mask-less pattern transfers onto a metallic substrate. EnFACE uses a novel acid-free, additive-free plating electrolyte containing low concentrations of metal salts (0.1 MCuSO$_4$), as the process requires electroplating under conditions of fast kinetics and low electrolyte conductivity. However, for electronic applications, industry requires the use of additives, which improve deposit properties such as thickness uniformity, strength, ductility, and conductivity. The use of pulsed current is also known to improve deposit properties such as grain structure, mechanical strength and throwing power. Therefore, in order to use EnFACE for fabrication of industrially useful products, the effect of additives on the electrochemical behaviour and deposit properties of this process needs to be assessed. In addition, the influence of current modulation; i.e. direct current vs pulsed current, on deposit properties also warrants investigation.

Potentiodynamic polarisation experiments were performed on additive-free and additive-containing EnFACE electrolyte (0.1 M CuSO$_4$). The additives tested were Copper Gleam A, Copper Gleam B, and chloride ions (Cl$^-$). The effect of two parameters: (i) additive type and (ii) additive concentration, on cathode polarisation were studied.

Copper films were electroplated on stainless steel substrates from electrolytes containing different concentrations of plating additives (0%, 17%, 33%, 50%, 100%, 200% of the industry recommended additive concentration). Both direct current (DC)

and pulsed current (PC) plating were used. The deposit was characterised using scanning electron microscope (SEM), electron backscattered diffraction (EBSD), tensile test machine (UTM), four-point probe and X-ray diffraction (XRD).

Cathode polarisation occurred when the additives were used individually. The combination of Copper Gleam B and Cl^- suggested synergistic inhibition, particularly in the diffusion-limited region. The addition of Copper Gleam A to the Copper Gleam B-Cl^- mix increased the limiting current and suggested plating acceleration. These effects are interpreted in terms of the adsorption-desorption behavior of the additives on the cathode surface.

SEM and EBSD images indicated that additives caused a concentration-dependent decrease in the grain size of the deposit in both the DC and PC plated deposit. This grain refinement resulted in an increase in yield and tensile strength, but reduced the ductility and resistivity of deposits. The PC-plated copper from the EnFACE electrolytes generally possessed better mechanical properties than its DC-plated counterparts, though both plating modes created copper films that can meet industry standards. The optimum additive concentration for the EnFACE electrolyte was 50% of the recommended value when using DC plating; while the optimum was only 33% when using PC plating.

ACKNOWLEDGEMENT

I would like to express my deepest gratitude to these people who became part of this research study until completion

To God be the glory

LIST OF CONTENTS

.

LIST OF FIGURES

1.0 Introduction

2.0 Critical review of the role of PEG, SPS and Cl⁻ in copper plating

3.0 Fundamental Aspects

4.0 Experimental

5.0 Results and Discussion: Electrochemical Characterisation of Additive-containing EnFACE electrolyte

6.0 Results and Discussion: Structures and Properties of Direct Current Copper plated from EnFACE Electrolyte with Additives

7.0 Results and Discussion: Structures and Properties of Pulse Current Copper plated from EnFACE Electrolyte with Additives

LIST OF TABLES

2.0 Critical review of the role of PEG, SPS and Cl⁻ in copper plating

3.0 Fundamental Aspects

4.0 Experimental

5.0 Results and Discussion: Electrochemical Characterisation of Additive-containing EnFACE electrolyte

6.0 Results and Discussion: Structures and Properties of Direct Current Copper plated from EnFACE Electrolyte with Additives

7.0 Results and Discussion: Structures and Properties of Pulse Current Copper plated from EnFACE Electrolyte with Additives

LIST OF SYMBOLS

Greek symbols

α	transfer coefficient	-
α_r	resistivity due to grain boundaries	μohms-cm
A	area of the electrode	cm^2
A_f	final area	cm^2
A_o	original cross section area	cm^2
β	Full width at half maximum peak intensity (FWHM)	-
β_e	broadening due to strain	°
β_L	broadening due to grain size	°
β_{total}	total peak broadening	°
Γ	fractional surface area	moles·cm^{-2}
δ_N	diffusion layer thickness	m
δ_p	pulsating layer	nm
δ_s	stationary diffusion layer	nm
ΔG_{bulk}	free energy due to formation of a new bulk	KJ·$mole^{-1}$
ΔG_{nucl}	free energy for nucleation of a seed	KJ·$mole^{-1}$
ΔG_{surf}	free energy due to creation of new surface	KJ·$mole^{-1}$
η	overpotential	V
η_c	crystallisation overpotential	V
η_{ct}	charge transfer overpotential	V
η_d	diffusion overpotential	V
η_r	chemical reaction overpotential	V
η_T	total overpotential	V
θ	duty cycle	-

θ_d	Bragg's angle	rad
θ_s	electrode coverage of adsorbed additives	-
K	dimensionless shape factor (0.9)	-
λ	x-ray wavelength	A
λ_m	electron mean free path in the material	nm
v	scan rate	V s^{-1}
ρ_o	bulk resistivity of the metal	μohms-cm
ρ_{gb}	resistivity due to grain boundary scattering	μohms-cm
σ_i	material constant for the starting stress for dislocation movement	Pa or MPa
σ_{site}	shortest distance for kink	nm
σ_y	yield strength	Pa or MPa
ϕ	applied potential	V
ϕ_o	potential at equilibrium conditions	V

Latin symbols

a	activity of the metal ion in solution	-
a_M	activity of the solid	-
A	atomic weight of the metal	g$\cdot$mol^{-1}
C	capacitance at additive coverage	Farad, F
C_b	bulk concentration	mol$^{.}$cm^{-3}
C_ε	slope of the line	-
C_o	capacitance at coverage zero	Farad, F
C_{sat}	capacitance at saturation	Farad, F
d	grain diameter	m
d_{hkl}	mean crystallite size	nm
d_s	grain size	nm
D	diffusion coefficient	m^2 s^{-1}

D_s	surface diffusivity of an ad-atom	-
e	strain	-
e_f	total strain at fracture, ductility	-
E	elastic modulus	Pa or N·m^{-2}
E	potential	V
E^o	standard electrode potential referenced to SHE	V
F	Faraday's constant	96,500 C/g-equivalent
$h_1,\ h_2,\ h_3$	deposit thicknesses at the recess	nm
Ha	thickness of the deposit at the exposed area	mm
Hb	thickness of the deposit at the edge/hole mouth	mm
Hc	thickness of the deposit at the centre of the through hole	mm
i	current density	mA·cm^{-2}
i_{add}	current density in the presence of additives	mA·cm^{-2}
$i_{addfree}$	current density in the absence of additives	mA·cm^{-2}
i_{AVE}	average current density	mA·cm^{-2}
$i_{d,lim}$	limiting current density (DC)	mA·cm^{-2}
i_{lim}	limiting current density	mA·cm^{-2}
i_o	exchange current density	mA·cm^{-2}
i_p	peak current density predicted by Randles Sevcik equation	A·cm^{-2}
i_{pa}	anodic current density	mA·cm^{-2}
i_{peak}	peak current density	mA·cm^{-2}
$i_{p,lim}$	limiting current density (PC)	mA·cm^{-2}
i_{pro}	current density at protrusions	mA·cm^{-2}
i_{rec}	current density at recesses	mA·cm^{-2}
I	applied plating current	mA or A
$I_{d,lim}$	limiting direct current	mA

$I_o(hkl)$	standard intensity of the plane	-
I_{peak}	peak current	mA
$I_{p,lim}$	limiting pulse current	mA
k_y	strengthening coefficient	MPa·m$^{1/2}$
L_f	film thickness	μm
L_f	final length	cm
L_o	original length of the specimen	cm
L_t	line thickness	cm
LP	Leveling Power	-
m	mass of the deposit	g
m_{actual}	measured weight after plating	g
$m_{theoretical}$	predicted weight using Faraday's equation	g
n	metal's valence/ number of electrons involved in reaction	-
n	number of diffraction peaks	-
P	applied load	Pa
PE	Plating Efficiency	%
Q	charge	Coulomb, C
R	gas constant	8.314 J mol^{-1} K^{-1}
R	material dependent grain boundaries reflected coefficient	-
R_g	grain resistance	μohms-cm
R_{gb}	grain boundary resistance	μohms-cm
R_1	resistance of a single grain boundary layer	μohms-cm
R_s	sheet resistance or sheet resistivity	ohms·sqr^{-1}
R_{Total}	total resistivity	μohms-cm
s	stress	N·m^{-2}
t	plating time	mins or s

t_+	ion transport or transference number of the Cu cation	-
t_{actual}	actual plating time	mins
t_{OFF}	pulse off time	ms
t_{ON}	pulse on time	ms
t_p	pulse period	s or ms
t_{res}	residence time	s
t_T	total pulse time	s
t_{theo}	theoretical plating time	mins
T	absolute temperature	K
$T*$	dimensionless pulse time	-
$T_c(hkl)$	texture coefficient of the (hkl) plane	-
TP	Throwing Power	%
UTS	Ultimate tensile strength	Pa or $N \cdot m^{-2}$
V	potential	V
YS	Yield strength	Pa or $N \cdot m^{-2}$

LIST OF ABBREVIATIONS

ACMA	Advanced Chemical and Materials Analysis
ASTM	American Society for Testing and Materials
BE	Backscattered Electrons
BKD	Backscattered Kikuchi Diffraction
BTA	Benzotriazole
CCD	Charge Coupled Device
CEAC	Curvature Enhanced accumulation Acceleration
CMP	Chemical Mechanical Planarization
CVD	Chemical Vapor Deposition
DC	Direct Current
DFT	Density Functional Theory
DPS	3-N,N dimethylaminodithiocarbomoyl-1-propanesulfonic acid
EBSD	Electron Backscatter Diffractometry
ECMD	Electrochemical Mechanical Deposition
EDS	Energy Dispersive Spectroscopy
EnFACE	Electrochemical nano and micro-Fabrication by flow and Chemistry
EO	Ethylene Oxide
FWHM	Full Width at Half Maximum
IC	Integrated Circuit
ICDD	International Centre for Diffraction Data
IPC	Institute for Interconnecting Packaging Electronic Circuits
JGB	Janus Green B
LP	Levelling Power
MEMS	Microelectromechanical Systems

MPS	3mercapto-1-propanesulfonate
MW	Molecular Weight
PAG	Polyakyl Glycol
PC	Pulse Current
PCB	Printed Circuit Board
PEG	Polyethylene Glycol
PO	Propylene Oxide
PPG	Polypropylene Glycol
QCM	Quartz Crystal Microbalance
SE	Secondary Electrons
SEM	Scanning Electron Microscopy
SERS	Surface Enhanced Raman Scattering
SHE	Standard Hydrogen Electrode
SiC	Silicon Carbide
SPS	bis(3-sulfopropyl)disulfide
SS	Stainless Steel
STM	Scanning Tunneling Microscope
ULSI	Ultra-Large Scale Integration
UTM	Universal Testing Machine
UTS	Ultimate Tensile Strength
US	Ultrasound
UV	UltraViolet
VLSI	Very-Large Scale Integration
WDS	Wavelength Dispersive Spectroscopy
XRD	X-ray Diffractomerty
YS	Yield Strength

Chapter 1

Introduction

1.1 Copper Use in PCB and Microelectronic Devices

Today's computers, integrated circuits (IC's) and microprocessors consist of tiny electronic devices that are typically mounted on a suitable platform called a Printed Circuit Board (PCB). An essential feature of this technology is the thin copper film found in these devices. The copper lines mainly serve as electrical channels that connect one micro-component to the next. Copper is the material of choice as it offers high conductivity, good corrosion resistance and high electromigration resistance. The main technique by which the lines are patterned and formed is called photolithography.

PCB provides the substrate onto which electronic components are mounted via soldering [1.1]. Copper lines are typically etched out from the copper-cladded pre-impregnated to provide conductive paths between mounted devices. Copper is plated in vias and through-holes and these features connect metal interlayers to each other as well as to the soldered component. On the other hand, in very-large (VLSI) and ultra-large scale integration (ULSI), copper is electrodeposited in trenches and vias and the inlaid metal serve as interconnects in and between transistors.

1.2 Photolithographic Process Description

Photolithography is the conventional method used in PCB and microdevice fabrication to transfer a pattern to a substrate [1.2]. Photolithography is a multi-step process and involves the use of light exposure through masks to project the image of a desired circuit. In Fig. 1.1, a photolithographic process to etch out a pattern in the SiO_2 thin film

is shown. The cleaned SiO_2 substrate, grown via oxidation (Fig. 1.1a), is initially coated with a light sensitive polymer photoresist and soft baked to evaporate and densify the photoresist (Fig. 1.1b). Two types of photoresist exist, one referred to as positive and the other as negative. In a positive photoresist, the exposed areas are decomposed leaving the unexposed areas in the substrate intact. The opposite occurs with the negative photoresist wherein the exposed areas harden and the unexposed regions dissolve.

An optical mask, typically on a glass plate containing the pattern, is aligned onto the substrate (Fig.1.1c). This set-up is exposed to uniform ultraviolet (UV) light. A developer solution is then applied to remove any undeveloped resist. Post baking is done to stabilise and further harden the developed photoresist and the substrate is subjected to a stripping process to remove any photoresist residues (Fig. 1.1d). The exposed SiO_2 film is etched through varying techniques such as wet etching or via reactive ion etching (Fig. 1.1e).
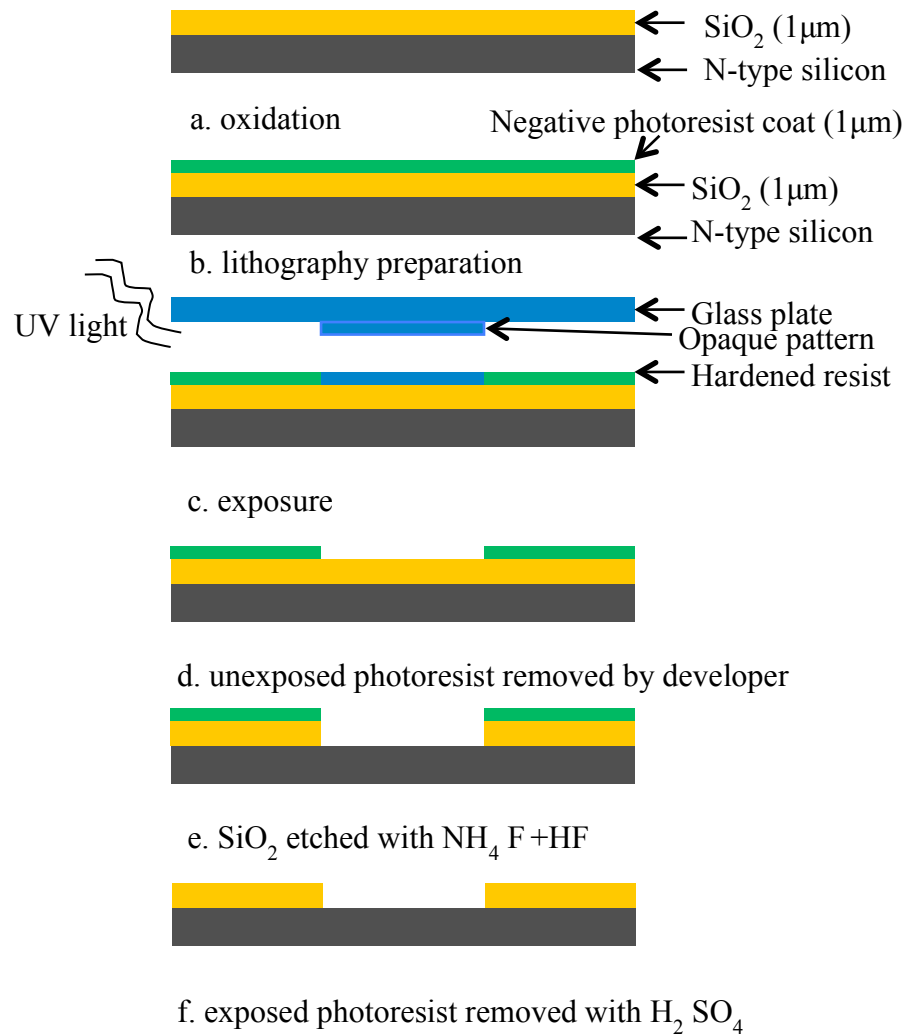
Figure 1.1 Schematic Diagram of the Photolithographic Process [1.3].

The major advantage of the photolithographic process is the ability for rapid mass production. However, although photolithography has found wide acceptance in the industry, this technique has several drawbacks [1.4]. Firstly, the process is typically multi-step, requiring the fabrication and stripping of several masks that ramp up operating cost. Secondly, the process uses copious amounts of chemicals that are expensive. Thirdly, photolitographic operations are done in a strictly controlled environment called a clean room that adds to production and maintenance cost. Finally,

the technique raises environmental concerns due to the use of large amounts of organic photoresists, as well as hazardous solvents and gases, which are difficult to store, handle and safely dispose.

1.3 Copper Electroplating in Device and PCB Fabrication

1.3.1 Interconnect Fabrication

In 1997, IBM initiated a paradigm shift in interconnect technology when it replaced the vacuum deposited aluminum with electroplated copper via the Damascene process [1.5]. This move created resurgence in interest on copper electroplating as the technique became the standard in the fabrication of interconnects in most electronic devices [1.3, 1.6].
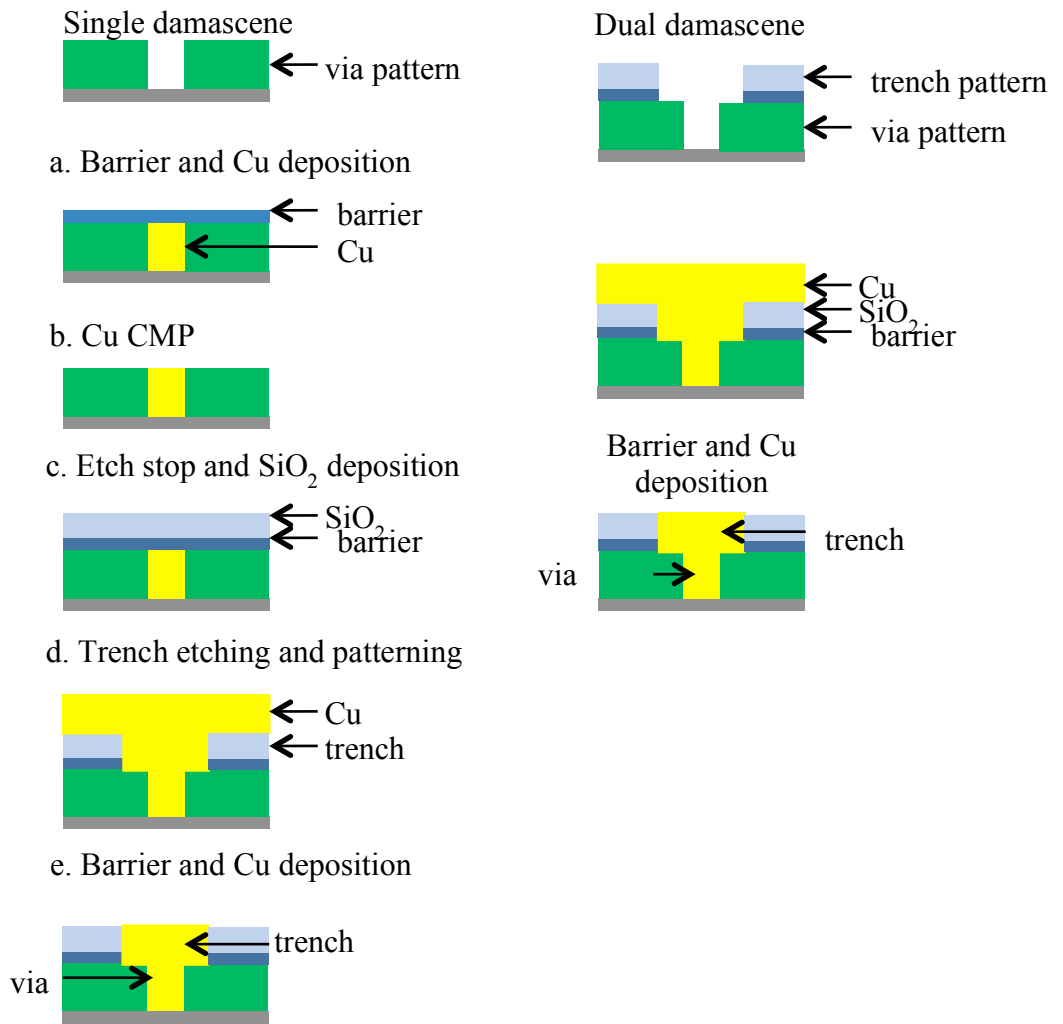
Figure 1.2 Schematic of the a) Damascene (left) and b) Dual Damascene Process (right) [1.7].

Figure 1.2 shows the steps for the Damascene and the Dual Damascene process. The Damascene process starts with via patterns created using photolithographic techniques (Fig. 1.2a). A barrier or seed layer, typically tantalum or tantalum nitride, is deposited (Fig. 1.2b). The barrier layer prevents copper out-diffusion into the silicon or silica substrate.

The next step is copper deposition via electroplating, and the metal fills target regions called vias. Excess copper is taken out using chemical mechanical planarisation (CMP) (Fig. 1.2c). Afterwards, silica is deposited on top of the filled via and a trench is formed using photolithography (Fig. 1.2d). This is followed by barrier layer deposition and copper electroplating to fill up the trench, and a final CMP to remove residual copper (Fig. 1.2e). The Dual Damascene is a logical contraction of the two-step process where via and trench etching are done initially followed by a single step copper electroplating for simultaneous filling of the two features.

The copper used as interconnects needs to be free of voids and seams. These defects cause several reliability issues with the deposited metal. When filling narrow trenches, defect formation was inevitable with traditional conformal plating. Such a problem was eventually solved with differential plating kinetics by using acid sulfate baths with plating additives [1.5].

1.3.2 PCB Fabrication

The PCB consists of layers of copper metallisation that electrically connects all electronic devices (e.g. transistors, capacitors, etc.) on the board. PCBs typically employ copper pattern plating to generate these connections. The copper pattern in the PCB is created via a number of steps.

Initially, the PCB is coated with a thin copper seed layer, as shown in Fig. 1.3a. Afterwards, the PCB's surface is coated with a photoresist film, which is the light sensitive polymer typically used in the photolithographic process. A patterned mask is placed on the photoresist-coated substrate, and this assembly is exposed to UV light (Fig. 1.3b). The photoresist in the exposed areas degrades and dissolves upon exposure to UV (Fig. 1.3c). The product is the PCB with an insulating film that bears the pattern of the mask, and with the rest of the areas exposing the copper seed layer (Fig. 1.3d).
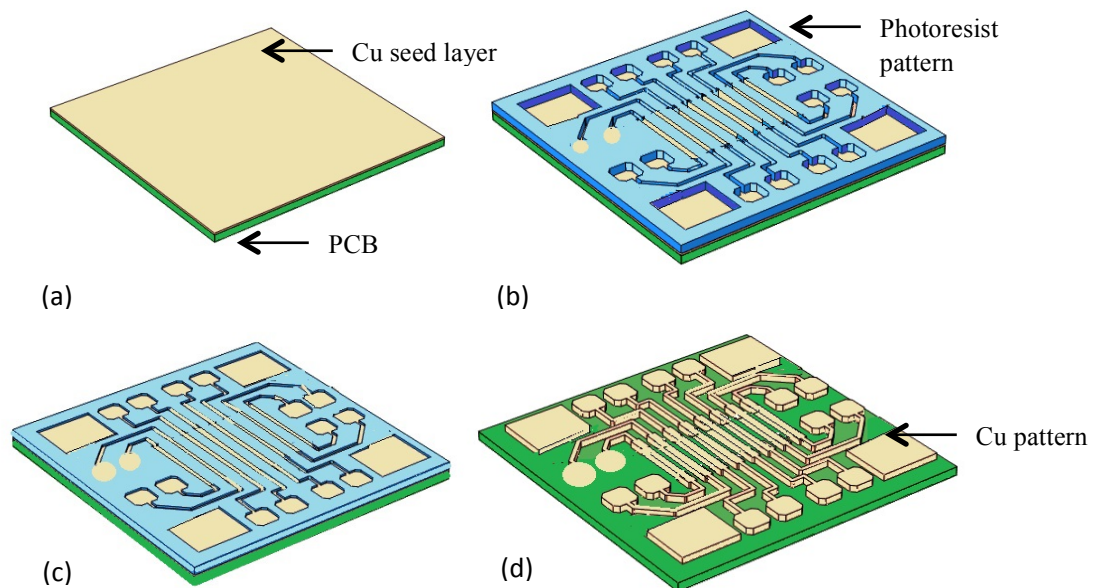
Figure 1.3 (a) The copper seed layer is applied to the PCB. (b) The PCB patterned with a photoresist using photolithography; UV degrades the photoresist in the areas uncovered by mask and exposes the seed layer. (c) Copper is electroplated on the exposed seed layer, consequently filling up the photoresist's cavities on the PCB. (d) The photoresist is stripped away and the seed layer is etched to reveal the desired copper pattern [Adapted from 1.8].

Copper plating commences with the PCB immersed in the electroplating electrolyte. This electrolyte typically consists of acidified copper sulphate ($CuSO_4$). The anodes used are solid copper bars. An applied potential between the PCB and the anodes results in metal plating on the exposed seed layer (Fig. 1.3c). Once the desired thickness is reached the plating is halted, and the remaining photoresist is stripped away. Finally, the thin copper seed layer is etched to electrically insulate the plated copper from each other (Fig. 1.3d).

1.4 The EnFACE Process

1.4.1 Process Description

Due to the growing interest to explore cost effective and 'greener' or more environmental friendly techniques, which could replace photolithography, several processes are being explored that appear to have great potential. Two of the more recent ones include ink jet printing [1.9, 1.10] and EnFACE [1.4]. The Electrochemical nano and micro-fabrication by Flow and Chemistry (EnFACE) technique is a one-step mask-less process that transfers a pattern directly from the tool to the substrate [1.11]. This technique was invented and developed by Prof. Sudipta Roy in Newcastle University, UK, and published in a disclosure in 2006 (International Publication No: WO 2006/010888) [1.12].
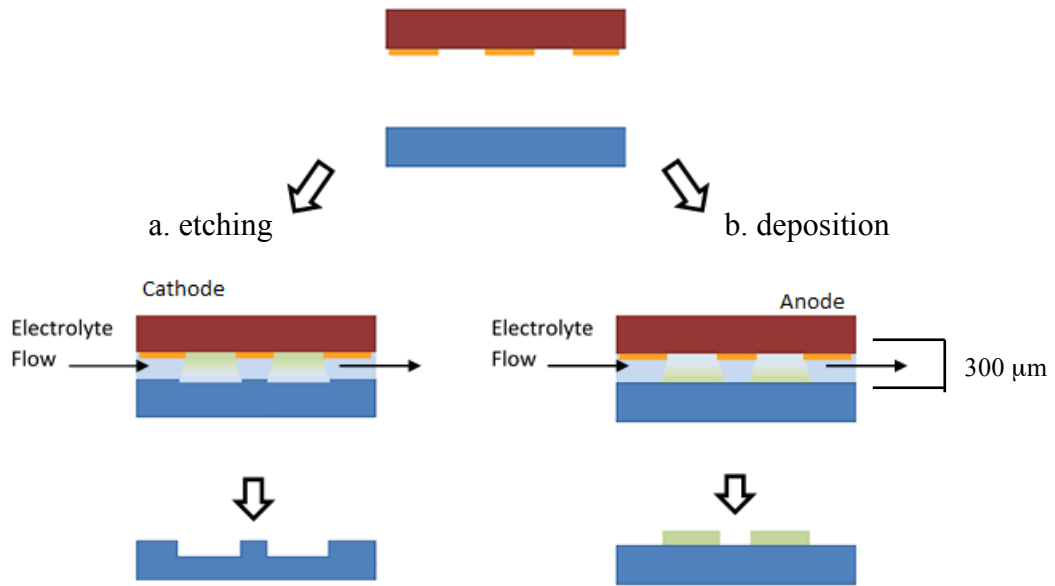
Figure 1.4 Schematic of the EnFACE process [1.4].

EnFACE technology involves a radical change in the reactor design and electrolyte composition, hence the terms 'flow' and 'chemistry' in its name. Figure 1.4 shows the EnFACE process flow for depositing and etching a metal. In the electrochemical reactor, the tool (cathode) and the work piece (anode) is placed at a close proximity [1.13], typically 300 μm apart. The electrodes are immersed in an electrolyte solution consisting of $CuSO_4$. The work piece can either be connected to the positive or negative terminal. When attached to the negative terminal, the work piece becomes the cathode and deposition occurs when current is passed (Fig. 1.4b). An innovation in the EnFACE process is that the opposite electrode or tool, in this case the anode, bears a pattern (Fig. 1.4a). These areas that are exposed in the anode, will deposit

metal in the opposite area of the cathode; conversely, the covered areas will inhibit copper deposition. On the other hand, if the positive terminal is used, the electrode becomes the anode and etching will occur. Similarly, the opposing electrode, which is the cathode, is patterned and areas, which are exposed in the cathode will create the etched areas in the anode (Fig. 1.4a).

Another innovation in the EnFACE process is the use of an acid-free, additive-free, low-copper concentration salt electrolyte. This chemistry gave optimum transfer pattern results in both etching [1.11] and deposition [1.14]. Schönenberger and Roy [1.11] have shown that current spreading is important to control to effect optimum pattern transfer. Current spreading may be minimised by using low-conductivity electrolytes; hence the need to eliminate acid and reduce the concentration of the copper salt. The EnFACE electrolyte offers several advantages over traditional acidified copper plating electrolytes. The absence of the acid allows easy handling and disposal of the electrolyte, and makes the process environment-friendly [1.4]. Furthermore, the presence of few components in the bath makes the electrolyte inexpensive and reduces operating costs.

1.4.2 Advantages of EnFACE

The EnFACE process offers two advantages. Firstly, it eliminates the need to perform multi-step photolithography due to its ability to transfer pattern into numerous substrates using a single tool. A single anode tool is estimated to successfully make 20 to 25 pattern transfers [1.13]. This translates to tremendous potential for reducing operating cost as well as reducing process time. Furthermore, the reduction of several

process steps lowers the chance of creating defects and simplifies fault-tracing in the production line.

Secondly, the EnFACE technique utilises only dilute solutions of $CuSO_4$ without acid addition [1.4]. This addresses the hazards and environmental drawbacks obtained from using traditional plating electrolyte in photolithography. Additionally, this could translate to significant savings in operating cost and lessening concerns in chemical handling and disposal. There is also a potential for infrastructure cost reduction since EnFACE process may not require the use of high-class clean rooms.

1.4.3 Developments in the EnFACE Process

Roy *et al*. [1.15] and Schönenberger and Roy [1.11] did some of the earliest research on EnFACE. Their work involved etching simple patterns onto a copper substrate using a direct current (DC). Good pattern transfers were influenced by three factors: (i) electrolyte conductivity, (ii) distance between anode and cathode, and (iii) electrolyte hydrodynamics. Microscale copper patterns were successfully transferred with the use of a novel vertical flow plating cell and an inter-electrode distance of 500 μm. Electrolytes consisting of acidified $CuSO_4$ produced sinusoidal etching profiles, while the solution with the lowest electrolyte conductivity (0.1 M $CuSO_4$) solution gave an acceptable rectangular etching profile. The improvement in etching profile was due to the reduction of current spreading in the substrate. Schönenberger and Roy [1.11] also performed EnFACE etching using pulsed current (PC). They observed that pulsed potential etching, instead of pulsed current etching, gave the best pattern transfer results.

The optimised pulse operating conditions include: (i) peak potential of 20V, (ii) pulse-on time of 1.0 ms, and (iii) duty cycle of 0.02.

Nouraei and Roy [1.16] proposed a mathematical model that described metal dissolution occurring at the substrate during EnFACE etching. They confirmed that etching in the acidified electrolyte produces a surface topography that is sinusoidal; whereas a non-acidified electrolyte produces a rectangular topography. This difference was caused by the formation of an oxide layer at the substrate surface in the non-acidified media.

Wu *et al*. [1.14] achieved successful plating pattern transfers via EnFACE in both DC and PC mode. Limiting current experiments were carried out using $CuSO_4$ solution and at different electrode gaps. The electrode gap was found to be vital in controlling the quality of the deposit and current efficiency. The use of small inter-electrode gaps prevented current spreading, which affected the feature size and caused line broadening. Copper line-widths of 120-200 μm were successfully fabricated, while reusability tests proved the robust nature of a single tool. They also successfully deposited copper patterns using pulse current plating set at these conditions: (i) current on/off times of 10/50ms, (ii) duty cycle, θ, of 0.17, (iii) peak current density of 276 mA·cm^{-2} (equivalent to average current density of 46 mA·cm^{-2}). They also observed that the use of pulse current did not cause significant reduction in current spreading compared to direct current. However, pulse current suppressed the evolution of roughness even at high plating thicknesses and thereby created a smooth copper deposit.

Widayatno and Roy [1.17, 1.18] implemented EnFACE on nickel, achieving similar degrees of success as with copper. However, while pattern transfer was successful, the nickel deposit showed poor replication of the pattern. This seemed to be the result of slow nickel plating kinetics and lack of stirring. A crucial problem that was encountered in the study was gas generation, which led to poor current density distribution in the electrodes.

Coleman and Roy [1.19] investigated the effect of ultrasound (US) agitation on the EnFACE process. A 20 kHz ultrasonic probe was employed to provide agitation, and the inter-electrode gap was set at 0.15 cm. Nickel deposits with target thickness of 4μm thick were plated using direct current plating and a 0.1 M $CuSO_4$ electrolyte. Plating with simultaneous US agitation created erratic potential fluctuations caused by: (i) a fully turbulent flow in the narrow channel between electrodes; and (ii) cavitation bubble collapse. Results indicate that plating using long current pulses with US applied during the off-time provided the best results; i.e. (i) stable potential response, (ii) smooth deposit and (iii) better copper adhesion to the substrate.

1.5 Statement of the Problem and Significance of the Study

The EnFACE technology is still under development and needs more research to further its growth. One study that is currently lacking is the effect of employing plating additives in the EnFACE process. To illustrate the importance of these chemicals, it is believed that the copper damascene process only became successful when the right types of additives were used [1.20, 1.21]. While knowledge on the effect of plating additives is well established on traditional copper plating electrolyte, the EnFACE electrolyte

chemistry is atypical and is significantly different from the standard plating electrolyte chemistries. This means that the effect of common plating additives, such as PEG, SPS and Cl⁻, or its commercial counterparts, such as the Copper Gleam series, may perform differently when used in the EnFACE electrolyte. Therefore, a comprehensive study needs to be performed to ascertain how additives would influence the EnFACE process. Of particular importance is the effect of additives on two important aspects of electroplating: a) the electrochemical behaviour of the electrolyte and b) the derived deposit properties such as the microstructure, strength, ductility, electrical resistivity, etc.

Studies of this nature would contribute to increasing knowledge on this novel technology, and help realise the process' full potential in terms of applicability or suitability for production in electronics and in other industries where copper plating is relevant as well. Additionally, if additives are proven to improve the quality of the EnFACE copper deposit, then this puts EnFACE a step closer to commercialisation. There is also the possibility that EnFACE may require less additives and would add to its appeal as a viable alternative to the conventional copper plating process.

1.6 Project Aims and Objectives

The primary aim of the study is to gain a fundamental understanding on the influence of additives when used in the EnFACE copper plating process. One feature of this research is that the additives that will be investigated are the commercially popular Copper Gleam additives. This makes the results of the study more relevant to industry practices and would offer greater practical value.

The research was conducted in two phases. In the first phase, the aim was to determine the effect of additives on the electrochemical properties of the EnFACE electrolyte. The study covered both single additive and multi-additive effects. The results revealed important information such as the influence of additives in the plating mechanism, important plating parameters such as the limiting current, and the additive dosage necessary to create deposits of acceptable quality.

Specific objectives under this study phase include:

i.   To compare the electrochemical behaviour, via polarisation experiments, of the standard copper electrolyte and the EnFACE electrolyte

ii. To determine the effect of varying concentrations of single additives; namely, Copper Gleam A, Copper Gleam B and Cl⁻ on the electrochemical behaviour of the EnFACE electrolyte

iii. To determine the effect of varying concentrations of mixtures of Copper Gleam A, Copper Gleam B and Cl⁻ on the electrochemical behaviour of the EnFACE electrolyte

In the second phase, the aim was to determine the impact of a) the type and b) the concentration of additive on deposit properties. In the second part, features such as grain size, grain shape, texture and defects were investigated. These microstructural features were correlated to the mechanical (e.g. yield strength, tensile strength and ductility) and electrical (e.g. resistivity and sheet resistance) properties of the plated copper. Furthermore, the studies were done under two plating modes: direct current (DC) and pulse current (PC) conditions. The overall focus of the second phase was to

obtain EnFACE copper deposits with properties (electrical and mechanical) conforming to PCB manufacturers' product standards.

Specific objectives under the second study phase include:

i. To electroplate copper using the additive-containing EnFACE electrolyte in direct and pulse plating current modes

ii. To determine the effect of varying concentrations of additive mixtures (Copper Gleam A, Copper Gleam B and Cl⁻) on the structure (e.g. grain size, grain shape, etc.) of EnFACE copper

iii. To determine the effect of varying concentrations of additive mixtures on the electrical properties (e.g. sheet resistance and resistivity) of EnFACE copper

iv. To determine the effect of varying concentrations of additive mixtures on the mechanical properties (e.g. yield strength, tensile strength and ductility) of EnFACE copper

v. To investigate the occurrence of self-annealing in EnFACE copper

References

1.1 Datta M, Romankiw LT (1989) Application of Chemical and Electrochemical Micromachining in Electronics Industry. J. Electrochem. Soc. 136(6); 285C-292C

1.2 Romankiw LT, Sullivan O (1997) Plating Techniques. Handbook of Microlithography, Micromachining, and Microfabrication. Vol 2 SPIE Press Bellingham Washington DC

1.3 Madou MJ (2002) Fundamental of Microfabrication: The Science of Miniaturisation. CRC Press Boca Raton FL London

1.4 Roy S (2009) EnFACE: A Mask Less Process for Circuit Fabrication, Circuit World 35(3); 8-11

1.5 Andricacos PC, Uzoh C, Dukovic JC, Horkans J, Deligiani H (1998) Damascene Copper Electroplating for Chip Interconnections. IBM J. Res. Dev. 42(5); 567-574

1.6 Franssila S (2010) Introduction to Microfabrication 2nd Edition John Wiley & Sons Ltd West Sussex United Kingdom

1.7 Pratt A PhD (2004) Overview of the Use of Copper Interconnects in the Semiconductor Industry. Advanced Energy Industries Inc Fort Collins Colorado 80525

1.8   Comsol.com (2016) Comsol multiphysics. (Online) Available at:
https://www.comsol.com [Accessed 31 May 2016]

1.9   Calvert P (2001) Inkjet Printing for Materials and Devices. Chemistry of
Materials 13(10); 3299-3305

1.10   Dorey RA, Rocks S, Dauchy F, Navarro A (2006) New Advances in Forming
Functional Ceramics for Micro Devices. Advances in Sci. and Tech. 45; 2440-
2447

1.11   Schönenberger I, Roy S (2005) Microscale pattern transfer without
photolithography of substrates. Electrochim. Acta 51; 809-819

1.12   PCT Gazette (2006) International Application numbers and corresponding
international publication number. Section III; 3093-3175

1.13   Schönenberger I (2004) Electrochemical microfabrication without
photolithography: copper substrates. MPhil Thesis School of Chemical
Engineering and Advanced Materials Newcastle University

1.14   Wu Q, Green TA, Roy S (2011) Electrodeposition of Microstructures using a
Patterned Anode. Electrochem. Comm. 13(11); 1229-1232

1.15   Roy S, Gupte Y, Green TA (2001) Flow cell design for metal deposition at
recessed circular electrodes and wafers. Chem. Engg. Sci. 56(17); 5025-5035

1.16   Nouraei S, Roy S (2009) Design of Experiments in electrochemical

         fabrication. Electrochem. Acta 54(9); 2444-2449

1.17   Widayatno T, Roy S (2013) Micropattern Transfer Without Photolithography

         of Substrate: Ni Electrodeposition using EnFACE Technology. PhD Thesis

         School of Chemical and Process Engineering Newcastle University UK

1.18   Widayatno T, Roy S (2014) Nickel Electrodeposition using EnFACE. J. of

         Appl. Electrochem. 44(4); DOI: 10.1007/s10800-014-0686-y

1.19   Coleman S, Roy S (2014) Effect of ultrasound on mass transfer during

         electrodeposition for electrodes separated by a narrow gap. Chem. Engg. Sci.

         113; 35-44

1.20   Vereecken PM, Binstead RA, Deligianni H, Andricacos PC (2005) The

         Chemistry of Additives in Damascene Copper Plating. IBM J. Res. and Dev.

         49(1); 3-18

1.21   Rusli E, Xue F, Drews T, Vereecken P, Andricacos P, Deligianni H, Braatz R,

         Alkire R (2007) Effect of Additives on Shape Evolution during

         Electrodeposition. J. Electrochem. Soc. 154(11); D584 – D597

Chapter 2

Critical Review of the Role of PEG, SPS and Cl⁻ during Copper Plating

2.1 Introduction to Copper Electroplating Additives

Electroplated copper is currently the primary electrical conductor in electronic devices (e.g. integrated circuits (ICs), actuators, microelectromechanical systems (MEMS) and in printed circuit boards (PCBs) [2.1, 2.2]. For interconnect technology, the shift to electroplated copper started in 1997 when IBM introduced the Damascene process and replaced the vacuum deposited aluminum metallisation [2.3]. Copper is preferred due to its high electrical and thermal conductivity, good corrosion resistance, and high electromigration resistance [2.2]. These properties improved the overall performance of semiconductor devices, and have kept the copper-based processes as the state of the art for the electronics industry today.

The semiconductor device industry places stringent demands on the properties of copper used for microelectronic interconnect applications. The copper needs to be defect-free because defects (e.g. voids and seams) can cause reliability problems such as electromigration and impurity trapping in the copper line [2.4]. Unfortunately, defect formation was inevitable with the traditional conformal plating, especially when used for filling narrow trenches. The problems associated with the traditional plating processes were eventually solved by controlling plating kinetics via the application of plating additives [2.3, 2.5, 2.6].

The predominant electroplating electrolyte used for copper interconnect applications is a mixture of copper sulphate ($CuSO_4$) and sulphuric acid (H_2SO_4). Plating may be accomplished with just these two electrolyte components. However, deposits from such electrolytes would typically lack several desirable qualities (e.g. fine-grained structures, good mechanical properties, etc.) unless other ingredients are added in the plating electrolyte. These supplementary chemicals are generically referred to as additives, and are used to impart the necessary characteristics required in the deposit.

Additives may be an organic or an inorganic (e.g. metallic, ionic and anionic) substance; each serving a specific purpose and used in relatively minute quantities [2.7]. Additives can influence both the plating mechanism and the ensuing metal deposit. Some of the most common effects include: polarisation of the cathode, grain refinement of the deposit, changes in crystal orientation and texture formation and changes in the physical properties of deposits [2.8]. Additives are often used in combination and synergistic effects are commonly observed. Indeed, today's microelectronics industry would not have prospered if additive-assisted copper electroplating process were not available.

The modern additive mixture for electronic copper plating consists of three major components: a suppressor such as polyethylene glycol (PEG), an accelerator bis-(3-sulfopropyl) disulfide($-S-C_3H_6-SO_3Na)_2$ (SPS), and a promoter such as chloride ions (Cl^-). Another type of suppressor, called a leveler, may also be added, such as Janus Green B. These additives are used in copper plating for different applications in the electronic industry such as: (i) forming copper metallisation on

wafers, (ii) filling microvias of IC substrates, and (iii) filling vias (50-100μm diameter) in PCBs.

The succeeding sections will discuss in greater detail the mechanistic role of three popular additives; namely, PEG, SPS and Cl⁻, in the copper plating process. The immediate section is an introduction to the properties of the additives. This will be followed by a discussion of the actions of these additives when used individually and in combination in the electrolyte. Another section will cover the action of these additives in trench and via filling. This will be followed by a discussion on the influence of additives on the properties of the copper deposit. The final section reports on the influence of additives in the pulse plating process.

2.2 Properties and Application of PEG, SPS and Cl⁻ in Copper Plating

2.2.1 PEG

Polyethylene glycol, PEG, is the product of the condensation polymerisation of ethylene oxide and water. This polymer is highly miscible in water. PEG solutions are stable and the molecule does not hydrolyse in storage at room temperature. However, pure PEG can undergo oxidative degradation in air at room temperature; and thus exposure of the compound to oxygen and high temperatures should be limited.

PEG is one of the most common suppressors used in copper plating [2.9]. PEG is called a carrier, a type of suppressor that increases polarisation resistance and reduces current to cause plating inhibition. Chemicals with similar molecular structure as PEG are also effective inhibitors, such as polypropylene glycol (PPG)

and triblock copolymers like PEG-PPG and EPE (combination of ethylene oxide (EO) and propylene oxide (PO) [2.10].

The molecular weight (MW) of PEG used in copper plating ranges from 1000 to 10,000g/mol. A commonly used MW is about 2000g/mol [2.11]. The typical concentration of PEG in the electrolyte is between 0.1 to 1g/L (300 to 1000ppm) [2.11, 2.12]. PEG molecules can degrade during electroplating via chemical processes such as radical decomposition and nucleophilic substitution [2.13]. Hence, the additive content in the electrolyte needs to be monitored and replenished to prevent a decrease in plating performance.

PEG belongs to the polyoxyethylene family of surface-active chemicals. The chemical structure of the PEG monomer is shown in Fig. 2.1. The designation for PEG is based on a number indicating the average molecular weight of the polymer; e.g. PEG-4000. It is believed that the oxygen in the PEG structure plays a role in PEG adsorption on the Cu surface based on a cation seizing mechanism. The strong inhibiting effect of PEG is also believed to be due to its inherently large molecular structure and its ability to interlink to further increase its size on the electrode surface [2.14, 2.15]. These mechanisms will be described in detail in Section 2.3.1.1.
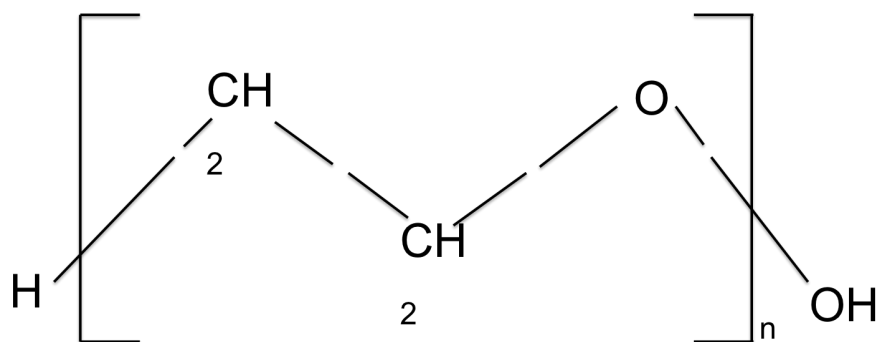
Figure 2.1 Chemical structure of polyethylene glycol (PEG) [Adapted from 2.16].

2.2.2 SPS

The bis-(3-sodiumsulfopropyl) disulfide ($C_6H_{12}Na_2O_6S_4$), also referred to as SPS, is an aliphatic compound that possesses a functionalised mercapto/disulfide group. SPS is derived from its potassium or sodium salt (1-propanesulfonicacid,3,3'-dithiobis-,disodium), which is miscible in water at room temperature.

Although studies have found a lot of suppressors and levelers, only few accelerators are known. SPS is the most commonly used and studied accelerator for the electronic copper plating process [2.17]. Accelerators deactivate the effect of suppressors, resulting to an increase in plating current and deposition rates. Other common accelerators include MPS (3-mercaptopropanesulfonic acid), which is a monomer of SPS, and DPS (3-N,N dimethylaminodithiocarbamoyl-1-propanesulfonic acid).The typical concentration of SPS in the plating electrolyte ranges between 0.002 to 0.01g/L (2 to 20ppm) [2.11, 2.12].

In contrast to suppressors, accelerators are often less stable in solution and are thus consumed at a high rate during plating. For example, SPS undergoes Cu-

catalysed oxidative decomposition that yields compounds such as DPS and MPS [2.11, 2.18]. Under typical plating conditions, SPS has a half-life of about 12 hours [2.18]. In the Damascene process, bath replacement during plating is necessary because the decomposition products of SPS are harmful to the super fill process.

Figure 2.2 shows the chemical structure of SPS and its monomer MPS. It is believed that SPS strongly adheres to the copper surface via the –[C-S-S-C]- portion of the molecule [2.19]. On the other hand, the disulfonic (-S-O_3-) part makes SPS highly soluble in the electrolyte [2.11, 2.20]. This is beneficial during plating as it prevents SPS incorporation in the deposit and extends the lifetime of the additive at the Cu surface. Furthermore, both the sulphate functional group and the S-S group in SPS, and the thiolate in MPS play an essential role in acceleration [2.17]. This mechanism will be described in greater detail in Section 2.3.1.2.
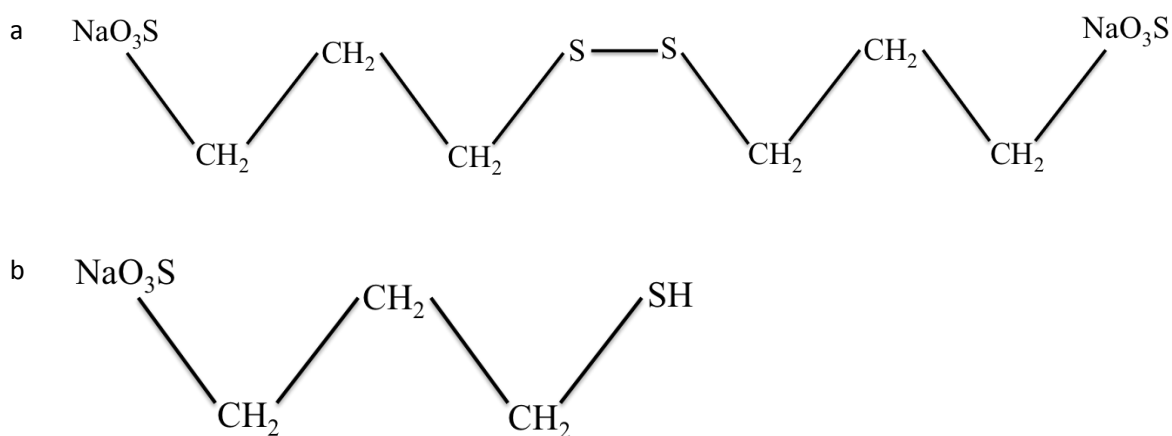
Figure 2.2 Chemical structure of (a) bis-(3-sodiumsulfopropyl) disulfide (SPS) and its monomer (b) MPS [2.21].

2.2.3 Cl^-

The chloride ion, Cl^-, is the anionic form of the element chlorine. Cl^- is colorless, diamagnetic, and in most cases highly soluble in water. Cl^- may be sourced from a number of salts (e.g. NaCl, KCl, $MgCl_2$) and acids (e.g. HCl).

Chloride ions are essential components of the copper plating electrolyte. When used without other addition agents, Cl^- can act as an accelerator or a suppressor depending on its concentration. Typically, Cl^- is an accelerator at low concentrations, and becomes a suppressor once the concentration goes beyond a critical amount. However, the principal use of Cl^- is in being a promoter in a multi-additive system [2.11, 2.22, 2.23]. The term promoter refers to the ability of Cl^- to initiate synergistic enhancement of suppression or acceleration with another additive.

For copper plating, Cl^- is typically sourced from HCl. High throwing power solutions require a Cl^- concentration of $0.05 - 0.10$g/L. For superfilling applications, Cl^- is used at a range of 0.02 to 0.10g/L, and nominally set at 0.05g/L [2.11].

2.3. Mechanistic Action of Additives in Copper Plating

Additives are known to behave differently when used alone and when used together with other additives. The use of multi-component additive systems is currently the preferred practice as additives are observed to show poor results when used alone yet shows remarkable effects when in combination with other additives [2.22, 2.23, 2.24].

This section expounds on the action of additives when used individually and collectively with other additives. The first part discusses the action of PEG, SPS and Cl$^-$ when added individually in the copper electrolyte. The succeeding part looks at multi-additive interactions between: (i) PEG and Cl$^-$; (ii) SPS and Cl$^-$; and (iii) PEG, SPS and Cl$^-$.

2.3.1 Single Additive Action

2.3.1.1 PEG

Many studies have observed the suppressive action of PEG on copper plating [2.25, 2.26. 2.27, 2.28, 2.29, 2.30]. An essential part of this suppression is the adsorption of PEG on the copper surface. Yokoi *et al*. [2.26] noted that PEG adsorption is potential-dependent in the absence of Cl$^-$ in the electrolyte, and occurs at 0.15 V$_{SHE}$. They also proposed that the presence of oxygen in the PEG structure allows the molecule to form a crown structure. Papke [2.31] earlier describes this crown as a helical structure with the oxygen lined inside the resulting tunnel. The Cu$^+$ or Cu^{2+} ions coordinate on the oxygen molecules of the helical PEG and form a pseudo-crown moiety that possesses a cationic state. The cationic PEG-Cu$^+$ crown can now attach to the negatively charged copper surface due to electrostatic attraction. Once adsorbed the large complex molecule can easily block other Cu^{2+}

ions from reaching the copper electrode, and thereby causes current suppression during plating. Stoychev and Tsvetanov [2.28] further suggested that the PEG-Cu$^+$ complex might also be detached from the surface and reside in the bulk electrolyte. In this manner, the complex can similarly induce plating suppression by impeding the overall transport of ions in the solution.

The PEG crown moiety may serve as an electron bridge to the seized Cu ions [2.32]. For example, Cu^{2+} can reduce to Cu$^+$ while attached to PEG. In such a case, PEG remains adsorbed to the copper surface due to the presence of the cation. Alternatively, a seized Cu$^+$ may also be reduced to Cu^0. In this instance, PEG will be released back to the solution since it lost the necessary charge to keep it attracted to the copper surface. The adsorption process will recommence once the PEG molecule is able to grab another Cu^{2+}.

When using PEG as a suppressor, two factors that are important to control are additive concentration and molecular (MW) [2.26]. For example in microvia filling, a minimum molecular weight of 2000 is needed for sufficient plating inhibition [2.33]. Plating suppression increases with an increase in either concentration or MW. The degree of polymerisation, which is related to MW, and the concentration of PEG do not cause suppression by influencing plating mechanisms, but by reducing the activity of Cu ions near the cathode.

2.3.1.2 SPS

Few studies reported on the effect of SPS on plating when used singularly in the electrolyte. While most studies reported the accelerating nature of SPS, it is believed that these reports have used SPS in the presence of Cl$^-$. On the other hand,

Tan *et al.* [2.34] clearly showed the action of SPS in copper plating in the absence of other additives. They observed a clear concentration-dependent inhibition with SPS at potentials of -0.5 to -0.8 V_{SHE}. They hypothesised that such inhibition was the result of a strongly adsorbed surface layer of the additive on copper. This adsorbed layer behaves similarly to an adsorbed PEG layer; i.e. it acts to prevent Cu ions from reaching the cathode surface.

Täubert *et al.* [2.35] agreed with the study of Tan *et al.* [2.34] and noted that the absorption/desorption behaviour of SPS in Cu is strongly dependent on the applied potential. They also observed that SPS adsorption on Cu (111) is relatively slow because the sulfate/H_2O adsorption phase acted as a barrier to SPS adsorption. Finally, while they expected that SPS molecules to spontaneously form densely packed, self-assembled monolayers on the copper surface, only disordered ad-layers were formed.

2.3.1.3 Cl⁻

Cl⁻ is known to be strongly adsorbed at the copper surface [2.32]. The adsorption state of Cl⁻ depends on the applied potential. From $+1.0$ to -1.0 V_{SHE}, an ordered ad-layer of Cl⁻ is present at the copper surface. At potentials more negative than -1.0 V_{SHE}, the Cl⁻ layer still exist but without its ordered structure. At potentials more positive than -1.0 V_{SHE}, the ad-layer layer is lost as the Cl⁻ completely desorbs from the surface. This clearly implies that at plating conditions, where the applied potential is negative, Cl⁻ is indeed present at the cathode.

Cl⁻ acts as an accelerator at concentrations less than 1mM. Cl⁻ accelerates copper deposition through the electron-bridge mechanism [2.25, 2.36, 2.37, 2.38]. The adsorbed Cl⁻ serves as a charge transfer site for Cu^{2+}. The Cu^{2+} are reduced at a

faster rate when it is attached to Cl⁻ than without Cl⁻ coordination because the energy

needed for the reduction process is also lower.

Cl⁻ becomes a suppressor at concentrations greater than 2mM [2.39, 2.40].

The Cu^+ dissolved in the anode reacts with Cl⁻ to form a film of CuCl. This film

passivates the anode and consequently suppresses plating current. Also, the cathode

may possess CuCl inclusions in the copper deposit when the plating is done at a low

current density.

2.3.2 Multiple-Additives Action: PEG, SPS and Cl⁻

2.3.2.1 PEG-Cl⁻

PEG is a weak suppressor in the absence of a promoter [2.41]; but plating

suppression is significantly increased when PEG is with Cl⁻ [2.25, 2.26, 2.27, 2.29,

2.42]. An immediate effect of Cl⁻ is the enhancement of PEG adsorption at the

cathode. Yokoi *et al*. [2.26] observed that PEG adsorption and plating suppression

occurred at all potentials in the presence of Cl⁻, whereas PEG adsorption occurred at

0.15 V_{SHE} in the absence of Cl⁻. Yokoi *et al*. [2.27] also proposed that this

suppression is a result of the formation of a PEG-Cu^+-Cl⁻ complex at the surface of

the cathode. This complex acts as a physical barrier and prevents Cu ions from

reaching the electrode. Some models have viewed this complex as exclusive to PEG

and Cl⁻, and Cu^+ was not necessary in the structure [2.29]. However, Feng *et al*.

[2.43] observed that the PEG-Cl⁻ complex does not exist in systems where Cu^{2+} is

absent; thereby proving the importance of Cu ions.

The existence of the PEG-Cu^+-Cl⁻ complex adsorbed on the cathode was

inferred using several techniques [2.32]: (i) analysing the electrochemical behaviour

of copper deposition and dissolution reactions, (ii) monitoring alterations in electric

conductivity and optical density of the solution, (iii) QCM measurements, (iv) surface-enhanced Raman spectroscopy (SERS) and (v) mass spectroscopy. On the other hand, Kondo *et al*. [2.21] observed the adsorbed PEG on copper in an electrolyte containing a PEG-Cl$^-$ mixture using the scanning electron microscope (SEM). They found PEG molecules with diameters of about 30nm adsorbed at the steps and edges of the growing copper crystal that prevented lateral crystal growth.

The actual structure of the PEG-based inhibiting layer remains debatable. Hill and Rogers [2.25] earlier proposed that the PEG chains are helically wound around the CuCl molecule, similar to proposals made by Sylvester and Tyler [2.44]. Using results from SERS analysis, Feng *et al*. [2.43] also proposed two structural models to describe the PEG-Cu$^+$-Cl$^-$ complex, which was based on the PEG–Cu(I) crown ether complex proposed by Yokoi *et al*. [2.26]. In both models, one of which is depicted in Fig. 2.3, Cu$^+$ is coordinated at three points; i.e. two with oxygen and the other with Cl$^-$. Cl$^-$ serves as the strong anchor that firmly attaches the complex to the Cu surface. Some Cu^{2+} ions that are seized by the complex may also be reduced to Cu$^+$ via chloride bridging. Hai *et al*. [2.14, 2.15] recently used cyclic voltammetry results and periodic plane-wave density-functional theory (DFT) calculations to propose a structure for the PEG-suppressor complex. They agreed with Feng *et al*.'s [2.43] PEG-Cu-Cl$^-$ structural model, but noted that this simple structure could not explain the strong suppressing capability of the complex molecule. They proposed an in-situ interlinking of the polyalkylene glycol (PAG) polymer chains, resulting to a hyper-branched PAG–Cu(I)–Cl coordination network that extends throughout the electrode surface.

The concentration of Cl⁻ in the PEG-Cl⁻ mixture also influences the morphology of the Cu deposit [2.45]. The formation of a monolayer of the Cl⁻ is essential to create a deposit of uniform thickness due to even suppression across the surface. This is expected at concentrations above 1mM Cl⁻. Below this critical concentration, non-uniform suppression occurs resulting in nodule formation [2.46].
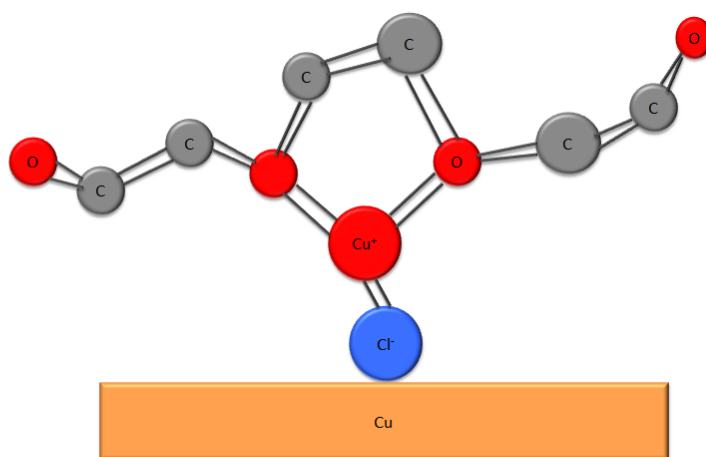
Figure 2.3 Structure of the PEG-Cu-Cl complex proposed by Feng *et al*. [2.43].

2.3.2.2 SPS-Cl⁻

The accelerating property of SPS is now known to be a consequence of its association with Cl⁻ in the plating electrolyte. Early reports by Bae and Gewirth [2.47] noted that Cl⁻ competes with adsorption cites on copper. However, Moffat and Ou Yang [2.48] showed that SPS could be physiosorbed on the adsorbed Cl⁻, thus revealing that SPS adsorption is not hindered by the presence of Cl⁻ at the surface. In situ scanning tunneling microscopy (STM) imaging proved that SPS [2.35] and MPS [2.49], a by-product of SPS reduction, is strongly adsorbed by the chloride adlayer present on the copper surface. Tan *et al*. [2.34] clearly demonstrated a transition from suppression to acceleration when Cl⁻ is added to an SPS-containing copper

electrolyte. The acceleration was concentration-dependent, with increasing suppression as SPS content increases.

Studies indicate that SPS undergoes several reactions in the electrolyte [2,14, 2.36, 2.50, 2.51], but a key process is the reduction of the SPS to its monomer MPS. Initially, SPS attaches to the halide promoter (e.g. Cl⁻) via physiosorption. The SPS-Cl⁻ molecule attaches to the Cu surface via similar a physiosorption mechanism. SPS may also attach to the already adsorbed Cl⁻ at the Cu electrode. The unstable SPS then transforms to MPS, via the reaction [2.36, 2.50]:

$$\frac{1}{2}SPS + H^+ + e^- \rightarrow MPS$$
<div align="right">Equation (2.1)</div>

Alternatively, Vereecken *et al.* [2.16], using rotating-disk polarisation experiments, suggested that SPS reduction does not just involve a simple faradaic process but needs Cu(I) to proceed via the reaction:

$$2Cu^+ + SPS + 2H^+ \rightarrow 2Cu^{2+} + 2MPS$$
<div align="right">Equation (2.2)</div>
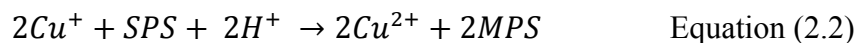
The MPS product is expected to dissociate from the surface at the end of the above reactions. However, MPS can rebind itself to the copper surface using its thiol or thiolate functional groups; or reattach to the adsorbed chlorides forming co-adsorption phases [2.51]. The MPS molecule acts as a possible catalytic pathway for copper plating and causes plating acceleration. The catalytic reaction pathway involves the initial reduction of Cu²⁺ to create cuprous thiolate [2.50, 2.52] according to the reaction:

$$2MPS + Cu^{2+} \rightarrow Cu(I)(thiolate)_{ad} + \frac{1}{2}SPS + 2H^+$$
<div align="right">Equation (2.3)</div>
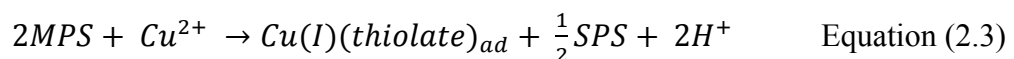
Healy *et al.* [2.36] suggested that both Cu^{2+} and Cu^0 is necessary for the rapid breakdown of SPS and MPS, with the copper disproportionation reaction a necessary first step to produce these species:

$$2Cu^+ \rightarrow Cu^0 + Cu^{+2}$$
<div align="right">Equation (2.4)</div>

Finally, the cuprous thiolate molecule is reduced to form copper:

$$Cu(I)thiolate_{ad} + H^+ + e^- \rightarrow Cu + MPS$$
<div align="right">Equation (2.5)</div>
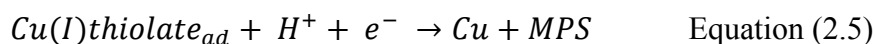
It is believed that Cu(I)thiolate is not the only product of the SPS-copper interaction. SPS form complexes with Cu (I) when Cl⁻ is present; and several studies proposed that this complex is the effective accelerant. Frank and Bard [2.18] earlier suggested a SPS-Cu(I) sulfonate complex. Schultz *et al.* [2.53] proposed a CuCl-SPS complex, wherein the sulfonate group is attached to the CuCl molecule. They used vibrational spectroscopic information, mass spectral data, and density functional theory calculations to predict the structure of the complex, as shown in Fig. 2.4. On the other hand, Tan *et al.* [2.34] suggested that the MPS thiol (R-SH) is an inhibitor, while the accelerant effect is due to the sulfonate ($R-SO_3$) group.
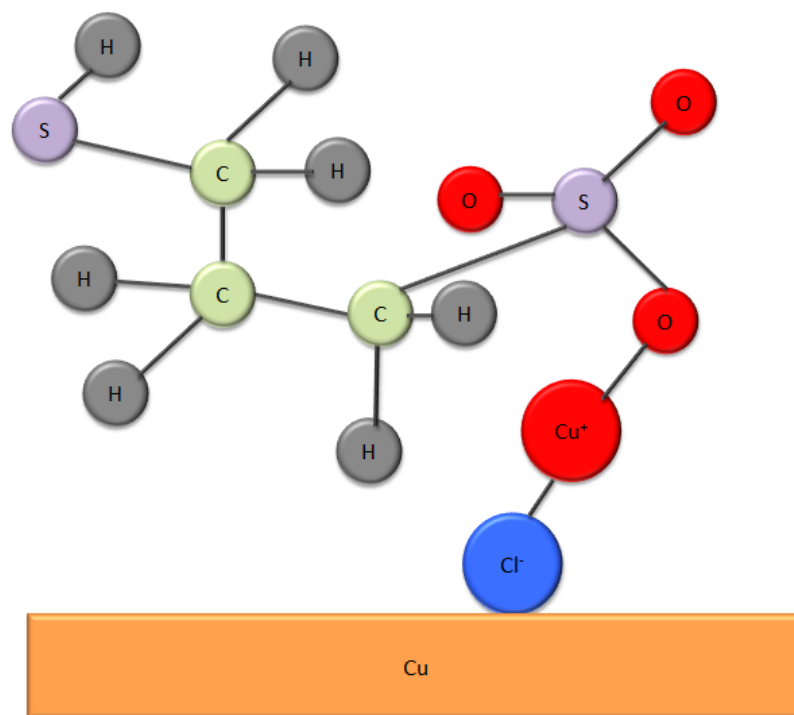
Figure 2.4 Sulfonate Cu-Cl complex structure proposed by Schultz *et al.* [2.52].

2.3.2.3 PEG-SPS-Cl⁻

Numerous works have studied the interaction of SPS, PEG and Cl⁻ in the copper plating. It is now clear that SPS serves as an antagonist to the PEG-based suppressor complex [2.54]. When SPS is added to the PEG/Cl⁻ system, a transition from suppression to acceleration occurs. The mechanism by which the SPS reactivates the inhibited copper surface is either by: (i) displacement of the PEG via competitive adsorption; or (ii) weakening of the PEG-to-surface bond. Using hysteretic voltammetry and rising chronoamperometric transient data, Moffat *et al.* [2.54] noted that PEG and SPS actively compete for surface sites, especially for promoter-mediated sites. Walker *et al.* [2.55] showed that the pre-adsorbed SPS/MPS prevents PEG adsorption using ellipsometric experiments.

Moffat *et al*. [2.54] also proposed that SPS could disrupt the PEG bond and causes PEG to break away from the PEG-Cl⁻ complex. The rate of PEG displacement from the surface increases with increasing overpotential. They believed that the anionic sulfonate end of SPS or MPS causes the disruption of the PEG layer, while the thiol/thiolate/disulfide group keeps the molecule attached to the surface. Finally, they suggested that the sulfonate end-group of SPS plays an important role in not only PEG displacement, but also in the SPS' propensity to strongly adsorb and segregate at the copper surface.

Basol and West [2.56] used electrochemical mechanical deposition (ECMD) pads to sweep the copper surface in an electrolyte containing a suppressor and an accelerator. They observed an increase in suppressor-to-accelerator surface coverage when the pad sweeps the wafer surface. After which, the accelerator re-adsorbs and displaces the suppressor. Although this study used commercial additives and not specifically PEG and SPS, it confirms the action of accelerators in a suppressor-containing electrolyte.

Willey and West [2.57] used a microfluidic cell to study the kinetics of suppressor displacement. They noted that when SPS and PEG were introduced simultaneously in the Cl⁻-containing electrolyte, deposition is suppressed at short times. This indicates that PEG is adsorbed faster than SPS, in agreement with the results of Tan and Harb [2.58]. However at longer times, the system shifts to plating acceleration instead of reaching the expected suppression plateau. Such implies that SPS reactivated the surface by displacing the adsorbed PEG.

Broekmann *et al*. [2.59] offered a detailed mechanism of SPS action in suppressor-containing electrolytes, shown in Fig. 2.5 [2.14, 2.15, 2.51]. They proposed that PEG/PAG suppression is due to a branched polymeric complex with $Cu(I)$ and Cl^- adlayers on the copper surface. Addition of SPS leads to SPS surface adsorption and eventual breakdown to MPS. MPS dissolves the complex layer via rupture of the surface-suppressor coordination bond. Furthermore, free MPS near the surface competes with PEG for $Cu(I)$, and prevents PEG re-adsorption. Finally, the team suggested that the accelerant is generated at the surface, and this generation is aided by copper reduction.
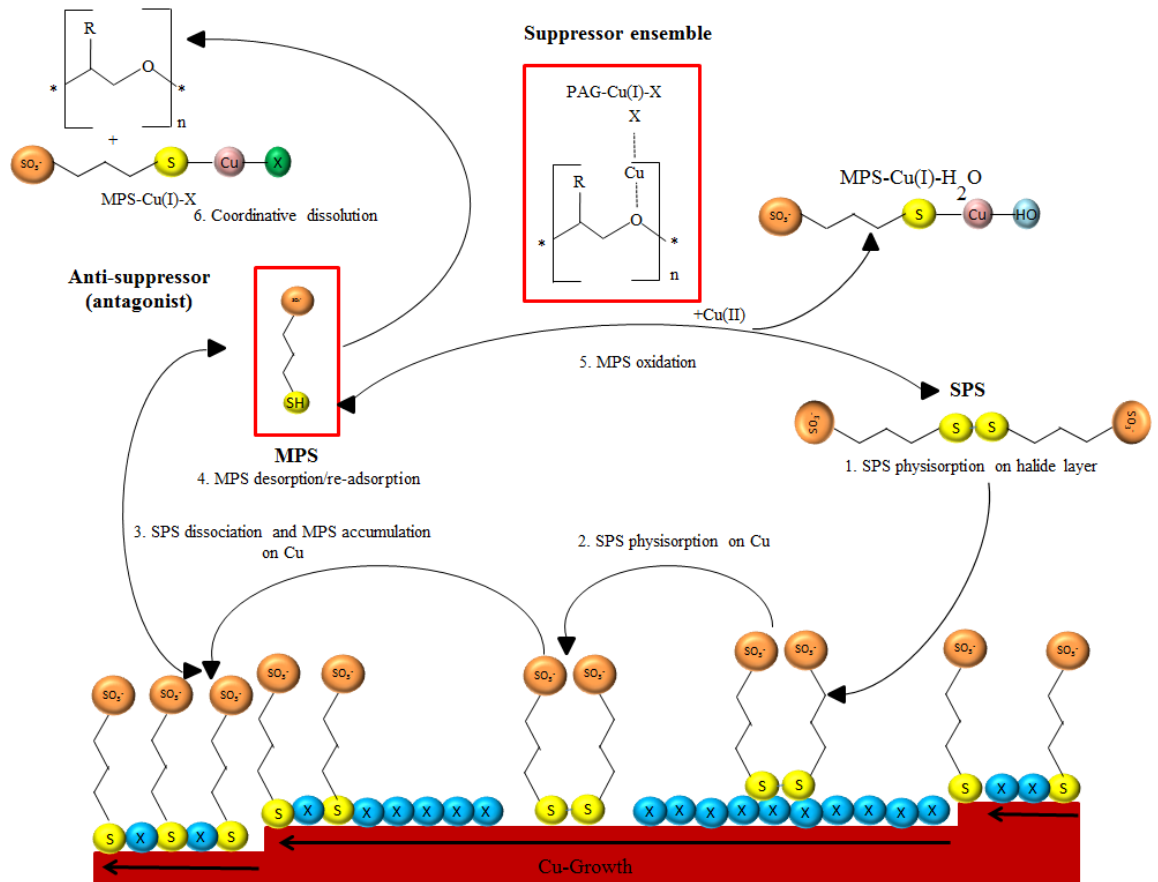
Figure 2.5 The action of SPS in the suppressor-containing electrolyte during copper plating [Adapted from 2.51].

2.4 The Action of Additives in Via and Trench Filling

The use of copper as interconnects in silicon chip fabrication brought about a whole new era in electrochemical processing. Key to this concept is the invention of the damascene, and eventually the dual-damascene process by Andricacos *et al.* [2.3]. An early obstacle in the implementation of copper electroplating in interconnect manufacture is the inability of the process to fill deep or high aspect ratio features (e.g. holes, trenches and vias) without forming defects [2.60]. Conformal plating, which deposits metal following the substrate's contour, as

expected to form voids and seams in the trench since plating will begin covering the top ridges before filling the recesses. Scientists realised that the way to fill trenches without creating defects is to induce differential plating rates. Differential plating is also known as superfilling, superconformal or bottom-up plating [2.3]. In differential plating, the metal deposits first at the bottom of the trench. The trench is gradually filled as plating proceeds towards the top and ends when metallisation is complete.

Superfilling was successful only after careful control of additives in the acid sulfate bath was done. While several commercial additives exist in the market, the damascene plating chemistry typically contains just three or four additives. The mixture includes a suppressor (e.g polyethers such as PEG), an accelerator (e.g. bis(3 sulfopropyl)-disodium-sulfonate(SPS), an additive enhancer (e.g. Cl^- ions), and a leveler (e.g. quaternary nitrogen compound such as Janus Green) [2.16].

In recent years, several studies attempted to explain the role of additives in the superfilling phenomenon. Currently, two mechanistic models are accepted. Bottom-up plating is explained as caused by: i) differential inhibition or ii) differential acceleration of plating kinetics.   In differential inhibition, a strong leveler prevents deposition in the elevated features on the plating substrate. In differential acceleration, a catalyst accumulates at the trench bottoms and promotes rapid plating in these areas. Which model prevails will depend on the composition and concentration of additives used [2.61]. The differential inhibition model is seen to be characteristic of baths possessing a strong leveler [2.22, 2.62], while the differential acceleration model is more fit in systems possessing an accelerator and a suppressor [2.63]. In baths possessing the three types of additives, dominance is dependent on the relative amounts of each additive.

The differential inhibition model is the first mechanism proposed to explain superfilling, and is essentially based on the theory of leveler action [2.60, 2.61, 2.64]. In this model (see Fig. 2.6), a strong leveler is believed to readily adsorb at the exposed surfaces found in the upper portions of the ridge. Consequently, the leveler inhibits metal deposition in these covered areas. On the other hand, trench bottoms remain free of the leveler since it takes time for the molecule to diffuse to and adsorb at these region. Therefore, trench bottoms will have less inhibition and plating is encouraged. Characteristic of the leveler-dominated baths are plating deposits with high impurity content, since levelers are incorporated in the deposit.

(a) (b) (c)
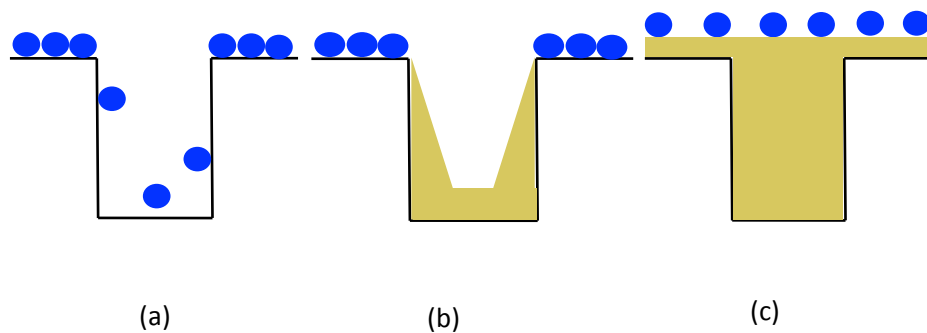
Figure 2.6 a) Difference in additive diffusion allows fewer levelers to reach recesses and thus plating inhibition occurs at the exposed portions. Deposition then starts at the b) bottom and c) progresses to the top.

Moffat *et al.* [2.63, 2.65] proposed the more recent differential acceleration curvature-enhanced accumulation acceleration (CEAC) model. The CEAC explains the existence of an accelerator catalyst complex present in the suppressor-accelerator containing electrolytes (see Fig. 2.7). This catalyst is adsorbed at specific regions on the substrate having a concave curvature, essentially found at trench bottoms, and promoting accelerated copper deposition. As the hole steadily fills up with the metal and less of the trench area is exposed, lesser amounts of the catalyst accumulate in

the region. Deposition, which is limited by the steadily declining amount of catalyst in the trench, continues until the hole is completely filled. The CEAC model has a very good correlation with actual deposit profiles and is applicable even for other systems such as gold and silver plating [2.66] and CVD of copper [2.67].

(a)   (b)   (c)
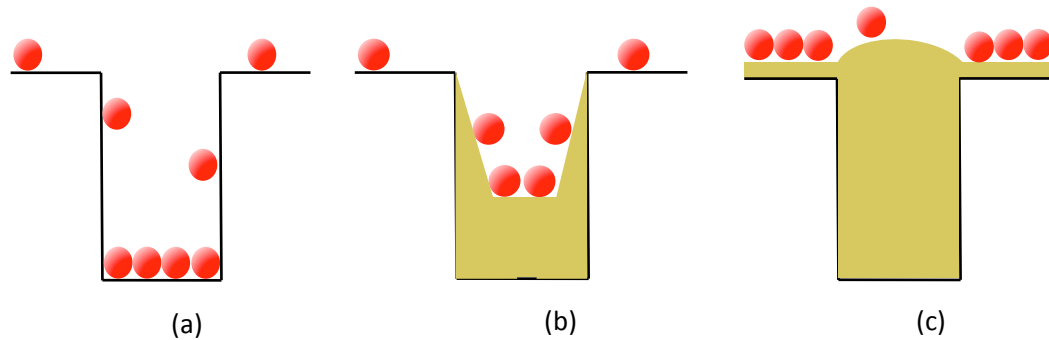
Figure 2.7 CEAC model explains that a) additive complex (red circle) accumulate at the concave surfaces found at recesses. b) The molecule complex accelerates metal deposition in these areas until trench is filled. c) At the top a change in surface curvature is experienced and complex diffuses to lower regions to promote leveling.

Dow *et al.* [2.68] developed a plating bath for through-hole filling applications that offered another alternative for additive use (see Fig. 2.8). The bath does not contain a carrier or an accelerator, but has two strong inhibitors: a quaternary amine and an amide. The action of both is dependent on adsorbed chloride ions on the cathode surface. This means that the inhibitor is concentrated in areas where chloride ions are adsorbed; primarily, the exposed surfaces and near through-hole entrances. These regions experience strong copper suppression. Conversely, regions with limited Cl$^-$ adsorption (e.g. center of the through-hole) will have lower amounts of the suppressor and deposition proceeds uninhibited.
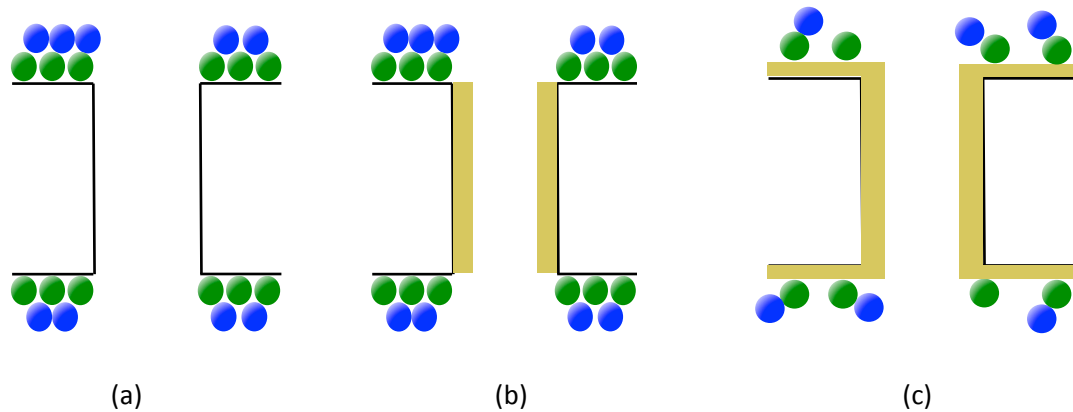
Figure 2.8 Schematic showing Dow *et al.*'s [2.68] concept where a) chloride ions (green circle) accumulates at through-hole entrances and attracts inhibitor molecules (blue circle), b) plating then starts at the center of the through hole and c) progresses to the entrance.

2.5 Effect of Additives on Copper Deposit Properties

2.5.1 Morphology

It is known that changes in the deposition process influences the microstructure and ensuing properties of deposits [2.69]. Electrodeposits are usually polycrystalline, consisting of fine crystals called grains, and regions of crystal orientation mismatch called grain boundaries. Furthermore, grain structures can be classified as: (i) columnar, (ii) equiaxed, (iii) dentritic, (iv) nodular and (v) fibrous as shown in Fig. 2.9 [2.70, 2.71]. The preferred grain structure depends on the application. For most plating applications, a fine-grained structure is desirable as it gives, among other things, better mechanical properties and brighter plate surfaces [2.72]. On the other hand, in electronics application the preferred grain morphology

is a bamboo-type grain structure where the grains are larger than device width [2.73]. This morphology increases resistance to electromigration.

(i) columnar

(iii) dendritic

(iv) nodular

(ii) equiaxed

(v) fibrous
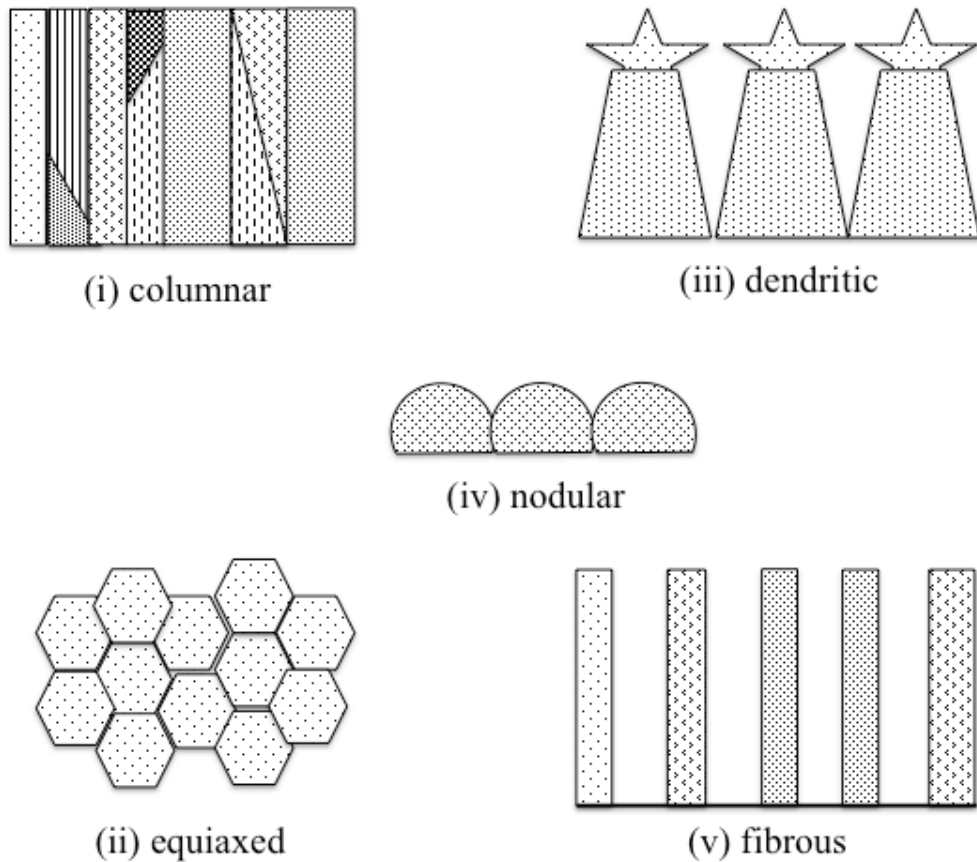
Figure 2.9 Schematic of grain structures [2.70, 2.71].

The possible grain structure that a deposit will assume depends on how additives affect crystal nucleation and growth. The reduction in grain size, or grain refinement, is one of the most significant morphological and microstructural effects of additives. Different additives promote grain refinement via different mechanisms. For example, brighteners can promote new nucleation sites hence creating fine deposits. Leveling agents create fine grains by inhibiting dendritic growth [2.74, 2.75, 2.76]. Winand [2.77] explains that the additive-induced inhibition promotes lateral growth of grains that creates dense and coherent deposit. Additive

concentration can also affect the plating morphology. Past literature suggest that low amounts of additives promote nucleation and create fine-grained deposits [2.69]. Other process parameters and factors that promote small grain structures include: (i) lower metal ion concentration, (ii) presence of additives, (iii) high current density, (iv) low bath temperature (as it enhances nucleation of new grains and retards grain growth), (v) low agitation and; (vi) high polarisation [2.70].

Crystallographic texture is another morphological feature that is important in electronics application. Texture refers to the distribution of crystallographic orientations in the metal. In copper films, the three most common grain orientations are the (111), (100) and (110) planes [2.78], with (111) being the most common due to having the lowest surface energy [2.79]. Although electroplated metals typically have randomly oriented grains, in some cases a preference in crystal growth orientation may be desirable. For example, in trench filling the barrier or seed layer morphology is controlled to induce Cu <111>texture [2.79]. This procedure is based on the fact that texture is largely dependent on the basis metal or the substrate [2.80]. The copper <111> texture is preferred since it shows higher resistance to void formation and can prevent excessive electromigration in interconnects [2.81, 2.82]. Current density and bath temperature are other factors that can also influence texture [2.9].

Self-annealing is a peculiar metallurgical process that occurs for electrodeposited copper. It refers to a phenomenon wherein the copper grain structure is unstable at room temperature and undergoes spontaneous grain growth even in the absence of thermal input [2.83, 2.84, 2.85]. During self-annealing, the grain size increases, the preferred texture changes, electrical resistivity is reduced by

20%, strength decreases, and ductility increases [2.83, 2.84, 2.85, 2.86, 2.87]. These changes in properties have strong implications on the performance of electroplated copper especially when used in microelectronics applications [2.88].

Self-annealing have been observed only in deposits plated from additive-containing electrolytes, and can initiate at any time [2.67, 2.89]. The process can last over a period of hours and may extend up to weeks [2.83]. Furthermore, observations in patterned thins films showed that grain growth initiates in regions close to the edges of features where the highest defect density are present [2.90], implying the influence of stress on the mechanism of self-annealing.

2.5.2 Mechanical Properties

The mechanical property of the plated copper is an important consideration especially when keeping up with the strict quality standards of the electronic industry. In printed circuit board (PCB) manufacturing, copper films experience enormous stresses during soldering and other thermal treatments [2.72, 2.91]. During service, additional stresses may come in from product handling or resistance heating. Electroplated copper lines are constantly expected to be robust enough to withstand these conditions [2.70].

A number of studies proved that mechanical properties are intimately related to the microstructural features of the plated copper [2.72, 2.92, 2.93, 2.94]. The grain structure can even be used to predict the ensuing mechanical properties of the deposit. Dini [2.95] provides a simple scheme that classifies grain structure with the corresponding mechanical properties of each (Table 2.1). Alternatively, a popular tool used by electroplaters is referred to as the Winand diagram. This diagram shows how the structure of the plated metal is influenced by polarisation, mass transport

and inhibition [2.77]. However, though useful in predicting microstructures, the diagram does not provide information on the consequent properties of the deposit.

Table 2.1 Mechanical Properties of Various Grain Sizes and Structures.

Grain type	Mechanical and physical property
Columnar	Low strength and hardness but exhibits high ductility.
Fine-grained	The size of the grains is usually 10-100nm. Deposits are hard and ductile.
Fibrous	The property of these deposits is between the columnar and fine-grained structure.
Banded	These grains have dimension of < 10nm, which are brought about by brighteners. Deposits can exhibit low ductility but high strength and hardness.

As mentioned earlier, plating additives are capable of creating different deposit morphology. For example, phenolsulfonic acid causes a fibrous structure in the copper deposit while tri-iso propanolamine or a brightener like SPS would create a fine-grained structure [2.9]. Different microstructures would often display different mechanical properties, and both grain size and grain shape can influence this outcome. The Hall-Petch relationship shows that tensile properties are inversely proportional to the square root of grain diameter [2.96]:

$$\sigma_y = \sigma_i + \frac{k_y}{\sqrt{d}} \qquad \qquad \text{Equation (2.6)}$$

where σ_y is the yield strength, d refers to the grain diameter and σ_i and k_y are material property constants. This means that the finer the grain structure, the stronger the deposit becomes. Thus, SPS, or any grain-refining additive for that matter, would create a strong deposit [2.97]. On the contrary, the phenomenon of self-annealing, where crystal grains grow spontaneously over time, will decrease the strength of the

metal. The Hall-Petch relation is experimentally true up to a size of about 10nm [2.98]. Below the 10nm limit, grain boundary sliding becomes a major contributor to deformation and failure, and thus strength subsequently goes down.

On the other hand, ductility of plated copper appears to be dependent not only on grain size but also shape. Ductility is generally lost with increasing tensile strength, and any changes in the microstructure that enhances the strength of metals will lower ductility. Hence, a fine-grained structure is expected to show poor ductility than a coarse-grained one. However, fine-grained equiaxed structures show more ductility than coarse and columnar grains, highlighting the effect of grain shape. For example, the columnar structure seen in deposits from additive-free baths is more prone to cracking during the solder float test [2.99]. Gelatin in copper baths created a fine yet fibrous grain structure that was also brittle [2.9]. Columnar grains are weak due to interferences in the converging grains. Parallel to the longitudinal direction, strain is prevented by the large grain boundary area found between adjacent grains. When plastic deformation is prevented from occurring then brittle fracture ensues. Additionally, ductility agents can improve other deposit properties such as thermal shock resistance [2.100].

Wilson [2.101] and Zakraysek [2.102] observed a thermally induced ductile-brittle transition in plated copper, with fractures coursing through grain boundaries (i.e. intergranular fracture). Lin and Sheppard [2.103] affirmed these observations, noting embrittlement in copper possessing columnar grains when at temperatures between 150 and 300°C. This behavior is explained to be associated with grain growth inhibition and resulting grain boundary weakening during anneal. Chlorides at the surface of deposits, which are likely assimilated from the plating bath, is seen

to significantly enhance vacancy motion. These chloride contaminations act as crack nucleation points (see Fig. 2.10) via the vacancy mechanism, and cause easy fracture even at temperatures as low as 150 $^{\circ}$C [2.102]. On the other hand, Lassila [2.104] postulated that segregated impurities, and not exclusively chloride substances, that cause the high-temperature brittleness in copper. Sole and Szendrei [2.105] confirmed Lassila's theory when they observed better reliability in copper deposited via an additive-free acid sulfate bath coupled with pulse plating.
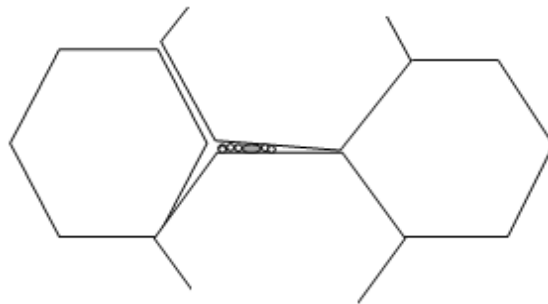
Figure 2.10 Schematic showing chloride ions (gray particle) settling at grain boundaries, encouraging void coalescence and becoming a crack initiation point. This crack nucleation and propagation mechanism leads to intergranular fracture.

Additives can degrade the properties of electrodeposited copper when tight controls are not implemented during plating [2.97]. Deposit cracking occurs when the breakdown products of additives, especially excess amounts of brighteners, and other contaminants are incorporated into the plating. This problem may be avoided by keeping the bath relatively pure by filtering, using activated carbon treatments, and by blending proper proportions of additives to prevent brightener imbalance.

2.5.3 Electrical properties

The main attraction in using copper in interconnect technology is based on the relatively high conductivity of this metal [2.79]. As the size of semiconductor devices shrink and metallisation line widths significantly decrease, a greater

emphasis on the use of high conductivity material in interconnects is placed. The two main advantages of using high conductivity metals are [2.7, 2.79] (i) the reduction of the overall interconnect time delay and (ii) the feasibility of using higher current densities at lower voltages, which minimises the heat generation and power requirements of the device. To illustrate, a 40% reduction in interconnect delay can be obtained by using copper (resistivity, ρ, of 1.7 $\mu\Omega\cdot$cm) instead of aluminum (ρ of 2.7 $\mu\Omega\cdot$cm) [2.106]. Clearly, any process that is used to form interconnects should be able to preserve the inherently good electrical properties of copper.

The primary mechanism of electrical conduction in metals is by electronic conduction. In this mechanism, free electrons act as charge carriers and are made to move through the metal by the action of an applied electric field. High conductivity results when electrons can move as freely as possible through the lattice. However, defects in the crystal structure such as alloying atoms, dislocations and grain boundaries can act as electron 'scattering centers'. These structures lower electron mobility by blocking the electron's path, consequently lowering total electron displacement and decreasing bulk electrical conductivity of the metal. For example, the electrical resistance of the grain boundary is two orders higher than that of the grain [2.107]. Furthermore, the scattering effect at the grain boundaries has an increasing influence on electrical resistivity as metal film thickness decreases [2.108]. Needless to say, defects are unwanted in applications where high electrical conductivity is important.

In interconnect applications, grain size and grain boundary characteristics have a large influence on the electrical properties of the copper films. The effect of

grain size on the total resistivity, R_{Total}, of the copper lines may be seen in the equation [2.109];

$$R_{Total} = R_g + R_{gb} = R_g + \frac{L_t}{dR_1} \qquad \text{Equation (2.7)}$$

where R_g is the grain resistance, R_{gb} is the grain boundary resistance, L_t is the line thickness, d is the mean grain diameter, and R_1 is the resistance of a single grain boundary layer. Clearly, the effect of grain size on conductivity is related to the grain boundary area, and that a reduction in grain size increases resistivity. Furthermore, as the interconnect line widths shrink, the bulk resistivity of copper is determined by a combination of surface scattering, grain boundary scattering and surface roughness scattering [2.79]. Grain boundary scattering becomes strongly dominant at line widths less than 100nm, and thus grain size should be made large to minimise the scattering effect.

Studies confirm that the lowest resistivities are found in copper deposits from additive-free baths, primarily due to the occurrence of the columnar, coarse-grained structures [2.110]. However, these baths are not suitable for electronic applications since the same coarse structure prevents proper hole filling. On the other hand, using additives result to the desired bottom-up filling action, but also causes grain refinement in the plated metal [2.3]. As mentioned earlier, the fine-grained structure is not particularly desirable in electronics application, and thus control of grain size becomes necessary. One technique to increase grain size in Damascene copper is the post-plating anneal treatment [2.79]. Similarly, the grain growth that occurs during self-annealing of plated copper would also be effective in reducing interconnect resistivity [2.79]. One factor that can offset the increase in resistivity caused by

additives is the purity of deposits. High purity deposits from additive-containing electrolytes exhibited conductivities similar to deposits from additive-free baths, despite the difference in grain size [2.110]. The absence of certain elements such as C, S and Cl appears to be responsible for the improvement in conductivity. The purity of the plated copper may be enhanced by using very high purity anodes and employing purified plating solutions.

Stress in the plated metal is another factor that influences conductivity. The stresses may result from a large defect density (e.g. dislocations, grain boundaries, voids) or from lattice mismatch at the plating interfaces. The magnitude of the stress, regardless if compressive or tensile, needs be low for good conductivity. One factor that influences the nature of the stress in the plated metal is the substrate [2.111, 2.112]. For example, Balakumar *et al.* [2.112] observed the formation of coarse-grained, low-resistivity copper when a low stress and highly (111)-oriented Cu seed layers were used. Additives can also induce stresses in the plated metal, and these stresses are enough to drive transformations such as those seen during self-annealing. Vas'ko *et al.* [2.113] noted a transition from highly compressive to slightly tensile stresses during self-annealing of copper plated from PEG-DPS containing electrolytes, and this drop in the magnitude of the stress coincided with a drop in the resistivity of the copper film.

Crystallographic texture can influence electrical behavior of the plated copper. Vas'ko *et al.* [2.113] noted that improvements in texture that reduces crystal misalignments across the grain boundary enhance the bulk conductivity of copper films. Additives can induce changes in texture and thus alter electrical properties of

deposits. However, this effect is relatively small compared to the effect of grain size and stress.

2.6 Additives in Pulse Current Plating

Pulse plating refers to an electrodeposition process that uses a current, or potential, that is alternated between two values [2.114, 2.115]. This is opposed to direct current (DC) plating, which uses a constant current that does not change with time. Pulses usually contain periods of applied current (on-time), followed by either a (ii) zero current (unipolar pulse), or (iii) a reversed polarity current (reverse pulse) [2.116]. This constantly changing current modifies the dynamics of the electrochemical processes during plating and changes the properties of deposits.

Studies by Lamb *et al.* [2.117], Popov *et al.* [2.118], Bakhvalov [2.119] and Hansal and Roy [2.116] on pulse plating and reverse pulse plating point showed that deposit morphology and properties are improved with a simple control of pulse parameters and without the need for additives. Pulse plating for copper deposition found early acceptance in the electrowinning, electroforming and bright-nickel undercoating industries [2.120]. On the other hand, the impetus to use pulse plating technique in electronics application, and primarily in PCB manufacturing, came when the limits of direct current (DC) were reached [2.116].

Pulse reverse plating is the appropriate technique for PCB manufacture. The process offers improved throwing power, important when filling vias and controlling pattern structures, as well as low porosity and smoother deposits when compared to DC plating [2.116]. For interconnect application, the same benefits are obtained from this technique and includes: i) improved gap filling performance, ii) reduction of film

roughness, iii) formation of uniform grains, iv) increase in mechanical strength without compromising ductility and v) reduction in interconnect resistivity [2.116, 2.118, 2.121].

Additives still play a key role during pulse plating. Most of the additives used from commercial sources are proprietary, and these are found to be as complex as those used in DC plating [2.116]. However, an additional requirement in additives used in pulse plating is the ability to withstand high and constantly shifting polarisation.

It is known that throwing power may already be enhanced by controlling pulse parameters [2.122, 2.123]; but the use of additives in pulse plating systems can further improve throwing power. Pearson and Dennis [2.124] observed that the use of polyethers, sulfopropyl sulfides and chloride ions with pulse reverse current in acid copper plating yielded better throwing power. Kou and Hung [2.125] cited improvements in macroscopic throwing power after addition of Cl^- and a commercial additive (AC-90) during pulse reversed plating of copper.

The synergistic effects of additives may vary during pulse plating. For instance, some additives in combination with Cl^- gave extra high polarisation, while benzotriazole with Cl^- showed depolarisation [2.116, 2.126]. These synergistic effects can result to improvements in plating characteristics [2.116]. For instance, Dyar *et al.* [2.127] introduced a low cost via metallisation process that uses pulse plating together with PEG and chloride as additives. This electrically-mediated process can fill vias with minimal copper deposition at the exposed surface. The process employs modified pulse reverse plating, wherein electrode polarity cycles

from positive to negative followed by a period of rest or off-time. During the forward pulse when the substrate is cathodic, copper deposits at the vias with the help of additives (see Fig. 2.11). When polarity reverses and the substrate becoming anodic, metal dissolution occurs and the parts that are the most exposed (i.e. the top portion of the structure) are immediately etched. This plating and etch cycles are repeated until the desired structure is obtained.

a) cathodic   b) anodic   c) resulting product
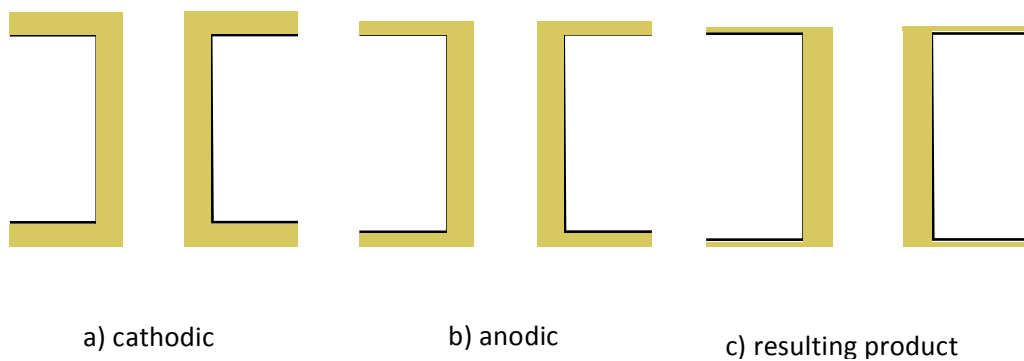
Figure 2.11 Schematic showing Dyar *et al*.'s [2.127] process where a) metal plating occurs when substrate is cathodic; b) after polarity reversal, substrate becomes anodic and etching occurs at the exposed region and c) final structure showing filled up via with minimal copper deposition on top portions.

The combination of pulse plating and additives can influence the morphology and the mechanical properties of deposits. Imaz *et al*. [2.128] successfully plated compact deposits using pulse plating in additive-free baths. Addition of thiourea in the electrolyte created a fine columnar structure, while gelatin created a fine equiaxed structure. However, both additives produced a rough deposit surface. This problem was eventually resolved by adjusting pulse parameters. Natter and Hempelmann [2.129] fabricated nanocrystalline copper by adding citric acid to the plating bath. Tao and Li [2.130] fabricated similar nanostructures using thiourea. Generally, a decrease in grain size improves mechanical properties of deposits. For

example, Tao and Li [2.130] observed higher elastic extension, wear resistance and nanoindentation hardness (~4.9 GPa) in nanocrystalline electroplated copper. Kou and Hung [2.125] noted higher ductility in pulse plated-copper using both additive-free and additive-containing electrolytes compared to DC-plated deposits.

Interestingly, since microstructures may be refined by controlling the pulse characteristics, then pulse plating can reduce the amount of plating additives needed to create the same morphological change. For example, Chang *et al.* [2.131] implemented defect-free trench and via filling even in leveler-free baths. Yin *et al.* [2.115] noted that pulsed current is important in enhancing mass transfer in the electrolyte, and this increases the efficacy and efficient consumption of additives. Kalantary *et al.* [2.132] observed good throwing power in additive-free baths using pulse reverse plating, but Holmbom and Jacobsson [2.133] observed that deposits lose brightness when additives are used with the same plating technique. Most studies agree that the positive effects of additives obtained in DC plating may come out differently when the same additive is used in pulse plating. Therefore, studies on additive effects should be an essential part of any attempt to optimise the pulse plating process.

In this chapter, a review of the role of three additives; namely, PEG, SPS and Cl^-, in the electroplating of copper was presented. The mechanistic actions of both the single- and multi-additives systems were discussed. The influence of these additives on the morphology and properties of the copper deposit were also covered. In the last section, the role of additives in the pulse plating process was reviewed.

References

2.1   Franssila S (2010) Introduction to Microfabrication. 2nd Edition John Wiley & Sons Ltd West Sussex United Kingdom

2.2   Madou MJ (2002) Fundamental of Microfabrication: The Science of Miniaturisation. CRC Press Boca Raton FL, London

2.3   Andricacos PC, Uzoh C, Dukovic JC, Horkans J, Deligiani H (1998) Damascene Copper Electroplating for Chip Interconnections. IBM J. Res. Dev. 42; 567-574

2.4   Shacham-Diamand Y (2009) Challenges in ULSI Interconnects Advanced Nanoscale ULSI Interconnects. Edited Shacham-Diamand Y, Ohba T, Datta M, Osaka T Springer NY

2.5   Dubin VM (2003) Electrochemical aspects of New Materials and Technologies in Microelectronics. Microelectron. Engg. 70; 461

2.6   Dubin VM (2012) Copper Electroplating for On-chip Metallization In Advanced Interconnects for ULSI Technology. M Baklanov, P Ho, E Zschech Eds. John Wiley & Sons, USA; 173-191

2.7   Landau U (1982) Plating New Prospect for an Old Art, Electrochemistry in Industry, New Directions Plenum Press New York

2.8   Oniciu L, Muresan L (1991) Some Fundamental Aspects of Levelling and Brightening in Metal Electrodeposition. J. Appl. Electrochem. 21; 565-574

2.9   Dini D. Snyder D (2010) Electrodeposition of Copper in Modern Electroplating: 5th Edition Edited by Mordechay Schlesinger Milan Paunovic John Wiley and Sons NY

2.10   Gallaway JW, West AC (2008) PEG, PPG, and Their Triblock

Copolymers as Suppressors in Copper Electroplating. J. Electrochem.

Soc. 55(10); D632-D639

2.11   Reid J (2008) Damascene Copper Electroplating in Handbook of

Semiconductor Manufacturing Technology. Y Nishi, R Doering editors

2nd Ed CRC Press NY USA

2.12   Qin Y, Li X, Xue F, Vereecken PM, Andricacos P, Deligianni H, Braatz

R, Alkire R (2008) Effect of Additives on Shape Evolution during

Electrodeposition III. Trench infill for on-chip interconnects. J of the

Electrochem Soc 155(3); D223-233

2.13   Won YS, Cho D, Kim Y, Lee J, Park SS (2010)   Degradation of

Poly(ethylene glycol) by Electrolysis During the Cu Electroplating: A

Combined Experimental and Density Functional Theory Study. J Appl

Polym Sci 117(4); 2083-2089

2.14   Hai NTM, Huynh TTM, Fluegel A, Arnold M, Mayer D, Reckien W,

Bredow T, Broekmann P (2012a) Competitive anion/anion interactions

on copper surfaces relevant for Damascene electroplating.

Electrochimica Acta 70; 286-295

2.15   Hai NTM, Krämer KW, Fluegel A, Arnold M, Mayer D, Broekmann P

(2012b) Beyond interfacial anion/cation pairing: The role of Cu(I)

coordination chemistry in additive-controlled copper plating.

Electrochimica Acta 83; 367-375

2.16   Vereecken PM, Binstead RA, Deligianni H, Andricacos PC (2005) The

Chemistry of Additives in Damascene Copper Plating. IBM J. Res. and

Dev. 49(1); 3-17

2.17   Barkey DP (2014) Acceleration Effect, (In) Copper Electrodeposition for Nanofabrication of Electronics Devices. Kondo K, Akolkar R, Barkey D, Yokoi M, (eds) Springer NY USA; 45-61

2.18   Frank A, Bard AJ (2003) The Decomposition of the Sulfonate Additive Sulfopropyl Sulfonate in Acid Copper Electroplating Chemistries. J. Electrochem. Soc. 150(4); C244-C250

2.19   Sarma RL, Nageswar S (1981) Electrodeposition of Copper in the Presence of 2-Mercaptoethanol. Surf. Tech. 12(4); 377-382

2.20   Reid J (1987) An HPLC Study of Acid Copper Brightener Properties. PC Fab. 10; 65-71

2.21   Kondo K, Matsumoto T, Watanabe K (2004) Role of additives for copper damascene electrodeposition; experimental study on inhibition and acceleration effects. J. Electrochem. Soc. 151(4); C250–C255

2.22   Kainuma S, Ishikura S, Hisatake K (1995) Giant Magneto resistance of Electrodeposited [CoNiCu/Cu] Multilayers. J. Magnetics Soc. of Japan 21; 557-560

2.23   Dow WP, Huang HS, Lin Z (2003) Interactions Between Brightener and Chloride Ions on Copper Electroplating for Laser-Drilled Via-Hole Filling. Electrochem. Solid-State Lett. 6(9); C134-C136

2.24   Beacom S, Riley B (1960) Further Studies of Leveling Using Radiotracer Techniques. J. Electrochem. Soc. 107(9); 785-787

2.25   Hill MRH, Rogers GT (1978) Polyethylene Glycol in Copper Electrodeposition onto a Rotating Disk Electrode. J. Electroanal. Chem.

86; 179-188

2.26   Yokoi M, Konishi S, Hayashi T (1984a) Adsorption behavior of polyoxyethyleneglycole on the copper surface in an acid copper sulfate bath. Denki Kagaku 52; 218–223

2.27   Yokoi M, Konishi S, Hayashi T (1983) Mechanism of the Electrodeposition and Dissolution of Copper in an Acid Copper-Sulfate Bath. 3. Effect of Cl− Ions, Denki Kagaku 51; 456-460

2.28   Stoychev DS, Tsvetanov C (1996) Behaviour of Poly(Ethylene glycol) During Electrodeposition of Bright Copper Coatings in Sulphuric Acid Electrolytes. J. Appl. Electrochem. 26(7); 741-749

2.29   Kelly JJ, West AC (1998a) Copper deposition in the presence of polyethylene glycol; I. Quartzcrystal microbalance study. J. Electrochem. Soc. 145(10); 3472–3476

2.30   Kelly JJ, West AC (1998b) Copper deposition in the presence of polyethylene glycol; II. J. Electrochem. Soc. 145(10); 3477–3481

2.31   Papke BL, Ratner MA, Shriver DF (1982) Conformation and ion-transport models for thestructure and ionic conductivity in complexes of polyethers with alkali metal salts. J. Electrochem. Soc. 129(8); 1694–1701

2.32   Yokoi M (2014) Supression Effect and Additive Chemistry, in Copper Electrodeposition for Nanofabrication of Electronics Devices. Kondo K, Akolkar R, Barkey D, Yokoi M, (eds), Springer NY, USA; 27-43

2.33   Dow WP, Huang HS, Yen MY, Chen HH (2005b) Influence of molecular weight of polyethylene glycol on microvia filling by copper

electroplating. J Electrochem Soc b 152(11); C769-C775

2.34 Tan M, Guymon C, Wheeler D, Harb J (2007) The Role of SPS, MPSA, and Chloride in Additive Systems for Copper Electrodeposition. J. Electrochem. Soc. 154(2); D78-D81

2.35 Täubert C, Kolb D, Memmert U, Meyer H (2007) Adsorption of the Additives MPA, MPSA, and SPS onto Cu(111) from Sulfuric Acid Solutions. J. Electrochem. Soc. 154(6); D293-D299

2.36 Healy JP, Pletcher D, Goodenough M (1992) The Chemistry of the Additives in an Acid Copper Electroplating Bath. J. Electroanal. Chem. 338; 155-165

2.37 Melnicki LS (1988) Electrochemical Technology in Electronics' in L Romankiw and T Osaka (Eds) PV 88–23 ECS Proceedings Series Pennington NJ; 95–103

2.38 Nagy Z, Blaudeau JP, Hung NC, Curtiss LA, Zurawski DJ (1995) Chloride ion catalysis of the copper deposition reaction. J. Electrochem. Soc. 142(6); L87–L89

2.39 Goodenough M, Whitelaw KJ (1989) Electrochemical Processing in ULSI Fabrication III. Trans. IMF 67; 57

2.40 Soares DM, Wasle S, Weil KG, Doblhofer K (2002) Copper ion reduction catalyzed by chloride ions. J. Electroanal. Chem. 532(1-2); 353–358

2.41 Dow WP, Huang HS, Yen MY, Chen HH (2005a) Roles of chloride ion in microvia filling by copper electrodeposition – II. J. Electrochem. Soc. a 152(2); C67-C76

2.42   Moffat TP, Wheeler D, Josell D (2004)a Superfilling and the Curvature Enhanced Accelerator Coverage Mechanism. The Electrochem. Soc. Interface Winter 2004

2.43   Feng ZV, Li X, Gewirth AA (2003) Inhibition Due to the Interaction of Polyethylene Glycol, Chloride, and Copper in Plating Baths: A Surface-Enhanced Raman Study J. Phys. Chem. B 107(35); 9415–9423

2.44   Sylvester N, Tyler J (1970) Dilute Solution Drag-Reducing Properties of Polymers. Ind Eng Chem Prod Res Devel 9; 548-553

2.45   Hebert KR (2005) Role of chloride ions in suppression of copper electrodeposition by polyethyleneglycol. J. Electrochem. Soc. 152(5); C283–C287

2.46   Yokoi M, Konishi S (1984b) Effect of polyoxyethylene surfactants on the hardness of copper electrodeposited from an acid copper sulfate bath. J. Surf. Finish. Soc. Jpn. 35; 421–427

2.47   Bae SE, Gewirth AA (2006) In Situ EC-STM Studies of MPS, SPS, and Chloride on Cu(100): Structural Studies of Accelerators for Dual Damascene Electrodeposition. Langmuir 22(25); 10315-10321

2.48   Moffat TP, Ou Yang LY (2010) Accelerator Surface Phase Associated with Superconformal Cu Electrodeposition, J. Electrochem. Soc. 157(4); D228-D241

2.49   Tu H, Yen PY, Yah S. Dow WP, Lee YL (2011) In Situ STM Imaging of Bis-3-sodiumsulfopropyl-disulfide Molecules Adsorbed on Copper Film Electrodeposited on Pt(111) Single Crystal Electrode. Langmuir *27*(11); 6801–6807

2.50   Farndon E, Walsh FC, Campbell SA (1995) Effect of thiourea, benzotriazole and 4,5-dithiaoctane-1,8-disulphonic acid on the kinetics of copper deposition from dilute acid sulphate solutions. J. Appl. Electrochem. 25; 574-583

2.51   Huynh TMT, Florian W, Hai NTM, Reckien W, Bredow T, Fluegel A, Arnold M, Mayer D, Keller H, Broekmann P (2013) On the role of halides and thiols in additive-assisted copper electroplating. Electrochim. Acta 89; 537– 548

2.52   Survila A, Kanapeckaite S, Pauliukaite R (1998) Polaragraphic behavior of Cu(II) solutions involving 3-Mercapto-1-Propanosulphonic Acid. Chemija 1; 21–26

2.53   Schultz ZD, Feng ZV, Biggin ME, Gewirth AA (2006) Vibrational spectroscopic and mass spectrometric studies of the interaction of Bis(3-sulfopropyl)-disulfide with Cu surfaces. J. Electrochem. Soc. 153(2); C97–C107

2.54   Moffat TP, Wheeler D, and Josell D (2004)b Electrodeposition of Copper in the SPS-PEG-Cl Additive System I. Kinetic Measurements: Influence of SPS. J. Electrochem. Soc. 151(4); C262-C271

2.55   Walker ML, Richter LJ, Moffat TP (2006) Competitive adsorption of PEG, Cl-, and SPS/MPS on Cu: an in situ ellipsometric study. J. Electrochem. Soc. 153(8); C557–C561

2.56   Basol BM, West AC (2006) Study on mechanically induced current suppression and super filling mechanisms. Electrochem. Solid-State Lett. 9(4); C77–C80

2.57   Willey MJ, West AC (2007) SPS adsorption and desorption during

copper electrodeposition and its impact on PEG adsorption. J.

Electrochem. Soc. 154 (3); D156-D162

2.58   Tan M, Harb JN (2003) Additive Behavior during Copper

Electrodeposition in Solutions Containing Cl⁻, PEG, and SPS. J.

Electrochem. Soc. 150(6); C420-C425

2.59   Broekmann P, Fluegel A, Emmet C, Arnold M, Roeger-Goepfert C,

Wagner A, Hai NTM, Mayer D (2011) Classification of suppressor

additives based on synergistic and antagonistic ensemble effects.

Electochim. Acta 56; 4724-4734

2.60   Andricacos PC (1999) Copper On-chip Interconnections: A

Breakthrough in Electrodeposition to Make Better Chips. Electrochem.

Soc. Interface 8(1); 32-37

2.61   Deligianni H, Horkans, J, Kwietniak K, Dukovic JO, Andricacos PC,

Boettcher S, Seo S-C, Locke P, Simon A, Seymour S, Malhotra S (2000)

Model in Superfilling in Damascene Electroplating: Comparison of

Experimental Feature Filling with Model Predictions, Lectrochemical

Processing in ULSI Fabrication III. PC Andricacos, PC Searson, C

Redsema-Simpson, P Allongue, JL Stickney, GM Oleszek. Editors. PV

2000(8); 145-149

2.62   Lin K-C, Shieh J-M, Chang S-C, Dai B-T, Chen C-F, Feng M-S (2002)

Electroplating Copper in Sub-100nm gaps by Additives with Low

Consumption and Diffusion Ability. J. Vac. Sci. Technol. B 20; 940-945

2.63   Moffat TP, Bonevich JE, Huber WH, Stanishevsky A, Kelly DR,

Stafford GR, Josell, D (2000) Superconformal Electrodeposition of

Copper in 500-90 nm Features. J. Electrochem. Soc. 147(12); 4524-4535

2.64   West AC (2000) Theory of Filling High-Aspect Ratio Trenches and

Vias in Presence of Additives. J. Electrochem. Soc. 147(1); 227-232

2.65   Moffat TP, Wheeler D, Witt C, Josell D (2002) Superconformal

Electrodepositon Using Derivatized Substrates. Electrochem. and Solid-

State Lett. 5; C110-C112

2.66   Baker BC, Freeman M, Melnick B, Wheeler D, Josell D, Moffat TP

(2003) Superconformal Electrodeposition of Silver from a $KAG(CN)_2$-

KCN-KSeCN Electrolyte. J. Electrochem. Soc. 150(2); C61-C66

2.67   Josell K, Sibum D, Wheeler TP, Moffat, Sung Gyu Pyo (2003)

Interconnect Fabrication by Superconformal Iodine-Catalyzed Chemical

Vapor Deposition of Copper. J. Electrochem. Soc. 150; C368-C373

2.68   Dow WP, Chen HH, Yen MY, Chen WH, Hsu KH, Chuang PY,

Ishizuka H, Sakagawa N, Kimizuka R (2008) Through-Hole Filling by

Copper Electroplating J. Electrochem. Soc. 155; D750-D757

2.69   Anderson D, Haak R, Ogden C, Tench D and White J (1985) Tensile

Properties of Acid Copper Electrodeposits. J. Appl. Electrochem. 15;

631-637

2.70   Paunovic M, Schlesinger M (1998) Fundamentals of Electrochemical

Deposition. John Wiley & Sons Inc Hoboken, NJ

2.71   Safranek W (1974) The Properties of Electrodeposited Metals and

Alloys, A Handbook. American Elsevier Publishing Company Inc New

York

2.72 Romankiw LT, Sullivan O (1997) Plating Techniques. Handbook of Microlithography, Micromachining, and Microfabrication. Vol 2 SPIE Press Bellingham Washington DC

2.73 Rosenberg R, Edelstein DC, Hu CK, Rodbell KP (2000) Copper Metallization for High Performance Silicon Technology. Annual Review of Materials Science 30; 229-262

2.74 Darken J (1979) Recent Progress in Bright Plating from Zincate Electrolyte. Trans. IMF 57; 145-145

2.75 Fisher GL (1978) Power Savings Using Sulfur-Activated Nickel Anode Materials. Plat. Surf. Finish. 65; 46-53

2.76 Loshkaryov MA, Loshkaryov YM (1978) Some Trends in the Influence of Surface-Active Substances on Electrode Processes. Surf. Technol. 6(6); 397-408

2.77 Winand R (1992) Electrocrystalization – theory and applications. Hydrometallurgy 29(1-3); 567-598

2.78 Knorr DB, Tracy DP (1995) A review of microstructure in vapor deposited copper thin films. Mater. Chem. Phys. 41(3); 206-216

2.79 Gupta T (2009) Copper Interconnect Technology. Springer Books, New York USA; 195-225

2.80 Shreir LL and Smith JW (1952) Cathode Polarization Potential during the Electrodeposition of Copper: III . Effect of the Cathode Base upon the Cathode Polarization Potential and the Crystal Structure of the Deposit. J. Electrochem. Soc. 1952 99(11); 450-456.

2.81 Vanasupa L, Joo YC, Besser PR, Pramanick S (1999a) Texture analysis

of damascene-fabricated Cu lines by X-ray diffraction and electron backscatter diffraction and its impact on electromigration performance. J. Appl. Phys. 85(5); 2583-2590

2.82 Sekiguchi A, Koike J, Maruyama K (2003) Microstructural influences on stress migration in electroplated Cu metallization. Appl. Phys. Lett. 83(10); 1962-1964

2.83 Harper JME, Cabral Jr C, Andricacos PC, Gignac L, Noyan IC, Rodbell KP, Hu CK (1999) Mechanisms for Microstructure evolution in electroplated Copper Thin Films near Room Temperature. J. Appl. Physics 86(5); 2516-3642

2.84 Cabral Jr C, Andricacos C, Gignac L, Noyan IC, Rodbel KP, Shaw TM, Rosenberg R, Harper JME (1998) Room Temperature Evolution of Microstructure and Reactivity in Electroplated Copper Films. Abstracts of the Advanced Metallization Conference (AMC) Colorado Springs Colorado

2.85 Ryu C, Kwon K, Loke A, Lee H, Nogami T, Dubin V, Kavari R, Ray G, Wong SS (1999) Microstructure and Reliability of Copper Interconnects. IEEE Trans. on Electron Devices 46(6); 1113-1120

2.86 Gangulee A (1972) The Structure of Electroplated and Vapor – Deposited Copper Films. J. Appl. Physics 43; 867-873

2.87 Ritzdorf T, Graham L, Jin S, Mu C, Fraser DB (1998) Self-annealing of electrochemically deposited copper films in advanced interconnect applications. Proc. Int. Interconnect technol. Conf. (New York: IEEE) 98; 166-168

2.88   Lee H, Wong S, Lopatin S (2003) Correlation of stress and texture evolution during self- and thermal annealing of electroplated Cu films. J. Appl. Phys. 93; 3796-3804

2.89   Brongersma SH, Richard E, Vervoort I, Bender H, Vandervorst W, Lagrange S, Beyer G, Maex K (1999) Two-step room temperature grain growth in electroplated copper. J. Appl. Phys. 86; 3642-3645

2.90   Lingk C, Gross ME, Brown WL (1998) X-ray diffraction pole figure evidence for (111) sidewall texture of electroplated Cu in submicron damascene trenches. J. Appl. Phys. 74(5); 682 – 684

2.91   Harding W, Di Bari G (1986) Testing of Metallic and Inorganic Coatings. ASTM Special Technical Publication 947 1916 Race St. Philadelphia, PA 19103

2.92   Michailova E, Vitanova I, Stoychev D, Milchev A (1993) Initial Stages of Copper Electrodepostion in the Presence of Organic Additives. Electrochimica Acta 38(16); 2455-2458

2.93   Hofer EM, Hintermann HE (1965) The Structure of Electrodeposited Copper Examined by X-Ray Diffraction Techniques. J. Electrochem. Soc. 112; 167-173

2.94   Rusli E, Xue F, Drews T, Vereecken P, Andricacos P, Deligianni H, Braatz R, Alkire R (2007) Effect of Additives on Shape Evolution during Electrodeposition. J. Electrochem. Soc. 154(11); D584 – D597

2.95   Dini JW (1993) Electrodeposition – The Materials Science of Coatings and Substrates. William Andrew Publishing/Noyes Electronic ISBN: 978-0-8155-1698-9; 195 – 237

2.96   Woodman AS, Taylor EJ, Anderson EB, Weil R (1993) Thin Metallic Films Electrochemical Society In Proc. 2nd International Symposium on Electrochemical Technology Applications in Electronics. LT Romankiw, M Datta, T Osaka, Y Yamazaki, Editors. Electrochem Soc Pennington NJ; 86-90

2.97   Yung E, Romankiw L, Richard C, Alkire (1989) Plating of Copper into Through-Holes and Vias. Electrochem. Soc. 136(1); 206-215

2.98   Schuh C, Nieh. TG (2003) Hardness and Abrasion Resistance of Nanocrystalline Nickel Alloys Near the Hall–Petch Breakdown Regime. Mat. Res. Soc. Symp. Proc.

2.99   Engelmaier and Kessler T (1978) Investigation of Agitation Effects on Electroplated Copper in Multilayer Board Plated-Through Holes in a Forced-Flow Plating Cell. J. Electrochem. Soc. 125(1); 36-43

2.100 Mayer LJ, Barbieri SC (1985) In Proc. AES 12th Plating in the Electronics Industry Symposium AESF Kissimmee FL

2.101 Wilson AD (1981) Fractography and Material Science. ASTM STP 733, L.N. Gilbertson and R.D. Zipp, Editors ASTM Philadelphia PA; 166-186

2.102 Zakraysek L (1983) Metallic Finish Systems in Microelectronic Components. IEEE Trans. on Components hybrids and manufacturing tech (4)4; 462-466

2.103 Lin K, Sheppard KG (1993) Mechanical Behavior of Electroplated Copper at Elevated Temperatures. Plat. and Surf. Finish. 80; 40-44

2.104 Lassila DH (1992) Shock Wave and High Strain Rate Phenomena in

Materials. MA Meyers, LE Murr, KP Staudhammer, Editors Marcel Dekker, New York; 543-545

2.105   Sole MJ, Szendrei T (1991) 'in Proc. AESF SUR/FIN 91' Session H Toronto 423 AESF Kissimmee Fl

2.106   Pratt A. PhD (2004) Overview of the Use of Copper Interconnects in the Semiconductor Industry. Advanced Energy Industries Inc Fort Collins Colorado 80525

2.107   Chopra KL (1967) Size Effects in the Longitudinal Magnetoresistance of Thin Silver Films. Phys. Rev. 155; 660-662

2.108   Van Attekum PM, Woerlee PH, Verkade GC, and Hoeben AAM (1984) Influence of grain boundaries and surface Debye temperature on the electrical resistance of thin gold films. Physical Review B 29(2); 645-650

2.109   Turner T (2000) Requirements for dual-damascene Cu-line width resistivity measurements. Solid State Technol. 43; 89-94

2.110   Preisser R, Dretschkow T, Fuerhaupter H (2003) Copper electroplating with improved stability, conductivity, and total cost of ownership: Copper Interconnects, New Contact Metallurgies/Structures, and low-k Interlevel Dielectrics II, G.S. Mathdad editor. The Electrochem Soc 2003(10); 33-39

2.111   Hara T, Sakata K, Yoshida Y (2002) Electrochemical determination of grain size of the EP-Cu. Solid State Lett. 5; C41-C43

2.112   Balakumar S, Kumar R, Shimura Y, Namiki K, Fujimoto M, Toida H, Uchida M, Tohru Hara (2004) Effect of Stress on the Properties of

Copper Lines in Cu Interconnects. Electrochem and Solid-State Lett. 7(4); G68-G71

2.113   Vas'ko VA, Tabakovic I, Riemer SC, Kief MT (2004) Effect of organic additives on structure, resistivity, and room-temperature recrystallization of electrodeposited copper. Microelectronic Engineering 75; 71–77

2.114   Ghaemi M, Binder L (2002) Effects of Direct and Pulse Current on Electrodeposition of Manganese Dioxide. J of Power Sources 102(1); 29-34

2.115   Yin KM, Jan SL, Lee CC (1997) Current Pulse with Reverse Plating of Nickel –Iron Alloys in Sulphate Bath. Surf. and Coat. Technol. 88(1); 219-225

2.116   Hansal EGW, Roy S (2012) Pulse plating. 1st edition Eugen G Lueze Verglag KK Germany

2.117   Lamb VA, Johnson E, Valentine DR (1970) Physical and Mechanical Properties of Electrodeposited Copper. J. Electochem. Soc. 117(9); 291C-341C

2.118   Popov KI, Totovski DC, Maksimovic MD (1983) Fundamental Aspects of Pulsating Current Metal Eletrodeposition VII: The Comparison of Current Density Distributions in Pulsating Current and Periodic Reverse Current Electrodeposition of Metals. Surf Tech 19(2); 181 -185

2.119   Bakhvalov GT (1966) New Technology of Electrodeposition of Metals: Current Reversal in Electroplating. Metallurgiya, Publishing House, Moscow

2.120   Chandrasekar MS, Pushpavanam M (2008) Pulse and pulse reverse

plating—Conceptual, advantages and applications. Electrochimica Acta 53(8); 3313–3322

2.121   Kim MJ, Cho SK, Koo H-C, Lim T, Park KJ, Kim JJ (2010) Pulse Electrodeposition for Improving Electrical Properties of Cu Thin Film. J. Electrochem. Soc. 157(1); D564-D569

2.122   Puippe J Cl, Ibl N (1980) Influence of Charge and Discharge of Electric Double Layer in Pulse Plating. J. Appl. Electrochem. 10(6); 775 - 784

2.123   White JR, Galasco RT (1988) Plat. Surf. Fin. 75 (1988) 122 - 126

2.124   Pearson T, Dennis JK (1990) The Effect of Pulsed Reverse Current on the Polarization Behaviour of Acid Copper Plating Solution containing Organic Additives. J. Appl. Electrochem. ISSN 0021-891X 20(2); 196 – 208

2.125   Kou SC, Hung A (2000) Studies of Acid Sulfate Copper Pulse Reversal Current Electrodeposition. Plat. Surf. Fin. 87(5); 140-144

2.126   Tantavichet N, Pritzker M (2006) Copper Electrodepostion in Sulphate Solutions in the Presence of Benzotriazole. J. Appl. Electochem. 36(1); 49-61

2.127   Dyar H, Taylor EJ, Sun J, Inman M (2004) A Low Cost Semiconductor Metallization/Planarization Process. Plat. and Surf. Finish. 91(3); 32-44

2.128   Imaz N, Garcia-Lecina E, Suarez C, Diez JA, Rodriguez J, Molina J, Garcia-Navas, V (2009) Influence of Additives and Plating Parameters on Morphology and Mechanical Properties of Copper Coatings obtained by Pulsed Electrodeposition. Trans. IMF 87(2); 64-71

2.129   Natter H, Hempelmann R (1996) Nanocrystalline copper for pulsed

electrodeposition: The effects of organic additives, bath temperature and pH. J. Physical Chem. 100(50); 19525-19532

2.130   Tao S, Li DY (2006) Tribological, Mechanical and Electrochemical Properties of Nanocrystalline Copper Deposits Produced by Pulsed Electrodeposition. Nanotech. 17(1); 65-78

2.131   Chang S-C, Shieh J-M, Dai BT, Feng MS (2002) Investigations of Pulse Current Electrodeposition for Damascene Copper Metals. J of Vac Sci and Tech B Microelectronics and Nanometer Structures 20(6); 2295-2298

2.132   Kalantary MR, Gabe DR, Goodenough MR (1993) Unipolar and Bipolar Pulsed Current Electrodeposition for PCB Production. J. Appl. Electrochem. 23(3); 231-240

2.133   Holmbom G, Jacobsson BE (1988) Through-hole Plating of Cu by Modulated Current Deposition. Surf. and Coat. Technol. 35(3); 333-341

Chapter 3

Fundamental Aspects

As this study involves an investigation on the effect of additives on the EnFACE process, it is necessary to review certain important topics to lay out a good foundation on the matter. This section starts out with a brief description of the process of electroplating and relevant concepts such as Faraday's law of electrolysis. This will be followed by a discussion on the thermodynamic aspects of plating citing such concepts like standard potential and the Nernst equation.

The succeeding section covers the kinetics of plating. Analysis of polarisation curves is one of the main features of the current research. This section will thus cover the rate controlling mechanisms of electroplating, such as charge-transfer and mass transport processes. The Butler-Volmer equation, which predicts the relationship of current density with overpotential, will also be discussed as this relates to how regions in the polarisation curves are ascertained.

3.1 The Electroplating Process

Electroplating, also known as electrodeposition, is an electrochemical process, which involves the use of an applied electrical current to reduce dissolved metal ions and form a metallic coat on a designated surface [3.1].
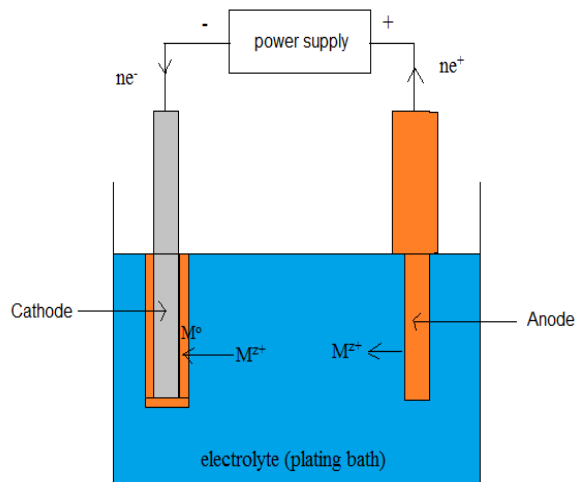
Figure 3.1 Schematic of the typical copper electroplating process.

The metal part to be plated is referred to as the cathode and the counterpart electrode is called the anode (Fig. 3.1). The two electrodes are connected to the appropriate terminals of an electrical source, typically a direct current (DC), and then immersed in an electrolyte solution called the plating electrolyte. The current source is then turned on and this initiates the reduction reaction that creates the deposit on the cathode. Simultaneously, an oxidation reaction occurs at the anode and proceeds at an equal rate to the cathode reaction. This set of red-ox reactions will involve an exchange of electrons and thus a conductive path is necessary to be maintained through the circuit. Also, while metals ions are being reduced in the cathode, the electrolyte is also continuously being replenished with ions from the anode when a dissolvable anode is used [3.2].

Electroplating is governed by Faraday's law of electrolysis. This equation predicts the amount of deposit created for any metal system as a function of the applied current and plating time:

$$m = \frac{IAt}{Fn}$$
Equation (3.1)

where m is the mass of the deposit (grams), I is the applied plating current (amperes), A is the atomic weight of the metal (g/mol), t is the time of plating (s), F is the Faraday's constant, 96,500 C/g-equivalent and n is the number of electrons interchanged.

In many cases, the actual amount deposited is observed to be smaller than predicted. This is due to the fact that side reactions, such as hydrogen evolution, that use some of the applied current. This value, when expressed as a percentage of the predicted amount, is called plating efficiency, PE, or current efficiency and is calculated as follows:

$$PE = \frac{m_{actual}}{m_{theoretical}} x100\%$$
Equation (3.2)

where m_{actual} is the measured weight after plating and $m_{theoretical}$ is the predicted weight using Faraday's equation.

3.2 Thermodynamics of Plating

3.2.1 Plating Overpotential

The electroplating reaction may simply be represented by the reduction reaction shown in Eqn. 3.3.

$$M^{z+} + z^{e-} \leftrightarrow M^0$$
Equation (3.3)

While the reaction above is simple, in reality the electroplating process is seen to occur as a series of several events which includes [3.3]: (i) dissolution of ionic species upon the metal changing it to a cation in the solution, (ii) convective motion of the cation towards the hydrodynamic boundary layer present at the cathode surface, (iii) diffusion of the metal ion through the boundary layer, (iv) adsorption of the charged species at the cathode surface, and (v) the reduction of the adsorbed cation creating the surface deposit. If the reduction reaction releases a by-product, then a final step will include the diffusion of these away from the interphase.

For electrodeposition to commence, an additional potential is needed to overcome the equilibrium reached between the metal ions in solution and the cathode. This additional potential, called polarisation or overpotential, is important in controlling the plating process. The total overpotential can be simply explained as the minimum energy needed to overcome the obstacles to the reduction reaction. These hindrances are actually related to the partial reactions happening during the electrodeposition process and each contributes to the value of total overpotential.

The reactions leading to electroplating each possess a corresponding overpotential. The charge transfer overpotential, $\eta_{ct,}$ refers to the overpotential necessary for the transfer of ionic species across the electrical double layer which exists at the interphase. The diffusion overpotential η_d, corresponds to mass transport processes, including both the movement of the metal ions from the bulk solution towards the interphase as well as the movement of by-products from the interphase to the bulk solution. This process is chiefly governed by diffusion although convective motion may also take place. The chemical reaction overpotential, $\eta_{r,}$ is an activation overpotential which relates to reactions, both homogenous and

heterogeneous, happening prior to electron transfer at the electrode. The presence of electrocatalysts may modify or even eliminate the effect of the reaction overpotential. Finally, the crystallisation overpotential, η_c, involves the deposit's crystallisation reactions occurring at the metal/metal-ion interface and refers to the process by which atoms are added or removed from the crystal lattice.

The above-described overpotentials can then be used to get the total overpotential, η_T:

$$\eta_T = \eta_{ct} + \eta_d + \eta_r + \eta_c \qquad \text{Equation (3.4)}$$

The production of hydrogen during the plating process is associated with another type of overpotential, called the hydrogen overpotential. As potential is increased in the plating process, water begins to breakdown in the cathode's vicinity producing H^+ and OH^- ions. Hydrogen ions may also come from acids placed in the electrolyte. When enough energy is supplied to overcome the hydrogen overpotential, the hydrogen reduction process is activated releasing hydrogen gas according to the reaction:

$$2H^+ + 2e^- \leftrightarrow H_{2(g)} \qquad \text{Equation (3.5)}$$

The hydrogen overpotential varies for each metal system. Hydrogen evolution may accompany a number of plating systems and tends to lower the overall plating efficiency.

3.2.2 Cell Potential and The Nernst Equation

Electrochemists have found that metals differ in their tendency to undergo reduction or oxidisation. This tendency may be measured via the standard electrode

potential, E^o, which essentially refers to the amount of energy needed or released when undergoing either of the half-cell reactions involved in a redox reaction.

While the overall potential of a pair of electrodes may be measured, it is not possible to measure each in isolation. Standard potential is thus measured by using a third electrode called the reference electrode [3.4]. The reference electrode has unchanging potential and would thus allow more accurate measurements to be done. For example, the copper reduction reaction:

$$Cu^{2+} + 2e^- \leftrightarrow Cu^0 \qquad \text{Equation (3.6)}$$

has a cathodic half-cell potential $E^o = 0.34$ V_{SHE}. In this notation, the subscript 'SHE' refers to the type of reference electrode used, which is the standard hydrogen electrode, and this reference bears an assigned potential of zero volts.

The potential difference occurring between a metal and its ion in the solution can be quantified using the Nernst equation [3.5]:

$$E = E^o + \frac{RT}{nF} \ln \frac{a}{a_M} \qquad \text{Equation (3.7)}$$

where E is the potential (volts), E^o is the standard electrode potential referenced to SHE, R is the gas constant, T is the absolute temperature in Kelvin, F is Faraday's constant, n is the metal's valence, a is the activity of the metal ion in solution and a_M is the activity of the solid (normal value is unity for a pure solid). Appropriately, the potential measured at the reduction site is called cathodic potential, while that measured at the oxidation site is referred to as anodic potential.

3.3 Kinetics of electroplating

In electroplating, the speed of metal deposition is seen to be largely dependent on two variables: electrode kinetics and mass transport of charged species to and from the bulk solution. Any one of these may control the overall rate of reaction and becomes the rate-determining step. Electrode kinetics refers to how fast the reactions are occurring at the interphase region, which may include charge transfer movement across the electrical double-layer, and electron exchange at the surface. Mass transport on the other hand may occur via diffusion, convection and migration. In most cases, conditions in the plating apparatus ensure that migration effects are reduced. Also, the effect of convection may be simplified and correlated with the purely diffusion-controlled mechanisms.

The fundamental equation that describes electrochemical kinetics is called the Butler-Volmer equation:

$$i = i_o \left[exp\left(\frac{(1-\alpha)nF\eta}{RT} \right) - exp\left(\frac{-\alpha nF\eta}{RT} \right) \right] \qquad \text{Equation (3.8)}$$

where i is the current density, i_o is the exchange current density, α is the transfer coefficient, F is the Faraday constant, R is the gas constant, and T is the temperature. The activation overpotential, η, refers to the additional voltage that drives the faradaic current and is expressed as:

$$\eta = \phi - \phi_0 \qquad \text{Equation (3.9)}$$

where ϕ is the applied potential, and ϕ_0 is the potential at equilibrium conditions. This equation shows that current density is dependent exponentially on the applied overpotential. However, certain simplifications can be made to the Butler-Volmer

equation at low and high overpotentials. These aspects are discussed in the forthcoming section.

3.3.1 Charge Transfer

Initially, when the potential is changed from equilibrium and the current still low, the plating reaction is dominated by the charge transfer mechanism. This refers to the movement of the charged species across an electrical double layer that exists near the surface. Different models were developed to explain the structure of the electrical double layer. Some of these include the Helmholtz, Gouy-Chapman, Stern, and Bockris-Devanathan-Muller models [3.6]. This layer is created every time a solid is immersed in a fluid medium. The driving force for the positive metal ions to cross this layer is electrostatic attraction as the cathode surface bears a negative charge when potential is applied. Once the ion reaches the surface, reduction proceeds and the crystalline metal deposit is created. At this point, the charge transfer process coupled with the reduction reaction is the rate-determining step in the plating sequence [3.7].

This stage is also governed by the Butler-Volmer relationship for current density, I, and overpotential, η. However, at low values of η, the exponential terms in the Butler-Volmer equation becomes:

$$\frac{\alpha nF\eta}{RT} \ll 1 \qquad\qquad \text{Equation (3.10a)}$$

$$\frac{(1-\alpha)nF\eta}{RT} \ll 1 \qquad\qquad \text{Equation (3.10b)}$$

and under these conditions, these exponentials may be approximated by the power series:

$$e^x = 1 + x + \frac{x^2}{2!} + \frac{x^3}{3!} + \cdots \qquad \text{Equation (3.11)}$$

Thus the first and second exponentials transforms to:

$$exp\left(\frac{(1-\alpha)nF\eta}{RT}\right) \approx 1 + \frac{(1-\alpha)nF\eta}{RT} \qquad \text{Equation (3.12a)}$$

$$exp\left(\frac{\alpha nF\eta}{RT}\right) \approx 1 + \frac{\alpha nF\eta}{RT} \qquad \text{Equation (3.12b)}$$

These equations may be substituted into the Butler-Volmer equation and yields:

$$i = i_o\left(\frac{nF\eta}{RT} - \frac{\alpha nF\eta}{RT} + \frac{\alpha nF\eta}{RT}\right) \qquad \text{Equation (3.13)}$$

Finally:

$$i = i_o\left(\frac{nF\eta}{RT}\right) \qquad \text{Equation (3.14)}$$

Equation 3.14 implies that at low overpotentials (< 0.01 V), the current possesses a linear relationship with the overpotential.

When the overpotential is high, the exponential form of the Butler-Volmer dominates. In the cathodic direction, the anodic partial current (first exponential term) in Eqn. 3.8 decreases and the cathodic partial current dominates:

$$exp\left(-\frac{\alpha nF\eta}{RT}\right) \gg \frac{(1-\alpha)nF\eta}{RT} \qquad \text{Equation (3.15)}$$

Thus, the Butler-Volmer equation may now be expressed as:

$$i = -i_o exp\left(-\frac{\alpha nF\eta}{RT}\right) \qquad \text{Equation (3.16)}$$

A special case of the Butler-Volmer relationship occurs for relatively high values of η. Beginning with Eqn. 3.11 and expressing it in absolute value of i:

$$|i| = i_o \exp\left(-\frac{\alpha nF\eta}{RT}\right)$$
Equation (3.17)

Taking the logarithm of both sides yields:

$$ln|i| = \ln i_o - \frac{\alpha nF\eta}{RT}$$
Equation (3.18)

or:
$$\frac{\alpha nF}{RT}\eta = \ln i_o - ln|i|$$
Equation (3.19a)

$$\eta = \frac{RT}{\alpha nF}\ln i_o - \frac{RT}{\alpha nF}\ln |i|$$
Equation (3.19b)

Taking the logarithm (log) of both sides:

$$\eta = \frac{2.303RT}{\alpha nF}\log i_o - \frac{2.303RT}{\alpha nF}\log|i|$$
Equation (3.20)

Expressing the constants in Eqn. 3.17 into simpler terms yields:

$$\frac{2.303RT}{\alpha nF}\log i_o = a$$
Equation (3.21a)

$$\frac{2.303RT}{\alpha nF} = b$$
Equation (3.21b)

In which case:

$$\eta = a - b\log|i|$$
Equation (3.22)

A similar approach may be used for cases when the anodic potential is large, and this will yield the equation:

$$\eta = a + b\log i$$
Equation (3.23)

Combining the anodic and cathodic process:

$$\eta = a \pm b\log i$$
Equation (3.24)

where *a* and *b* are constants. Equation 3.24 reveals that for large cathodic and anodic values values, η and log*i* have a linear relationship. This equation is called the Tafel equation, which was empirically derived in 1905.

The predicted Butler-Volmer exponential relationship is expected to persist with further increase in potential. However, in reality after reaching a certain level of potential, the curve departs from the expected trajectory and reaches a plateau. This divergence is due to the emergence of mass transport controlled processes. In this case, charge transfer considerations are insufficient, and mass transfer begins to play a major role [3.8].

3.3.2 Mass Transport

Since surface reaction rates are dependent on the supply of metal ions to the electrode, then transport between the reaction site and the bulk is important. Diffusion governs mass transport processes if the concentration gradient is the driving force for material movement [3.9]. The diffusion layer thickness is dependent on the change in the concentration gradient when the electrode surface is reached. The thickness of the diffusion layer, δ_N, is defined by the Nernst diffusion layer model as shown in Fig. 3.2.

The Nernst diffusion model states that there are two zones that exist in the vicinity of the electrode. At a distance closer to the electrode, a stagnant diffusion layer exists in which materials are transported only through diffusion. This is called the Nernst diffusion layer. Beyond this layer, the bulk solution is well stirred and convective forces dominate over other transport processes.

At low applied overpotentials, the concentration of the reacting species at the electrode surface is kept high since reduction reactions are slow. This concentration gradient will increase as the overpotential is increased and more ions at the surface are reduced rapidly. At a certain point, the applied potential is enough to cause instantaneous reduction, and metal ions are reduced as soon as they reached the electrode. Since concentration at the surface is zero, the state of maximum concentration gradient and maximum diffusion is reached.

The plating process is now dependent only on the rate of transport of the reacting species to the electrode. The corresponding current density at which this occurs is called the limiting current density, i_{lim}. In the polarisation curve, the limiting current density manifests as a plateau current where any increase in potential would not increase current density since the maximum rate of reduction and electron exchange has been reached. Also, the transition area called mixed control region explains the point wherein both charge transfer and mass transport controlled processes are present and acts in combination.
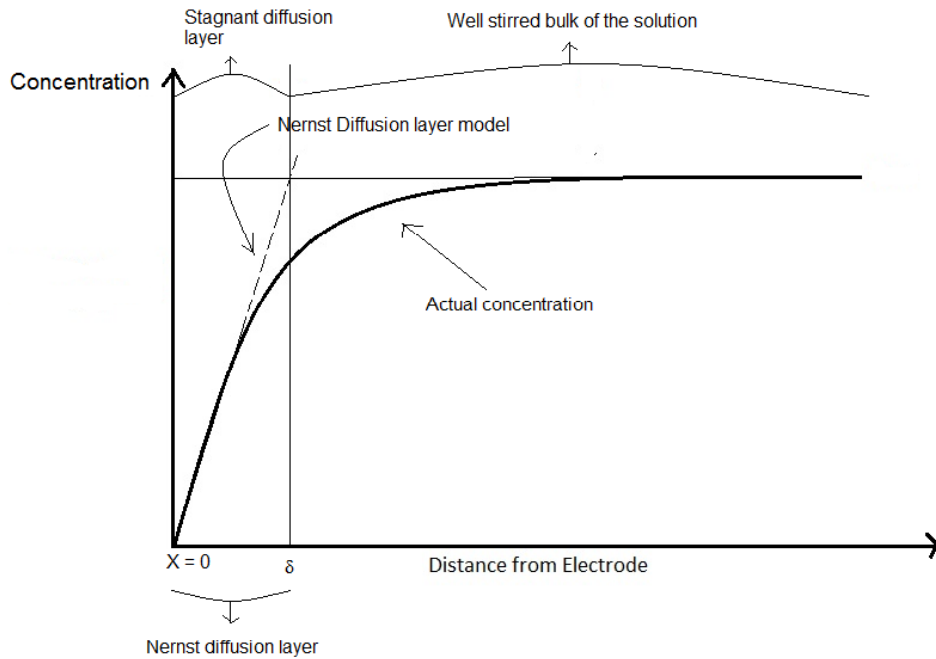
Figure 3.2 A plot of concentration profile at the vicinity of an electrode showing the Nernst diffusion layer (δ_N= Nernst diffusion layer thickness) [Adapted from 3.10].
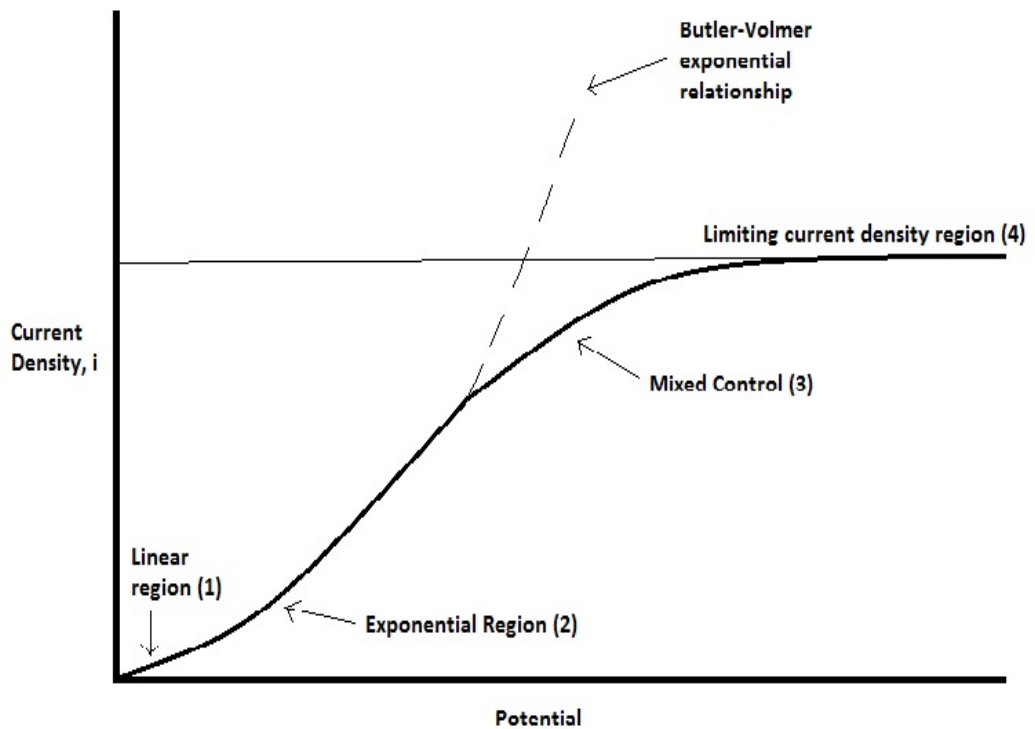
Figure 3.3 Current-Potential regions (1) Linear; (2) Exponential; (3) Mixed Control and (4) Limiting current density [Adapted from 3.11].

At this point, the concept of charge-transfer and mass transport has been explained and a description of the expected polarisation behaviour may now be introduced. The overall polarisation data for metal reduction resembles that of Fig. 3.3. The curve will typically show four regions. These sections are described as linear (1), exponential (2), mixed control (3) and limiting current region (4) [3.10]. Initially there is a linear increase in current density at low overpotentials. The second region shows the case where potential-current relationship is exponenial. The first two sections are essentially governed by the Butler-Volmer relationship and reactions occurring in this region are dominated by non-diffusional reactions; specifically the charge transfer mechanism. The mixed control region explains a transition from charge transfer to mass transfer or diffusion-dominated mechanisms. The last region is characterised by a region of plateau in the curve and signifies that reactions are governed by mass-transfer limitations only. This plateau occurs at the mass-transport limiting current density, i_{lim}. The limiting current density, i_{lim}, may also be theoretically estimated using:

$$i_{lim} = \left(\frac{nFD}{\delta_N}\right) C_b \qquad \text{Equation (3.25)}$$

where D is the diffusion coefficient, C_b is the bulk concentration, δ_N is the Nernst diffusion layer thickness (see Fig. 3.2), n is the number of electrons involved in the reaction and F is Faraday constant. Finally, the subsequent current increase in the curve after the plateau would indicate hydrogen reduction and gas evolution in the cathode.

3.4 Crystallisation at the Plating Interphase

Electrocrystallisation is the process by which the metal, formed after reduction of the ions that crossed the double layer, is incorporated into the crystal lattice [3.12, 3.13]. Metal deposition starts with the formation of an adatom at the surface (see Fig. 3.4). The adatom is unstable on account of a high surface energy when it sits freely on the surface. However, it can become stable by (i) attaching to a kink, an edge or a step, or (ii) generating new nuclei.

The process to attach an atom to a kink or a step is governed by surface diffusion. The ad-atom typically looks for the kink with the shortest distance, σ_{site}, from its location, as shown in Fig. 3.5. The adatom will be able to attach to this kink if it can cover the distance σ_{site} before the end of its residence, t_{res}. This may be expressed by the equation [3.14]:

$$\sigma_{site} \leq \sqrt{D_s * t_{res}}$$
<div align="right">Equation (3.26)</div>

where D_s is the surface diffusivity of the ad-atom. This implies that sufficient time is necessary for ad-atoms to reach favoured sites and crystallise.
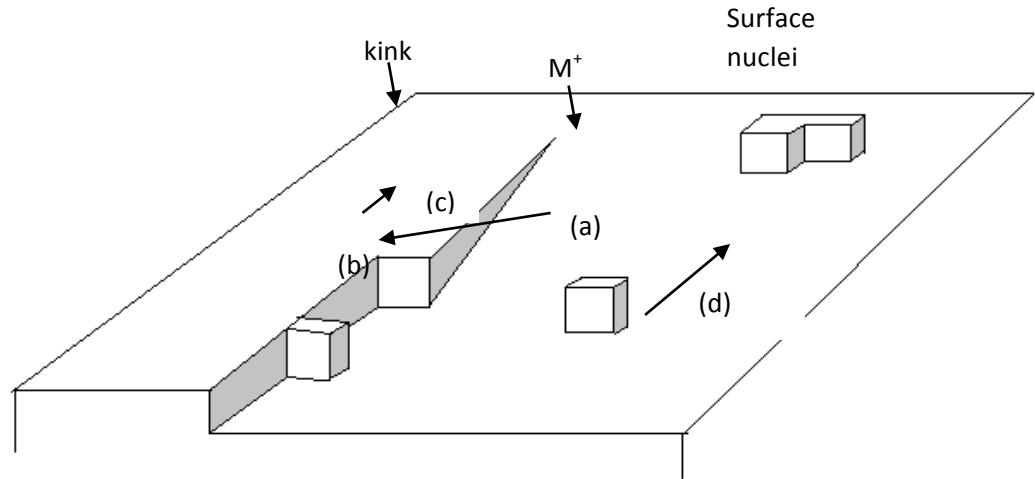
Figure 3.4 Schematic showing the process of electrocrystallisation during electrodeposition. a) Metal ion is reduced and forms an adatom, b) surface diffusion of adatoms towards stable sites and c) incorporation into a kink; d) formation of a nuclei [Adapted from 3.15].
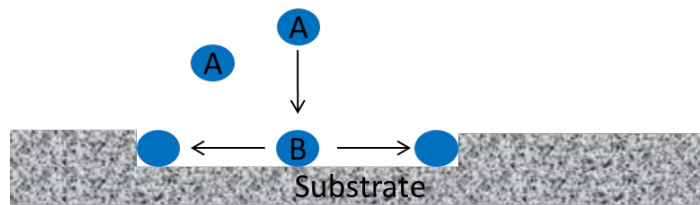
Figure 3.5 Schematic of an adatom moving into a kink or step site within a distance, σ_{site} [Adapted from 3.14].

On the other hand, if kink attachment is difficult, then nuclei formation occurs (see Fig. 3.6). The process to generate new 'seeds' or nuclei is typically difficult. It initiates under conditions of high overpotential because it requires a considerable amount of energy. The free energy change for the nucleation of a seed, ΔG_{nucl}, may be expressed by [3.14]:

$$\Delta G_{nucl} = \Delta G_{bulk} + \Delta G_{surf} \qquad \text{Equation (3.27)}$$

where ΔG_{bulk} is the free energy change due to formation of a new bulk, and ΔG_{surf} is the free energy change due to the creation of a new surface . ΔG_{bulk} is negative while the ΔG_{surf} is positive. A stable nucleus is formed when the ΔG_{nucl} is zero or negative:

$$\Delta G_{nucl} \leq 0 \qquad\qquad \text{Equation (3.28)}$$

ΔG_{nucl} will correspond to a critical radius, which is the minimum size of clustered adatoms necessary to form a stable seed. The number of nuclei formed is influenced by the bath composition as well as by current density [3.13]. Once created, the nuclei begin to grow rapidly at conditions of low overpotential.
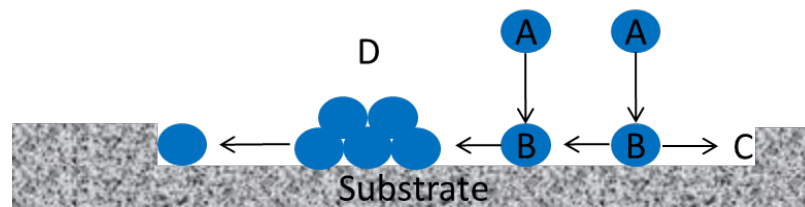
Figure 3.6 Schematic showing how a new deposit nucleus is formed if kink attachment is not favourable [Adapted from 3.14].

Current density can influence both nucleation and growth of the crystalline deposit. The current density has a strong effect on deposit's thickness, quality and morphology. Figure 3.7 shows the effect of different current densities on the morphology of the plated metal. At low current densities, the crystal structure, as well as defects such as screw dislocations, is well formed. As the current density is increased, less ordered structures such as nodules, dendrites and whiskers are formed. At high current densities near the limiting current density, the deposit is often powdery and burnt. Hydrogen evolution is also likely at this level and its

incorporation in the metal may lead to problems. In practice, plating is not done at current densities greater than 0.6 of the limiting current value to ensure the creation of compact deposits [3.16].
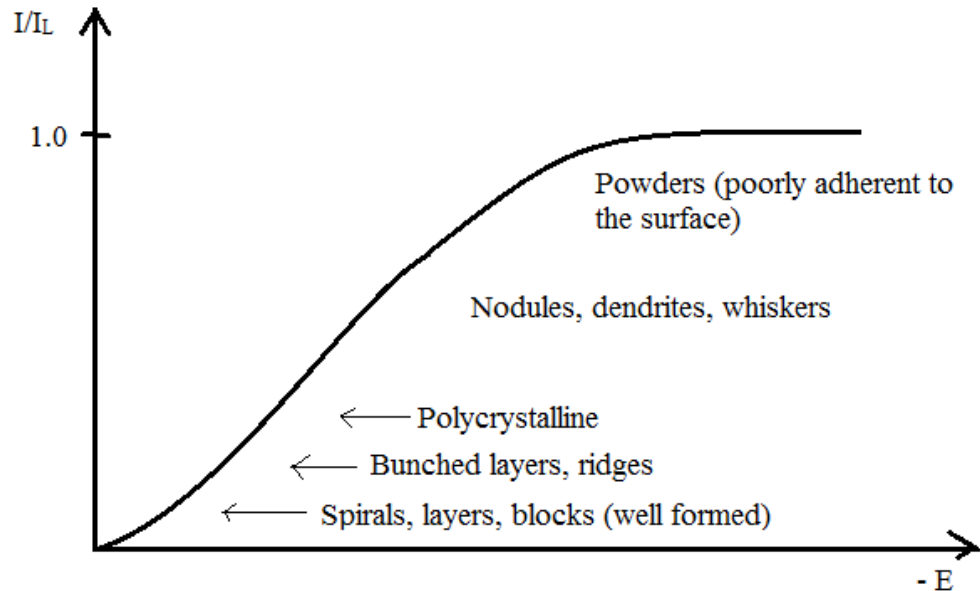
Figure 3.7 Generalised plot of normalised current display (I/I$_L$) as a function of current density [Adapted from 3.16].

3.5 Additives in the Plating Process

3.5.1 Types of Additives and Their Functions

The traditional classification of additives, which is based on its effect on the deposit, broadly lists these chemicals either as levelers, carriers, brighteners and wetting agents [3.17, 3.18, 3.19, 3.20]. The more modern approach, on the other hand, classifies additives according to its effect on deposition kinetics. For example, in copper plating the additives is categorised into two types: suppressors and accelerators. A suppressor generally creates an inhibiting effect and thereby making copper deposition difficult. An accelerator promotes or hastens metal plating [3.21,

3.22]. A common third component is the leveler, though this substance could be classified as a type of suppressor [3.23].

The action of suppressors maybe seen at two levels; i.e. at the bulk or macroscale, and at the microscale. The suppressor called carrier is added to control deposition at the macroscale; while levelers affect deposition at the microscale. The action of carriers is based on increasing the polarisation resistance of the electrode and causing current suppression. This suppression is due to the adsorption of the carrier at the cathode surface. The adsorbed carrier effectively increases the diffusion layer thickness and regulates the attachment of Cu ions onto the cathode. Carriers create deposits with finer grain structure, and improve overall plating distribution Typical carriers used in copper plating are polyalkylene glycol type polymers, with molecular weight of at least 2000g/mole [3.23]. The most popular polyethers used are polyethylene glycol (PEG) (Fig. 3.8a) and polypropylene glycol (PPG) [3.20, 3.24].

(a)   (b)   (c)
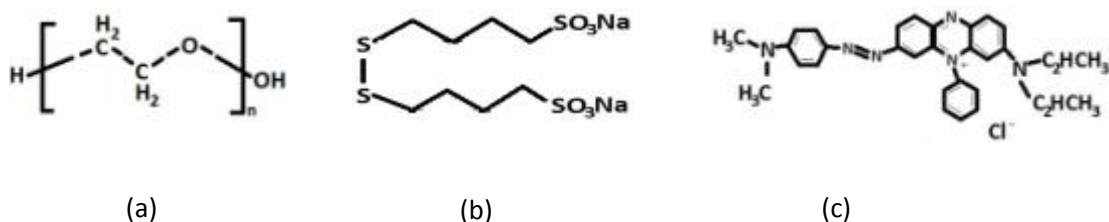
Figure 3.8 Chemical structure of common copper plating electrolyte additives: a) polyethylene glycol (PEG), b) bis(3-sulfopropyl)disulfide (SPS) and c) Janus Green B (JGB).

Accelerators are added to speed up the rate of metal deposition and cause grain refinement. A large class of accelerator called brighteners could create deposits that are shiny or having a high degree of specular reflection. The shiny appearance is

a result of two factors: i) fine grain structure [3.25], and ii) highly oriented texture [3.26]. Weil and Paquin [3.27] argued that these two aforementioned characteristics are not the exclusive conditions for a bright surface. They found that bright deposits should also have no large defects like crevices and deep grain boundaries, nor protrusions that extend (~15μm) considerably from the surface plane. Alternatively, some brighteners are preferentially adsorbed on particular active plating sites (e.g. lattice kinks, steps, and other surface projections) and block crystal growth at these areas.

The typical copper bath accelerator belongs to the mercapto family [3.28, 3.29], such as propane sulfonic acids that are derived with surface-active groups containing pendant sulfur atom. Two of the most commonly used copper brighteners are bis(3-sulfopropyl)disulfide (SPS) (Fig. 3.b) and 3-mercapto-1-propanesulfonate (MPS) [3.30].

Levelers are used to produce deposits that are thicker in the small recesses and thinner on the small protrusions. Similar to the suppressing action of carriers, levelers create a flat deposit on an uneven surface albeit at the microprofile [3.31]. Levelers, together with brighteners, suppress deposition at micropeaks and encourage preferential deposition at the microvalleys [3.19]. Levelers are often considered as a supplementary component that reduces surface roughness of deposits, creating a mirror-like finish in the plated products [3.10]. The typical leveler for acid copper bath is an aromatic polymer, containing nitrogen functionalities, such as thiourea, benzotriazole (BTA) and an azo dye like Janus Green B (JGB) (Fig. 3.8c) [3.32, 3.33].

Leveling can be classified as either geometric or true leveling. Geometric leveling occurs when deposits of lower surface roughness are produced by a uniform current distribution. On the other hand, true leveling is the result of using additives in the bath [3.10, 3.19].

The leveling power of additives may be estimated using several approaches. Watson and Edwards [3.34] offered a simple equation for the leveling power, *LP* :

$$LP = \frac{i_{rec} - i_{pro}}{i} \qquad \text{Equation (3.29)}$$

where i_{rec}, i_{pro} and i (see Fig. 3.9) refer to the current densities at recesses, at protrusions and average current density, respectively. The above equation takes into account the inhibition, as reflected by current densities, occurring in recesses and protrusions. It is expected that current density and plating rate is high at protrusions when the electrolyte is additive-free. When additives are present in the electrolyte, the additives settle at protrusions causing a concentration-dependent reduction in current density. However, this equation is only applicable when only a single type of additive controls leveling, which is not always the case in practical plating. Lainier [3.35] proposed a formula that is more appropriate for multi-additive systems and is as follows:

$$LP = \frac{h_1 - h_2}{h_3} \qquad \text{Equation (3.30)}$$

where h_1 , h_2 and h_3 are the deposit thicknesses at the recess, on the even surface and at the center of the recess.
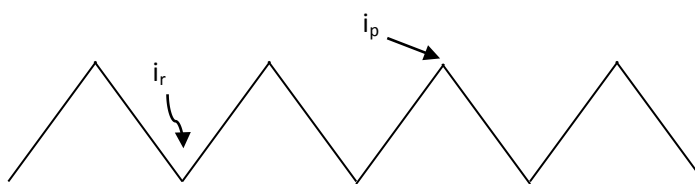
Figure 3.9 Location of i_r and i_p in relation to the features at the substrate's surface.

Chloride ions (Cl⁻) are found to be essential components of the copper plating electrolyte. Small amounts of Cl⁻ can act as an accelerator, catalysing the rate-determining reduction reaction of cupric ions [3.20, 3.24, 3.36]. However, beyond a critical amount, an excess of chloride ions suppresses copper deposition by forming a coating of copper chloride at the surface [3.37]. More importantly, Cl⁻ ions are added to enhance the effect of other additives like PEG [3.38] and SPS [3.39]. The use of multi-component additive systems is currently the preferred practice as additives are commonly observed to show poor results when used alone yet shows remarkable effects when in synergistic combination with other additives [3.40].

3.5.2 Fundamental Actions of Additives in the Plating Electrolyte

Various mechanisms are proposed to explain the action of additives in the plating process [3.17, 3.19, 3.38, 3.41, 3.42, 3.43]. From the point of view of the rate determining process, these mechanisms can be simply classified as either diffusion-controlled or non-diffusional mechanism [3.17]. While diffusion-controlled mechanisms often dominate, it is believed that a mixture of the two mechanisms (diffusion and adsorption) commonly occurs.

Non-diffusional mechanisms affect processes that are not dependent on mass transport of materials, such as the charge transfer during metal ion reduction or the activation-dependent reactions occurring at the interphase. Examples of non-diffusional mechanisms include: (i) electrosorption of additives on the electrode surface, (ii) formation of complexes, (iii) ion-pairing, (iv) interfacial tension change and (v) chemical film formation. These mechanisms are present in different types of plating systems. For Cu plating, the most commonly encountered are the electrosorption and the complex formation mechanisms.

Electrosorption of additives is the most common non-diffusional mechanism. In this concept, additives are viewed as a foreign substance at the cathode's surface that either interferes or facilitates appropriate reactions [3.18, 3.44]. Electrosorption is structure sensitive and requires certain compatibility, in terms of size, shape and chemical structure, between the metal and additive.

One of the most important consequences of electrosorption is the modification of the free energy required for the charge transfer process. This results in the commonly observed changes of the current-potential relationship in the additive-containing electrolyte [3.45]. By covering areas of the electrode, the adsorbed additives can also enhance overvoltages, create kinetic heterogeneity in electrodeposition, shorten the mean free path between adatoms, and block crystal growth areas [3.46]. Most of the actions of additives are associated with its interaction with the electrode interface. Levelers are strongly adsorbed on the surface of high current density regions on the electrode such as protrusions. Consequently, these areas will experience plating inhibition while other regions undergo deposition. Suppressors have a similar mechanism with levelers. Suppressors are adsorbed on

the surface and form a monolayer film. For example, PEG forms a glycol film at the interface [3.47] that inhibits deposition and suppresses the plating rate. Brighteners are known to have several actions on the deposit: i) diffusion-controlled leveling, ii) grain refining, and iii) randomisation of crystal growth [3.48]. Regardless of the mechanism, these actions appear to be dependent either on additive surface coverage or high rates of adsorption and desorption process [3.48].

Diffusion-controlled mechanisms refer to the rate-determining processes as being diffusion dependent; e.g. the diffusion of the additives or the electroactive species towards the electrode, or even the surface diffusion of adsorbed atoms [3.17]. The possibility that cathode kinetics is governed by mass transport of additive from the bulk towards the electrode is made logical by the fact that copper ion concentration is about 10^3 to 10^5 times more than the additive. The scarcity of additives in the electrolyte requires that it be mobile enough to affect reactions near the electrode. Agitation or stirring improves convective diffusion of additives, and thus affects the polarisation behaviour of the cathode. Therefore, stirring can play a major role in unmasking diffusion-controlled mechanisms [3.48].

The transport of metal ions in solution can also be influenced by additives. Additives may also affect diffusion-dependent processes during plating. Roy and Pintauro [3.49] studied the effect of PEG, Cl$^-$ and Copper Gleam on mass transfer in a copper electrolyte. They observed that polymer adsorption on the surface not only influenced plating kinetics, but changed the hydrodynamic boundary layer due to slip of the adsorbed polymers at the electrode surface. Bonou *et al.* [3.47] observed that PEG can form a complex with Cu^{2+} while in solution which changed the transport of the ionic species.

The synergistic or antagonistic effect of additives is sometimes explained by the formation of complex molecules in the electrolyte. These complexes, either formed with the metallic ions or with other species, offer alternative kinetic routes for metal ion discharge [3.18]. An example is seen in an effect referred to as induced absorption. In this process, the additive complex attracts an abundance of metal ions in the electrode vicinity and increases deposit nucleation. Another important effect of complex formation is called ion bridging. In ion bridging, the complex facilitates electron transfer to the metal ions and effectively improves the ion reduction rates. On the contrary, some complexes are known to inhibit deposition; e.g. benzotriazole in copper [3.50]. In this case, the complex increases the required energy and overpotential for nucleation. Such is observed when PEG is used together with Cl^- [3.20, 3.51] and forms the strongly inhibiting complex, PEG-Cu^+-Cl. Additionally, Tan *et al.* [3.52] explained that the increase in accelerating effect of SPS when used with chloride ions is due to the Cl^--sulfonate complex.

3.5.3. Influence of Additives on Electrochemical Parameters

3.5.3.1 Cathodic Polarisation

A large number of copper additives (e.g. PEG, JGB, thiourea and Cl^-) are inhibitors and these substances polarise the cathode. Figure 3.10 shows the effect of cathode polarisation on the i-V curve due to additives. A polarised cathode will display lower current density at a given applied potential [3.8]. Consequently, the obtained polarisation curve is shifted to lower current densities or higher overpotentials when compared to the plot of an additive-free electrolyte.

On the other hand, an accelerator depolarises the cathode and induces a shift in the polarisation curve to lower overpotentials. Interestingly, some additives like

SPS will polarise the cathode when used alone in the plating electrolyte [3.52]. However, SPS shows its depolarising characteristics when present with other additives such as Cl⁻ [3.52].
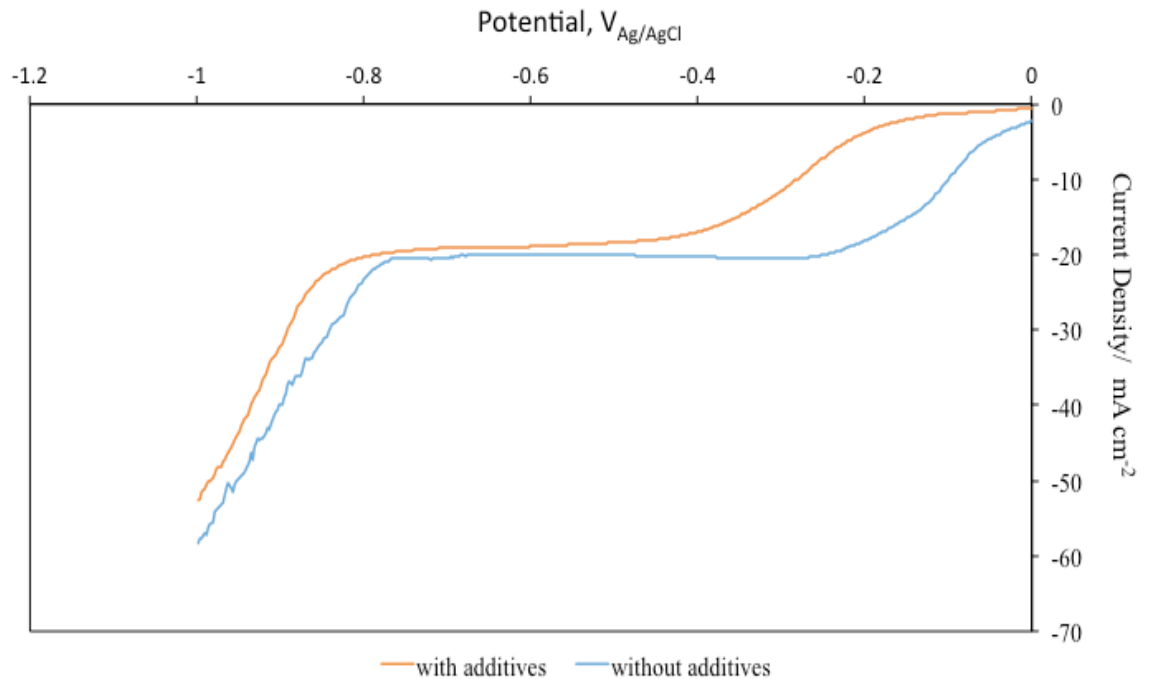
Figure 3.10 Polarisation curve of a copper sulfate electrolyte with and without Copper gleam additive (unpublished data from the author's laboratory).

It is believed that the increase in polarisation may be traced to the influence of additives on the different types of overpotentials related to plating; namely, charge transfer (η_{ct}), diffusion (η_d), chemical reaction (η_r) and crystallisation (η_c) overpotentials [3.15]. For example, η_d is affected when the additive enters the diffusion layer, typically as a colloid, and affects ion transport through this region. Another example is seen where η_c is affected when additives hinder surface diffusion of adatoms in the nucleating crystal.

The proposed mechanism by which additives influence polarisation can be via electrosorption at the electrode surface [3.46]. The adsorbed additives increases overvoltages by decreasing the available area for reduction and causing changes in the effective current density.

Since additive action in the plating electrolyte is affected by the quantity of electrosorbed species on the cathode surface, it is important to acquire a quantitative measure of the amount of additives adsorbed. Polarisation curves can be used to give an estimate of the amount of adsorbed additive. Additives cause a shift in the polarisation curve, and this shift may be used to calculate the additive surface coverage. At a specified potential, the fractional surface area, Γ covered by the additive may be calculated using the equation [3.49]:

$$\Gamma = 1 - \frac{i_{add}}{i_{addfree}}$$
<div align="right">Equation (3.31)</div>

where i_{add} and $i_{addfree}$ refer to the current densities in the presence and absence of additives, respectively. Roy and Pintauro [3.49] successfully used this equation to predict surface coverage of copper gleam during plating, and study convective mass transfer behaviour of the additive in copper electrolytes.

An alternative approach to measuring additive electrosorption is to look at the surface coverage of metal ions on the electrode. The presence of additives lowers the amount of metal ions adsorbed at the plating interface. Therefore by measuring the change in the amount of total metal ions adsorbed after additive use, then one can infer the amount of additives adsorbed. Brett and Brett [3.6] derived the total amount of metal ion at the electrode's surface using a slow potential scan. The single layer metal ion surface coverage, Γ (moles/cm^2), is taken from the equation [3.6]:

$$\Gamma = \frac{Q}{nFA} \qquad\qquad \text{Equation (3.32)}$$

where Q refers to the charge, n is the number of electrons involved in reduction, F is the Faraday's constant and A is the area of the electrode. The charge, Q, is derived from the area under a voltammogram (Amp/V) curve divided by the potential scan rate (V/s). The curve used is typically from a cyclic voltammetry test. It can be deduced from the equation that, since Q is proportional to the surface coverage, a higher area under the polarisation curve would imply that larger number of metal ions have been discharged at the surface. In the presence of additives, the value of Q is lower because metal ions at the surface are blocked.

3.5.3.2 Electrical Double layer

Additives have also been observed to enter and alter the structure of the electrical double layer existing at the electrode-liquid interface. One consequence of this alteration is the decrease in the electrical capacitance of the layer. The capacitance decreases in proportion to the amount of adsorbed molecules until it reaches a saturation point. This change in capacitance is distinct and may even be used to measure the electrode coverage of adsorbed additives, θ_s, as follows [3.53]:

$$\theta_s = \frac{C_o - C}{C_o - C_{sat}} \qquad\qquad \text{Equation (3.33)}$$

where C_o is the capacitance at coverage zero, C is the capacitance at additive coverage θ_s, and C_{sat} is the capacitance at saturation.

Although not often observed, there are some reported cases where the electrical capacitance is increased by additives. Examples include triethyl-benzyl-ammonium chloride [3.54] or Cl⁻ [3.55] when used in Cu plating. This is believed to

be due to an increase in the active areas on the cathode surface after additive adsorption.

3.5.3.3 Plating Kinetics

Additives may affect the mass transport characteristics of metal ions in solution. This occurs when the additive forms a complex with the ionic species and changes the mobility of the ion [3.47]. Plating rate is also influenced in cases where the rate determining is the diffusion of the additives towards the cathode; as seen during the superfilling of vias [3.30, 3.56].

The charge transfer step can also be changed after additive electrosorption. This may result to (i) changes in reaction pathway and (ii) alterations in the values of kinetic parameters such as the exchange current density (i_o) and transfer coefficient (α). Thiourea in acidified $CuSO_4$ caused a reduction in the i_o that resulted in plating inhibition [3.57]. They proposed that is a result of the formation of different complex molecules at the electrode surface. On the other hand, thirourea [3.57] and Cl^- [3.55] can reduce α, indicating that the simple electron transfer process that occurs in additive-free electrolytes is now aided by an intermediate compound existing at the interface.

3.5.3.4 Electrocrystallisation

Additives can affect electrocrystallisation by influencing the nucleation and growth processes in several ways [3.58]. The most basic way is additives blocking the active areas on the electrode surface where metal crystallisation could occur. This action hinders nucleation and inhibits plating. On the other hand, some additives can reduce the free energy of nucleation thus decreasing the critical radius necessary for

the formation of a stable seed. Alternatively, additives can reduce the surface mobility of adatoms resulting to lesser growth and more frequent nuclei formation.

Additives can also alter the direction of growth of crystals. For example, benzothiazolium derivatives suppress the perpendicular growth while encouraging the lateral growth of electrodeposited copper [3.59]. This 'birth-and-spread' mechanism results to a level copper deposit of uniform thickness. Some additives can induce deposits to possess a 'texture' or preferred crystallographic orientation. Triethyl-benzyl-ammonium chloride induces a strong [110] texture in copper deposits [3.60], while Cl^- influences simulstaneously the surface quality, crystallographic orientations and morphology of the deposited copper [3.61].

3.5.4 Understanding Additive Action via Polarisation Studies

Electroanalytical techniques such as polarography, voltammetry and impedance measurements are often employed to reveal information regarding additive effects [3.62, 3.63]. A voltammetry or polarisation measurement is the commonly employed technique since it offers high sensitivity to a large concentration range of both organic and inorganic species in an electrolyte. Polarisation data, consisting of current-potential (i-V) plots are obtained using either potentiodynamic or galvanodynamic. Analyses of these plots allow the ability to detect both kinetic and mechanistic parameters of plating [3.62]. In potentiodynamic mode, the potential between the reference and the working electrodes is controlled, while current between the counter and working electrode is being measured. In contrast, galvanodynamic mode varies the applied current between the counter and working electrodes, while the potential between the working and reference electrodes

is measured. The mode of current or potential application may also be varied; two of the most common are the single linear sweep and cyclic linear sweep modes [3.63].

The potentiodynamic and galvanodynamic polarisation tests often give very similar results [3.64]. However, galvanodynamic tests require that the polarisation behaviour of the metal is known precisely so that the correct range of current may be applied and maximum polarisation occurs. This makes the galvanodynamic test more cumbersome, and hence less popular than the potentiodynamic test. Potentiodynamic tests are used in the study of plating mechanisms; including investigations that aim to reveal the action of additives in the plating bath [3.17]. This test is also used in corrosion studies to create Tafel curves, a semi-log plot of potential vs. current, and obtain information such as corrosion potential and corrosion current density. Other information that may be taken from polarisation results include: (i) a quantitative measure of the limiting current and the thickness of the boundary layer; (ii) an estimate metal ion surface coverage; and (iii) an understanding of the influence of mechanical agitation of the plating solution.

The limiting current, $i_{\lim}$, is essentially the highest current density at which practical plating may be done, and this parameter bears special significance in the plating operation. Plating at or near $i_{\lim}$ can be desirable since this yields high plating rates. However, this practice could also create rough, dendritic, burnt or powdery deposits [3.65]. Some studies proposed that the ratio of the operating current to $i_{\lim}$, and not the absolute value of the operating current alone, is responsible for the coarse deposits [3.66]. Any ratio beyond 0.6 would tend to yield dendritic deposits. This means that plating operators need to look for the right current density that yields good plating rates while avoiding dendritic or coarse deposits.

Some studies have attempted to use polarisation measurements to quantify the amount of additives present in the plating electrolyte. For example, Bindra *et al*. [3.67] used the rotating disk electrode to determine the amount of PEG and PPG in copper sulfate bath. Different amounts of additives were mixed into the bath and subsequent potential measurements between the reference and working electrodes were taken at each level. A plot of potential against additive concentration is then derived, and this curve was used as the standard for determining unknown additive amounts.

3.6 Fundamentals of Pulse Current Plating

3.6.1 Definition, Advantages and Application of Pulse Plating

Direct current (DC) plating has been the traditional way of conducting electroplating of numerous metals. In this process, a constant direct current (DC), which is defined as unidirectional flow of electric charge, is applied on the cathode for electrodeposition. Pulse current (PC) plating is another method by which electroplating may be conducted. A pulsed current is defined as interrupted direct current in which the current is continuously fluctuated. This train of pulses may be described by a current waveform, and can be programmed to a desired variation (e.g. unipolar, bipolar or pulse reverse, pulse on pulse, etc.). By intermittently changing the applied current, the dynamics of electrodeposition is altered. For example, pulse plating uses high currents applied over a short interval, which induces high nucleation rates. These changes in plating mechanisms often results to positive changes in deposit morphology, deposit properties and process attributes A detailed

discussion of the effect of pulsed current on the different plating mechanisms is presented in a succeeding section.

Table 3.1 Advantages of pulse plating over direct plating.

Properties / Process	Effect of pulse plating
Deposit morphology	• Finer grain structure • Lower porosity and roughness • Denser deposit
Mechanical and electrical properties	• Higher tensile strength • Higher elongation • Higher conductivity
Plating physical attributes	• Better deposit adhesion • Higher throwing power • Higher plating rates • Improved thickness distribution • Ability to fill sub-micron trenches • Better control of alloy composition/ ability to plate complex alloy layers • Reduced deposit stress • Enhanced corrosion protection • Reduced hydrogen embrittlement
Process	• Less post treatment step • More flexibility of metal content in bath • Reduction or complete elimination of additives

The advantages in using pulse plating are numerous, and these are listed in Table 3.1 [3.14, 3.65, 3.68, 3.69]. The most important practical advantage of pulse plating is its ability to improve the quality of the deposit. Some of the results of pulse deposition are finer grains, porosity reduction, higher deposition rate, low inclusion level and improvements in mechanical and physical properties [3.14].

An apparent disadvantage of pulse plating is that it requires an advanced and therefore more expensive rectifier than that needed for DC plating. The highly sophisticated design of the pulse rectifier makes it costly to manufacture.

One advantage of pulse plating is its flexibility in terms of the possible combinations of pulse parameters current densities, pause time and frequencies [3,14, 3.70, 3.71]. However, these numerous combinations also pose a disadvantage in finding the optimum plating settings. The determination of these optimum settings requires a lot of planning and feasibility testing, and such would entail additional time and cost.

Numerous applications of pulse plating for electronics applications have been cited and include [3.14, 3.68, 3.69]: (i) fabrication of connectors and switch contacts; (ii) wire bond pads in leadframes; (iii) making circuit paths for high-density circuitry; (iv) pulse etching of metal patterns; and (v) through-hole plating in PCBs.

One application where pulse plating finds considerable acceptance is in copper plating of PCBs, specifically in high density interconnection manufacture where plating of though-holes and vias is critical [3.14, 3.72]. The use of traditional DC plating created issues of non-uniform copper plating called 'dog-boning' (Fig. 3.11).
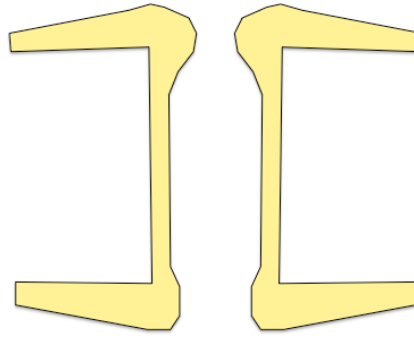
Figure 3.11 The 'dog-boning' phenomenon in through-hole plating.

A thicker deposit is formed due to a higher current density occurring at the edges of through-holes. Pulse reverse plating was successful in addressing the 'dog-boning' issue and significantly improved the surface-to-hole throwing power. During the reverse pulse, excess copper at the edges dissolves and renders the overall deposit thickness more uniform [3.73]. Pulse plating also offers the ability to plate at a higher current density. This means that plating may be done at a higher deposition rate leading to higher product throughput. Finally, the high current density used in pulse plating creates a fine-grained deposit structure, which improves the strength and the reliability of plating components.

3.6.2 Pulse Plating Parameters

Pulse plating parameters plays a significant role on the resulting properties of the plated metal. Better understanding of pulse plating parameter effects on the deposit properties is essential to obtain the desired results. Compared to DC plating, pulse plating has several variables that may be controlled such as: i) polarity, (ii) frequency, (iii) duty cycle, and (iv) peak current density [3.14]. The succeeding section identifies these important pulse plating parameters.

3.6.2.1 Polarity

The way to understand the pulse plating parameters is by understanding a pulse waveform. Pulse waveforms may be two types: (i) unipolar and (ii) bipolar. Figure 3.12a shows a typical unipolar pulse waveform, with the included terms that names some features of the waveform. In a unipolar waveform, all pulses are set in one direction only, either anodic or cathodic depending on the intended application. Pulse plating is typically unipolar in the cathodic direction. A bipolar waveform mixes anodic and cathodic pulses, as shown in Fig. 3.12b. The process called pulse reverse plating uses a bipolar waveform.

Aside from the above mentioned waveforms, there are many other variations including [3.68]: (i) pulse-on-pulse, (ii) duplex pulse, (iii) periodic reverse pulse superimposed on high frequency pulse, (iv) square-wave pulse and (v) sine-wave pulse. The number of variables that need to be controlled increases with the complexity of the waveform, and this makes it more difficult to understand the influence of waveform on deposit characteristics.
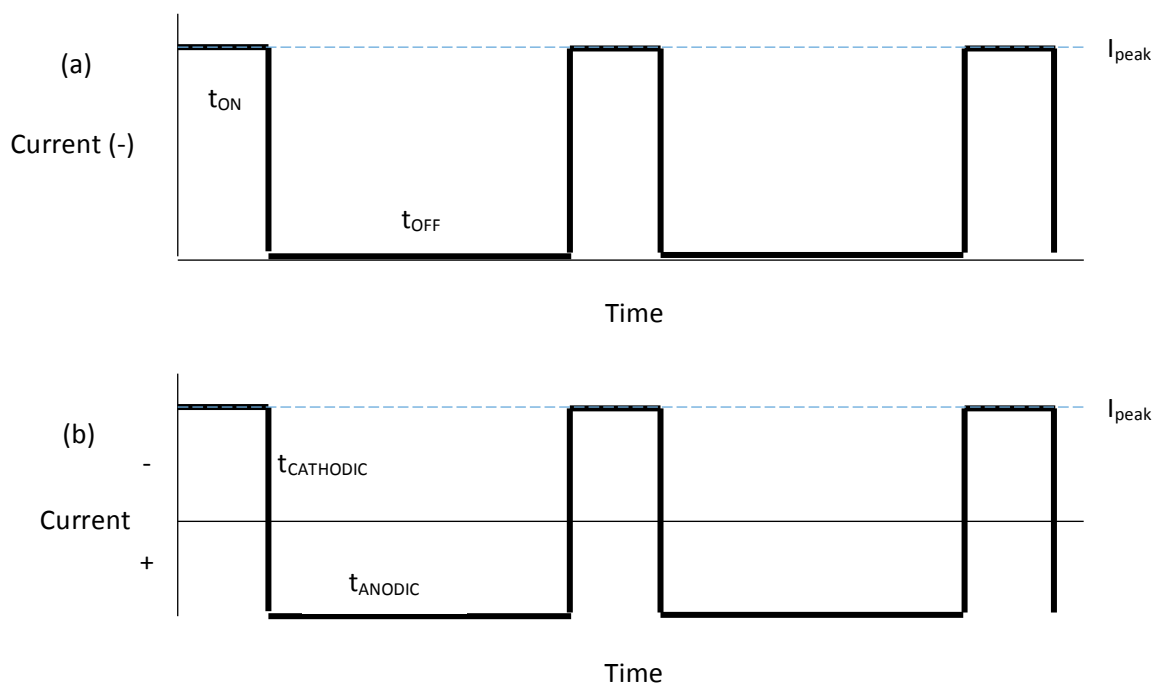
Figure 3.12 Plot of (a) unipolar pulse and (b) bipolar pulse waveform showing t_{ON}, t_{OFF} and I_{peak}.

3.6.2.2 Frequency

The term on time, t_{ON}, refers to the time the current is applied, while off time, t_{OFF}, is the duration when the current is turned off. The period refers to the duration of one pulse cycle and is expressed as the sum of t_{ON} and t_{OFF}.

A common way to express period is by using the term frequency. Frequency describes the number of pulse cycles per second, expressed in units of hertz (Hz). For example, a 1000 Hz operation means a pulse period of 1 millisecond. The frequency can range from 200 to 10,000 Hz in a typical pulse plating operation.

3.6.2.3 Duty cycle

Another important pulse parameter is the duty cycle, θ. Duty cycle is the ratio of the pulse width, t_{ON}, over the pulse period. Duty cycle may be expressed by the equation:

$$\theta = \frac{t_{\mathrm{ON}}}{t_{\mathrm{ON}} + t_{\mathrm{OFF}}} \qquad\qquad \text{Equation (3.34)}$$

In practice, pulse plating usually involves a duty cycle of 5% or greater at a t_{ON} from micro- to milliseconds.

3.6.2.4 Peak current density

Peak current, I_{peak}, refers to the highest applied current in a cycle (Fig. 3.12). One of the advantages of pulse plating is the ability to apply a high current density, which benefits deposit structure and plating rates. However, if these high levels of current densities are used in DC mode, deposits will come out burnt and dendritic. However, because the current is applied intermittently the benefits of using high current are retained.

The average current density (i_{AVE}), in pulse plating is defined as:

$$i_{\mathrm{AVE}} = i_{\mathrm{peak}} \ x \ \theta \qquad\qquad \text{Equation (3.35)}$$

It is reasonable to assume that PC plating will deposit metal at the same rate as DC plating when the average current density of the two operations is similar.

It is also worth mentioning that when the applied operating current in DC plating is near the mass transport limiting current, a coarse and dendritic deposit is created. The applied i_{peak} in PC plating typically exceeds the DC limiting current. This level of current is indeed enough to create such coarse microstructures. However, a completely opposite structure is obtained when this large current is applied only at very short intervals. The excess current induces rapid nuclei formation, but is prevented from promoting crystal growth. The resulting microstructure is therefore fine-grained and compact [3.14].

3.6.3 The Action of Pulsed Current in the Plating Process

The application of a pulsed current affects different aspects of the plating process. The interphase boundary between the electrode surface and adjacent electrolyte resembles a simple parallel plate capacitor and is called the electrical double layer. When the current is turned on, a majority of the current applied is used to charge the double layer. At this point, deposition does not occur until after maximum capacitance is reached when the current is used for the faradaic processes and electrocrystallisation [3.14]. This means that the current should be applied long enough to allow charging of the layer (~0.1 to 1ms) as well as permit deposition. Conversely, when the current is switched off, the double layer is discharged. The charging and discharging process have to be repeated for each and every individual pulse. However, since discharging also needs a finite time to complete, then the off-time should be long enough to allow full discharge of the layer (see Fig. 3.13). These conditions would help define the range of operating values for t_{ON} and t_{OFF}.

Another process affected by pulsed current is mass transport in the plating system. When the current is applied at t_{ON}, metal ions present in the vicinity of the electrode are reduced. This creates a concentration depletion layer adjacent to the electrode. As the ions near the electrode surface are reduced, they have to be replenished by transport from the bulk electrolyte. This process occurs during the off-time, and requires that the t_{OFF} is long enough to ensure concentration recovery. The change in concentration gradient typically occurs over the total pulse time, and

this requires that high mass transport rates should be maintained in pulse plating systems [3.14].

Pulse plating also results in the formation of two distinct diffusion layers in the vicinity of the interphase: (i) pulsating layer, δ_p and; (ii) stationary diffusion layer, δ_s as shown in Fig. 3.13 [3.14]. The thickness of the depletion layer is influenced by I_{peak}, though the maximum thickness will be limited by the diffusion coefficient of the metal ions in the electrolyte. A distinct advantage with pulse plating is that mass transport in the system can now be influenced by pulse parameters, aside from the usual control of stirring rate.
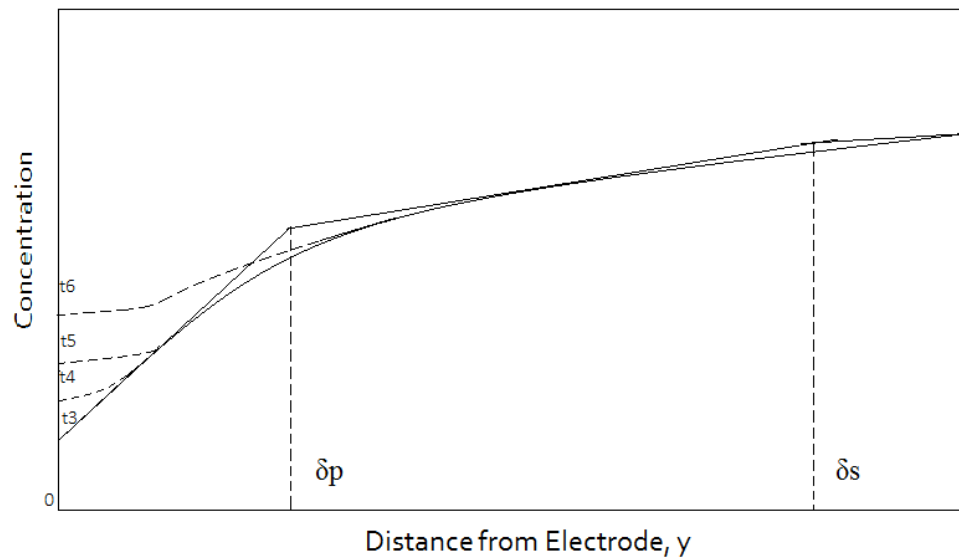
Figure 3.13 Two layers from pulse plating: pulsating layer, δ_p and stationary diffusion layer, δ_s [Adapted from 3.14].

A third process that a pulsed current can influence is electrocrystallisation. Electrocrystallisation is when adatoms or adions are incorporated in the crystal lattice by either building up of old crystals or creation of new crystals [3.13]. During

the on-time, nucleation and growth happens and will temporarily stop during the off-time until the current is on again to form new nuclei [3.74]. The formation of new crystals can be enhanced when there is high overpotential, high amount of adatoms and low surface diffusion rates. The application of short pulses of high current density leads to high overpotential and favours nucleation. Consequently, finer grains are formed in the deposit. Also, finer grains are produced due to the increase in nucleation sites available in each and every pulse [3.75].

3.6.4 Determination of Operating Peak Current Density in PC Plating

One of the most important advantages of pulse plating is its flexibility in terms of the possible combinations of pulse parameters that one can employ to gain a particular effect on the deposit [3,14, 3.70, 3.71]. However, these numerous combinations would also pose a disadvantage in trying to look for the optimum operation settings. Some guidelines on choosing the appropriate operating t_{ON} and t_{OFF} were already mentioned in the previous section. This section describes the steps involved when determining a suitable operating peak current density for a typical copper plating system.

The calculation of the operating peak current, I_p, starts with the determination of the pulse limiting current, $i_{p,lim}$. Roy and Landolt [3.13], using equations proposed by Cheh [3.76, 3.77] and Chin [3.78], showed that the ratio of $I_{p,lim}$ to the limiting current under DC, $I_{d,lim}$, can be expressed by:

$$\frac{I_{p,lim}}{I_{d,lim}} = \frac{1+2\left(\frac{I_{pa}}{I_{d,lim}}\right)T^* \cdot \sum_{m=1}^{\infty} \frac{\exp(\lambda_m(1-\theta))-1}{\lambda_m[\exp(\lambda_m)-1]}}{1-2\,T^* \cdot \sum_{m=1}^{\infty}[\exp(\lambda_m)-1]} \qquad \text{Equation (3.36)}$$

where T^* is the dimensionless pulse time given by $T^* = Dt_T/\delta^2_s$ (D is diffusivity, t_T is total pulse time, and δ_s is the thickness of the outer stagnant layer); and the summation term $\lambda_m = \Pi^2 T^*(m-1/2)^2$ (m is the summation variable).

For unipolar pulses, I_{pa} is set to 0, and Eqn. 3.36 transforms to:

$$\frac{I_{p,lim}}{I_{d,lim}} = \frac{1}{1-2\,T^* \cdot \sum_{m=1}^{\infty} [\exp(\lambda_m)-1]} \qquad \text{Equation (3.37)}$$

Once the current ratio is obtained, a corresponding $I_{d,lim}$ may be used to determine $I_{p,lim}$. The $I_{d,lim}$ may be theoretically determined using Eqn. 3.25, or experimentally measured by way of polarisation experiments on the corresponding electrolyte in DC mode. Also, the computed $I_{p,lim}$ may now be converted to $i_{p,lim}$ by using the equation:

$$i_{p,lim} = \frac{I_{p,lim}}{A} \qquad \text{Equation (3.38)}$$

where A is the deposit area.

The $i_{p,lim}$ may now be used to calculate the i_{peak}. Two conditions needs to be met when calculating the peak current density, i_{peak} [3.14]:

Condition I: $\qquad\qquad\qquad\qquad i_{ave} < i_{p,lim} \qquad\qquad\qquad$ Equation (3.39)

where i_{ave} is the average current density given in Eqn. 3.35.

Condition II: $\qquad\qquad\qquad\qquad i_{peak} < i_{p,lim} \qquad\qquad\qquad$ Equation (3.40)

These conditions set on $i_{p,lim}$ are schematically represented in Fig. 3.15. Condition I and II ensure that mass transport conditions are favourable during plating

to prevent the formation of dendritic deposits [3.76, 3.77]. A third criterion may also be considered, which states:

$$i_{d, lim} < i_{peak} < i_{p, lim} \qquad\qquad \text{Equation (3.41)}$$
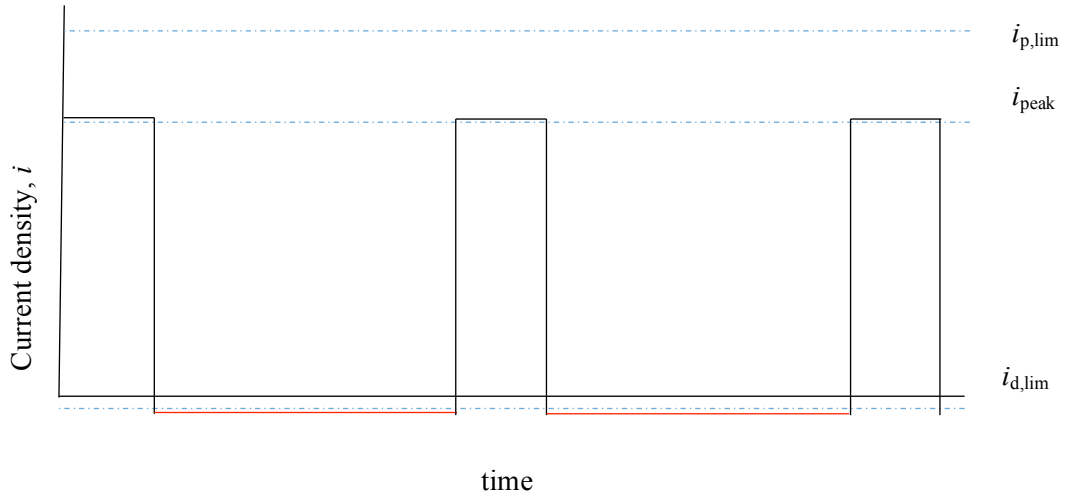
Figure 3.14 Schematic representation of the operating i_{peak} in relation to the $i_{p,lim}$ and $i_{d,lim}$.

While the first two conditions set the maximum value of i_{peak}, the third condition sets the minimum value. It is preferable to use high peak currents, often close to the $i_{p,lim}$ value, to i) increase plating rates and ii) encourage high nucleation that creates a fine grain structure.

In this chapter, a review of the thermodynamics and kinetics of the electroplating process was presented. The fundamentals of additive action were discussed, together with a brief overview of the basics of the pulse plating process.

References

3.1   Davies CW (1967) Electrochemistry. Newness London

3.2   Eyring H (1970) Electrochemistry. Academic Press New York

3.3   Dini D, Snyder D (2010) Modern Electroplating: 5th Edition" Edited by Mordechay Schlesinger, Milan Paunovic, John Wiley and Sons NY

3.4   Bard AJ, Faulkner LR (1980) Electrochemical Methods: Fundamentals and Applications. 2nd ed New York, Wiley

3.5   Vetter K (1967) Electrochemical Kinetics: Theoretical and Experimental Aspects. Academic Press Inc (London) Ltd

3.6   Brett C, Brett A (1994) Electrochemistry: Principles, Methods, and Applications. Oxford University Press New York; 95-186

3.7   Bockris J O'M (1954) Modern aspects of Electrochemistry 1st ed Butterworths London; 180-276

3.8   Koryta J, Dvorak J, Bohackova V (1970) Electrochemistry. Methuen London

3.9   Plieth W (2008) Electrochemistry for Materials Science. 1st edition Elsevier BV Oxford UK

3.10 Paunovic M, Schlesinger M (1998) Fundamentals of Electrochemical Deposition. John Wiley & Sons Inc

3.11 Paunovic M, Schlesinger M (2000) Modern Electroplating. 5th edition John Wiley & Sons Inc

3.12 Ibl N, Puippe JC, Angerer H (1978) Electrocrystallization in pulse electrolysis. Surf. Technol. 6(4); 287-300

3.13 Roy S, Landolt D (1997) Determination of the practical range parameters

during reverse-pulse current plating. J. Appl. Electrochem. 27(3); 299-307

3.14   Hansal EGW, Roy S (2012) Pulse plating. 1ˢᵗ edition Eugen G Lueze

       Verglag KK Germany; 250-350

3.15   Winand R (1992) Electrocrystalization – theory and applications.

       Hydrometallurgy 29(1-3); 567-598

3.16   Romankiw LT, Sullivan O (1997) Plating Techniques Handbook of

       Microlithography, Micromachining, and Microfabrication. Vol 2, SPIE

       Press Bellingham Washington DC

3.17   Oniciu L, Muresan L (1991) Some Fundamental Aspects of Levelling and

       Brightening in Metal Electrodeposition. J. Appl. Electrochem. 21(7); 565-

       574

3.18   Franklin TC (1987) Some Mechanisms of Actions of Additives in

       Electrodeposition Processes. Surf. and Coat. Technol. 30(4); 415 – 428

3.19   Kruglikov SS, Kudriavtsev NT, Vorobiova GF, Antonov AYa (1965) On

       the Mechanism of Levelling by Addition Agents in Electrodeposition of

       Metals. Electrochim. Acta 10(3); 253-261

3.20   Hill MRH, Rogers GT (1978) Polyethylene Glycol in Copper

       Electrodeposition onto a Rotating Disk Electrode. J. Electroanal. Chem.

       86(1); 179-188

3.21   Schoenberg LN (1971) The Structure of the Complexed Copper Species in

       Electroless Copper Plating Solutions. J. Electrochem. Soc. 118(70); 1571-

       1576

3.22   Paunovic M, Arndt R (1983) Surface Preparation and Finishes for Metals.

       J. Electrochem. Soc. 130; 794-799

3.23 Reid J (1987) An HPLC Study of Acid Copper Brightener Properties. PC Fab 10; 65-71

3.24 Healy JP, Pletcher D (1992) The Chemistry of the Additives in an Acid Copper Electroplating Bath. J. Electroanal. Chem. 338(1-2); 155-165

3.25 Liebreich E (1935) The Effects of Film Formation on the Structure of Electrodeposited Metallic Coatings. Downloaded by Newcastle University on 24/10/2013 21:20:09,1188-1194

3.26 Blum W, Beckman A, Meyer W (1941) General Principles and Methods of Electroplating. Trans. Electrochem. Soc. 80(1); 249-299

3.27 Weil R, Paquin R (1960) The Relationship between Brightness and Structure in Electroplated Nickel. J. Electrochem. Soc. 107(2); 87-91

3.28 Broekmann P, Fluegel A, Emnet C, Arnold M, Roeger-Goepfert C, Wagner A, Hai NTM, Mayer D (2011) Classification of Suppressor Additives Based on Synergistic and Antagonistic Ensemble Effects. Electrochim. Acta 56(13); 4724-4734

3.29 Moffat TP, Wheeler D, Josell D (2004) Superfilling and the Curvature Enhanced Accelerator Coverage Mechanism. The Electrochem. Soc. Interface 13(4); 46-52

3.30 Moffat TP, Bonevich JE, Huber, WH, Stanishevsky A, Kelly DR, Stafford GR, Josell D (2000) Superconformal Electrodeposition of Copper in 500-90 nm Features. J. Electrochem. Soc. 147(12); 4524-4535

3.31 Gardam GE (1946) Polarisation in the Electrodepositon of Metals. Downloaded by Newcastle University on 24/10/2013 19:05:27

3.32 Taephaisitphongse P, Cao Y, West AC (2001) Electrochemical and Fill

Studies of a Multi-component Additive Package for Copper Deposition. J. Electrochem. Soc. 148(7); C492-C497

3.33   Vereecken PM, Binstead RA, Deligianni H, Andricacos PC (2005) The Chemistry of Additives in Damascene Copper Plating. IBM J. Res. and Dev. 49(1); 3-18

3.34   Watson SA, Edwards J (1957) An investigation of the mechanism of leveling in electrodeposition. Trans. IMF 34, 167-198

3.35   Lainier VI (1967) Modern Electroplating (Soyremennaya Galvanoteknica). USSR; 26 - 35

3.36   Melnicki LS (1988) in L Romankiw and T Osaka (Eds) Electrochemical Technology in Electronics PV 88-23 ECS Proceedings Series Pennington NJ; 95-103

3.37   Goodenough M, Whitelaw KJ (1989) Electrochemical Processing in ULSI Fabrication III. Trans. IMF 67; 57-60

3.38   Kainuma S, Ishikura S, Hisatake K (1995) Giant Magneto resistance of Electrodeposited [CoNiCu/Cu] Multilayers. J. Magnetics Soc. of Jpn. 21 (4_2); 557-560

3.39   Dow WP, Huang HS, Lin Z (2003) Interactions Between Brightener and Chloride Ions on Copper Electroplating for Laser-Drilled Via-Hole Filling Electrochem. Solid-State Lett. 6(9); C134-C136

3.40   Beacom S, Riley B (1960) Further Studies of Leveling Using Radiotracer Techniques. J. Electrochem. Soc. 107(9); 785 - 787

3.41   Brenner A (1963) Electrodeposition of Alloys: Principles and Practice. Academic Press, New York

3.42 Fabricus G, Sundholm G (1985) The effect of additives on the electrodeposition of copper studied by the impedance technique. J. of Appl. Electrochem. 15(6), 797-801

3.43 Michailova E, Vitanova I, Stoychev D, Milchev A (1993) Initial Stages of Copper Electrodepostion in the Presence of Organic Additives. Electrochim. Acta 38(16) 2455-2458

3.44 Roth CC, Leidheiser H (1953) The Interaction of Organic Compounds with the Surface during the Electrodeposition of Nickel. J. Electrochem. Soc. 100(12); 553-565

3.45 Nunez M (2005) Metal Electrodeposition. Nova Science Publishing Inc

3.46 Delahay P, Trachtenberg I (1958) Adsorption Kinetics and Electrode Processes. II. American Chemical Society J. Am. Chem. Soc. 80(9); 2094-2100

3.47 Bonou L, Eyraud M, Denoyel R, Massiani Y (2002) Influence of additives on Cu electrodeposition mechanisms in acid solution: direct current study supported by non-electrochemical measurements. Electrochim. Acta 47(26); 4139-4148

3.48 Kardos O, Foulke DG (1962) Advances in Electrochemistry and Electrochemical Engineering. Vol 2 CW Tobias ed Interscience New York

3.49 Roy S, Pintauro PN (1993) Analysis of Convective Mass Transfer by Potential Relaxation. J. Electrochem. Soc. 140(11); 3167-3175

3.50 Leung TYB, Kang M, Corry BF, Gewirth AA (2000) Benzotriazole as an Additive for Copper Electrodeposition Influence of Triazole Ring Substitution. J. Electrochem. Soc 147(9); 3326-3337

3.51 Stoychev D, Tsvetanov D (1996) Behavior of Poly(Ethylene glycol) During Electrodeposition of Bright Copper Coatings in Sulphuric Acid Electrolytes. J. Appl. Electrochem. 26(7); 741-749

3.52 Tan M, Guymon C, Wheeler D, Harb J (2007) The Role of SPS, MPSA, and Chloride in Additive Systems for Copper Electrodeposition. J. Electrochem. Soc. 154(2); D78-D81

3.53 Amblard J, Maurin G, Wiart R (1978) Electrocristallisation -Aspect fondamentaux, Les techniques de l'ingenieur 3; 1-23

3.54 Varvara S, Muresan L, Popescu IC, Maurin G (2003) Kinetics of copper electrodeposition in the presence of triethyl-benzyl ammonium chloride. J. Appl. Electrochem. 33(8); 685-692

3.55 Goldbach S, Messing W, Daenen T, Lapicque F (1998) Coupled effects of chloride ions and branch chained polypropylene ether LP-1™ on the electrochemical deposition of copper from sulfate solutions. Electrochim. Acta 44(2–3); 323-335

3.56 Moffat TP, Wheeler D, Witt C, Josell D (2002) Superconformal Electrodepositon Using Derivatized Substrates. Electrochem. and Solid-State Lett. 5; C110-C112

3.57 Stanković ZD, Vuković M (1996) The influence of thiourea on kinetic parameters on the cathodic and anodic reaction at different metals in H_2SO_4 solution. Electrochim. Acta 41(16); 2529-2535

3.58 Muresan L, Varvara S (2005) Leveling and brightening mechanisms in metal electrodeposition In Metal Electrodeposition. Nunez M ed Nova Science Publishers New York USA; 2-45

3.59   Nichols RJ, Bach CE, Meyer H (1993) The effect of three organic additives on the structure and growth of electrodeposited copper: An in-situ Scanning Probe Microscopy Study Ber Bunsenges Phys. Chem. 97(8); 1012-1020

3.60   Muresan L, Varvara S, Maurin G, Dorneanu S (2000) The effect of some organic additives upon copper electrowinning from sulphate electrolytes. Hydrometallurgy 54(2-3); 161-169

3.61   Pradhan N, Krishna PG, Das SC (1996) Influence of chloride ion on electrocrystallisation of copper. Plat and surf finish 83(3); 56-63

3.62   Okinaka Y (1985) Electroanalytical Methods for Research and Development in Electroplating. Plat. and Surf. Finish. 72; 34-43

3.63   Rogers T (1987) Electroanalytical Methods in the Plating Industry, An Overview. Plat. and Surf. Finish. 74; 51-52

3.64   Kelly JJ, Tian C, West AC (1999) Leveling and Microstructural Effect of Additives for Copper Electrodepostion. J. Electrochem. Soc. 146(7); 2540 – 2545

3.65   Schwartz M (1994) Deposition from Aqueous Solutions: An Overview book chapter in Handbook of deposition technologies for films and coatings: science, technology and applications edited by Rointan F. Bunshah 2nd edition Noyles publication

3.66   Landau U (1982) Plating New Prospect for an Old Art, Electrochemistry in Industry New Directions. Plenum Press New York

3.67   Bindra PS, David A, Galasco RT, Light DN (1985) Copper Plating Bath Having Increased Plating Rate, and Method. Eur. Pat. Appl. EP 114647

3.68 Chandrasekar MS, Pushpavanam M (2008) Pulse and pulse reverse plating—Conceptual, advantages and applications. Electrochim. Acta 53(8); 3313–3322

3.69 Osero N (1986) An Overview of Pulse Plating. Plat. and Surf. Finish. 73(3); 20-22

3.70 Piuppe J-C, Leaman F (1986) Theory and Practice of Pulse Plating. Am Electroplaters and Surf. Finishers Society

3.71 Yung EK, Romankiw LT, Alkire RC (1989) Plating of Copper into Through-Holes and Vias. Electrochem. Soc. 136(1); 206-215

3.72 Kenny S, Reents B, and Zosel J (2005) Plating high aspect ratio PCBs. Printed Circuit Design & Manufacture 22(1); 22-29

3.73 Kanani, N (2006) Electroplating: Basic Principles, Processes and Practice. Elsevier Ltd Oxford UK; 131 -135

3.74 Renzai-Kalantary M (1990) Pulse electroplating of copper for printed circuit technology. PhD thesis Loughborough University UK

3.75 Devaraj G, Guruviah S (1999) Pulse plating. Materials Chemistry and Physics. 25(5), 439 - 461

3.76 Cheh HY (1971) Electrodeposition of Gold by Pulsed Current. J. Electrochem. Soc. 118; 551-557

3.77 Chen HY (1971) The Limiting Rate of Deposition by P-R Plating. J. Electrochem. Soc. 118; 1132-1134

3.78 Chin DT (1983) Mass Transfer and Current-Potential Relation in Pulse Electrolysis. J. Electrochem. Soc. 130; 1657-1667

Chapter 4

Experimental

This chapter presents a description of the methods used in doing several experiments including: (i) polarisation experiments on standard and EnFACE electrolytes with additives; (ii) direct current (DC) electroplating of additive-containing EnFACE electrolyte; (iii) pulse current (PC) electroplating of additive-containing EnFACE electrolyte; (iv) characterisation of plated specimens; and (v) assessment of the throwing power of additive-containing EnFACE electrolyte in DC plating.

4.1 Polarisation experiments

Polarisation experiments were conducted to reveal the influence of additives on cathode polarisation; and thereby gain an understanding of the mechanisms of additive action in the EnFACE electrolyte. In this study, polarisation tests were conducted primarily under a potentiodynamic mode. A potentiodynamic polarisation test involves studying the change in current (between the working and counter electrode) as the applied potential (between the working and the reference electrode) is varied over a specified range. While both potentiodynamic and galvanodynamic tests can give the same result, the potentiodynamic test is more popular owing to ease of implementation, and the ability to yield considerable amount of information (e.g. kinetic and thermodynamic information, limiting current, etc.) from a single test [4.1].

4.1.1 Materials and Apparatus

Figure 4.1 shows a schematic of the polarisation experiments. The test apparatus consisted of a current source, a classic three-electrode cell, and a current or potential measuring instrument. The three-electrode configuration is appropriate to use when control of potential between the working and the reference electrode is important, as in a potentiodynamic polarisation test. The working electrode was a 0.5 cm diameter copper disc encased in an inert, non-conductive polymer, and the counter electrode was a 1cm × 1cm copper sheet. The reference electrode, which was inserted in a luggin capillary, was Ag/AgCl/saturated KCl (+ 0.197 V_{SHE}). The tests were carried out in a 300 ml cylindrical glass cell, and without mechanical agitation. Mechanical agitation was not applied to the system to eliminate hydrodynamic effects that complicates analysis of polarisation curves [4.2].
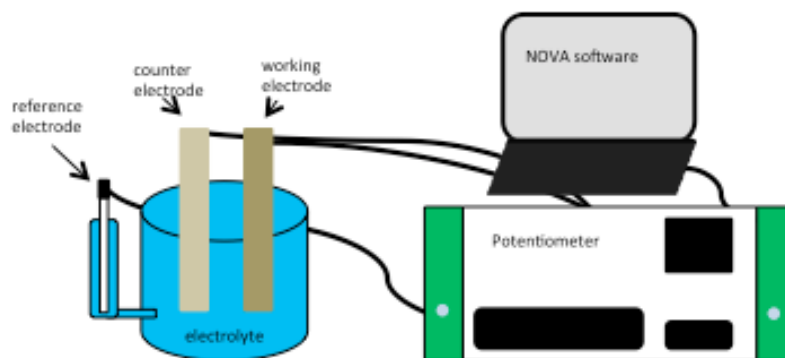
Figure 4.1 Schematic of the polarisation test apparatus.

Technical grade $CuSO_4$ (Sigma Aldrich) and reagent grade H_2SO_4 (Sigma Aldrich) were used to prepare plating electrolytes. The commercial plating additives used were Copper Gleam HS–200 A, Copper Gleam HS–200 B (Dow Chemicals), and laboratory grade 37% HCl (Sigma Aldrich). The manufacturer's description of the plating additives is found in Appendix 1.

4.1.2 Polarisation Test Procedure

Prior to each polarisation tests, the copper electrode was polished using 4000 grit silicon carbide (SiC). The copper rod was washed with ethanol then air-dried. The test electrolyte was poured into the electrolyte chamber, and the three electrodes were immersed in the solution. Polarisation measurements were then performed.

Potentiodynamic polarisation was performed with an applied potential sweep from 0 to -1.0 V at a scan rate of 0.02 V/s. The resulting current was measured using an Autolab potentiostat (PGSTAT101). Data were analysed using the software NOVA version 1.7 and a plot of current vs potential (i-V curve) was obtained. All polarisation tests were corrected for ohmic drop. The NOVA software is electrochemistry software used by the Metrohm autolab. In this software, the desired settings for the electrochemical test (such as potential scan range, scan rate, step size, etc.) can be controlled. The interface displays a real time plot of the potential and the measured current.

4.1.3 Preliminary Studies on the Effect of Additives on Standard and EnFACE Copper electrolyte

Table 4.1 lists the chemistry of the electrolytes used in the different polarisation tests. The polarisation studies looked at the effect of additives on the polarisation behaviour of a standard acid-copper sulfate electrolyte (S-0 and S-100) and the EnFACE electrolyte (E-0 and E-100). The chemistry of the standard acid copper electrolyte, consisting of H_2SO_4 and $CuSO_4$, in accordance to recommended settings by Rohm and Haas [4.3]. The Copper Gleam additive series is a commercially available additive that is widely accepted in the plating industry. A

commercial additive (ie. Copper Gleam) was chosen for the study because these additives are used by the industry; and thus our results would be more relevant to current applications. The additives chosen represent the suppressor (Gleam B) and accelerator (Gleam A) type additives used in electronic plating applications. The chloride ion on the other hand offers synergistic effects for both types. Copper Gleam B was believed to be an inhibitor, while Copper Gleam A was the accelerator. This was eventually confirmed by the results of polarisation experiments. HCl was used as the chloride ion source. Low and high concentration of additives were used in the polarisation experiments to see a more logical trend on its effect.

Table 4.1 Composition of the standard and EnFACE electrolytes used for initial polarisation experiments.

Sample Designation	Experiment settings	$CuSO_4$ (M)	H_2SO_4 (M)	Copper Gleam B (ml/L)	Copper Gleam A (ml/L)	HCl (ppm)
E-0	EnFACE electrolyte without additives	0.1	×	×	×	×
E-100	EnFACE electrolyte with recommended additive concentration	0.1	×	10	0.50	70
S-0	Standard electrolyte without additives	0.63	2.04	×	×	×
S-100	Standard electrolyte with recommended additive concentration	0.63	2.04	10	0.50	70

4.1.4 Study on the Effect of Additives on EnFACE Electrolyte

After the preliminary tests, further experiments investigated the effect of concentration of individual additives; i.e. Copper Gleam B, Copper Gleam A and Cl⁻, on the cathode polarisation behaviour in the EnFACE electrolyte. Plating additives are often used in combination rather than singularly. Nevertheless, by using these additives in isolation, the true effect of each component will be revealed. Table 4.2 lists the electrolyte settings used in this round of experiments. The recommended values for each type of additive were obtained from literature [4.3]. The effect of additive concentration on electrolyte polarisation was further studied by varying the amount of additives used in the electrolyte. Three concentration levels, which were lower than the recommended dosage, were chosen (e.g. see samples C-17, C-33 and C-50).

Table 4.2 Electrolyte compositions used for determining the effect of single additives on EnFACE electrolyte.

Sample Designation	Experiment settings	$CuSO_4$ (M)	Copper Gleam B (ml/l)	Copper Gleam A (ml/l)	HCl (ppm)
A-17	EnFACE electrolyte with different Gleam A concentrations	0.1	×	0.09	×
A-33		0.1	×	0.17	×
A-50		0.1	×	0.25	×
A-100	EnFACE electrolyte with recommended Gleam A concentration	0.1	×	0.50	×
B-17	EnFACE electrolyte with different Gleam B concentrations	0.1	1.7	×	×
B -33		0.1	3.3	×	×
B-50		0.1	5.0	×	×
B-100	EnFACE electrolyte with recommended Gleam B concentration	0.1	10	×	×
C-17	EnFACE electrolyte with different Cl⁻ concentrations	0.1	×	×	12
C-33		0.1	×	×	23
C-50		0.1	×	×	35
C-100	EnFACE electrolyte with recommended Cl⁻ concentration	0.1	×	×	70

Table 4.3 Electrolyte compositions used for determining the effect of mixed-additives on EnFACE electrolyte.

Sample Designation	Experiment settings	CuSO$_4$ (M)	Copper Gleam B (ml/l)	Copper Gleam A (ml/l)	HCl (ppm)
ABC-17	EnFACE electrolyte with different concentrations of Gleam A, Gleam B and Cl$^-$	0.1	1.7	0.09	12
ABC-33		0.1	3.3	0.17	23
ABC-50		0.1	5.0	0.25	35
ABC-100	EnFACE electrolyte with recommended Gleam A, Gleam B and Cl$^-$ concentration	0.1	10	0.50	70
ABC-200	EnFACE electrolyte with high Gleam A, Gleam B and Cl$^-$ concentration	0.1	20	1.0	140
BC-17	EnFACE electrolyte with different Gleam B and Cl$^-$ concentrations	0.1	1.7	×	12
BC-33		0.1	3.3	×	23
BC-50		0.1	5.0	×	35
BC-100	EnFACE electrolyte with recommended Gleam B and Cl$^-$ concentration	0.1	10	×	70

The effect of different concentrations of multi-additive mixtures; i.e. (i) Cl$^-$ and Copper Gleam B (BC electrolyte) and (iii) Copper Gleam A-Copper Gleam B-Cl$^-$ (ABC electrolyte), were investigated. The electrolyte composition settings for these experiments are shown in Table 4.3. Other additive combinations (e.g. Copper Gleam A and Cl$^-$) were not investigated, as these mixtures are not used in actual plating applications.

4.2 Copper Plating in Direct Current Mode

Electroplating of copper was conducted to determine the influence of additives on the different properties of the EnFACE deposit. Generally, electroplating in the industry is done via two techniques: (i) direct current (DC) and (ii) pulse current (PC) plating. In this study, these two techniques were used to plate copper to verify the effect of the mode of current application on the deposit properties. The following describes the methods used for DC plating, while Section 4.3 describes the methods used for PC plating.

4.2.1 Materials and Apparatus

Figure 4.2 shows a schematic of the fixtures used for direct current (DC) plating. The two-electrode cell was appropriate because plating was done by controlling the applied current between the working and the counter electrode (i.e. galvanostatic mode), and thus a reference electrode was not necessary. A dog-boned shaped 308 stainless steel (SS) substrate was the cathode, with dimensions as shown in Fig. 4.3. Alligator clips were used to hold the SS substrate and provides the electrical connection. Stainless steel was chosen as the substrate since the copper film can be easily peeled off for the ensuing characterisation techniques. These substrates were manufactured to the specifications of the IPC-TM-650 standard [4.4]. A copper rod with an immersed area of $58.1cm^2$ was the anode. The resulting anode-to-cathode area ratio was 2:1. For efficient plating, the value of the area ratio should be a minimum of 1:1. The current source used was the Thurlby Thandar PL-303 power supply.

All plating solutions were prepared using technical grade $CuSO_4$ and reagent grade H_2SO_4. Similarly, Copper Gleam HS–200 A, Copper Gleam HS–200 B (Dow Chemicals), and reagent grade 37% HCl solution were used as additives.
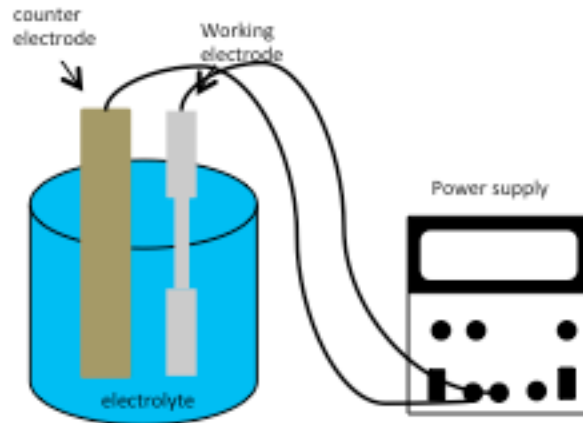
Figure 4.2 Two-electrode cell apparatus used for plating copper in DC mode.
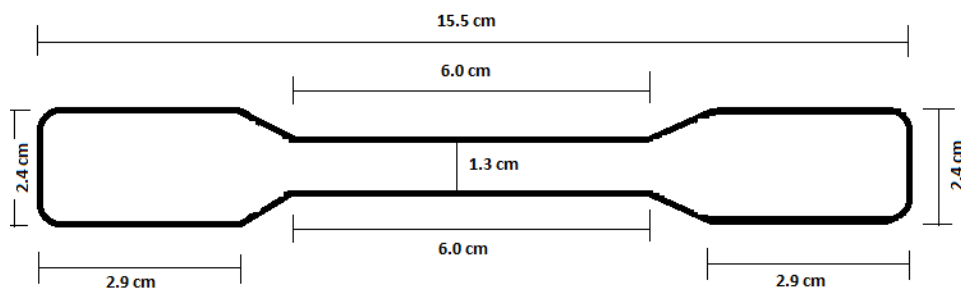
Figure 4.3 Schematic of the stainless steel coupon used as plating substrate for thin film tensile tests.

4.2.2 DC Plating Procedure

Prior to plating, the SS substrates were cleaned to remove dirt and residual oxides by using the following procedures:

(1) Specimen was dipped in concentrated nitric acid for 1 minute

(2) Rinsed in water for 1 minute

(3) Mechanically polished using silicon carbide sheets starting at grit #220 to #4000

(4) The back part of the substrate was insulated with photoresist to control the plating area then air dried for a few minutes.

(5) The exposed part was swabbed with acetone for 30 seconds and left to dry at room temperature.

The different electrolytes used for DC copper plating is shown in table 4.4. The desired deposit thickness was set at 25 μm, which is equivalent to the copper film thickness that the electronics industry requires for printed circuit boards. Plating thickness was measured using a Mitutuyo digimatic micrometer (MDC- 25PJ) with an accuracy of ± 0.0001in (2μm).

Table 4.4 Electrolyte compositions used for DC electroplating experiments.

Designation	Settings	CuSO$_4$ (M)	H$_2$SO$_4$ (M)	Gleam B (ml/L)	Gleam A (ml/L)	HCl (ppm)
E-0	EnFACE electrolyte only	0.1	x	x	x	x
E-17	17% of the recommended concentration	0.1	x	1.7	0.09	12
E-33	33% of the recommended concentration	0.1	x	3.3	0.17	23
E-50	50% of the recommended concentration	0.1	x	5.0	0.25	35
E-100	Recommended concentration	0.1	x	10	0.5	70
E-200	High concentration (double of the recommended concentration)	0.1	x	20	1.0	140
S-100	Standard	0.63	2.04	10	0.5	70
S-0	Standard w/o additives	0.63	2.04	x	x	x

Exploratory plating runs were conducted to determine plating efficiency. The plating efficiency was calculated by comparing the actual weight of the deposit to the theoretical weight, at a plating current density equal to 40% of the limiting current density, i_{lim}. These limiting currents, as shown in Table 4.5, were obtained from earlier polarisation experiments. The theoretical plating time, t_{theo}, for a deposit thickness of 25 μm was calculated using Faraday's law:

$$m = \frac{IAt}{Fn} \qquad\qquad \text{Equation (4.1)}$$

where m is the mass of the deposit (grams), I is the current (amperes), A is the atomic weight of the metal (g/mol), t is the plating time (s), F is the Faraday's constant, 96,500 C/g-equivalent and n is the metal's valence. The actual plating time, t_{actual}, was then obtained by adjusting the theoretical plating time to accommodate plating inefficiencies to enable 25μm thick copper deposits:

$$t_{actual} = \frac{t_{theo}}{\left(\frac{\% \, efficiency}{100\%}\right)}$$

Equation (4.2)

Table 4.5 Plating parameters used for DC electroplating of different electrolytes.

Settings	Limiting current density, $i_{lim,}$ (mA·cm⁻²)	Plating current 40%I_{lim} (mA)	Plating time, theo (min)	Efficiency (%)	Adjusted Plating time (min)
E-0	5.30	68	536	87	615
E-17	5.29	68	536	86	623
E-33	4.95	63	579	91	623
E-50	4.58	58	629	92	669
E-100	4.20	54	675	94	705
E-200	4.17	53	688	96	708
S-100	19.20	245	149	97	146
S-0	20.00	255	143	97	152

After the allotted deposition time was reached, the SS coupons were removed from the solution and washed with deionised water for one minute. The surface was dried using a lint free cloth. The plated copper films were carefully peeled off from the SS substrate, and were prepared for subsequent characterisation.

4.3 Plating in Pulsed Current Mode

4.3.1 Materials and Apparatus

Copper plating experiments using pulsed current was carried out using a pulse rectifier (Plating Electronics) attached to the two-electrode plating apparatus, as for the DC plating experiments. All other experimental apparatus were the same, except for an oscilloscope (Agilent 300 series), which was used to monitor the pulse characteristics. All the chemicals used for PC plating were similar to those used in DC plating (see Section 4.2.2).

4.3.2 Determination of PC plating parameters

As described in Section 3.6, a unipolar PC plating operation requires three plating parameters; i.e. peak current, I_{peak}, duty cycle, θ, and pulse period, t_p. The following describes how each parameter was determined for this study.

4.3.2.1 2^k Factorial Experiments to Determine Operating Duty Cycle and Total Pulse Time.

To empirically determine θ and t_p, a 2^k factorial experiment was implemented [4.5]. A 2^k factorial experiment is a screening test designed to determine the factors that can affect a particular response. The 2^k refer to a series of test with k factors set at 2 levels (high and low). Two factors (i.e. θ and t_p) were studied, and Table 4.6 shows the settings used for the 2^2 tests. Copper was electroplated using the additive-free EnFACE electrolyte, E-0, and the peak current was kept constant at 40% of i_{lim}. The responses used to assess the quality of the deposit includes: (i) plating efficiency, and (ii) ease-of-peel of the deposit from the substrate. Plating efficiency is

important to maximise yield from a plating process. Ease-of-peel is important as it ensures that the coupon is cleanly separated from the SS substrate, and allows subsequent characterisation of the copper film.

Table 4.6 Values of duty cycle and pulse period used in the 2^K factorial experiments, and the corresponding plating efficiency and deposit thickness obtained from each setting.

Duty Cycle, θ	Total pulse time (ms)	Efficiency (%)	Thickness (nm)
0.25	100	68	30
	20	53	25
0.50	100	58	25
	20	52	25

Table 4.6 also shows the efficiencies and thickness obtained from the different setting combinations. Furthermore, Fig. 4.4 shows images of the electrodeposited copper films, which were assessed according to efficiency and ease-of-peel. Results indicated that the best settings were $\theta = 0.25$ and $t_p = 100$ms.
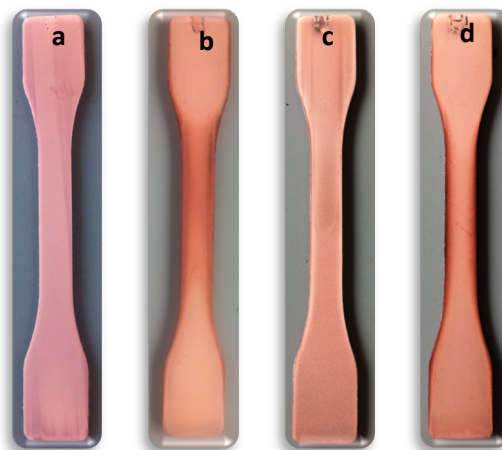
Figure 4.4 Electrodeposited copper film at current density = $40\%I_{p,lim}$ (a) $\theta = 0.25$, $t_p = 100$ms (b) $\theta = 0.25$, $t_p = 20$ms (c) $\theta = 0.50$, $t_p = 100$ms and (d) $\theta = 0.50$, $t_p = 20$ms.

Similar factorial experiments were done to determine the operating pulse settings for the electrolyte with additives. The additive-containing EnFACE electrolyte, E-100, was investigated. In this test, t_p was set to 100ms, as the previous test proved that t_p at 20ms yielded poor plating quality, and only θ was varied (0.50 and 0.25).

The current efficiency and thickness measured for the experiment settings are shown in Table 4.7, while Fig. 4.5 shows images of the electrodeposited films. Although θ of 0.5 and 0.25 yielded the same plating thickness, considerable difference in the plating efficiency was observed. This suggests that at θ of 0.5 the solution was not allowed to recover fully to achieve a high plating efficiency. Thus, judging on plating efficiency and ease-of-peel, the optimum settings for pulse deposition was found at $\theta = 0.25$ at a total pulse time of 100ms.

Table 4.7 Results of pulse plating experiments on electrolyte with additives.

Total pulse time (ms)	Duty Cycle, θ	Efficiency (%)	Thickness (μm)
100	0.50	70	25
	0.25	96	25

Figure 4.5 Copper films deposited at $0.4i_{p,lim}$ and (a) $\theta = 0.25$, $t_p = 100$ ms; (b) $\theta = 0.50$, $t_p = 100$ ms.

4.3.2.2 Calculation of the Operating Peak Current Density in Pulse Current Plating

Recall that in chapter 3.6.4, for a unipolar pulse, the ratio of $I_{p,lim}$ to the limiting direct current, $I_{d,lim}$, was expressed using Equation 3.36:

$$\frac{I_{p,lim}}{I_{d,lim}} = \frac{1}{1 - 2\,T^* \cdot \sum_{m=1}^{\infty} [\exp(\lambda_m) - 1]} \qquad \text{Equation (3.36)}$$

where T^* is the dimensionless pulse time given by $T^* = Dt_T/\delta_s^2$ and the summation term $\lambda_m = \pi^2 T^*(m - 1/2)^2$. The term D refers to diffusivity, t_p is the total pulse time and δ_s is the thickness of the stagnant layer adjacent to the cathode. $I_{d,lim}$ of the electrolyte is experimentally determined via polarisation experiments in DC mode. The appropriate values of the following parameters for the studied electrolyte (0.1 M $CuSO_4$) were as follows:

Table 4.8 Parameters used to determine $I_{p,lim}$.

D	diffusion coefficient	5.64×10^{-6} cm^2 s^{-1}
t_T	total pulse cycle time	1.0×10^{-1} s
δ	steady state diffusion layer thickness	1.0×10^{-2} cm
m	summation variable	10

Using these values, the ratio was obtained:

$$\frac{I_{p,lim}}{I_{d,lim}} = 3.2957$$

Using the $i_{d,lim}$ of each electrolyte and the above ratio, the corresponding $i_{p,lim}$ was calculated and is presented in Table 4.9. This $i_{p,lim}$ values may now be used to calculate the i_{peak}.

Table 4.9 Calculated pulse limiting current density for the different electrolytes.

Electrolyte designation	$i_{d,lim}$ (mA·cm^{-2})	$i_{p,lim}$ (mA·cm^{-2})
E-0	5.30	17.47
E-17	5.29	17.43
E-33	4.95	16.31
E-50	4.58	15.09
E-100	4.20	13.84
E-200	4.17	13.74
S-100	19.2	63.28
S-0	20	65.91

Two conditions need to be met when calculating the peak current, i_{peak} [4.5]:

$$\textbf{Condition I}: \quad i_{ave} < i_{p,lim} \qquad \text{Equation (4.3)}$$

where $i_{ave} = i_{peak} * \theta$ and θ is the duty cycle

$$\textbf{Condition II}: \quad i_{peak} < i_{p,lim} \qquad \text{Equation (4.4)}$$

These two conditions ensure that mass transport conditions are favourable during plating and thus prevent the formation of dendritic deposits [3.76, 3.77]. A third condition may also be considered, which states:

$$i_{d,lim} < i_{peak} < i_{p,lim}$$
<div align="right">Equation (4.5)</div>

Following these criteria, it was decided to set i_{peak} at 40% of $i_{p,lim}$, which is similar to the plating condition used during DC plating. Finally, Table 4.10 shows the corresponding i_{peak} for the electrolytes tested.

Table 4.10 Operating peak current density for the different electrolytes used in the PC plating experiments.

Electrolyte designation	i_{peak} $(mA \cdot cm^{-2})$
EP-0	6.99
EP-17	6.97
EP-33	6.52
EP-50	6.04
EP-100	5.54
EP-200	5.50
SP-100	25.31
SP-0	26.37

4.3.3 PC Plating Procedure

Substrate preparation and cleaning followed the same procedure used in preparing substrates for DC plating (see Section 4.2.2).

Table 4.11 Pulse plating parameters used for electroplating experiments.

Settings	Pulse limiting current density, $i_{p,lim}$ (mA·cm^{-2})	Plating current, 40% of $I_{p,lim}$ (mA)	Plating time (min)	Efficiency (%)	Adjusted Plating time (min)
EP-0	17.47	223	645	64	1022
EP-17	17.43	223	645	74	885
EP-33	16.31	208	690	77	909
EP-50	15.09	193	747	78	971
EP-100	13.84	177	814	85	971
EP-200	13.74	175	820	83	978
SP-100	63.28	808	178	86	209
SP-0	65.91	842	171	86	202

The unipolar pulse form was used for plating. The operating pulse parameters used were $\theta = 0.25$ at a t_p of 100ms. The actual plating time for a deposit thickness of 25 um was calculated using Faraday's law and was adjusted to accommodate plating inefficiencies, as shown in Table 4.11. Finally, the electrolyte compositions used in the PC plating experiments were similar to those used in the DC plating runs (see Table 4.4).

4.4 Characterisation of Electrodeposited Copper Film

Different characterisation tools were used to analyse the influence of additives on the different properties of the copper deposits. The properties investigated include electrical (four-point probe), morphological (SEM, EBSD, XRD) and mechanical (UTM) properties. The next sections described in detail the

methods used to conduct these analyses. Each section will begin with a description of the operating principles of each technique followed by the methods used for the test.

4.4.1 Four-point probe

4.4.1.1 Principle of Resistivity measurements

The four-point probe is used to measure the sheet resistance and bulk resistivity of thin films, and is particularly useful for measuring semiconductor parameters. The use of the four-probe arrangement is advantageous because it reduces measurement errors due to: (i) the resistances of the probes; (ii) spreading resistance of each probe; and (iii) contact resistance between the metal probe and the test material. This means that the four-probe arrangement allows accurate measurements of low resistance values.

The apparatus consists of four-equally spaced, collinear probes, as shown in Fig. 4.6. A high impedance current source is attached to the two outer probes, while high impedance voltmeter is connected to the two inner probes. To do a test, the probes are first located at the center of the thin film. A controlled amount of current is passed through the two outer probes, while the voltage drop in the two inner probes is monitored. These two parameters are used to obtain resistivity.
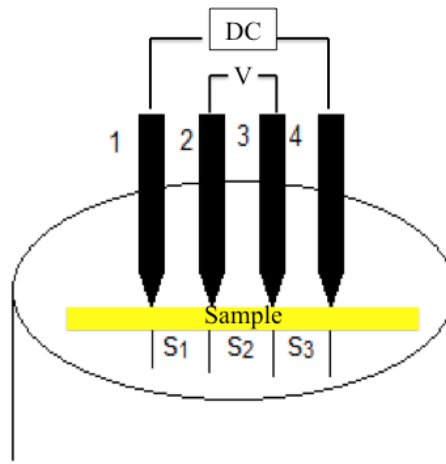
Figure 4.6 Schematic of the collinear four-point probe instrument used for thin film sheet resistance and resistivity measurements.

Two types of resistivity are derived from the test; namely, sheet resistivity and bulk resistivity. Sheet resistance or sheet resistivity, R_s (ohms/sq) is based from the equation:

$$R_s = \frac{\pi}{ln2} \frac{V}{I}$$
Equation (4.6)

where I is the current applied in the two outer probes and V is the potential measured in the inner probes. Sheet resistance is a measure of the resistivity of films possessing a uniform thickness. The advantage of using this parameter is that it is independent of the scale of film contact and thus can be used to compare the electrical resistivity of devices that are different in terms of size.

The bulk resistivity, ρ (ohms·cm) is calculated from R_s using the equation:

$$\rho = R_s L_f$$
Equation (4.7)

where L_f is the film thickness. Bulk resistivity is particularly important for semiconductor applications since it can be directly related to the impurity levels in the doped silicon wafer.

4.4.1.2 Test procedure

The entire coupon was used for the four point probe testing. The probe spacing, s (see Fig. 4.6), was 62.5 mils (1.58 mm). To do a test, a starting current of 0.01 A was passed through the two outer probes and the voltage was measured in the two inner probes. The Signatone Pro4 system was used to help analyse and collect resistivity data during the test. Measurements were made from 0 to 168 hours after plating with the intention of detecting the self-annealing phenomenon. Data was recorded at 30 minutes time interval in the first 24 hours. After which, data was recorded at 1-day interval up to 7 days. A Pro4 software control the four point probe equipment. A real time graph will be displayed in the data interface and a data logger is used to collect and stored data for a user-specified time. The data will be exported in excel for data management. The software used the ASTM Standard F84-99 for error compensation due to probe spacing and proximity to the edge of the conducting layer.

4.4.2 X-ray diffraction

4.4.2.1 Operating Principle

X-ray diffractometry (XRD) is a multi-purpose, non-destructive technique for studying crystalline structures. Information from an XRD test yield a wealth of information including crystallographic structure, phase compositions, textures or preferential growth directions, crystal size, and stresses in the phases [4.6].
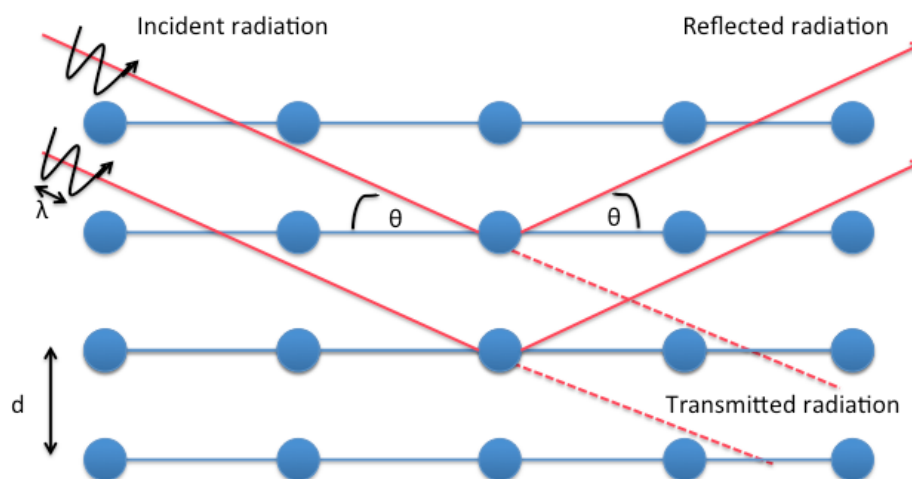
Figure 4.7 Schematic representation of Bragg's law. Constructive interference occurs for an incoming electromagnetic wave with a wavelength, λ, scattered at an angle, θ, by lattice planes having interplanar distance, d_{hkl}, if Bragg's equation is satisfied [Adapted from 4.7].

Diffraction refers to the constructive interference of scattered electromagnetic radiation as a result of the interaction of the radiation with an ordered or periodic structure. XRD is based on studying the diffraction patterns created when the crystal, which possesses the necessary ordered structure for the scattering center, is illuminated with x-rays. These patterns consist of interference peaks that reflect the periodicity of the analysed material.

Bragg's law is the fundamental principle governing diffraction, as depicted in Fig. 4.7, and is important for analysing diffraction patterns. The Bragg's law essentially describes the condition at which diffraction occurs. The Bragg's Law in equation form is as follows [4.8]:

$$2d_{hkl}sin\theta_d = n\lambda \qquad \text{Equation (4.8)}$$

where λ is the wavelength of the X-ray, θ_d is the diffraction angle, n is the order of diffraction (a whole integer 1,2,3..etc), and d_{hkl} is the interatomic distance between crystal planes.

The XRD equipment consists of two main parts: the X-ray tube and a goniometer (see Fig. 4.8). The X-ray tube with a typical tungsten filament acts as the source of x-ray radiation. The test specimen is placed in the sample holder, and is made incident with x-rays at different angles. Test specimens may be in bulk, in sheet, or in powdered form. During operation, cold water is supplied under the anode holder to cool the sample and prevent melting due to high temperature. The data is collected by a detector moving on an angle 2θ, while the sample moves at an angle θ. Figure 4.9 shows the typical data from a scan; i.e. diffraction intensity is plotted against diffraction angle, 2θ. Each of the peaks represents a scattering event triggered by a unique set crystal planes.
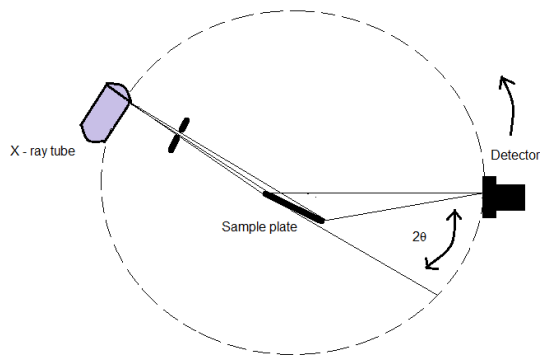
Figure 4.8 Schematic representation of a typical x-ray diffractometer.
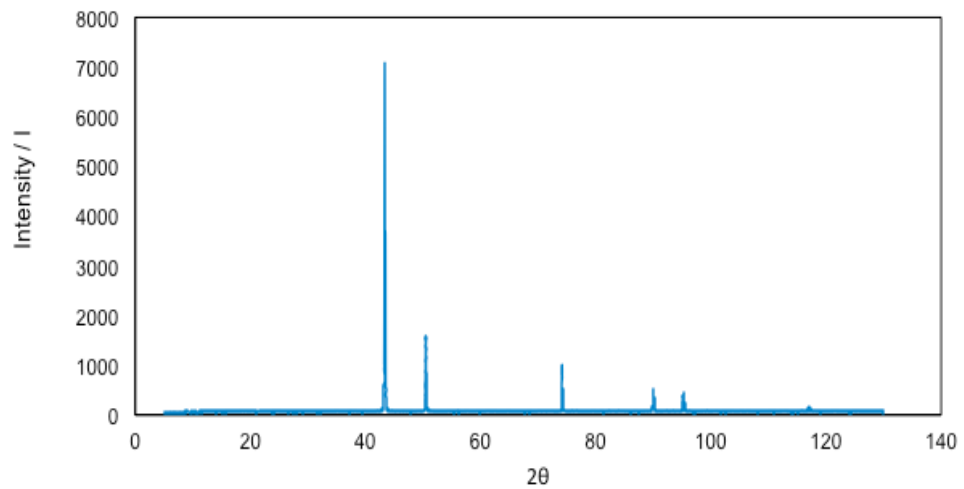
Figure 4.9 Example of a diffraction pattern from an XRD test.

4.4.2.2 Grain size, Microstrain and Texture Analysis

A majority of the application of XRD is for phase identification, and this analysis depends primarily on the positions of the peaks (i.e. 2θ values) in a diffraction pattern. However, the shapes of these peaks may also provide additional information about the crystal such as crystallite size, plastic deformation or microstrain, and even vacancy and impurity element concentrations.

Changes in crystallite size can cause changes in the peak width. For example, a decreasing crystal size causes peak broadening. Scherrer's equation describes the relationship between the mean crystallite size, d_{hkl}, and peak width, β:

$$d_{hkl} = \frac{K\lambda}{\beta cos\theta_d} \qquad \text{Equation (4.9)}$$

where K is a dimensionless shape factor (typical value of 0.9), λ is the X-ray wavelength, β is the full width at half the maximum peak intensity (FWHM) in radians, and θ_d is the Bragg angle.

The Scherrer equation is applicable when estimating the crystal size in between 100 and 200 microns. Furthermore, the Scherrer grain size should be considered as the lower bound of the particle size range because several factors can contribute to the width of a diffraction peak. These factors include: (i) microstrain, (ii) crystal lattice imperfections (dislocations, stacking faults, grain boundaries, coherency strain, etc.), and (iii) instrumental effects. Only when the contribution of these factors is measured to be zero would the Scherrer equation accurately give the grain size value.

The Williamson-Hall method is another technique that is used to calculate both grain size and microstrain [4.9]. This method assumes that the total peak broadening, β_{total}, is the sum of the broadening due to grain size, β_L, and the broadening due to strain, β_e. Size broadening may be taken from Scherrer equation:

$$\beta_L = \frac{K\lambda}{d_{hkl}cos\theta_d} \qquad\qquad \text{Equation (4.10)}$$

while strain broadening is described by the following equation:

$$\beta_e = C\varepsilon tan\theta_d \qquad\qquad \text{Equation (4.11)}$$

where $C\varepsilon$ is the microstrain.

Therefore, β_{total} may be expressed as:

$$\beta_{total} = \beta_L + \beta_e = \frac{K\lambda}{d_{hkl}cos\theta_d} + C\varepsilon tan\theta_d \qquad\qquad \text{Equation (4.12)}$$

and multiplying this equation with $cos\theta_d$ yields:

$$\beta_{total}cos\theta_d = \frac{K\lambda}{d_{hkl}} + C\varepsilon sin\theta_d \qquad\qquad \text{Equation (4.13)}$$

Equation 4.12 assumes the form of the linear equation: y = mx + b. A plot of

βcosθ vs sinθ, called the Williamson-Hall plot, will then yield a straight line. The

slope of this line, $C\varepsilon$, is then used to calculate the strain and the y-intercept, $\frac{K\lambda}{d_{hkl}}$, is

used to calculate the grain size.

The Williamson-Hall technique is simple and easy to use. A perceived

weakness of this method is that it considers too many assumptions. Therefore, the

values obtained using the Williamson-Hall approach is only accurate when certain

conditions are met. On the other hand, it can be useful for comparative studies where

it may reveal trends in the crystallite size/strain of different products.

Copper texture may also be revealed using x-ray diffraction data. Texture

may be assessed from the value of I_{111}/I_{200}, which is the ratio of the integral peak

intensities of (111) and (200). A maximum I_{111}/I_{200} value of 2.17 indicates no texture

or randomly oriented grains, while larger ratios indicates strong texture [4.10].

Alternatively, texture in plated films may be assessed using the texture coefficient of

the (hkl) plane, T_c(hkl) [4.11]:

$$T_c(hkl) = \frac{I(hkl)/I_o(hkl)}{\left(\frac{1}{n}\right)\sum_n I(hkl)/I_o(hkl)} \qquad \text{Equation (4.14)}$$

where, I(hkl) is the measured intensity of the chosen (hkl) plane, I_o(hkl) is the

standard intensity of the plane (JCPDS data) and n is the number of diffraction

peaks. A T_c(hkl) that is close to unity (1) indicates a randomly distributed crystal

orientation, while a T_c(hkl) greater than 1 means the (hkl) plane is preferentially

oriented.

4.4.2.3 Test Procedure

The X-ray diffractometer (XRD) was used for estimation on the grain size as well as analysis of the crystal structure and residual strain or microstrain. The copper film was cut using a sharp blade, and a 2×2 cm^2 portion was reserved for XRD analysis. The relatively large area of the specimen ensures that the center area of the specimen is analysed. It is important to exclude the sides from analysis because this region could contain residual stress created during the cutting procedure, and such stress will add to the inherent microstrain of the deposit. The specimens were stored in a desiccator at room temperature. Testing of copper specimens commenced after two days of storage to ensure that all time-dependent microstructural changes in the deposits had completed.

The films were characterised at the Advanced Chemical and Materials Analysis (ACMA) laboratory at Newcastle University. The equipment used was a PANalytical XPERT-PRO MPD, powered by a Philips PW3040/60 X-ray generator and fitted with an X'Celerator detector. The data were collected using a scanning X'Celerator detector with scan range of 5 to 130, step size of 0.004178 and nominal time per step of 10.16s. Fixed anti-scatter and divergence slits of 0.19mm were used together with a beam mask of 10mm and all scans were carried out in continuous mode.

Phase identification was done using the software PAN analytical High Score Plus together with the ICDD Powder Diffraction File 2 database [4.12], the American Mineralogist Crystal Structure Database [4.13] and the Crystallography Open Database [4.14]. The High score plus software is integrated in the XRD

equipment and used to control and input the parameters for the characterisation. The measured scans were automatically stored in the pre-set database. The High score plus is capable of profile-fitting to get the Full Width at Half Maximum (FWHM), which is useful for crystallite size and microstrain calculation.

4.4.3 Tensile test

4.4.3.1 Operating principle of Universal Testing Machine

The universal testing machine (UTM) is one of the most versatile equipment for measuring mechanical properties. The machine can be made to do a variety of mechanical tests including tensile, compressive, shear and flexural tests.

The tensile test is conducted to determine the tensile properties of a material. Standards such as ASTM E-8 and ISO 6892-1 are the most commonly used when testing bulk metals. A typical tensile test begins with a standard specimen, of known dimensions, being fixed on the sample grips of the UTM (see Fig. 4.10). The extensometer is attached to the specimen and set at the gage length. A tensile or pulling force is then applied to the specimen by the movement of the crosshead. The tensile load is applied at a defined stress or strain rate. Controlling the stress and strain rate is important since it can influence the measured mechanical properties. The load is continuously applied until fracture of the specimen occurs. The mating pieces of the failed specimen are usually analysed to reveal fracture characteristics of the material.
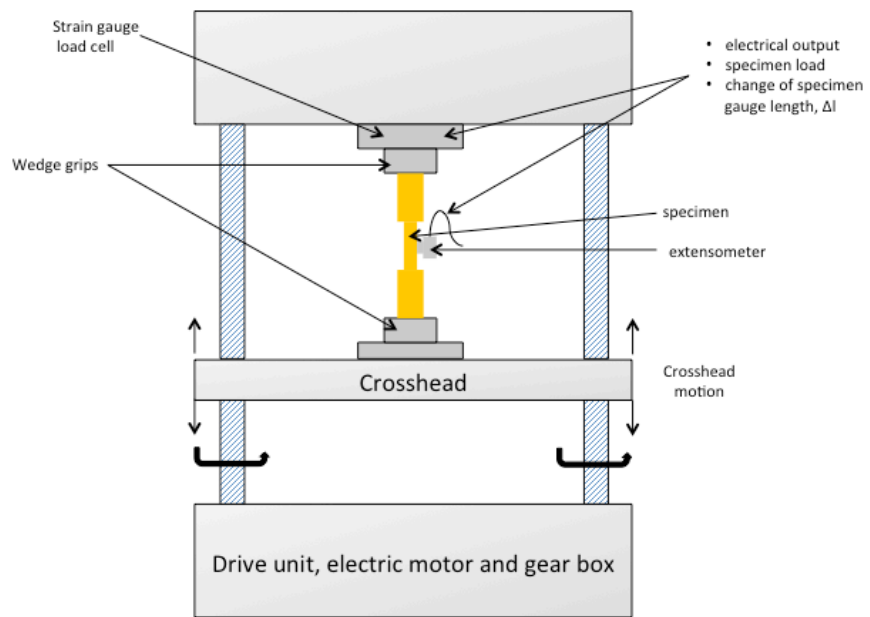
Figure 4.10 Schematic representation of the tensile test with the UTM.

The typical data from the tensile test is shown in Fig. 4.11. Load and elongation data from the test is converted to engineering stress, s, and engineering strain, e, and is plotted to yield the stress-strain (s-e) curve. The equations for s and e are as follows [4.8]:

$$s = \frac{P}{A_o}$$ Equation (4.15)

$$e = \frac{L_f - L_o}{L_o}$$ Equation (4.16)

where P is the applied load, A_o is the original cross-sectional area, L_f is the final length, and L_o is the original length of the specimen.
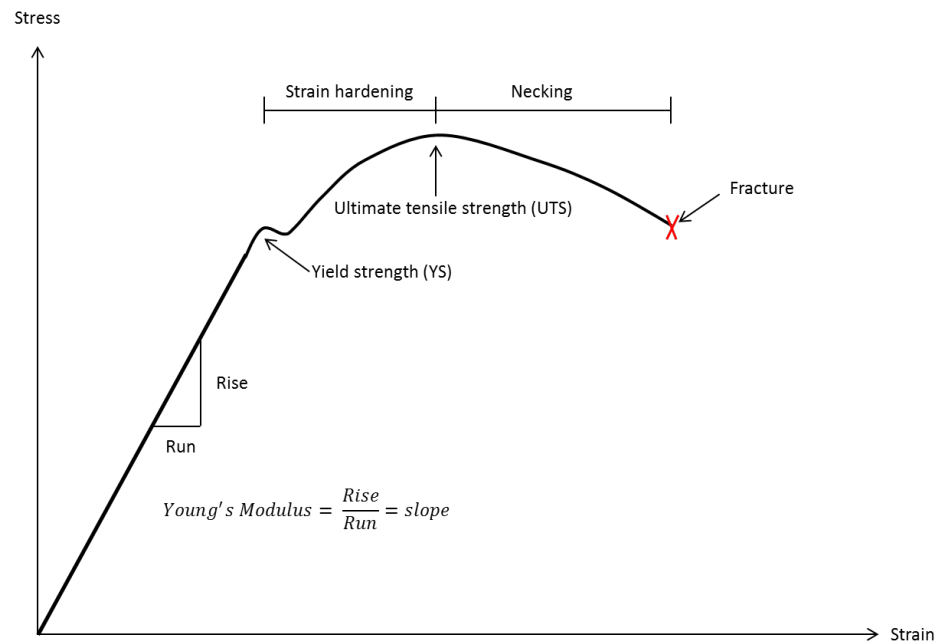
Figure 4.11 Typical stress-strain curve derived from the tensile test.

Several important properties are derived from the s-e curve including:

(i)   Elastic modulus, E

The elastic modulus, also known as Young's modulus, is a measure of a material's stiffness. It is derived from the slope of the initial linear region of the s-e curve.

(ii)   Yield strength (YS), σ_y

The yield strength is the minimum stress necessary to create plastic deformation in the material. YS may be taken from the s-e curve plot either by looking at the (i) stress corresponding to the plateau at the end of the linear region or (ii) or measuring the stress needed to create a specified amount of plastic deformation (0.2 or 0.3% offset yield strength).

(iii)   Ultimate tensile strength (UTS), σ_f

        The ultimate tensile strength is the highest stress that a material can withstand. This is taken from the stress corresponding to the highest point in the s-e plot. At the UTS, the specimen develops a neck where subsequent fracture will occur.

(iv)   Ductility, e_f

        The e_f refers to the total strain at fracture, and may be taken from the corresponding strain at the end of the s-e curve after elastic strain is deducted. Ductility may be taken from the change in length, L, or the reduction in area, A, of the specimen after the test:

$$e_f = \frac{L_f - L_o}{L_o} x100\% = \frac{A_o - A_f}{A_o} x100\% \qquad \text{Equation (4.17)}$$

where L_f is the final length, L_o is the original length, A_f is the final area and A_o is the original cross-sectional area of the specimen.

4.4.3.2 Test procedure

        The mechanical properties of the copper foil were determined using a Tinius Olsen H50KS tensile tester. The Horizon software was used for data collection (e.g. real-time plot of strain versus stress) and analysis. The foils were carefully peeled off from the steel substrate to prevent unnecessary structural damage on the specimen that could influence the mechanical properties of specimens. Three specimens were tested for each of the setting in both DC and PC plating. All tests were done at room temperature with crosshead speed of 10mm/min and tensile load of 500N. All tensile tests followed ASTM–E 345, which is the standard for determining tensile properties of metallic foils. The stress-strain (s-e) curve for each run was digitally recorded by

the equipment software. Tensile properties such as the 0.2% offset yield stress, ultimate tensile stress, and ductility were subsequently derived from the s-e curve.

4.4.4 SEM and EBSD

4.4.4.1 Operating Principle

The scanning electron microscope, SEM, is considered one of the most useful and the most versatile microscopes for materials characterisation. SEMs can provide topographical, morphological and compositional information about a material. The advantages of the SEM include [4.15]: (i) ease of use, (ii) rapid data collection and analysis, (iii) capacity for large specimens, (iv) option to do concurrent simultaneous chemical analysis (e.g. energy-dispersive (EDS) and wavelength-dispersive (WDS) spectroscopy, and electron-backscattered diffraction (EBSD), (v) images possess a depth of field giving a 3-D like quality to images, (vi) ability to image rough surfaces, and (vii) samples require minimal preparation.
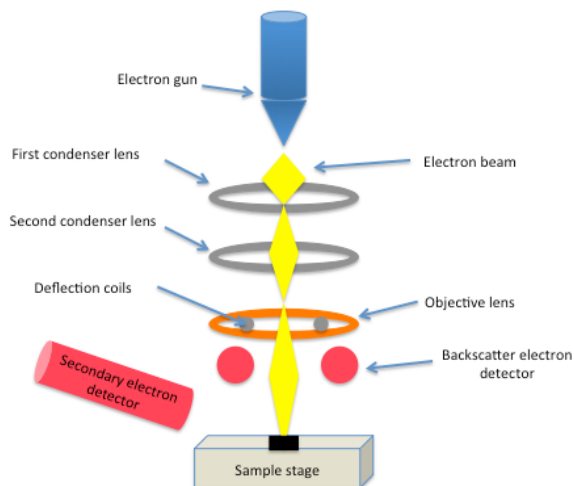
Figure 4.12 Illustration of scanning electron microscope with both the secondary and backscatter electron detector [Adapted from 4.7].

Figure 4.12 shows a schematic representation of the SEM. An electron gun is initially heated and emits a stream of electrons. Electromagnetic condenser lenses shapes and focuses this stream of electrons to create a beam of electrons that is made incident on the sample. The sample is made to take a positive charge and this further attracts electron interaction [4.16].
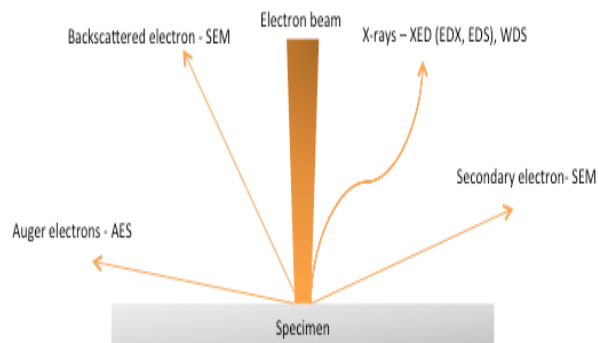
Figure 4.13 Illustration of the different products resulting from the interaction of the primary electron beam and the sample.

When the beam hits the sample, two types of electrons are produced: (1) secondary electrons and (2) backscattered electrons (shown in Fig. 4.13). Secondary electrons (SE) are produced when atoms absorb some of the incident energy and release their own electrons. A SE detector, which possesses a positive charge of about 300V, picks up these secondary electrons and uses the information to produce the image. In the SEM, the beam is continuously scanned over the material. SE typically come from surface atoms, and thus is best used for imaging surface features.

Backscattered electrons (BE) are electrons that are reflected from the surface due to inelastic collision of the incident beam with the atoms of the analysed

specimen. BE may originate not only from the surface but also from a greater depth in the material. Since the energy of BE is affected by atomic mass, BE are best used for creating a phase contrast image. In this type of imaging, contrast (black or white) is created due to difference in the atomic weight of the scanned or imaged phases.

The electron backscattered diffraction (EBSD), also known as the backscattered Kikuchi diffraction (BKD), is an attachment to the SEM that allows analysis of microstructures revealing grain morphology, microtextures, phase identities, defects and crystal strain. The EBSD extends the usual advantages gained by using the SEM as the EBSD offers the ability to do concurrent, rapid diffraction analysis and yield crystallographic information and imaging with resolution less than 0.5 um.

EBSD data is collected by positioning the electron beam to hit the SEM specimen at fairly small angles ($\sim20^{o}$), as shown in Fig. 4.14. This small angle of incidence to the specimen surface allows the production and escape of diffraction emissions from the material. The electron beam probes the surface of the sample point by point across a grid of positions in the scanning electron microscope. At each point, the backscattered electrons are collected by a detector. The detector comprises of a scintillator screen coupled by a lens to an imaging detector such as a charge coupled device (CCD) camera. The result is an electron backscatter diffraction pattern, also referred to as Kikuchi lines, that is processed by a computer for indexing. EBSD results are analysed in real time and yields rapid microstructural information. An example of an EBSD image with an accompanying pole figure is shown in Fig. 4.15. Each color in this phase map denotes a crystallographic plane that would be identified by the pole figure.
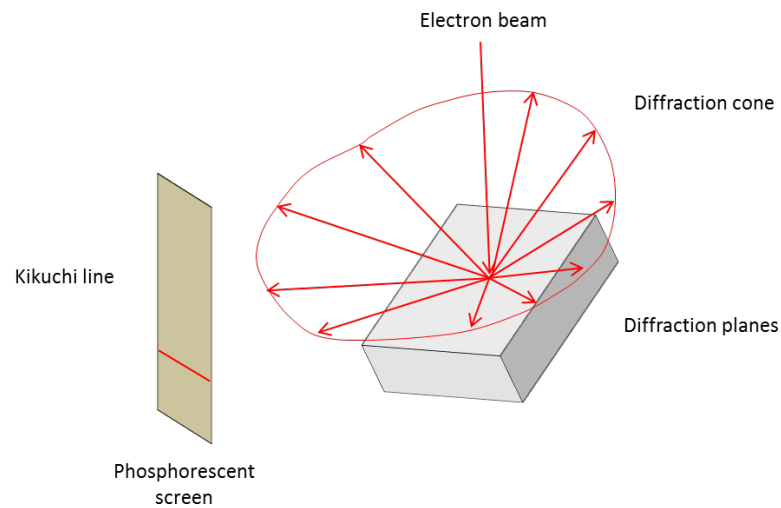
Figure 4.14 Schematic of the production of Kikuchi lines during an EBSD test.
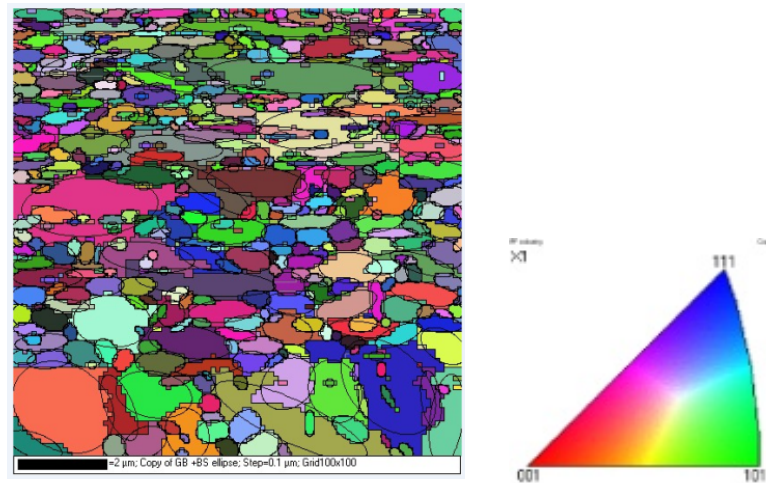
Figure 4.15 Example of an EBSD phase map and corresponding orientation legend.

4.4.4.2 Test procedure

Microstructural analysis (e.g. grain size and grain shape analysis) of the plated copper foils was performed using a JEOL JSM-5300LV SEM with an EBSD system was used. The software TANGO (HKL channel5 system) was used for the EBSD image analysis. Tango is a post-processing software that allows users to

obtain a number of information from an EBSD image, including grain size analysis, misorientation profile, strain contouring and recrystallised fraction component.

The copper film was cut using a sharp blade to a 1x1 cm^2 size. The specimens were cleaned using the following procedure:

(1) Dipped in 18 M HCl for 30 seconds

(2) Rinsed in water for 30 seconds

(3) Swabbed with acetone to remove organic substances

The copper films were mounted on an aluminum stub and loaded in the SEM. Sample imaging was done at 250X and 2500X magnifications.

4.5 Measurement of the Throwing Power of Additive-containing EnFACE electrolyte in DC Plating

Throwing power is the ability to create deposits of uniform thickness. This ability is important in electronics applications. In PCBs, for example, electroplated copper films of uniform thickness are necessary to provide good electrical conduction. The throwing power of the solution is poor when used for plating recessed areas such as through-holes and vias. Since the EnFACE process was earmarked for copper plating applications in the electronics industry, then we need to assess the throwing power of the EnFACE electrolyte with additives in comparison with that of the standard electrolyte used in the industry.

4.5.1 Materials and Apparatus

The Printed Circuit Boards (PCB) were supplied by Merlin Circuit Technology Ltd., UK. The company provided 6 x 6 inches boards with through

holes (200μm, 350μm and 500μm) as shown in Fig. 4.16. The PCB's possessed a layer of electroless copper that makes the boards conductive, and another layer of flash-plated copper (<5μm) to avoid oxidation of the electroless copper.

A two-electrode cell was used, which is appropriate for DC plating. Two copper plates with an immersed area of 75 cm^2 each were used as the anode.
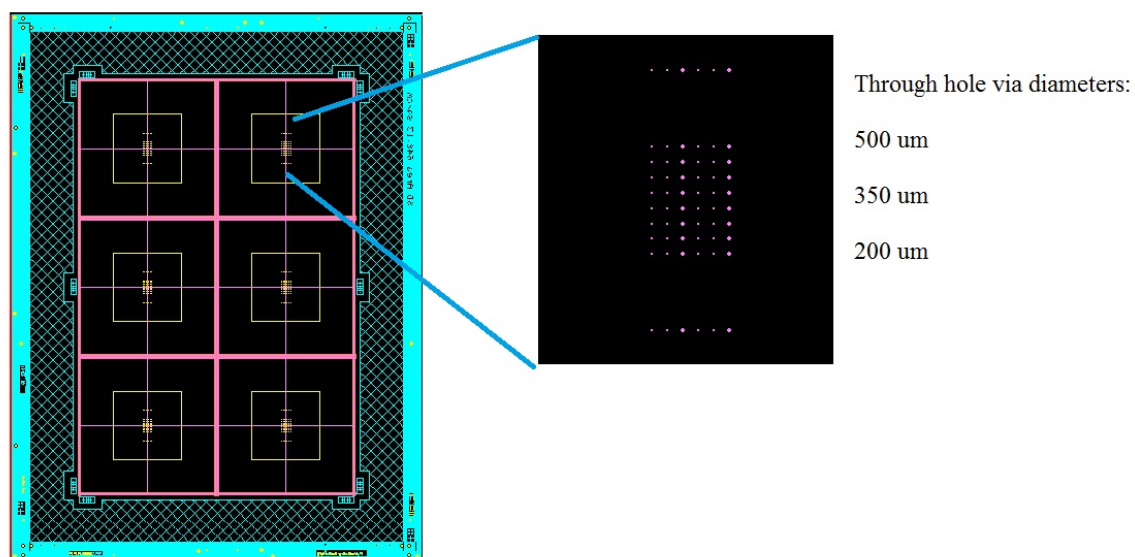
Figure 4.16 PCB design from Merlin Technologies Ltd.

All plating solutions were prepared using technical grade CuSO$_4$ and laboratory grade H$_2$SO$_4$. The additives used were Copper Gleam HS-200A, Copper Gleam HS-200B (Dow chemicals) and laboratory grade 37% HCl (Sigma Aldrich) solution. The Slotetch 584 salt (Schoetter Surface Technology) was used as copper etchant.

The copper deposit was characterised using Yenway optical microscope (CX40 optical). The data was analysed using Image J. The Image J software is an

image processing software that lets the user measure the thickness of a deposit, grain size analysis etc.

4.5.2 Plating Procedure

To prepare the boards for copper plating, the layer of flash-plated copper was etched using an acidified Slotetch 584 salt solution. The solution consisted of 60 g/L Slotetch salt and 10 ml/L 18M sulphuric acid. The PCB was etched for 5 minutes, with an estimated etch rate of 0.7 μm/minute in the absence of agitation.

After etching, the PCB substrate was prepared using the following procedures:

(1) One side of the PCB was uniformly coated using photoresist (Rapid electronics) leaving a plating area of $15 cm^2$. Coating was done to control the area where deposits will plate, and minimise the applied operating current.

(2) The coated PCB was baked in an oven (Thermo Scientific[TM]) for 20 minutes at 50^oC to cure the photoresist.

(3) Steps 1 and 2 were repeated on the other side of the PCB.

Table 4.12 lists the composition of the different electrolytes, while Table 4.13 shows the plating parameters used in these experiments. The desired deposit thickness was set at 25μm, which again is the copper film thickness that the electronics industry requires for PCB's. The plating time for this deposit thickness was calculated using Faraday's equation (Equation 4.1).

Table 4.12 Composition of electrolytes used for throwing power experiments (DC plating).

Designation	CuSO₄ (M)	H₂SO₄ (M)	Gleam B (ml/L)	Gleam A (ml/L)	HCl (ppm)
E-0	0.1	x	x	x	x
E-33	0.1	x	3.3	0.17	23
E-50	0.1	x	5.0	0.25	35
S-100	0.63	2.04	10	5	70

Table 4.13 Plating parameters used for throwing power experiments.

Settings	Plating current 40% of $I_{d,lim}$ (mA)	Plating time (min)
E-0	68	536
E-33	63	579
E-50	58	629
S-100	245	149

At the end of plating, the PCBs were removed from the solution and washed with deionised water for 1 minute. The surface was dried with lint free cloth and stored.

The four specimens (E-0, E-33, E-50 and S) were sent to Merlin technologies Ltd. for microsectioning. These specimens were then shipped back to the University of Strathclyde for further characterisation.

The specimens were mounted on a polymer resin for microscopy analysis. The thickness of the deposit was measure at the exposed area (H_a), edge/hole mouth (H_b) and center (H_c) of the through hole as shown in Fig. 4.17. Throwing power was assessed using the equation:

$$TP = \frac{H_c}{H_a} \; x \; 100$$

Equation (4.18)
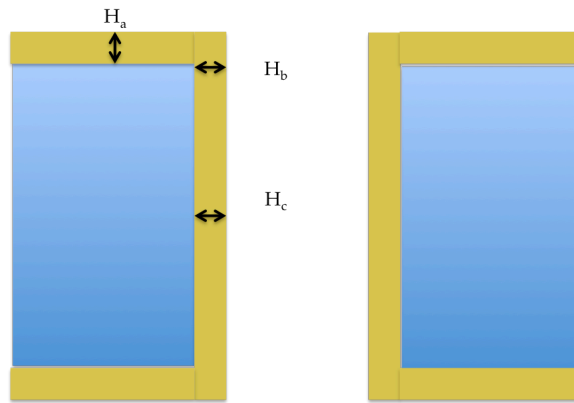
Figure 4.17 Illustration of the exposed area (H_a), edge/hole mouth (H_b) and center (H_c) area of the through hole.

In this chapter, the methods to conduct (i) polarisation and (ii) DC and PC plating experiments on the standard and EnFACE electrolytes were described. The chapter also included a brief description of the operating principles and the methodology of the different characterisation techniques performed on the plated copper films. Finally, the method to assess the throwing power of the additive-containing EnFACE electrolyte in DC plating was presented.

References

4.1   Yang L (2008) Techniques for corrosion monitoring. 1st edition Woodhead Publishing CRC Press Abington Cambridge England

4.2   Roy S, Pintauro PN (1993) Analysis of Convective Mass Transfer by Potential Relaxation. J. Electrochem. Soc. 140(11); 3167-3175

4.3   Rohm and Haas (2007) Copper Gleam HS-200 vertical acid copper for PWB metallization application. Electronic Materials Circuit board technologies CB07N009 Rev.1

4.4   IPC-TM-650 Test Methods (1980) Number 2.4.18, Tensile Strength and Elongation of Copper Foil. The Institute for Interconnecting and Packaging Electronic Circuits, Northbrook, IL

4.5   Hansal EGW, Roy S (2012) Pulse plating. 1st edition Eugen G Lueze Verglag KK Germany

4.6   Cullity BD, Stock SR (2001) Elements of X-Ray Diffraction. 3rd ed Prentice-Hall Inc; 167-171

4.7   Moller P, Nielsen LP (2013) Advanced Surface technology. Vol 2 Moller and Nielsen, Denmark

4.8   Callister WD, Rethwisch DG (2014) Materials science and engineering: an introduction. 6th ed John Wiley and Sons Inc. Hoboken NJ USA

4.9   Williamson GK, Hall WH (1953) X-ray line broadening from filed aluminum and wolfram. Acta. Metall. 1(1); 22–31

4.10   Cherkaoui M and Capolungo L (2009) Atomistic and continuum modelling of nanocrystalline materials: Deformation mechanisms and scale transition. Springer New York USA; 9-12

4.11   Liao CN, Lin CY, Huang CL, Lu YS (2013) Morphology, Texture and Twinning Structure of Cu films prepared by Low-Temperature Electroplating. J of The Electrochem Soc 160(12); D3070-D3074

4.12   The International Centre for Diffraction data – ICDD Powder Diffraction File 2 database. ICDD.com. N.p (1999) Web. 28 Sept. 2014

4.13   Mineralogical Society of America - The American Mineralogist Crystal Structure Database. Minsocam.org. N.p (2010) Web. 16 Oct. 2014

4.14   Crystallography Open Database. Crystallography.net. N.p (2012) Web. 28 May 2014

4.15   Goldstein J, Newbury DE, Joy DC, Lyman CE, Echlin P, Lifshin E, Sawyer L, Michael JR (2003) Scanning Electron Microscopy and X-ray Microanalysis, 3rd Ed Springer-Verlag New York USA

4.16   Wilkinson A, Britton T (2012) Strains, planes, and EBSD in materials science. Materials today 15(9); 366–376

Chapter 5

Results and Discussion: Electrochemical Characterisation of Additive-containing EnFACE Electrolyte

The effect of additives on the plating deposit may be traced from the way it alters the mechanisms involved in the electroplating process. A change in cathode polarisation is just one of the manifestations of the additive's influence on the plating process. This section details the results of electrochemical analysis done on additive-containing EnFACE and standard copper electrolytes, and discusses the important implications of these results. All polarisation curves were obtained using a scan rate of $0.02V\ s^{-1}$.

5.1 Effect of Additives on Standard Copper Electrolyte

To establish a benchmark for the EnFACE electrolyte, the effect of additives on a standard copper electrolyte were studied first. The cathodic polarisation curves for the additive-free (S-0) and the standard electrolyte (S-100) with additives (i.e. Copper Gleam A, Copper Gleam B, and Cl⁻) at the industry-recommended concentrations are shown in Fig. 5.1. The curves possessed the regions of the typical polarisation plot. As a review, section A possesses the linear and exponential part of the curve where non-diffusional, kinetically-controlled reactions dominate plating. Section B, seen at the plateau corresponding to the limiting current density, i_{lim}, represents the region where mass transport-controlled reactions dominate. Finally,

section C represents other reactions that occur at higher potentials, such as the hydrogen evolution reaction.

The polarisation curve for the additive-containing standard electrolyte (S-100) is clearly shifted to lower current densities and more negative potentials compared to the additive-free standard electrolyte (S-0). Region A is more pronounced, and the start of the mixed-mode and limiting current regions occurred at more negative potentials. These results indicated plating suppression, which is a well-known effect of additives on electrode polarisation [5.1]. Section A, the activation controlled region, appeared to be the most affected by additives by showing the largest degree of shift among the three regions. This indicated the strong influence of additives on the non-diffusional mechanisms (i.e. charge transfer reactions) in the electrolyte. This is reasonable when one considers that additives, similar to Cu^{2+}, are known to adsorb at the cathode surface. The bulky molecular structure of additives can easily disrupt the electrical double layer, and consequently change the mechanics of charge transfer through this layer.

There was a slight decrease in i_{lim} when additives were used in the standard electrolyte. The i_{lim} measured were -20 mA cm^{-2} and -19.20 mA cm^{-2} for the additive-free and additive-containing electrolytes, respectively. The small difference between the i_{lim} values suggested that mass transport reactions were not considerably affected by additives. The amount of additive is small compared to the amount of ions (i.e. coming from the acid and copper salt) present in solution; and such a small quantity would probably not hinder ion movement in the electrolyte.

Finally, there was no significant difference between section C in the S-100 and S-0 polarisation curve, indicating that hydrogen evolution was unaffected by the additives.
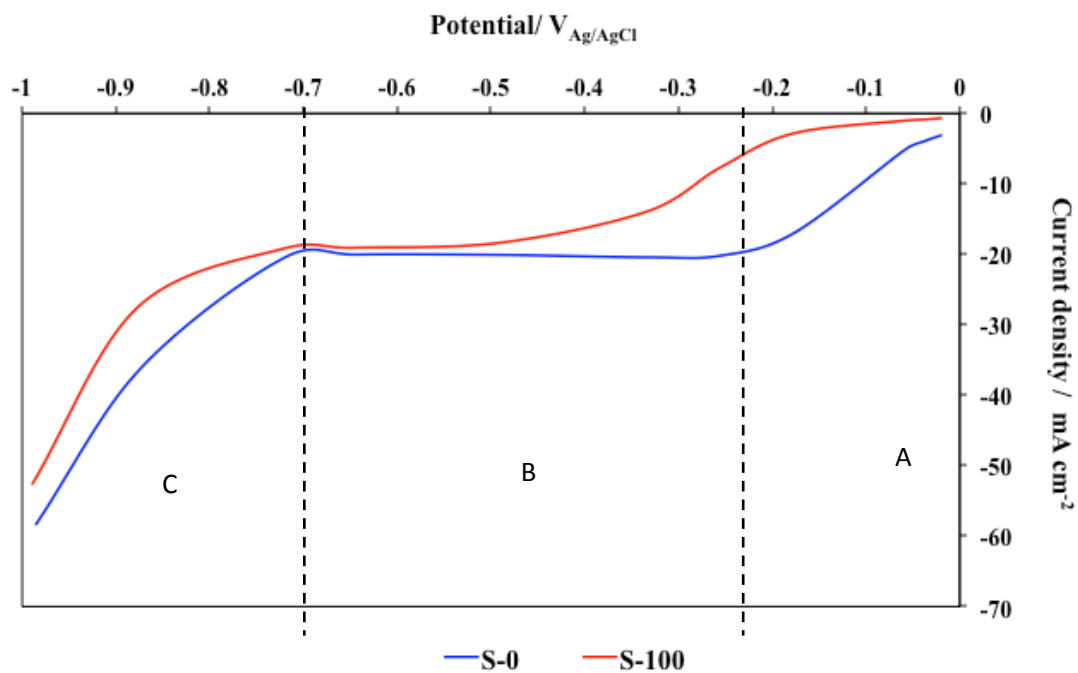
Figure 5.1 Potentiodynamic polarisation curves for standard plating electrolyte with (S-100) and without (S-0) additives; showing the kinetically controlled (A), mass-transport-limited (B), and hydrogen evolution (C) regions.

5.2 Effect of Additives on EnFACE Electrolyte

5.2.1 Potentiodynamic Experiments
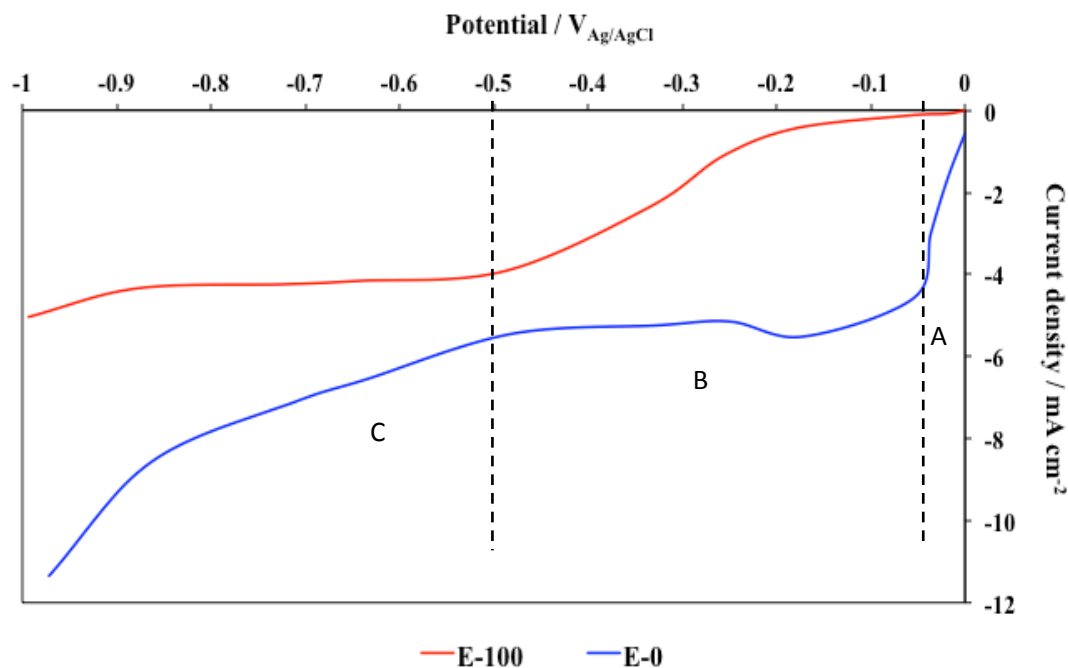
Figure 5.2 Potentiodynamic polarisation curves for EnFACE electrolyte with (E-100) and without additives (E-0).

Figure 5.2 shows the cathodic polarisation curves for the additive-free (E-0) and additive-containing (E-100) EnFACE electrolyte. The plot for E-100 electrolyte was shifted to lower current densities and more negative potentials; similar to what was observed in the S-100 electrolyte. The largest degree of shift in E-100 was observed in the kinetically controlled region section A. An appreciable shift to more negative potentials was also seen in the mass transport-limited region section B.

These results lead to two conclusions. First, the additives had a strong effect on the non-diffusional plating mechanisms in the EnFACE electrolyte, similar to what was seen in the standard electrolyte. Second, the additives also had considerable influence on the mass transport of copper ions in the EnFACE electrolyte; in contrast with the standard electrolyte. This may be due to two factors: (i) the low concentration of copper and (ii) the absence of acid in the EnFACE electrolyte. Due to the low population of Cu^{2+} in the EnFACE electrolyte, Cu^{2+} diffusion in the bulk solution was now altered by the presence of additive molecules.

To summarise, these results suggested that the additives had a similar effect on the polarisation behaviour in the EnFACE electrolyte as in the standard electrolyte; i.e. additives increased the cathode polarisation that resulted to plating inhibition.

5.2.2 EnFACE vs Standard Copper Electrolyte

5.2.2.1 Comparison of Additive-free Electrolytes

Figure 5.3 compares the polarisation curves obtained from the additive-free electrolytes, S-0 and E-0. Table 5.1 presents the limiting current density, i_{lim}, and the potential at which i_{lim} occurred. S-0 possessed a wide activation controlled region (i.e. region A), which transitioned to i_{lim} at about -0.25 $V_{Ag/AgCl}$. Region A of E-0 was short, and transitioned to i_{lim} at -0.05 $V_{Ag/AgCl}$. However, the slope of region A in both electrolytes is almost similar.

The mass transfer limiting currents, i_{lim}, for S-0 and E-0 are listed in Table 5.1, and shows that the i_{lim} of E-0 is about 75% lower than the i_{lim} of S-0. The i_{lim} for copper deposition from an acid-containing electrolyte such as S-0, $i_{\text{L,S-0}}$, and an acid-free electrolyte such as E-0, $i_{\text{L,E-0}}$, may be expressed by:

$$i_{L,S-0} = nFD \frac{C_{Cu,S-0}}{\delta_N} \qquad \text{Equation (5.1)}$$

$$i_{L,E-0} = nFD \frac{C_{Cu,E-0}}{\delta_N(1-t_+)} \qquad \text{Equation (5.2)}$$

where n is the oxidation number of Cu, F is the Faradays number, D is diffusivity of Cu in the electrolyte, C_{Cu} is the concentration of Cu^{2+}, δ_N is the thickness of the Nernst diffusion layer, and t_+ is the ion transport or transference number of the Cu cation. The ion transport number of Cu^{2+} becomes important in the EnFACE electrolyte because the electrolyte conductivity is wholly dependent on this cation.

Assuming that the diffusion layer for Cu^{2+} is similar in the two electrolytes, then (1) and (2) transforms to:

$$\frac{i_{L,S-0}}{i_{L,E-0}} = \frac{C_{Cu,S-0}}{C_{Cu,E-0}}(1-t_{Cu}) \qquad \text{Equation (5.3)}$$

Using the concentration of Cu^{2+} in the two electrolytes and the ion transport number of Cu^{2+} in the EnFACE electrolyte (t_+=0.358; [5.2]) the theoretical ratio of the limiting currents is equal to 4.04. On the other hand, the values shown in Table 5.1 yields an experimental value of the ratio equal to 3.92, which is similar to the

calculated theoretical value. This proves that the polarisation behaviour of the EnFACE electrolyte is primarily influenced by the low concentration of Cu^{2+}.

Results indicated that the EnFACE electrolyte has an inherently high cathode polarisation, in agreement with past studies. Taft and Messmore [5.2] observed that copper deposition for acid-free electrolytes was successful only at low current densities. At higher current densities, deposits were loose and spongy. This is an indication of the low i_{lim} in acid-free electrolytes; and the observed spongy deposit is a typical consequence of doing plating beyond i_{lim}.

The EnFACE electrolyte has low conductivity due to the low copper ion concentration and the absence of sulfuric acid; and this characteristic may have contributed to its high polarisation and low i_{lim}. The primary role of the acid and its influence in polarisation has already been extensively studied. Struyk and Carlson [5.3] proposed that the fundamental function of the acid in the plating electrolyte is to improve electrical conductivity and allow faster movement of charged species in the medium. In this manner, the acid reduces both anodic and cathodic polarisation [5.4]. Skowronski and Reinsoso [5.5] noted that specific conductivity of the electrolyte doubles when acid concentration is raised from 50 g/L to 100 g/L and at the level of 200 g/L, the resistivity further drops from 4.2 - 4.3 to 1.6 - 1.9 µΩ-cm. The low i_{lim} in the EnFACE electrolyte implies low deposition rates; and such can have an impact on actual plating operations.
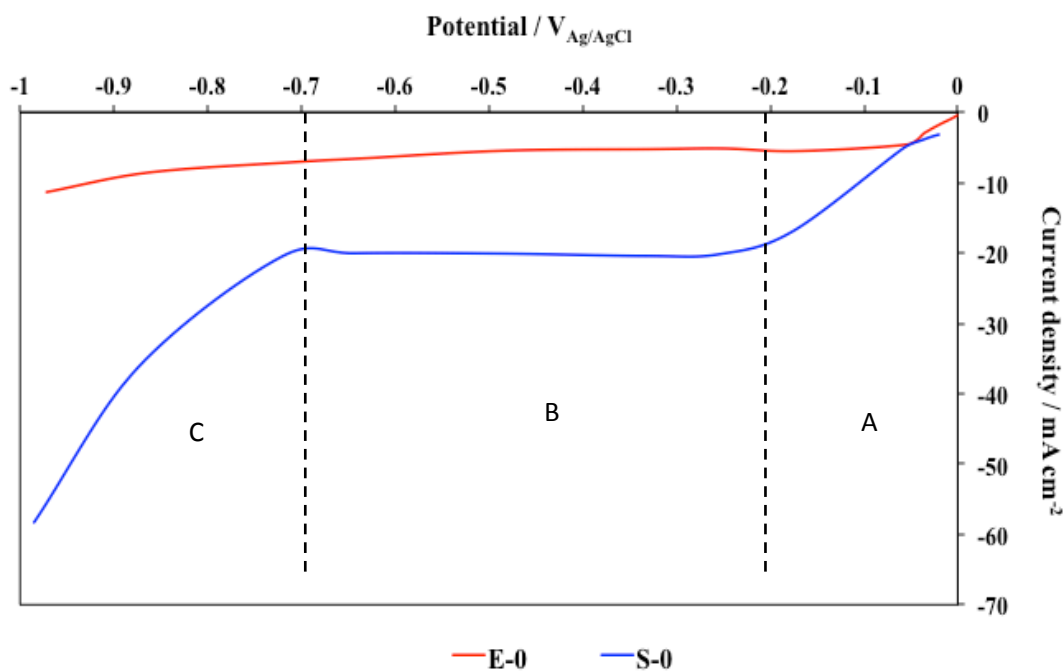
Figure 5.3 Comparison of polarisation curves of the EnFACE (E-0) and standard copper (S-0) electrolyte without additives.

Table 5.1 Summary of results of potentiodynamic experiments on additive-free standard and EnFACE plating electrolytes.

Plating electrolyte type	Without additive	
	Limiting current density, i_{lim} (mA·cm^{-2})	Potential at i_{lim} (V$_{Ag/AgCl}$)
Standard, S-0	-20.00	-0.25
EnFACE, E-0	-5.30	-0.20

Hydrogen evolution (HE) in the E-0 electrolyte occurred at a lower voltage

(-0.5 V$_{Ag/AgCl}$) than in the S-0 electrolyte (-0.8 V$_{Ag/AgCl}$). This indicated lower

hydrogen overpotential in the EnFACE electrolyte due to the absence of the acid and

the low concentration of Cu salt. It is known that hydrogen overpotential is

influenced by different factors including i) the nature of the cathode, ii) pH and the iii) applied current density [5.6].

It is known that performing voltammetry tests in unstirred solution results in the appearance of the peak current, i_p; while the same test in stirred solution results to the occurrence of the characteristic limiting current phenomenon, i_{lim}. The appearance of i_p is related to the increase in the thickness of the Nernst diffusion layer in the unstirred solution during the polarisation test. The Randles-Sevcik equation can be used to predict the value of i_p, as follows:

$$i_p = 0.4463nFAC\sqrt{\frac{nFvD}{RT}} \qquad \text{Equation (5.4)}$$

where, n equals the number of electrons involved in the redox reaction, v is the scan rate (V s^{-1}), A is the electrode area (cm^2), D is the diffusion coefficient of the analyte (cm^2 sec^{-1}), T is the absolute temperature (K), R is the universal gas constant (8.314 J mol^{-1}K^{-1}) and F is Faraday's constant (96485 C mol^{-1}). This equation is best used in conditions of rapid kinetics or in relatively slow potential scan rate [5.7, 5.8, 5.9]. Using Equation 5.4, the calculated i_p for S-0 and E-0 are 13 and 5.17 mA cm^{-2}, respectively.

Interestingly, all polarisation curves had no feature indicating i_p and instead had i_{lim}, despite all tests being done in unstirred solutions. This may be due to the use of working electrodes with small areas (i.e. 1 cm diameter) in the polarisation tests, and the presence of some natural convection in the solution.

5.2.2.2 Comparison of Additive-containing Electrolytes

Figure 5.4 compares the polarisation curves of the standard (S-100) and EnFACE (E-100) electrolytes containing additives; while Table 5.2 lists important information derived from these curves. These results mirror those obtained from the additive-free electrolytes. The huge difference in the i_{lim} of S-100 (-19.20 mA·cm^{-2}) and E-100 (-4.20 mA·cm^{-2}) is still apparent. Interesting information is obtained when the additive-induced change in the i_{lim} is computed. In the standard electrolyte, additives caused a drop of about 11% in the i_{lim} value; while in the EnFACE electrolyte, the reduction was about 20%. This implies that additives had a greater influence on polarisation in the EnFACE chemistry than in the standard electrolyte.

These results may be explained by considering the fractional additive surface coverage in each electrolyte. At a specified potential, the fractional surface area, Γ covered by the additive may be calculated [5.10]:

$$\Gamma = 1 - \frac{i_{add}}{i_{addfree}} \qquad \text{Equation (5.5)}$$

where i_{add} and $i_{addfree}$ refer to the current densities in the presence and absence of additives, respectively.
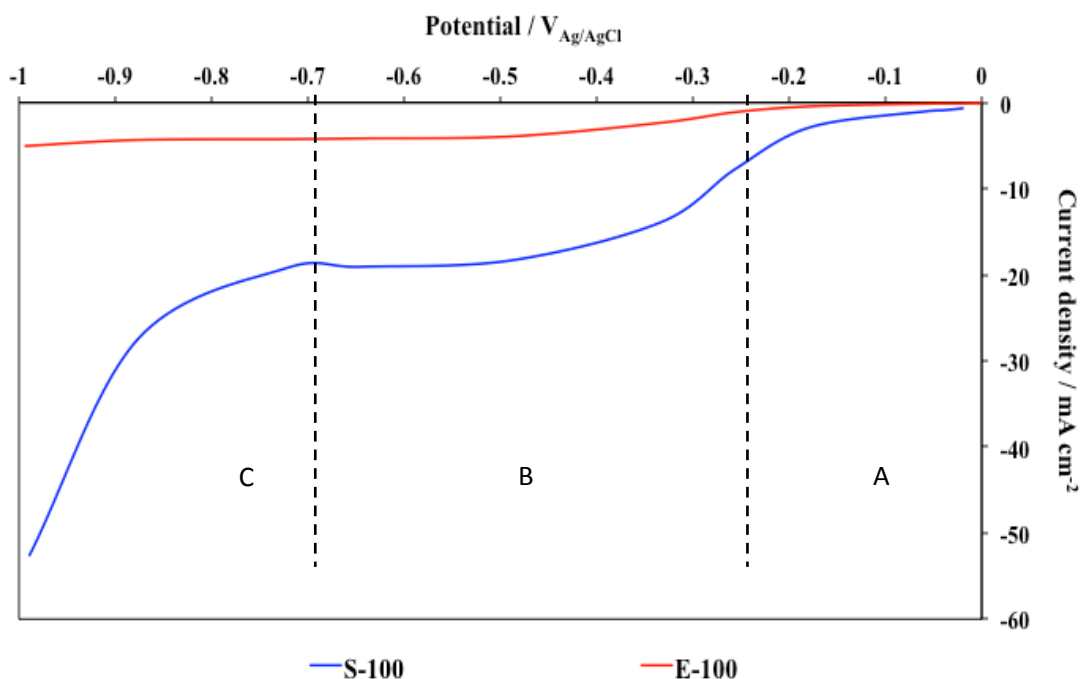
Figure 5.4 Comparison of polarisation curves for EnFACE (E-100) and standard electrolyte (S-100) with recommended amounts of additives.

Table 5.2 Summary of results of potentiodynamic experiments on standard and EnFACE plating electrolytes with additives.

Plating electrolyte type	With additive	
	Limiting current density, i_{lim} (mA·cm^{-2})	Potential at i_{lim} ($V_{Ag/AgCl}$)
Standard, S-100	-19.20	-0.45
EnFACE, E-100	-4.20	-0.40

Figure 5.5 presents a comparison of the additive coverage between S-100 and E-100 electrolytes. In both electrolytes, additive surface coverage was highest at low applied potentials, and then steadily decreased at higher potentials. The reduction in additive surface coverage at higher potentials may be explained several ways.

Additives may be lost during Cu^{2+} reduction as the additive became trapped in the nucleating crystal and was incorporated in the deposit. In fact, incorporated additives are a common concern for metal platers since these impurities could modify the ensuing properties of the deposit [5.11, 5.12]. Alternatively, Pasquale *et al*. [5.13] proposed that the adsorbed additive-ion complexes might be released from the electrode surface when the anchor atoms (e.g Cl^-) or molecules become enclosed by the growing deposit. On the other hand, it can be observed that greater additive coverage occured in the EnFACE electrolyte than in the standard electrolyte. A high surface coverage allows additive molecules to exert a greater influence on polarisation, and thus explain the high polarisation observed in the EnFACE electrolyte. The higher additive coverage in the EnFACE electrolyte would again be due to the EnFACE chemistry. A low copper salt content means there are less Cu^{2+} competing with additive molecules for space at the interface; thereby resulting to higher additive adsorption efficiency at the surface.
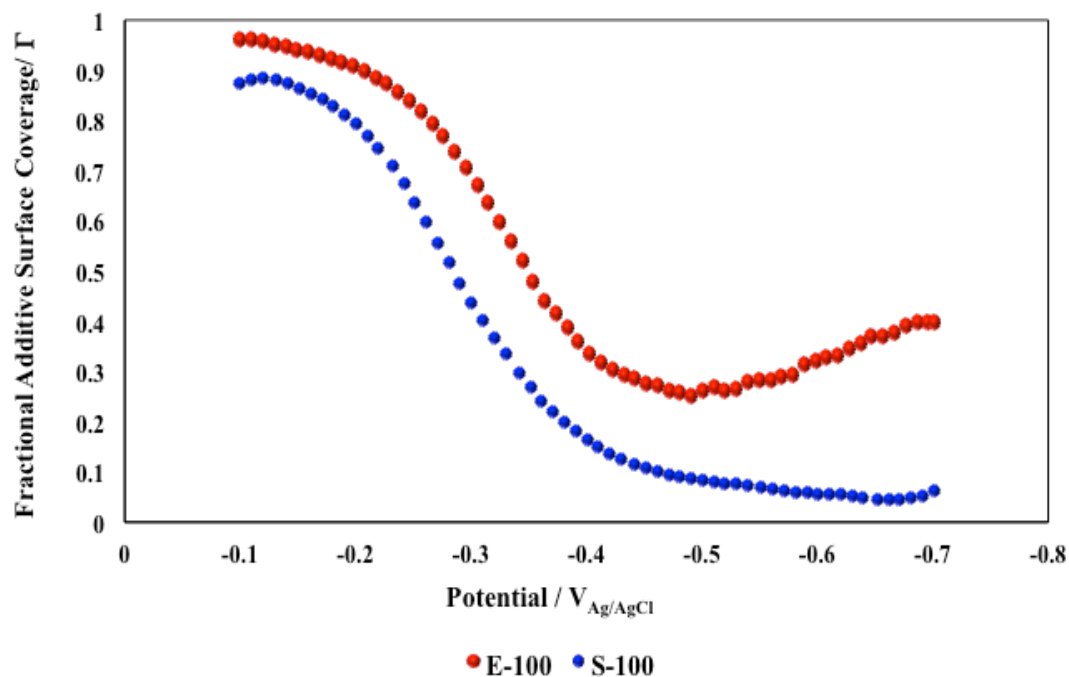
Figure 5.5 Plot of surface coverage versus potential for the standard (S-100) and EnFACE electrolyte (E-100) with additives.

5.3. Effect of Individual Additives on EnFACE Electrolyte

It is known that additives exhibit different behaviour when used individually and when used in combination with other additives. This section discusses the influence of different concentrations of individual additives on cathode polarisation in the EnFACE electrolyte.

5.3.1 Suppressor: Copper Gleam B

Figure 5.6a shows the polarisation curves for the plating electrolyte containing four different concentrations of Copper Gleam B. It is evident that increasing Copper Gleam B concentration: (i) caused the kinetically-controlled

regions to extend to more negative potentials; (ii) shifted the mixed control region and (iii) the onset of the i_{lim} plateau to more negative potentials. The i_{lim} decreased with increasing additive concentration, although the reduction in i_{lim} was not proportional to the increase in additive amount. Electrolytes B-33, B-50 and B-100 had similar i_{lim} values (4.93-4.95 mA·cm^{-2}). Figure 5.6b shows the additive surface coverage at different Copper Gleam B. The surface coverage in B-33, B-50 and B-100 did not show significant differences after it reached a potential of about -0.35 $V_{Ag/AgCl}$.

The results confirm that Copper Gleam B is a strong suppressor. While we can only speculate on the actual chemical components of Copper Gleam B, it is likely that Copper Gleam B would be a large organic molecule of high molecular weight like PEG. Therefore, our discussion on the action on Copper Gleam B will be based on the suppressive action of PEG. The strong inhibiting effect of PEG in the conventional acid-copper electrolyte is well known [5.1, 5.14]. Hill and Rogers [5.1] noted that adsorption, and consequently the suppressive action, of PEG is potential dependent and starts at around -150 mV$_{SHE}$. This behaviour was similarly observed in the current study. Chen *et al*. [5.15], using electrochemical impedance spectroscopy (EIS), explained that this inhibition is due to PEG-Cu+ complexes that are adsorbed at the electrode interphase. However, most research agrees that the inhibiting characteristics of PEG are more pronounced when a promoter (Cl$^-$) is present in the electrolyte [5.14, 5.16].
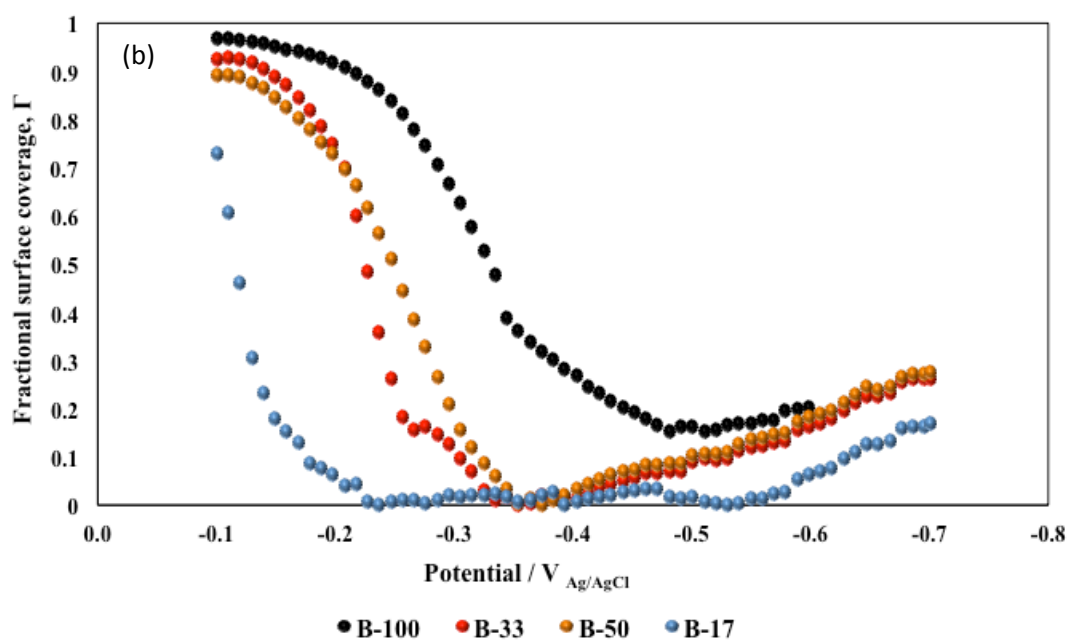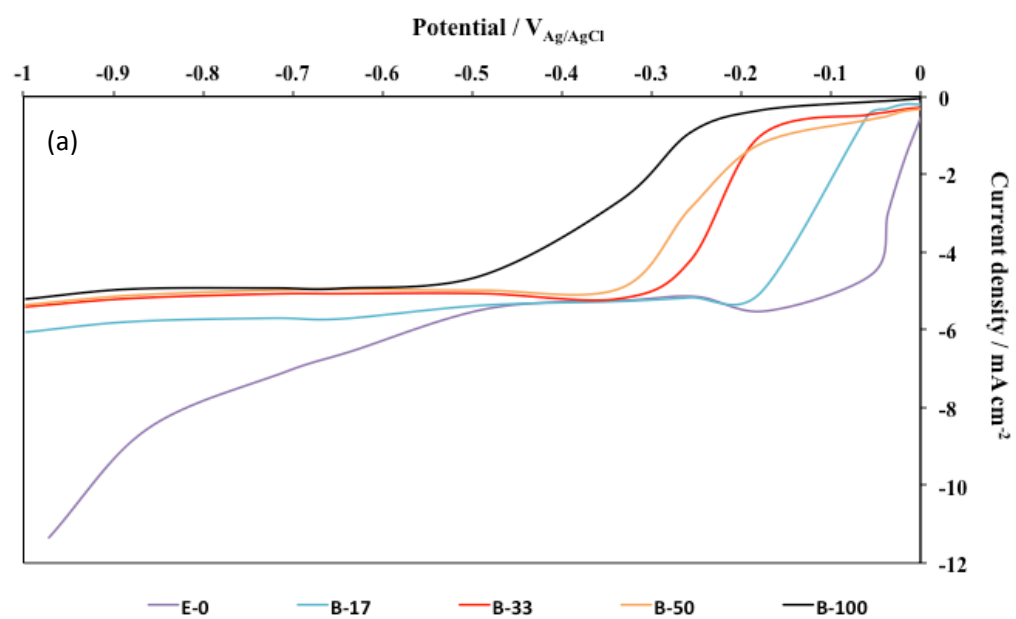
Figure 5.6 a) Cathodic polarisation curve and b) fractional additive surface coverage of the EnFACE electrolyte with varying concentrations of Copper Gleam B.

The observation that i_{lim} reached a maximum at B-33, and did not increase with additional additives is consistent with a polarisation plateau [5.17]. As discussed earlier, the polarisation plateau refers to a critical concentration where further addition of additives does not yield an appreciable increase in polarisation. Since the additive concentration in B-33 is about three times lower than the recommended, then using this additive dosage would be advantageous in practical application as it offers the chance to save on additive consumption and reduce operating cost. However, it needs to be mentioned that Copper Gleam B alone is a weak polariser, and is never used alone in the copper electrolyte. Thus, future work dealing on looking for the optimum additive concentration, which aims to get maximum polarisation at the lowest cost, should best consider multi-additive set-ups.

5.3.2 Accelerator: Copper Gleam A

Figure 5.7a shows the polarisation behaviour of the EnFACE electrolyte with different concentrations of Copper Gleam A; while Fig. 5.7b presents the additive surface coverage in these plating electrolytes. Again, the charge transfer region of the i-V curve was missing, and only the mixed-control and i_{lim} region were present. No significant shift in the polarisation curve was observed at low concentrations of Copper Gleam A (e.g. A-17 and A-33). However, at higher Gleam A concentrations, the curve shifted to lower i that indicated plating inhibition. Both the mixed-control and i_{lim} regions were changed, although the latter exhibited a greater shift. Inhibition was also found to be concentration-dependent, similar to those seen in Copper Gleam B.

Interestingly, Fig. 5.7b shows that surface coverage of Copper Gleam A increased as the applied potential becomes more negative, in contrast with the adsorption behavior observed in the suppressor Copper Gleam B. Also, additive coverage increased with increasing Copper Gleam A concentration.

The inhibiting effect of Copper Gleam A is somewhat surprising as accelerators are expected to depolarise the cathode [5.18]. However, several works, such as those of Kang *et al.* [5.19], Dow *et al.* [5.20] and Tan *et al.* [5.21], reported similar concentration-dependent inhibiting behaviour for the accelerator SPS when used as the lone additive in the conventional acid-copper sulfate electrolyte. Tan *et al.* [5.21] proposed that suppression was the result of the Cu(I)-thiolate complex present at the cathode. It is therefore probable that similar mechanisms are at play in the Copper Gleam A-containing EnFACE electrolyte.

The increase in adsorption of Copper Gleam A at more negative potentials means that additive adsorption and acceleration was a function of potential. Tan *et al.* [5.21] reported similar potential-dependent acceleration in SPS, a consequence of SPS reduction to MPS being also potential-dependent.
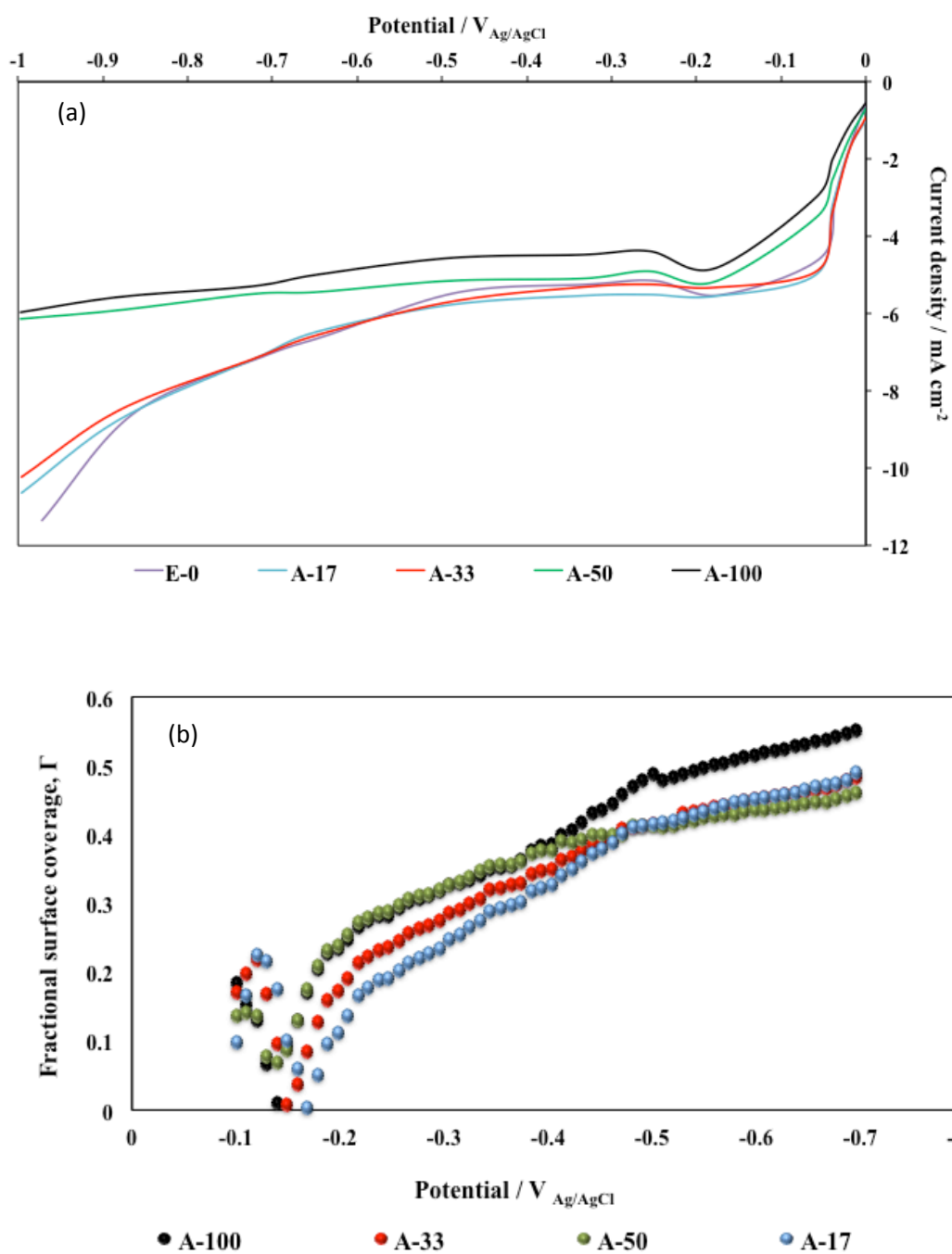
Figure 5.7 a) Cathodic polarisation curve and b) fractional additive surface coverage for the EnFACE electrolyte with different concentrations of Copper Gleam A.

5.3.3 Promoter: Cl⁻

Figure 5.8a and b shows the cathodic polarisation curve and additive surface coverage of the EnFACE electrolyte with different concentrations Cl^-, respectively. The i-V curves of the Cl^--containing electrolytes lacked the charge-transfer region and started at the mixed-control region. Cl^- shifted the curves to lower i both in the mixed-control and i_{lim} regions, indicating plating inhibition. The degree of inhibition progressively increased with increasing amounts of Cl^-, suggesting concentration-dependent polarisation in the electrolyte.

Figure 5.8b indicates that Cl^- adsorption was initially high at low potentials, approached a minimum at around -0.2 to -0.3 $V_{Ag/AgCl}$, and then subsequently increased at the more negative potentials. The trend in the curves suggested that surface coverage increased with increasing Cl^- concentration, with the exception of C-33 that gave unexpected results.

Past studies reported the ability of Cl^- to increase cathode polarisation in copper electrolytes [5.22, 5.23, 5.24, 5.25]. Soares *et al.* [5.24] proposed that this is due to the formation of a passive layer of CuCl at the cathode when the Cu^{2+} concentration of the electrolyte exceeds 1mM. The recommended Cl^- concentration used in this study is about 2mM; thus, it is conceivable that the formation of the said CuCl film caused the observed polarisation. At concentrations less than 1mM, Cl^- acts as a depolariser and can catalyse the Cu^{2+} reduction reaction [5.26, 5.27].

Results indicated that Cl^- adsorption is also potential dependent. Moffat *et al.* [5.28] reported similar potential dependency in Cl^- adsorption. The minimum

adsorption occurring at around -0.2 to -0.3 $V_{A/AgCl}$ is consistent with the observed

ordered adsorption state of Cl^- at low applied overpotentials. On the other hand, the

increase in adsorption at more negative potentials is due to the creation of a more

disordered Cl^- adlayer at the cathode.
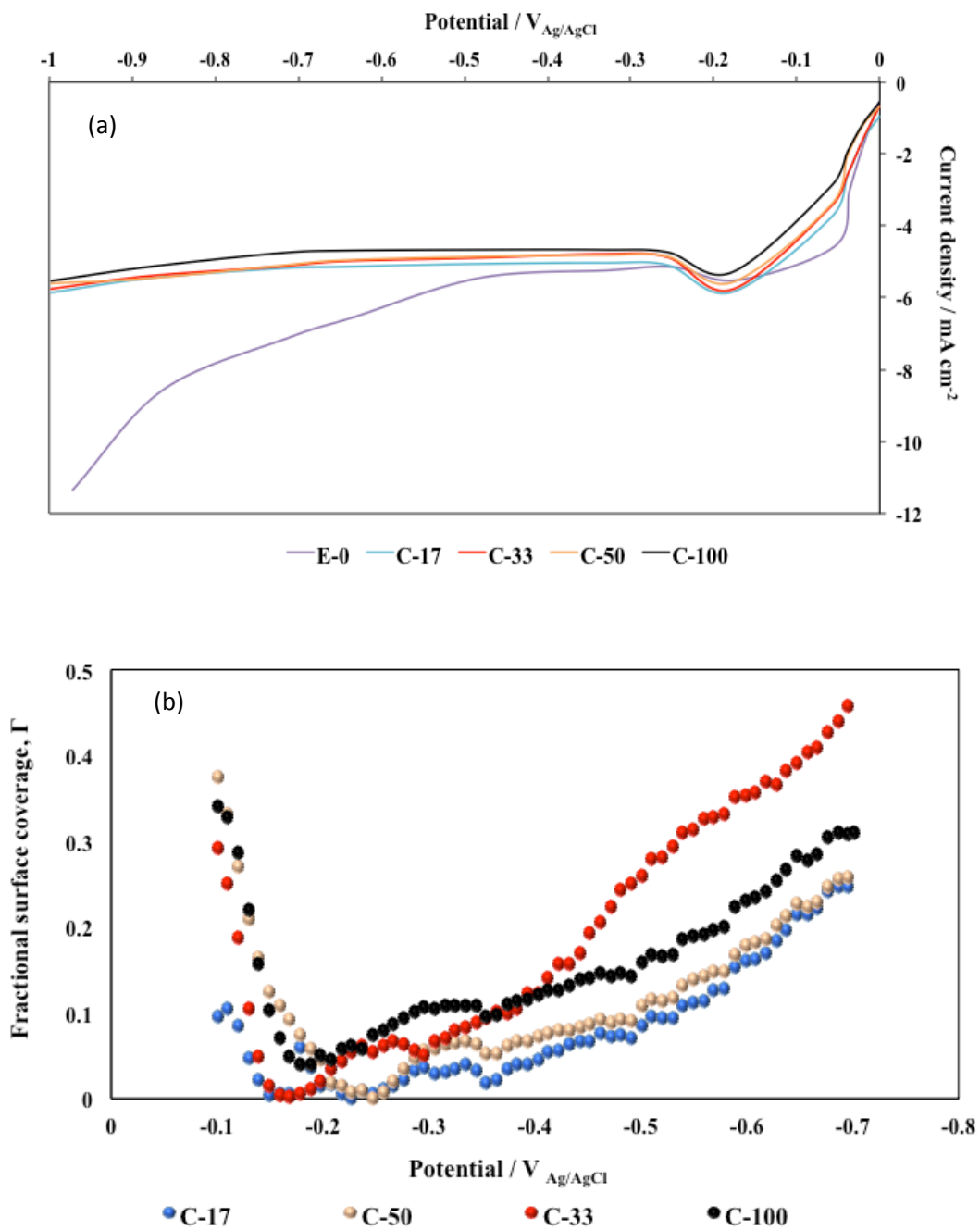
Figure 5.8 a) Cathodic polarisation curve and b) fractional additive surface coverage for the EnFACE electrolyte with different concentrations of Cl⁻.

5.3.4 Comparison of the Effect of Individual Additives
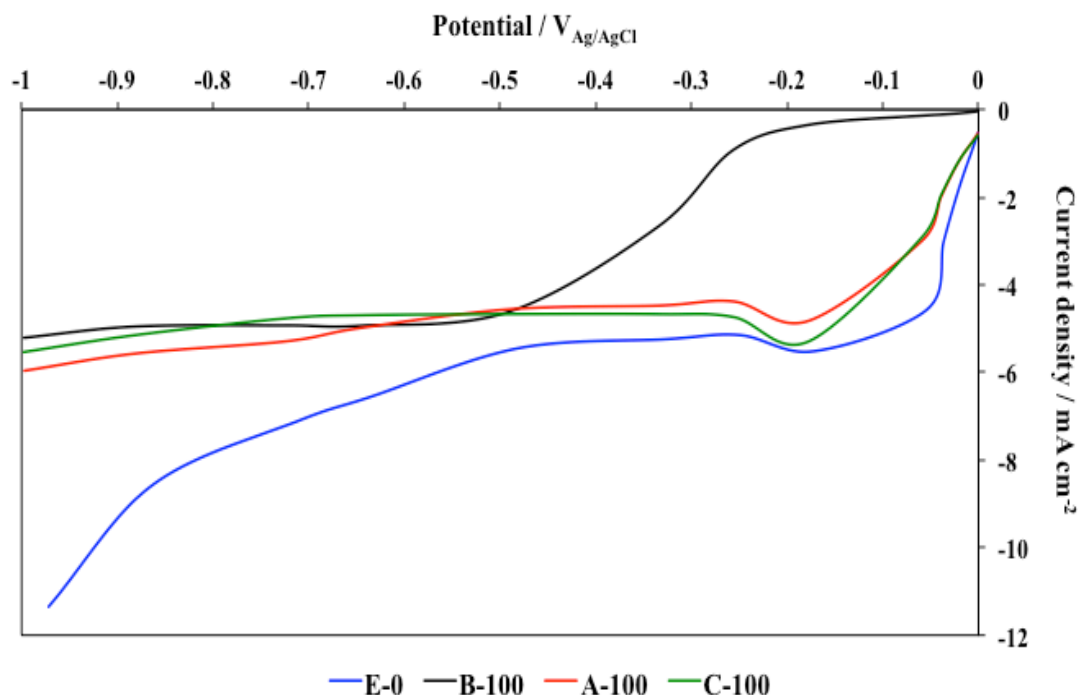
Figure 5.9 Cathodic polarisation curves of EnFACE electrolyte without (E-0) and with single additives Copper Gleam A (A-100), Copper Gleam B (B-100) and Cl⁻ (C-100).

Figure 5.9 presents the cathodic polarisation curves of the EnFACE plating electrolyte before (E-0) and after addition of Cl⁻ (C-100), Copper Gleam B (B-100) and Copper Gleam A (A-100). When added separately the three additives caused cathode polarisation in the EnFACE electrolyte. However, the degree of polarisation or inhibition, which is judged from the amount of shift to lower i and higher potentials, depends on the type of additive. Copper Gleam A and Cl⁻ created similar although modest levels of inhibition. Copper Gleam B caused significant polarisation, especially at the charge-transfer regions.

The strong inhibition seen in Copper Gleam B may be linked to the degree of adsorption and consequent surface coverage of the cathode by the additives. A larger molecule can cover a bigger surface and cause greater suppression. The molecules of Copper Gleam B is believed to be relatively larger compared to the molecules of Copper Gleam A and Cl⁻, as would be if one were a PEG-type and the other an SPS type-additive. Interestingly, the i_{lim} in the electrolytes with single additive were similar. This suggests that i_{lim} is independent of the type of additive used. The steady value of the i_{lim} may be caused by mass transport-limited reduction of Cu^{2+}. Finally, the additives increased the hydrogen overpotential and hydrogen evolution occurred at a higher potential.

5.4 Effect of Mixed Additive in EnFACE Electrolyte

5.4.1 Effect of Copper Gleam B and Cl⁻

Figure 5.10a shows the cathodic polarisation curve for the EnFACE plating electrolyte with Cl⁻ (C-100), Copper Gleam B (B-100), and Copper Gleam B-Cl (BC-100) at industry recommended concentrations; and Fig 5.10b presents the additive surface coverage in these electrolytes. The B-100 and BC-100 plots were quite similar, displaying the full sigmoidal shape of the curve. The charge-transfer region of the B-100 and BC-100 electrolyte did not have significant difference. At the mixed control and the i_{lim} region, the BC-100 plot shifted to lower i values. To illustrate, BC-100 electrolyte has an i_{lim} of about 3.0 mA·cm⁻², while the B-100 and C-100 electrolytes have i_{lim} of 5.0 mA·cm⁻². This indicates that a further increase in

plating suppression occurred after the two additives were combined, and confirms the synergistic effect of Cl^- and Copper Gleam B on plating suppression.

The current results are consistent with past studies that observed the strong plating inhibition caused by the combination of a suppressor (PEG) and a promoter (Cl^-) [5.12, 5.17, 5.18, 5.29]. Using the PEG model, studies suggest that inhibition was due to the presence of the PEG-Cu^+-Cl^- complex at the cathode [5.30, 5.31]. Feng *et al*. [5.32] proposed that Cl^- acts as a strong anchor and secures the PEG-Cu^+ complex to the cathode surface. Hai *et al*. [5.33] further suggested that the PEG branches could interlink creating a large network of interlinked suppressor complex that effectively covers a huge area of the substrate surface.
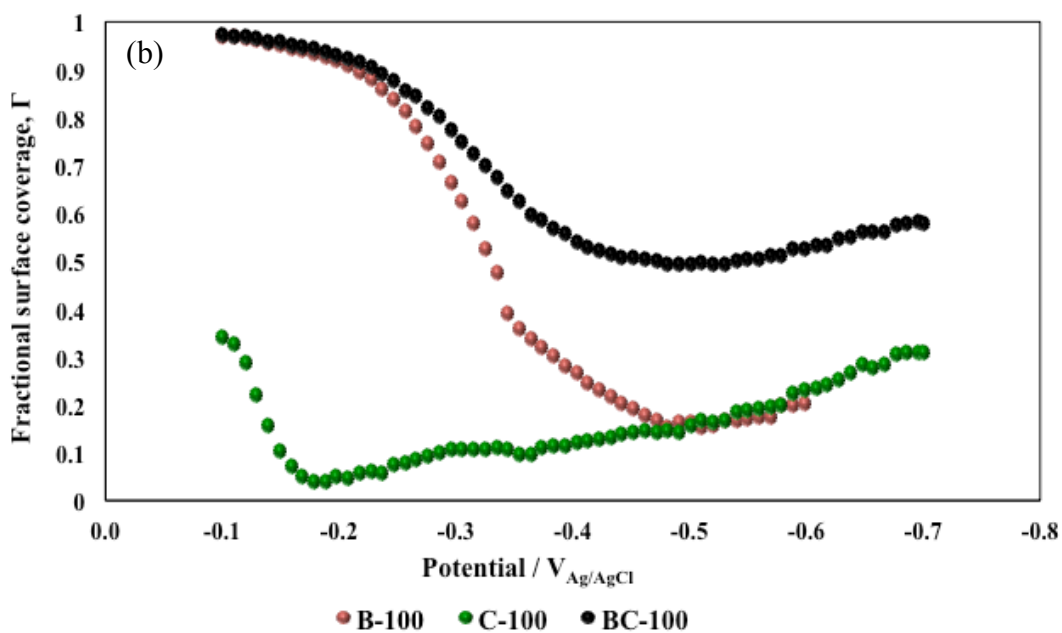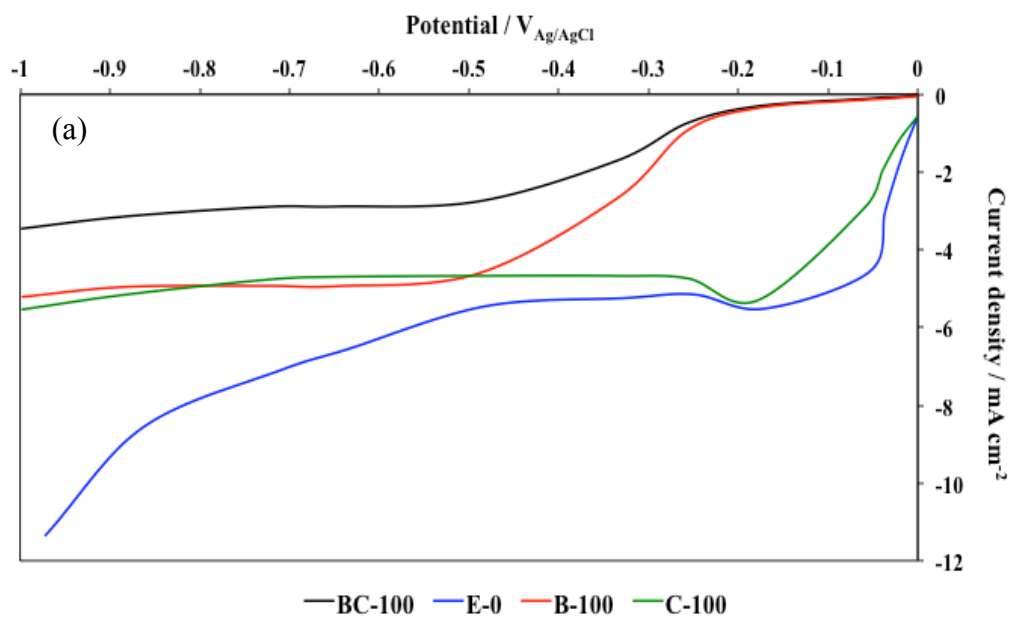
Figure 5.10 a) Cathodic polarisation curve and b) fractional additive surface coverage for the additive-free (E-0) and additive-containing Cl⁻ (C-100), Copper Gleam B (B-100) and Copper Gleam B-Cl⁻ (BC-100) EnFACE electrolyte.

The synergistic effect of Copper Gleam B and Cl⁻ may also be explained by looking at Fig. 5.10b. Clearly, the Copper Gleam B- Cl⁻ (BC-100) mixture had higher additive surface coverage compared to individual Copper Gleam B (B-100) and Cl⁻ (C-100) additions. This coverage also does not drop steeply even at high potentials. This suggests very strong surface attachment of the additive molecules, and correlates well to the strong polarisation behaviour observed.
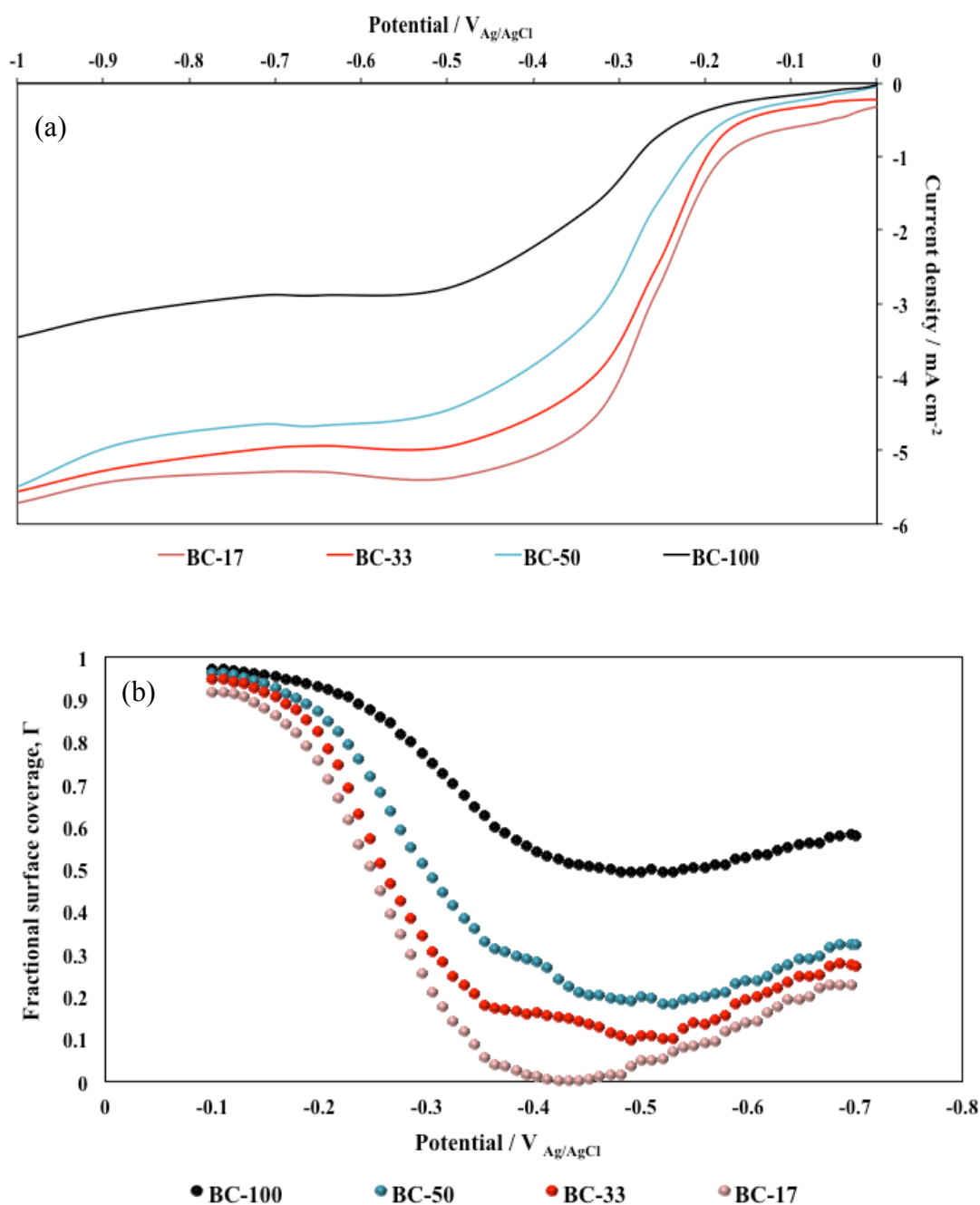
Figure 5.11 a) Cathodic polarisation curve and b) fractional additive surface coverage for the EnFACE electrolyte with different concentrations of the Copper Gleam B- Cl⁻ (BC) mixture.

Figure 5.11a shows the effect of varying concentrations of the Copper Gleam B- Cl⁻ mixture on cathode polarisation; while Fig. 5.11b shows the additive surface coverage in these electrolytes. The four curves possessed sigmoidal shapes. Clearly, increasing additive concentration increased cathodic polarisation and plating inhibition, as seen in the progressive shift of the curves to higher potentials and to lower i_{lim}. The trend indicates a concentration-dependent polarisation, similar to what was observed in the single-additive experiments. The result is also consistent with Fig. 5.11b that shows an increase in additive surface coverage with increasing additive concentration.

5.4.2 Effect of Copper Gleam A-Copper Gleam B- Cl⁻

The effect of combining all three additives; i.e. Copper Gleam A, and Copper Gleam B, Cl⁻ on cathodic polarisation of the EnFACE electrolyte is shown in Fig. 5.12a. Figure 5.12b shows the additive surface coverage in the different electrolytes. It was seen earlier that the mixture of Copper Gleam B and Cl⁻ electrolyte caused synergistic inhibition at the diffusion-limited regions. However, an interesting phenomenon was seen with the addition of the accelerator, Copper Gleam A, to the Copper Gleam B-Cl⁻ electrolyte. While the charge-transfer region appeared unaffected, the mixed control and i_{lim} region were found shifted to higher current densities. The upward shift in the i-V curve suggests that Copper Gleam A caused plating acceleration in the mass-transport region. Finally, Fig. 5.12b confirms that the additive surface coverage was reduced after Copper Gleam A was added to the Copper Gleam B-Cl⁻-containing (BC) electrolyte.

The accelerating effect of Copper Gleam B, when used with Copper Gleam A and Cl$^-$ that was seen in the EnFACE electrolyte is similar to those reported when SPS is added to PEG-Cl$^-$-containing conventional copper electrolytes [5.21, 5.32]. It is believed that the accelerator SPS reacts with CuCl to form the Cu(I) thiolate molecule [5.33]. The thiolate molecule can decrease the effect of the PEG-Cl$^-$-Cu complex suppressor at the cathode surface; either by directly competing with the suppressor for the Cu ion, or by weakening the bond between the suppressor and the cathode surface. In both ways, the SPS reduces the presence of the PEG molecule in the cathode, consistent with the observed reduction of additive surface coverage after the addition of Copper Gleam A in the Copper Gleam B-Cl$^-$ mixture shown in Fig. 5.12b. It is thus likely that similar mechanisms caused the acceleration observed in the EnFACE electrolyte.

Figure 5.12 a) Cathodic polarisation curve and b) fractional additive surface coverage for the EnFACE electrolyte without (E-0) and with different types of additives: Copper Gleam B (B-100), Copper Gleam B-Cl⁻ (BC-100), and Copper Gleam A-Copper Gleam B- Cl⁻ (ABC-100).

Figure 5.13a and b shows the polarisation curves and the additive surface coverage for different concentrations of the mixed Copper Gleam A-Copper Gleam B-Cl⁻ (ABC) in the plating electrolyte, respectively. As the amount of additives was increased, the curves shifted to more negative η values and lower values of i in both the charge- transfer and diffusion-limited regions. Similar to what was previously observed in earlier electrolytes, this result indicated concentration-dependent plating inhibition. However, beyond the recommended concentrations no appreciable increase in plating inhibition was observed, as suggested by the similar i-V curves of ABC-100 and ABC-200.

These results indicated that plating inhibition was dependent on the amount of additives used. A concentration-dependent suppression is logical because higher amounts of additives in the electrolyte correlate to more molecules being adsorbed at the cathode, as proven by Fig. 5.13b that shows additive surface coverage increased with increasing additive concentrations. However, it appears that plating suppression reached a maximum after a certain amount of additive was used. This occurred at the 100% additive concentration, and no appreciable cathode polarisation was observed beyond this value. This result is consistent with the 'polarisation plateau' reported for additive-containing electrolytes [5.17].

The electrochemical behaviour of the EnFACE electrolyte with additives is similar to that of a standard Cu plating electrolyte. The suppression and acceleration phenomenon accompanying the use of additives were all observed in the EnFACE. This implies that the EnFACE electrolyte could behave similarly and give

comparable results as the standard electrolyte when used in actual service. On the other hand, the inherently low limiting current of the EnFACE electrolyte could be a disadvantage, since this leads to lower plating rates. However, plating rates may be improved by other techniques such as mechanical stirring of the electrolyte that increases the mass transport.

In summary, the effect of additives on cathodic polarisation in both EnFACE and standard copper solutions were described. The primary effect of additives, either when used individually or in combination, is to induce cathode polarisation. This polarisation was manifested as a decrease in the measured current and a shift of plating processes to higher overpotentials.
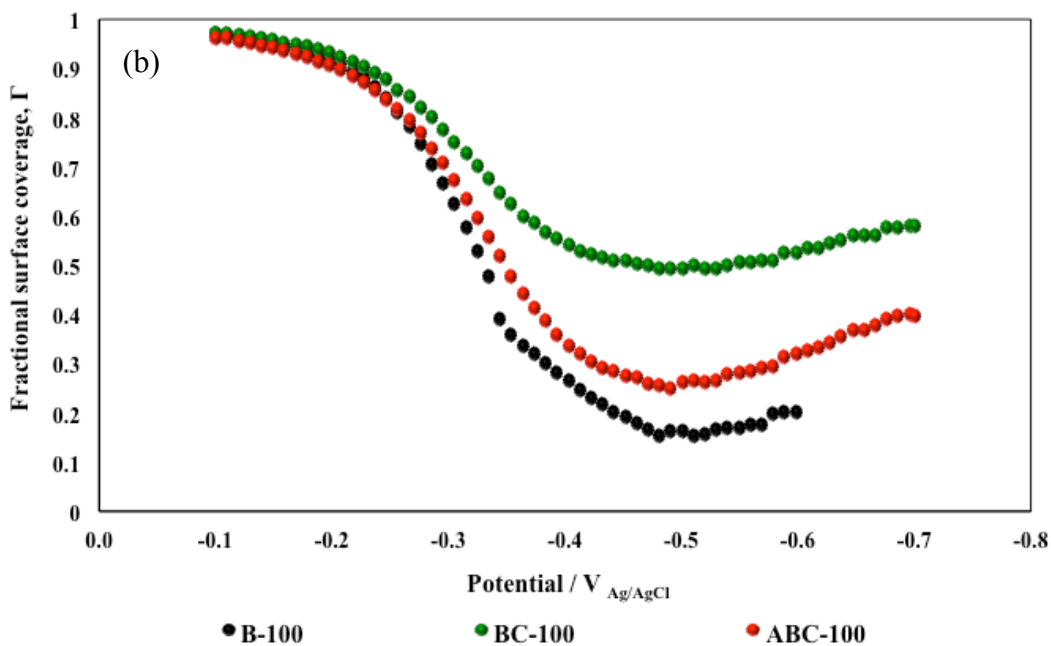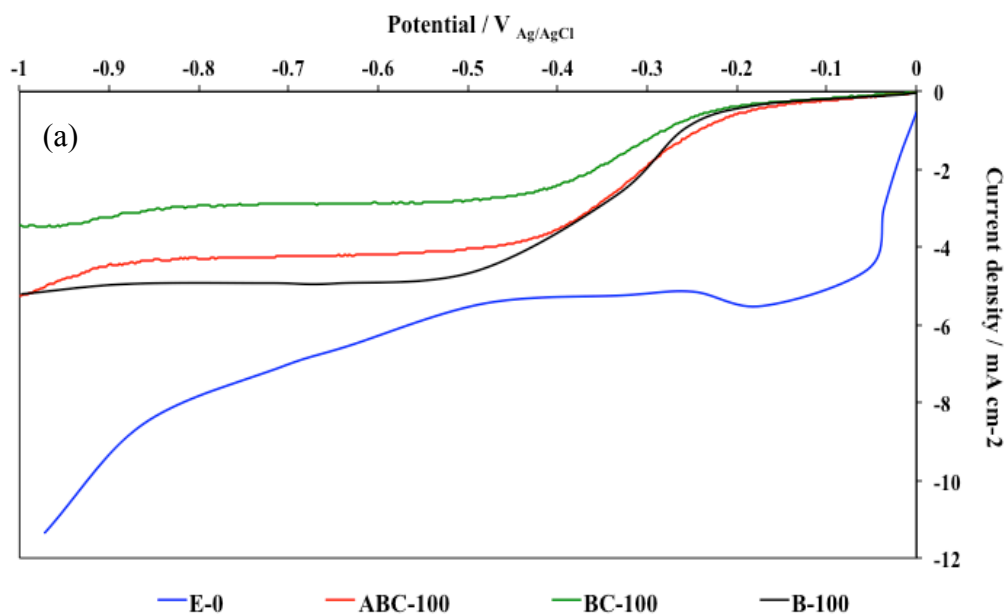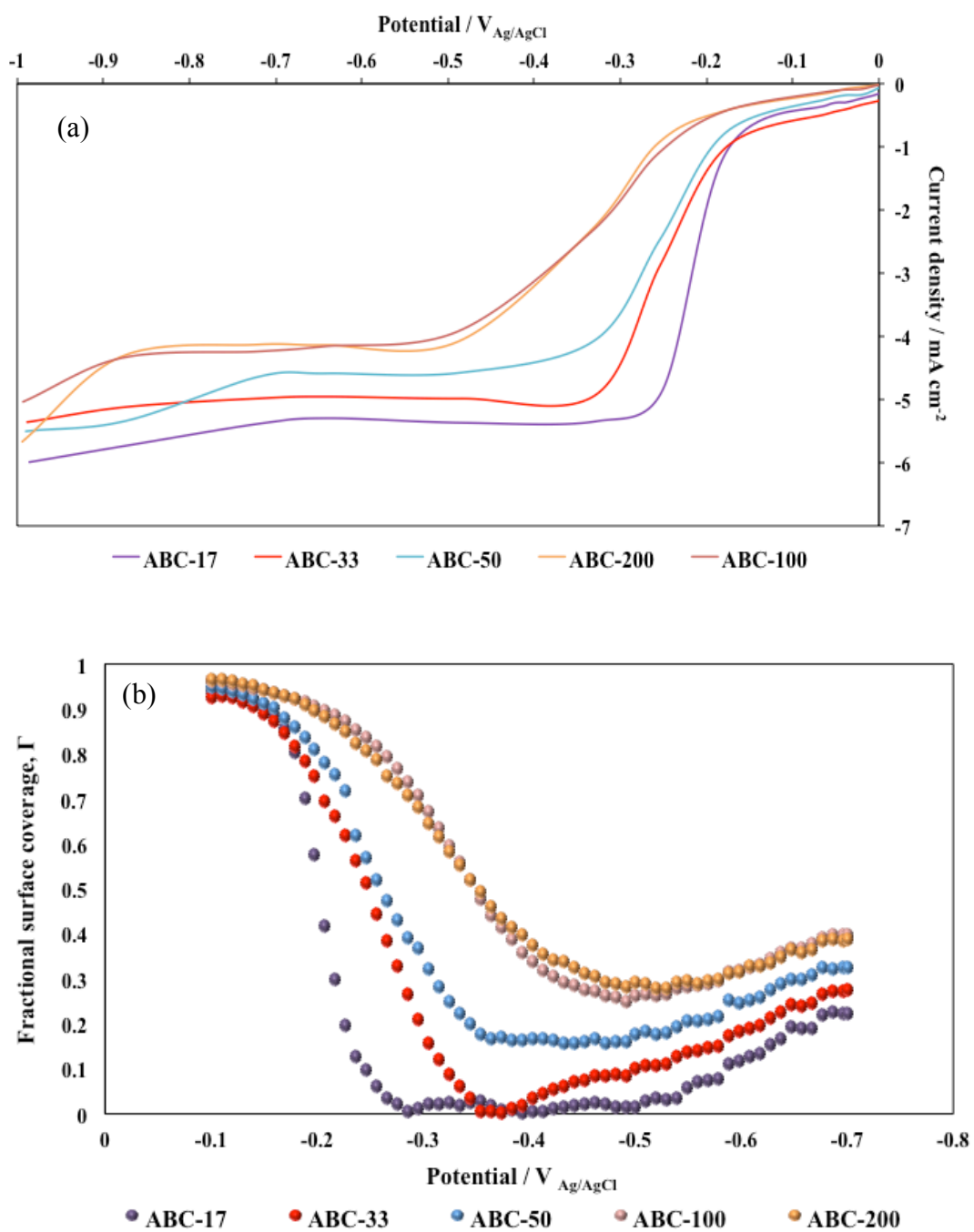
Figure 5.13 a) Cathodic polarisation curve and b) fractional additive surface coverage for the EnFACE electrolyte with different concentrations of the Copper Gleam A- Copper Gleam B- Cl⁻ (ABC) additive mixture.

References

5.1 Hill MRH, Rogers GT (1978) Polyethylene Glycol in Copper Electrodeposition onto a Rotating Disk Electrode. J Electroanal Chem 86; 179-188

5.2 Taft R, Messmore HE (1931) The Electrodeposition of Copper in Presence of Gelatin. J Phys Chem 35(9); 2585-2618

5.3 Struyk C, Carlson AE (1946) Electrodeposition of Copper. Mon Rev Am Electroplat Soc 33; 923-925

5.4 Kimber G, Napier D, Smith D (1967) Electrodeposition at rotating cathodes from acidified copper sulphate solution. J of Appl Chem 17(2); 29–35

5.5 Skowronski S, Reinsoso EA (1927) The specific resistivity of copper refining electrolytes and methods of calculation. In proceedings of the 51st General meeting of the American Electrochemical Society, Philadelphia, USA

5.6 Gabe DR (1997) The role of hydrogen in metal electrodeposition processes. J of Appl Electrochem 27(8); 908-915

5.7 Randles JEB (1952) Kinetics of rapid electrode reactions. Trans Faraday Soc 48; 828-832

5.8 MacLeod AJ (1993) A note on the Randles-Sevcik function from electrochemistry. Appl Math and Comp 57(2-3); 305-310

5.9 Compton RG, Banks CE (2010) Understanding Voltammetry. 2nd edition Imperial College Press, University of Oxford, UK

5.10 Roy S, Pintauro PN (1993) Analysis of Convective Mass Transfer by Potential Relaxation. J Electrochem Soc 140(11); 3167-3175

5.11 Moffat TP, Wheeler D, Edelstein MD, Josell D (2005) Superconformal film growth: Mechanism and quantification. IBM J of Research and Development 49(1); 19-36

5.12 Kang M, Gewirth A (2003) Influence of Additives on Copper Electrodeposition on Physical Vapor Deposited (PVD) Copper Substrates. J of the Electrochem Soc 150(6); C426-C434

5.13 Pasquale MA, Gassa LM, Arvia AJ (2008) Copper electrodeposition from an acidic plating bath containing accelerating and inhibiting organic additives. Electrochim Acta 53; 5891-5904

5.14 Kelly JJ, West AC (1998) Copper Deposition in the Presence of Polyethylene Glycol I. Quartz Crystal Microbalance Study. J Electrochem Soc 145; 3472-3476

5.15 Chen H-M, Parulekar SJ, Zdunek A (2008) Interactions of Chloride and Polyethylene Glycol in Acidic Copper Sulfate Electrolyte. J of the Electrochem Soc 155(5); D341 – D348

5.16 Ko, SL, Lin JY, Wang YY, Wan CC (2008) Effect of molecular weight of polyethylene glycol as single additive in copper deposition for interconnect metallization. Thin Solid Films 516(15); 5046 – 5051

5.17 Oniciu L, Muresan L (1991) Some Fundamental Aspects of Levelling and Brightening in Metal Electrodeposition. J of Appl Electrochem 21; 565-

574

5.18   Healy JP, Pletcher D (1992) The Chemistry of the Additives in an Acid
         Copper Electroplating Bath. J Electroanal Chem 338; 155-165

5.19   Kang M, Gross ME, Gewirth AA (2003) Atomic Force Microscopy
         Examination of Cu Electrodeposition in Trenches. J Electrochem Soc 150;
         C292-C301

5.20   Dow WP, Huang HS, Yen MY, Chen HH (2005) Roles of chloride ion in
         microvia filling by copper electrodeposition – II. J Electrochem Soc 152;
         C77-C88

5.21   Tan M, Guymon C, Wheeler D, Harb J (2007) The Role of SPS, MPSA,
         and Chloride in Additive Systems for Copper Electrodeposition. J
         Electrochem Soc 154(2); D78-D81

5.22   Kao YL, Li KC, Tu GC, Huang AC (2005) Microstructural Study of the
         Effect of Chloride Ion on Electroplating of Copper in Cupric Sulfate-
         Sulfuric Acid Bath. The Electrochem Soc 152(9); C605 – C611

5.23   Upadhyay DN, Yegnaraman V (2000) Effect of Thiourea and substituted
         thioureas on copper underpotential deposition in gold. Mater Chem Phys
         62(3); 247-253

5.24   Soares DM, Wasle S, Weil KG, Doblhofer K (2002) Copper ion reduction
         catalyzed by chloride ions. J Electroanal Chem 532; 353-358

5.25   Holzle MH, Apsel CW, Will T, Kolb DM (1995) Copper Deposition onto
         Au(111) in the Presence of Thiourea. J Electrochem Soc 142(11); 3741-

3749

5.26 Pearson T, Dennis JK (1990) The Effect of Pulsed Reverse Current on the Polarization Behaviour of Acid Copper Plating Solution containing Organic Additives. J of Appl Electrochem 20(2); 196 – 208

5.27 Nagy Z, Blaudeau JP, Hung NC, Curtiss LA, Zurawski DJ (1995) Chloride Ion Catalysis on the Copper Deposition Reaction. J Electrochem Soc 142; L87-L89

5.28 Moffat TP, Ou Yang LY (2010) Accelerator surface phase associated with super conformal Cu electrodeposition. J Electrochem Soc 157(4); D228– D241

5.29 Kelly JJ, Tian C, West AC (1998) Leveling and Microstructural Effects of Additives for Copper Electrodeposition. J of Electrochem Soc 146(7); 2540 – 2545

5.30 Chen Q, Wang Z, Cai J, Liu L (2010) The influence of ultrasonic agitation on copper electroplating of blind vias for SOI three-dimensional integration. Microelectronic Engg 87(3); 527 – 531

5.31 Kondo K, Yamakawa N, Tanaka Z, Hayashi KJ (2003) Copper Damascene Electrodeposition and Additives. J Electroanal Chem 559; 137-142

5.32 Feng ZV, Li X, Gewirth AA (2003) Inhibition due to the interaction of polyethylene glycol, chloride, and copper in plating bath: A surface-enhanced raman study. J Phys Chem B 107(35); 9415–942

5.33 Hai NTM, Huynh TTM, Fluegel A, Arnold M, Mayer D, Reckien W,

Bredow T, Broekmann P (2012) Competitive anion/anion interactions on copper surfaces relevant for Damascene electroplating. Electrochim Acta 70; 286-295

Chapter 6

Results and Discussion: Structures and Properties of Direct Current-plated Copper from EnFACE Electrolyte with Additives

Additive-induced changes in the electrochemical behaviour of the plating solution are known to create changes in deposit properties. While Chapter 5 discussed the electrochemical effects of additives, this chapter focuses on the more tangible implications of using additives. The current chapter presents the results of varying characterisation tests conducted on copper films produced via direct current (DC) plating using additive-containing EnFACE electrolytes. The final section contains the results of through-hole plating tests on the EnFACE electrolyte, which was conducted to assess the applicability of the electrolyte to the PCB manufacturing industry.

6.1 Morphology and grain size

Figure 6.1 shows the SEM images (planar view) of the copper deposits of the EnFACE electrolyte with different additive concentrations (see table 4.5), together with the product of the standard copper electrolyte. The products of the additive-free electrolytes possessed coarse microstructure, while the deposits from the additive-containing electrolytes appear compact and fine. As the amount of additive in the EnFACE electrolyte increased, the surface roughness of the deposit noticeably decreased. Indeed, at 100% (E-100) and 200% (E-200) additive concentrations, the deposits appeared smoothest and the most compact. In terms of appearance, the deposit from the S-100 electrolyte was similar to the deposit of

the E-33 electrolyte. This indicates that even at low concentrations the influence of additives is substantial.

Since surface roughness is related to grain size, the observed reduction in surface roughness could indicate a fine-grained structure in the deposit [6.1]. In fact in the industry, a 'bright' or shiny deposit is a good indication of a compact, non-dendritic structure. However, attempts to measure the grain size from the micrographs proved difficult since the grain structure was not easily discernible even when viewed at high magnifications. Therefore, it became necessary to use another imaging technique that allowed accurate visualisation of grain morphology. Electron back-scatter diffraction (EBSD) was chosen because the technique allows grain size and grain orientation analysis without the need to alter the surface condition of the metal.

(a) E-0	(b) E-17	(c) E-33
(d) E-50	(e) E-100	(f) E-200
(g) S-0	(h) S-100	
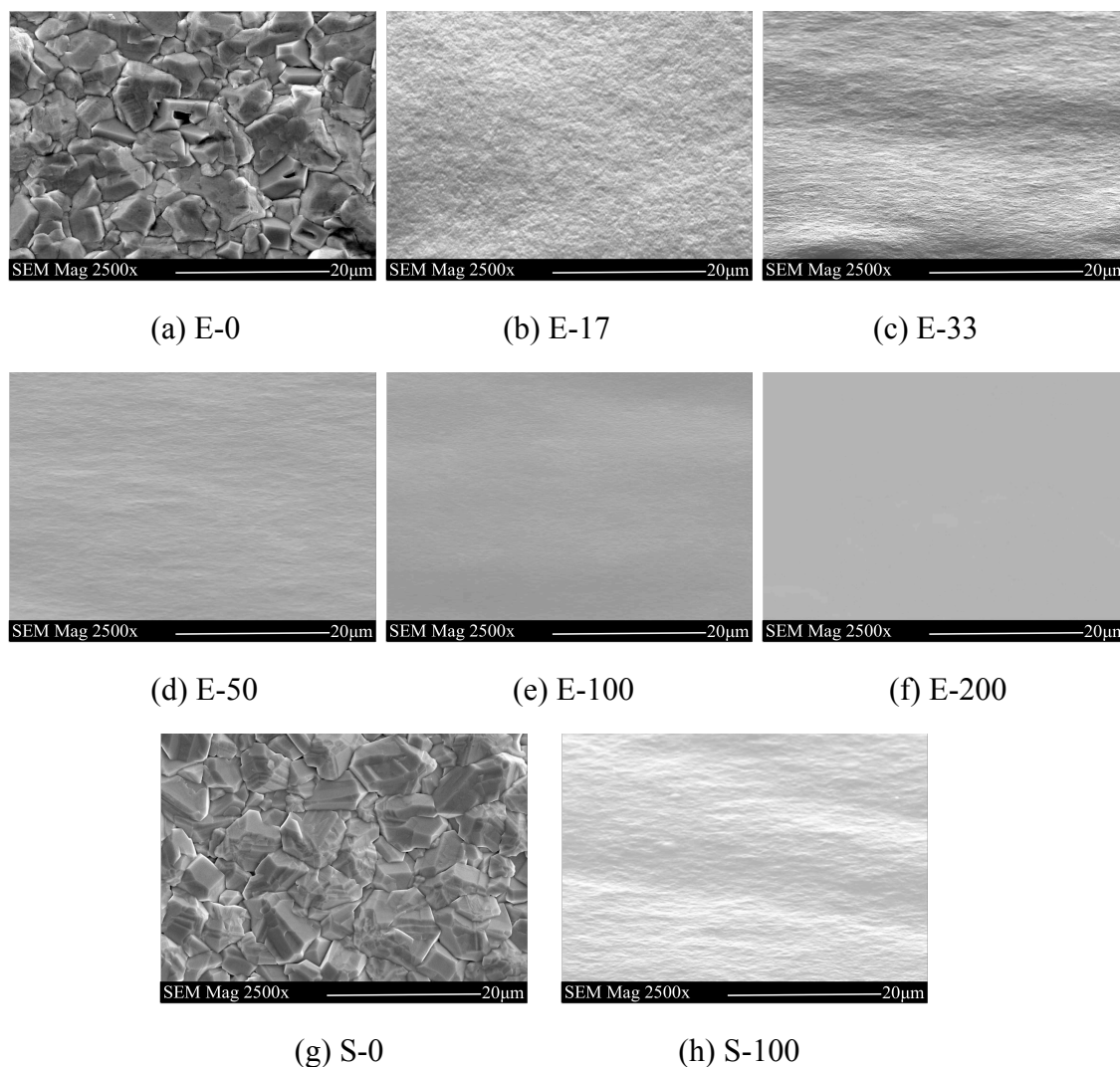
Figure 6.1 SEM images of copper deposits from EnFACE electrolyte with different additive concentration: a) 0% (E-0), b) 17% (E-17), c) 33% (E-33), d) 50% (E-50), e) 100% (E-100), f) 200% (E-200); g) 0% (S-0) and h) 100% (S-100) - standard electrolyte. These percentages are relative to the industry recommended additive concentration of 10 ml/L Copper Gleam B, 0.5 ml/L Copper Gleam A, and 70 ppm Cl⁻.

Figure 6.2 shows the corresponding EBSD maps for the products of the EnFACE electrolyte with different levels of additive concentration and of the standard copper electrolyte. The EBSD images show not only the grain size of deposits but also the crystal or grain orientations. With respect to orientation, each color on the map represents an electron diffraction plane. These planes may be

identified by using the inverse pole legend shown in Fig. 6.2g. Grain orientation maps can give information on preferred orientation or texture in the deposit. Compared to the XRD, the texture information given by EBSD is taken from a much smaller area. This is an advantage when trying to investigate weak textures in fine-grained materials. However, the small probe area of the EBSD is unsuitable for analysing coarse-grained materials because the EBSD will detect significant textures in these cases.

Table 6.1 gives a summary of the grain size of deposits measured using the EBSD image analysing software, TANGO (HKL Technology A/S, 2001). TANGO can be used to study EBSD orientation maps and extract crystallographic information such as grain size, texture data, phase distribution and recrystallisation. The grain structure map was obtained by adjusting band contrast (i.e. noise reduction and wild spikes extrapolation) to clearly reveal grains. The grain size parameter used is the major and minor axis of a fitted ellipse, and the software automatically measured the grain size based on the delineation of all of the grain boundaries. Figure 6.3 presents a plot of deposit grain size as a function of additive concentration in the EnFACE and standard electrolytes. In Fig. 6.3a, the scale range is quite large and thus the effect of additive concentration on grain size is not readily apparent. Figure 6.3b shows the plot in the range 17 to 200% additive concentration, and this figure gives a better representation of additive effect.

a) E-17   b) E-33   c) E-50

d) E-100   e) E-200   f) S-100

g) inverse pole legend
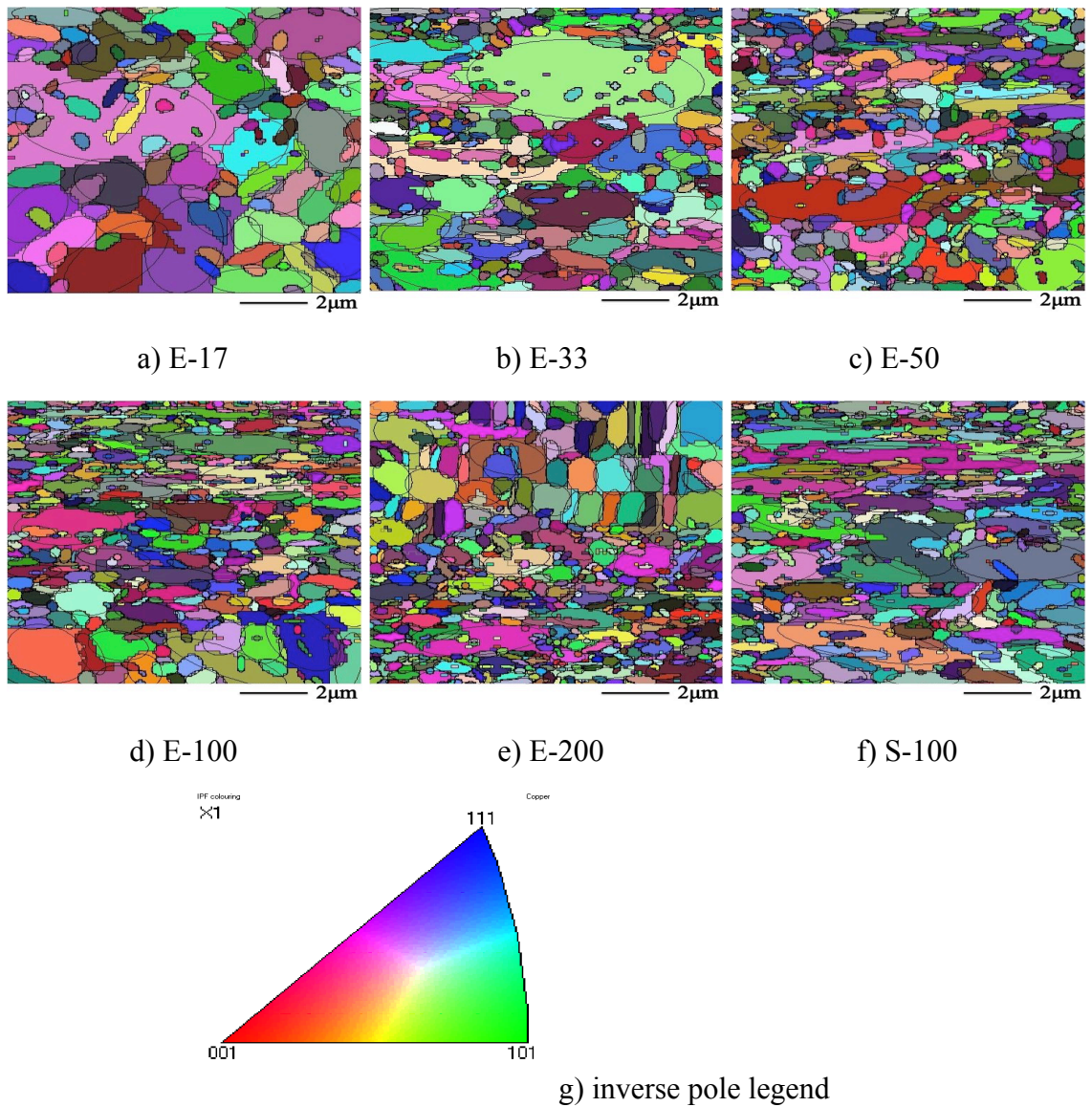
Figure 6.2 EBSD images of copper deposits from EnFACE electrolyte with different additive concentration: a) 17% (E-17), b) 33% (E-33), c) 50% (E-50), d) 100% (E-100), e) 200% (E-200), and f) S-100 - standard electrolyte. These percentages are relative to the industry recommended additive concentration of 10 ml/L Copper Gleam B, 0.5 ml/L Copper Gleam A, and 70 ppm Cl⁻. The calibration bar represents a length of 2 μm. The different colors in the EBSD map represent different crystals planes as described by the g) inverse pole legend.

Table 6.1 EBSD grain size measurements of deposits of the additive-containing and additive-free EnFACE (E) and standard (S) electrolytes.

Sample designation	Grain size (nm)
E-0	9016 ± 312
E-17	758 ± 62
E-33	523 ± 51
E-50	466 ± 38
E-100	407 ± 35
E-200	400 ± 42
S-100	431 ± 96
S-0	11524 ± 426
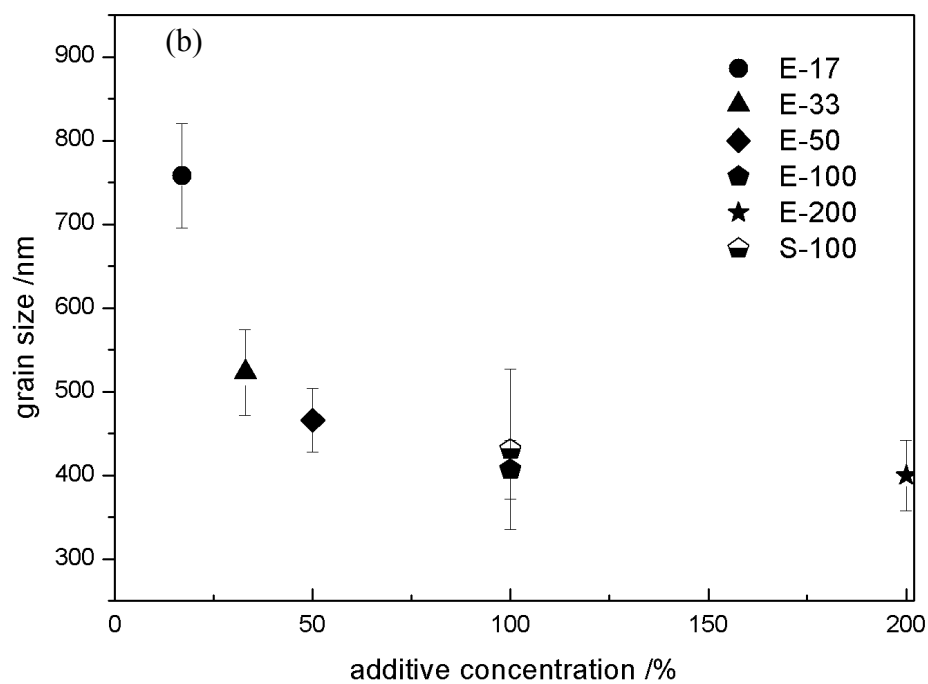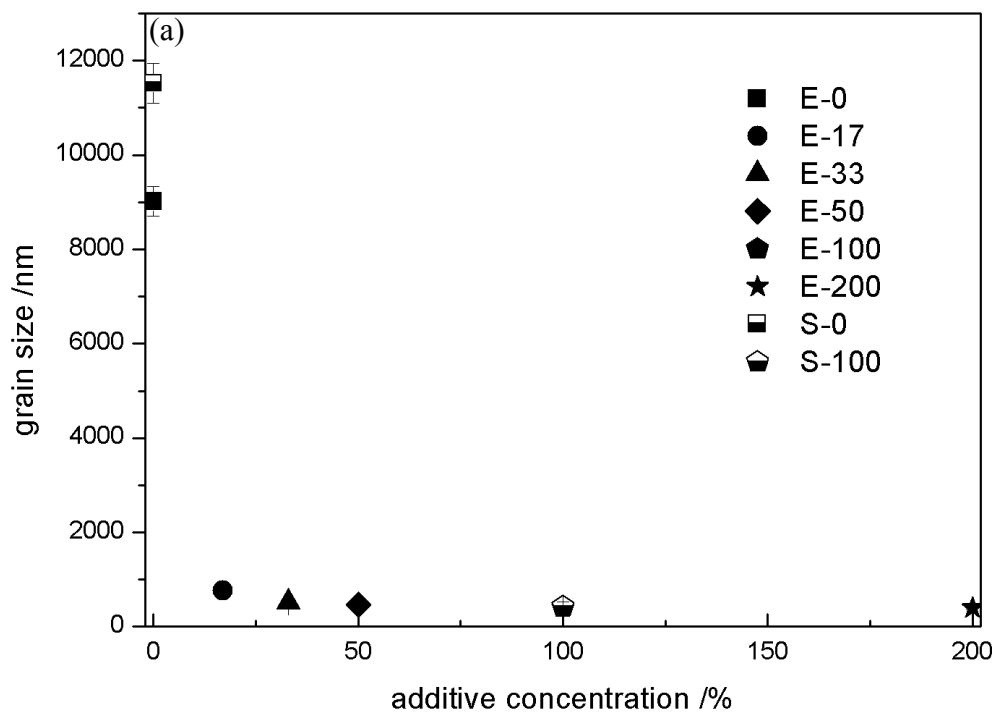
Figure 6.3 a) Plot of grain size versus additive concentration for the additive-containing EnFACE electrolyte. b) Zoomed-in image of the plot in the additive concentration range of 17% to 200%.

The EBSD results clearly indicated that as the amount of additives increased, the deposit grain size decreased. For example, there was a 10 times reduction in grain size from the product of the E-17 electrolyte relative to that of the E-0 electrolyte; while a 20 times reduction in grain size occurred when the additive concentration was increased to 100% (E-100). However, it appears that the decrease in grain size was not significant beyond the 100% concentration. The grain sizes in the products of the E-100 and E-200 appear to be almost identical, with the difference possibly the result of statistical variance. Furthermore, in agreement with the observed similarity in appearances, the grain sizes of the deposits from the S-100 electrolyte and the E-50 electrolyte are in proximity of each other.

Similar to the conclusions made from SEM analysis, the EBSD results indicated that additives created a finer grain structure in the deposit, and that the decrease in grain size was proportional to the concentration of additives used. However, as the concentration increased beyond 100%, the decrease in grain size was marginal. This indicated that the reduction due to additives levels off after the 100% concentration. Such is consistent with our previous polarisation studies that reported a polarisation plateau (see Chapter 5), which is the concentration at which maximum electrode polarisation occurs [6.2]. Beyond this critical concentration, no further increase in polarisation is expected; and thus the grain-refining action of additives was consequently suppressed.

Past studies have reported the benefits of additives in DC plating using the conventional acid-copper sulphate baths [6.2, 6.3, 6.4, 6.5]. Additives affect deposit morphology by (i) inducing grain refinement of the deposit [6.6, 6.7], or by (ii) changing crystal orientation and creating deposit texture [6.2]. Additives can influence nucleation and growth of deposits during plating [6.8]. For instance, brighteners can improve nucleation rates by lowering the energy for nuclei formation [6.3, 6.9]. Alternatively, adsorbed additives can promote nucleation by acting as physical barriers to diffusing surface ad-atoms thereby preventing kink/step attachment [6.7]. Grain refinement could even be synergistic when different types of additives are present in the electrolyte. While numerous studies have reported similar observations in conventional copper baths [6.2, 6.6, 6.7], these observations may be the first report on how additives affect the grain structure of the products of the EnFACE electrolyte. Finally, since grain refinement has important implications on the mechanical and electrical properties of the plated copper, these properties were measured and are reported in succeeding sections.

The EBSD orientation maps hints at the occurrence of the (111) texture in the microstructure. This is seen in the predominance of bluish areas in the EBSD maps. However, since the EBSD data was taken from a small area, the result may not be representative of the specimen. To obtain more accurate information on grain texture, the XRD was employed since it can simultaneously scan a greater area of the specimen. The results of XRD analysis are presented in the next section.

6.2 Microstrain and crystallographic texture

Figure 6.4a and b shows the XRD patterns of electrodeposited samples from the EnFACE electrolyte at different additive concentrations, and from the standard copper electrolyte, respectively. Five prominent peaks with the corresponding diffraction planes were found in the XRD plots. Also, there is no significant difference between the diffraction patterns of the deposits from the EnFACE electrolyte and that of the standard electrolyte.
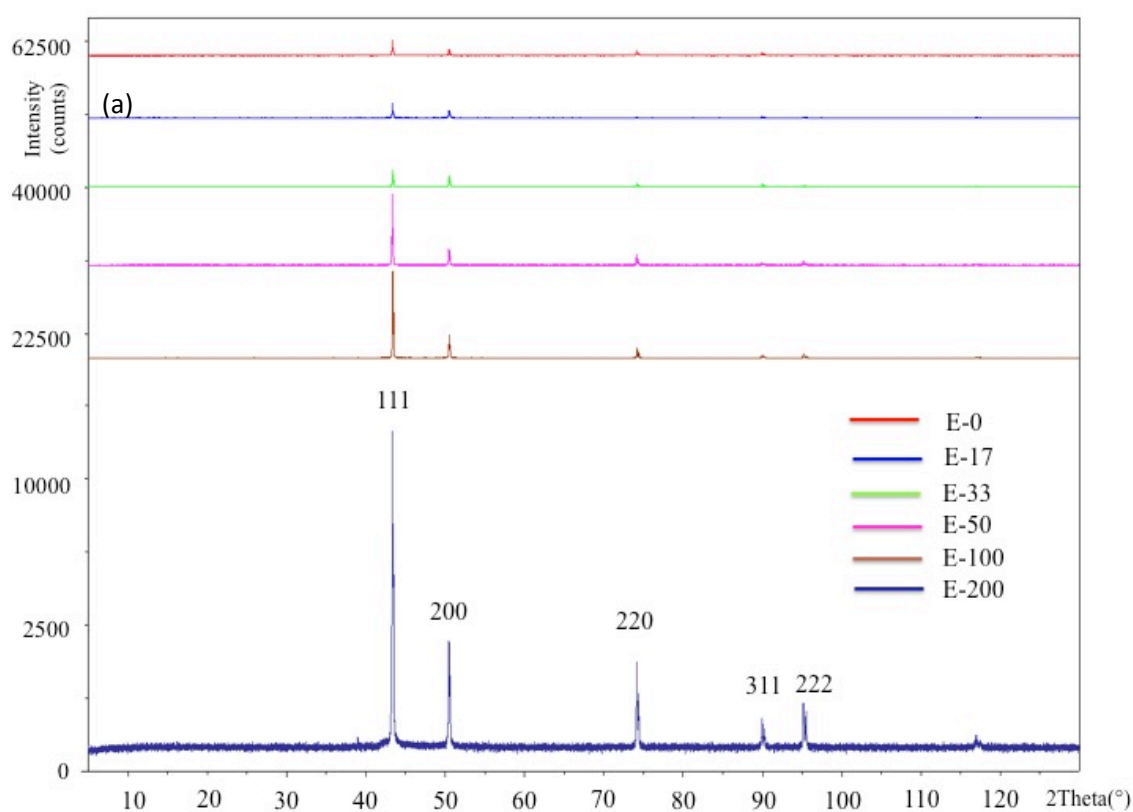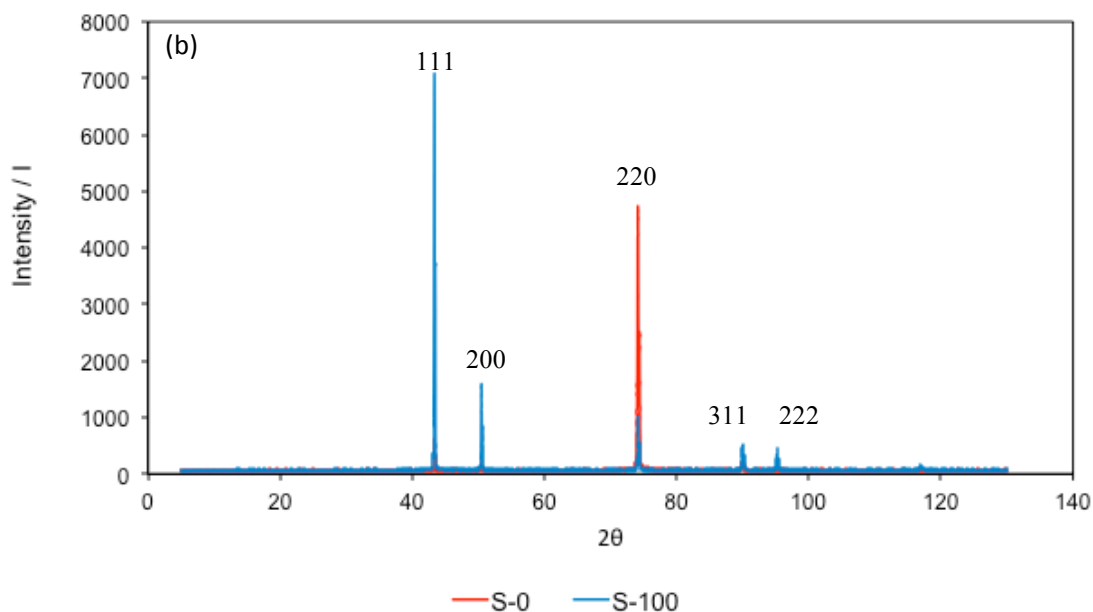
Figure 6.4 XRD scans of electrodeposited copper films from a) EnFACE electrolyte with different additive concentration; and b) standard copper electrolyte. EnFACE electrolyte scans were shifted along the intensity axis except the high concentration setting. However, the intensity of the peaks was not adjusted to reveal the true intensity.

Figure 6.5a to 6.5d gives a close-up view of the individual XRD peaks. A closer examination of the individual peaks revealed the existence of well–defined doublets. The doublets could be due to the presence of kα1 (1.54406 Å) and kα2 (1.5444 Å) components since monochromatisation was not carried out during the scan.

The XRD data indicated that as the amount of additives increased, progressive broadening of intensity peaks at relevant diffraction planes, (111) and (200) occurred. The highest broadening was seen in the product of the E-200 electrolyte. The Scherrer's equation (Eqn. 4.9) shows that the peak width is

inversely proportional to the crystallite size; and therefore peak broadening may indicate grain size refinement.

Alternatively, the residual strain or microstrain in the grains can also contribute to peak broadening. The contribution of grain size and microstrain to the peak broadening was determined using the Williamson-Hall equation (Eqn. 4.12).
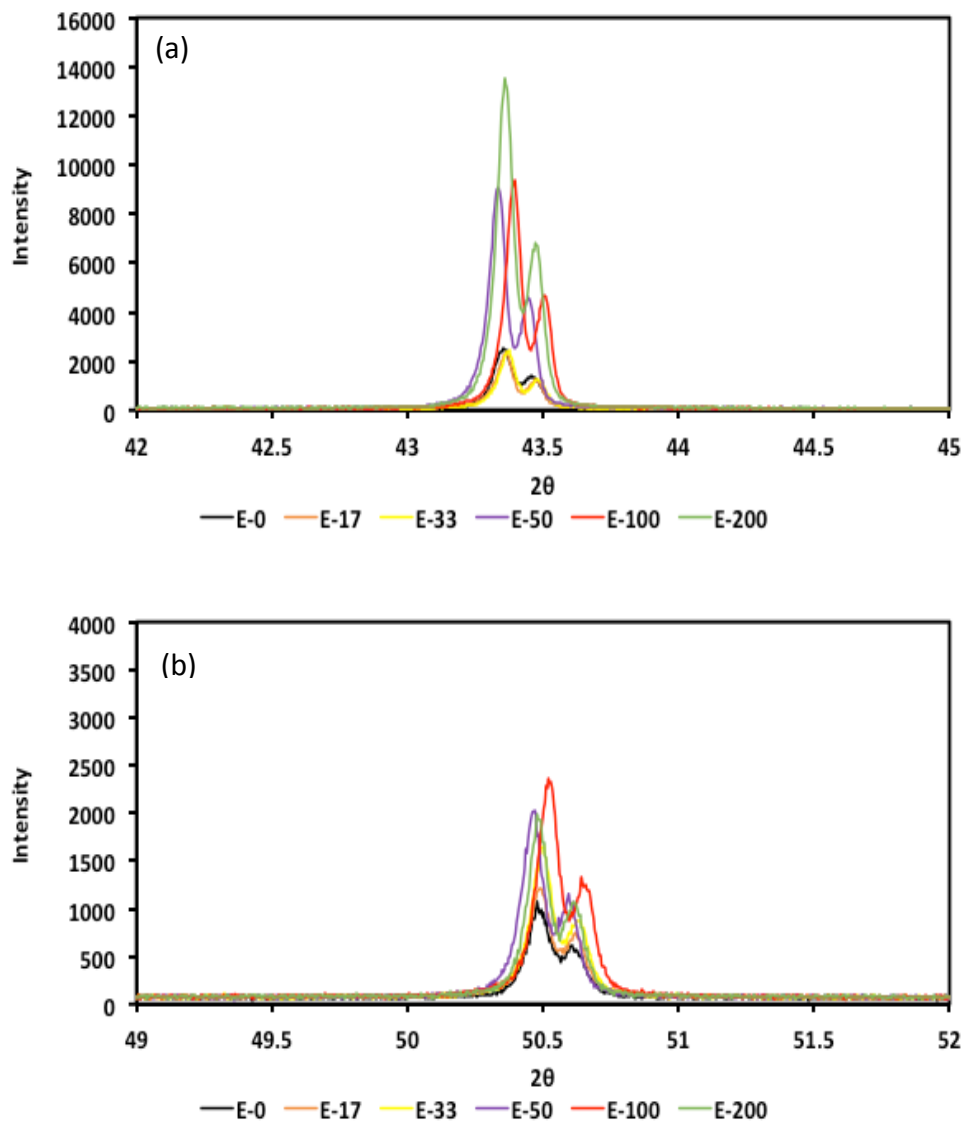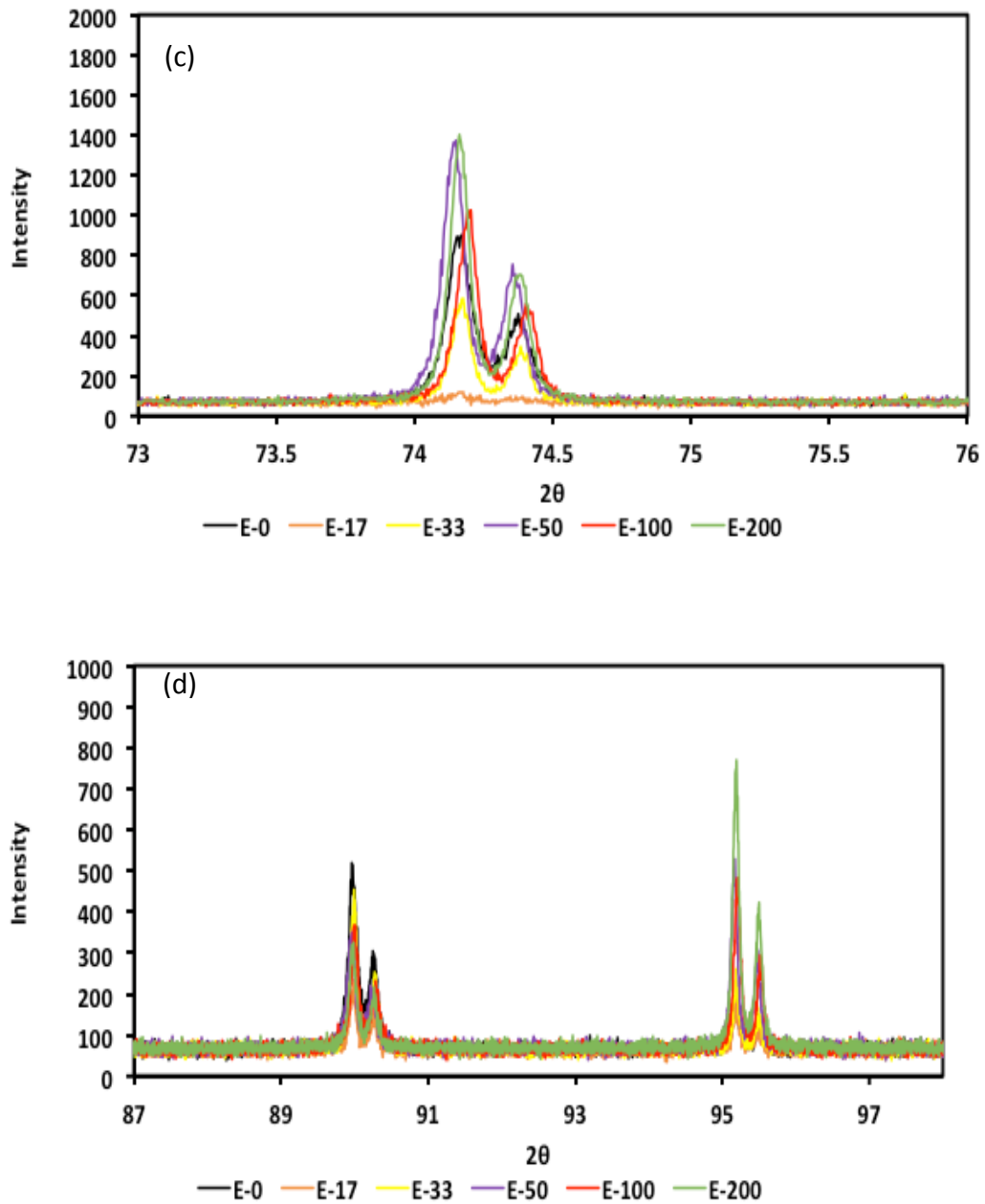
Figure 6.5 XRD plots of the deposits of the EnFACE electrolyte with additives; shown are the strong diffraction peaks corresponding to the (a) 111 (b) 200 (c) 220 and (d) 311 and 222 planes.

Table 6.2 presents the calculated crystallite size (via Scherrer's equation) and microstrain (via Williamson-Hall technique) for the products of the EnFACE electrolyte at different additive settings. Figure 6.6 shows a plot of microstrain in

the deposits of the different additive-containing EnfACE electrolytes. The data

gives a clear indication of the effect of addition agents on crystallite size and

microstrain. As the amount of additives was increased, both crystallite size and

microstrain decreased.

Table 6.2 Calculated crystallite size (Scherrer's equation) and microstrain
(Williamson–Hall technique) of EnFACE copper at different additive
concentration.

Sample designation	Crystallite size (nm)	Microstrain (%)
E-0	1167 ± 129	0.161 ± 0.084
E-17	320 ± 55	0.055 ± 0.006
E-33	257 ± 90	0.043 ± 0.015
E-50	259 ± 72	0.036 ± 0.002
E-100	196 ± 12	0.024 ± 0.005
E-200	176 ± 3.2	0.021 ± 0.005

The results, as shown in Table 6.2, confirm the EBSD results and simply

validate the grain-refining action of additives [6.10, 6.11, 6.12]. However, it

needs to be mentioned that Scherrer's equation is most applicable for crystallite

sizes less than 200 to 300 nm. This means that the quantitative estimates of the

grain size may not be completely accurate especially if grains sizes are well

beyond this limit. Indeed, when the Scherrer measurements are compared with the

EBSD results, significant differences were noted. In this case, the EBSD results

are considered the more accurate data for the grain size analysis.
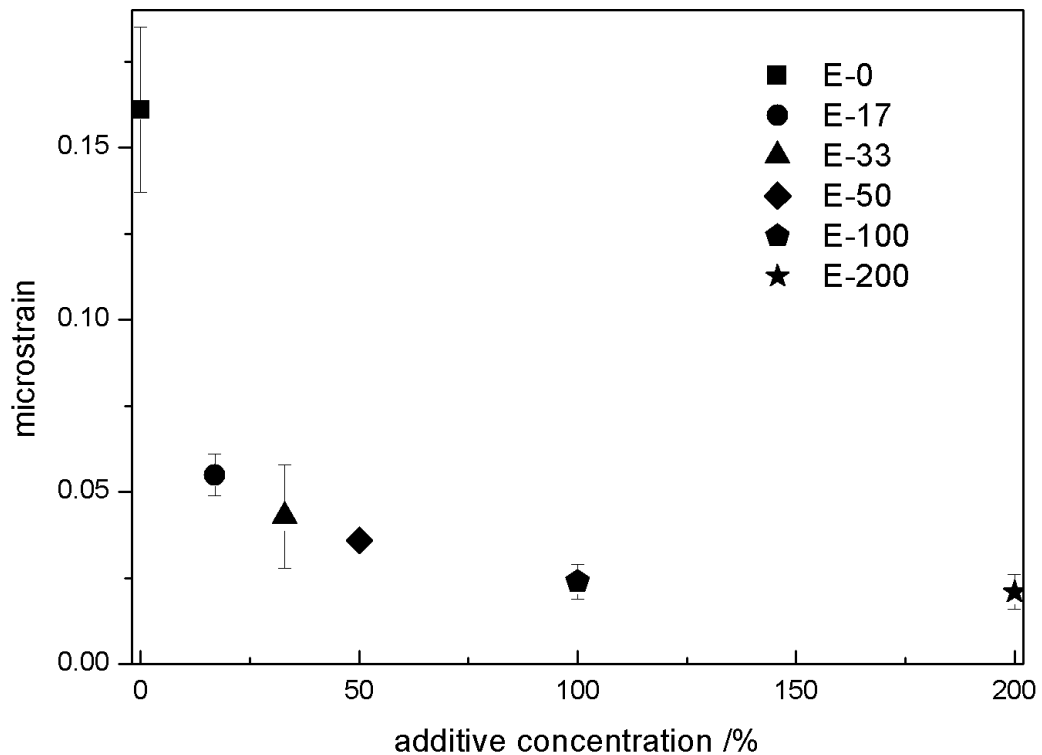
Figure 6.6 Plot of microstrain in the deposit of the different additive-containing EnFACE electrolytes.

The microstrain in the deposits decreased with increasing amounts of additives. High levels of microstrain are often caused by non–uniform lattice distortions and high dislocation densities in the crystal lattice. Dislocations and strains are primarily created during the process of crystal growth. A fast growth process typically creates greater disorder and forms more dislocations in the grains because it does not give time for atoms to arrange themselves in an orderly manner. Therefore, the low levels of microstrain seen with the products of the additive-containing EnFACE electrolytes could be a result of low dislocation densities, which is probably a result of an additive- controlled growth of the crystallites [6.13].

The diffraction intensity of the (111) plane was the highest among the peaks, followed by (200) and (220). The peak intensity of the (111) plane was found to increase proportionally to the additive amount. An increase in the peak intensity of a crystal plane suggests the formation of a well-defined crystal structure in the Cu deposits [6.14]. Alternatively, peak intensities can also increase due to the occurrence of preferred orientation or texture in deposits.
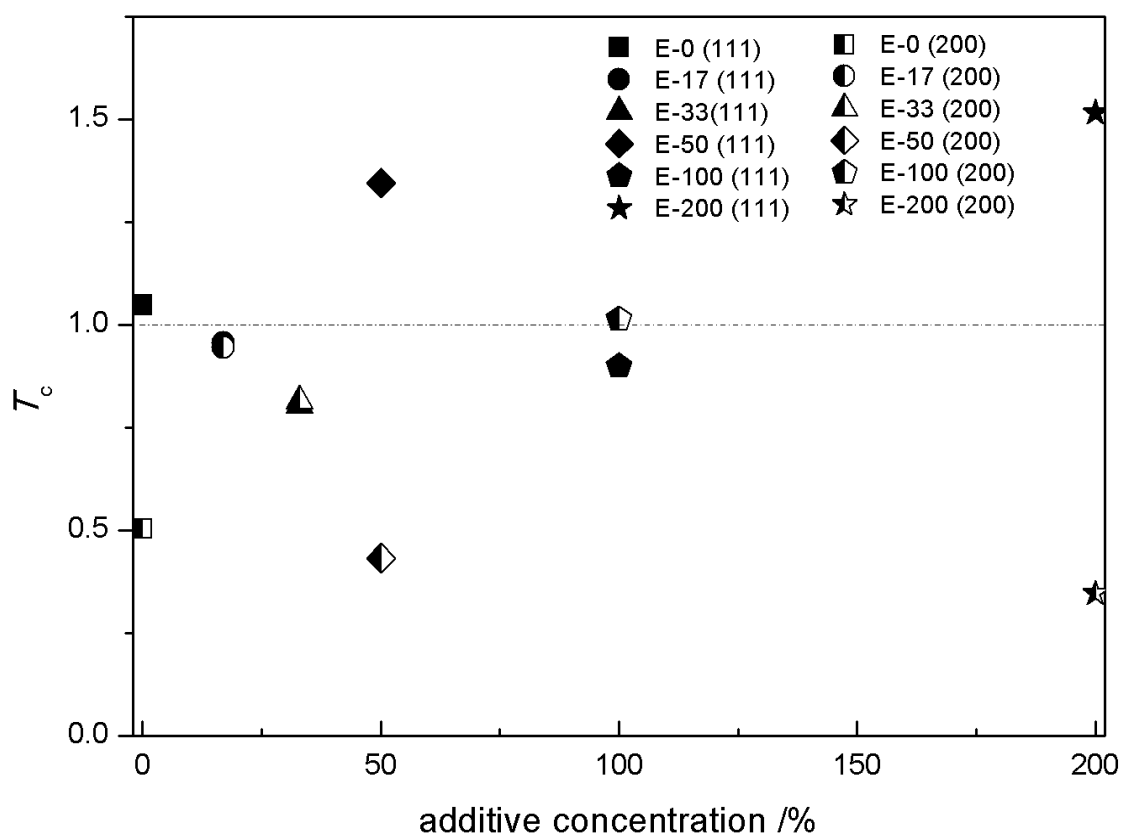
Figure 6.7 Plot of texture coefficient for the (111) and (200) in the deposits of the different EnFACE electrolytes. A T_c value above 1.0 (dotted line) indicates the occurrence of texture.

Texture in the Cu films was assessed using the texture coefficient of the (hkl) plane, T_c(hkl), as seen in Eqn. 4.14. The texture coefficient for the two strongest peak corresponding to (111) and (200) were calculated, and is shown in

Fig. 6.7. A T_c(hkl) that is close to unity indicates a randomly distributed crystal orientation, while a T_c(hkl) greater than 1 means the (hkl) plane is preferentially oriented.

For the DC-plated Cu, the (111) texture was detected in certain deposits (i.e. E-0, E-50 and E-200); but there was no definite trend in the occurrence of the (111) texture with respect to additive concentration. There was no preferential orientation for (200) in the copper deposits.

Some of the copper foils exhibited a strong (111) texture. The strong diffraction intensities observed in the (111) plane is considered normal for copper films. Microstructure evolution in thin films is governed by surface energy minimisation. This mechanism results to the (111) grain texture in copper electrodeposits because the (111) is the plane of highest density and possesses the least energy [6.15]. Film texture has strong implications on thin film behavior owing to the anisotropy of properties in different crystal planes. For example in copper films, the elastic modulus in the <111> is about 2.9 times higher than in the <100> [6.16]. The <111> can also affect the electrical performance of interconnect lines [6.17].

Interestingly, the occurrence of texture was not strongly dependent on additive concentration. In contrast, some studies reported seeing textural changes in copper deposits proportional to additive concentration [6.13].

6.3 Film resistivity and self-annealing

Figure 6.8 show the electrical resistivity, ρ, of the electrodeposited copper thin films from both the standard copper (S) electrolytes and the EnFACE (E)

electrolytes containing different levels of additives. The deposit of the standard electrolyte possessed lower resistivity than the deposit of the EnFACE electrolyte. To illustrate, the ρ ranged from 2.17 to 2.41 μohm/cm for the additive-free and additive-containing EnFACE electrolytes, respectively. In contrast, the ρ is 2.16 and 2.37 μohm cm for the additive-free and additive-containing S electrolytes, respectively. Also, the ρ of the copper films from the EnFACE electrolyte increased with increasing additive concentration.
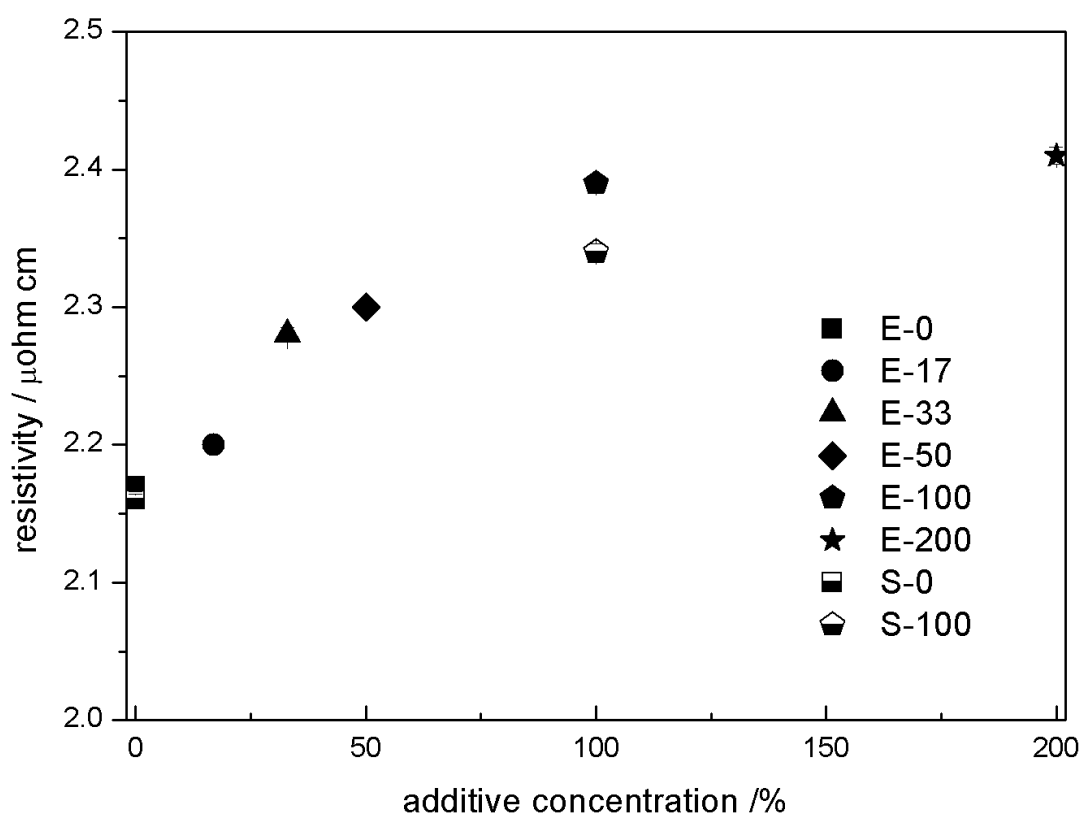
Figure 6.8 Resistivity measurements of electrodeposited copper films of the EnFACE (E) electrolyte with varying additive concentrations and the standard (S) electrolyte.

Results indicated that additives increased the resistivity of the plated copper. This was true in both the EnFACE and the standard copper electrolytes.

Matthiessen's rule states that bulk or total ρ of a metal is the sum of resistivity contributions from defects (e.g. alloy impurities, dislocations, grain boundaries, and surfaces) and lattice vibration (i.e. phonons). It is then reasonable to assume that the increase in ρ may be explained by the significant reduction of grain size and the consequent increase in grain boundary area of the deposit. For polycrystalline metals, the Mayadas-Shatzkes [6.18] model describes the resistivity due to grain boundaries, α_r using the equation:

$$\frac{\rho_{gb}}{\rho_o} = 1 - \frac{2}{3}\alpha_r + 3\alpha_r{}^2 - 3\alpha_r{}^3 \ln\left(1 + \frac{1}{\alpha_r}\right) \qquad \text{Equation (6.1)}$$

where ρ_{gb} is the resistivity due to grain boundary scattering, ρ_o is the bulk resistivity of the metal (1.68 x10^{-8} ohm m), and $\alpha_r = \frac{\lambda}{G}\frac{R}{1-R}$; where R is the material dependent reflection coefficient in the grain boundary ($R_{Cu} = 0.24$), and λ is the electron mean free path in the material ($\lambda_{Cu} = 39$ nm) [6.19]. Clearly, the above equation indicates that increasing grain size decreases the resistivity due to grain boundaries; and consequently the bulk resistivity of copper.

Self-annealing is a known consequence of additives on copper plating [6.20]. This phenomenon refers to the spontaneous increase in deposit grain size at room temperature. Self-annealing can lower ρ and reduce the strength of plated copper. In the current study, self-annealing was studied by monitoring the change in ρ over time. Figure 6.9a and 6.9b shows the ρ of different copper films measured over a period of 24 and 168 hours, respectively. Table 6.3 summarises the film ρ measured at the start and at the end of the 168-hour period.

The ρ of deposits of certain electrolytes (i.e. E-33, E-50, E100, E200 and S-100) progressively decreased over time, and eventually reached a stable value within the first 24 hours after plating. Beyond the 24 hours, no significant reduction in ρ was observed. There was no observed reduction in ρ in the deposit of the electrolytes without additives (S-0, E-0), and with the least amount of additives (E-17). The stable or final ρ of copper was proportional to the amount of additives in the electrolyte; i.e the most resistive deposit was obtained from the electrolyte with the highest amount of additive (E-200). The transition time from high to low ρ also takes longer when additives are present.

Table 6.3. Summary of the electrical resistivity of the copper deposits of the EnFACE and standard electrolytes (0-168 hours).

Sample designation	Peak ρ (μOhm·cm)	Final ρ (μOhm·cm)	Difference, (μOhm·cm)	Change (%)
E-0	2.18	2.17 ± 0.006	0.01	0
E-17	2.21	2.20 ± 0.006	0.01	0
E-33	2.34	2.28 ± 0.005	0.06	-2.6
E-50	2.40	2.30 ± 0.003	0.10	-4.2
E-100	2.43	2.39 ± 0.005	0.04	-1.6
E-200	2.47	2.41 ± 0.006	0.06	-2.4
S-100	2.41	2.34 ± 0.006	0.07	-2.9
S-0	2.17	2.16 ± 0.006	0.01	0
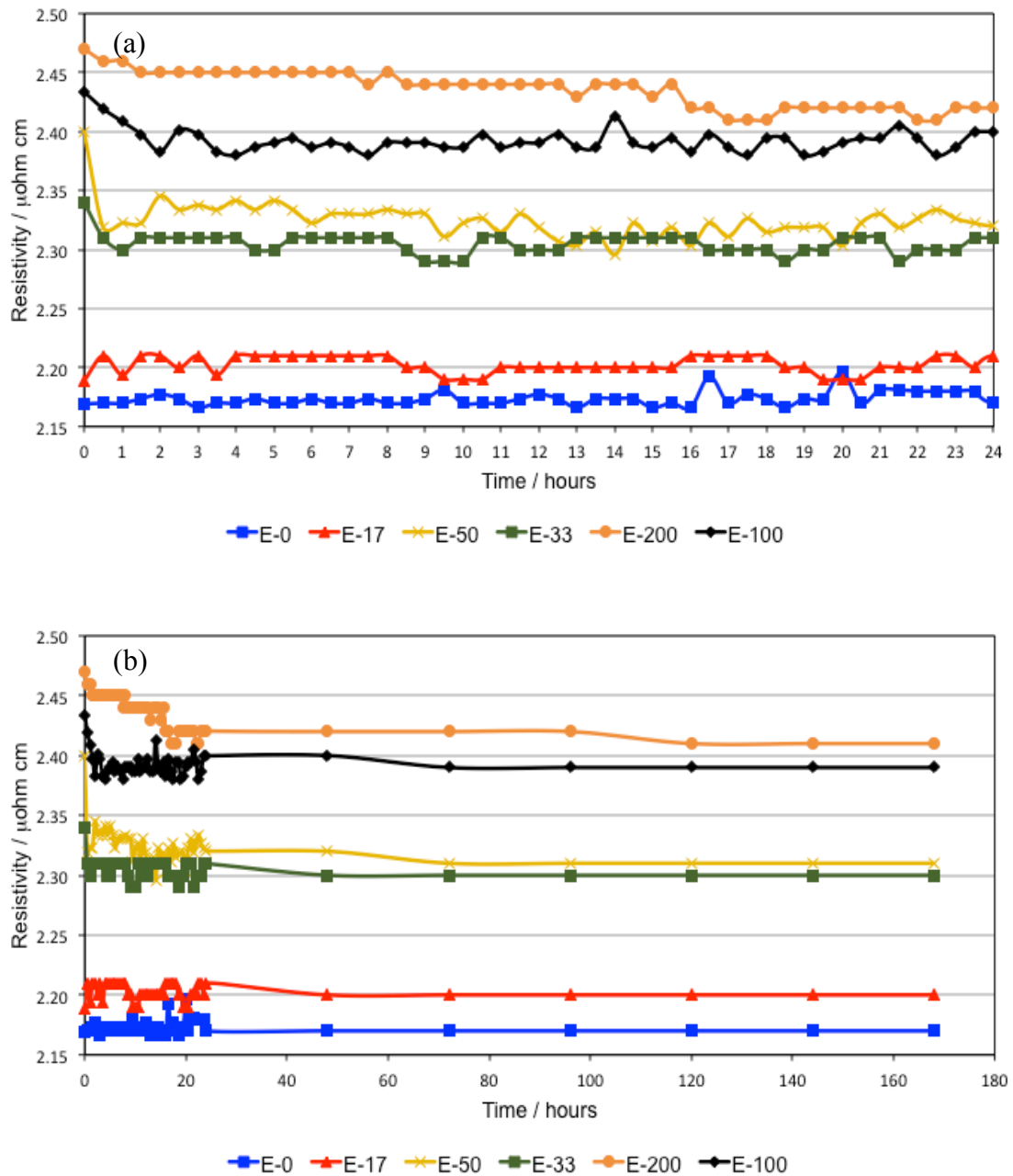
Figure 6.9 Resistivity of the copper films of the EnFACE and standard electrolyte with different additives measured in the first a) 24 hours and b) 168 hours after deposition.

The occurrence of self-annealing in electroplated copper is believed to be additive-related [6.21, 6.22], since self-annealing was not observed in the deposits of additive-free electrolytes. This agrees with the current observation that the

deposits from the electrolytes with no, or the least amount of, additives did not show significant changes in ρ over time.

The drop of ρ over time in the deposits of the additive-containing EnFACE electrolytes suggested the occurrence of self-annealing. However, the observed reduction in resistivity of the electroplated copper was much lower compared to literature values. Self-annealing is known to reduce the ρ to about 75% of the as-deposited value [6.23]. As seen in Table 6.3, the % change in ρ ranges from 1.6 to 4.2% only.

The minimal reduction in ρ suggested that self-annealing was not actually occurring in the copper film; and additional proof was needed to ascertain its occurrence in the specimens. Since self-annealing is accompanied by microstructural evolution, specifically by changes in grain sizes via grain growth, then this could also be detected by other analytical tools such as the SEM or XRD. Image analysis via SEM is more accurate and preferred, but is difficult to implement in this case since deposit grains were difficult to image. The XRD technique was employed owing to its simplicity of use. XRD analysis was done on the plated copper at different time intervals after plating. A change in grain size would be detected in the change in peak widths of the corresponding diffraction pattern.
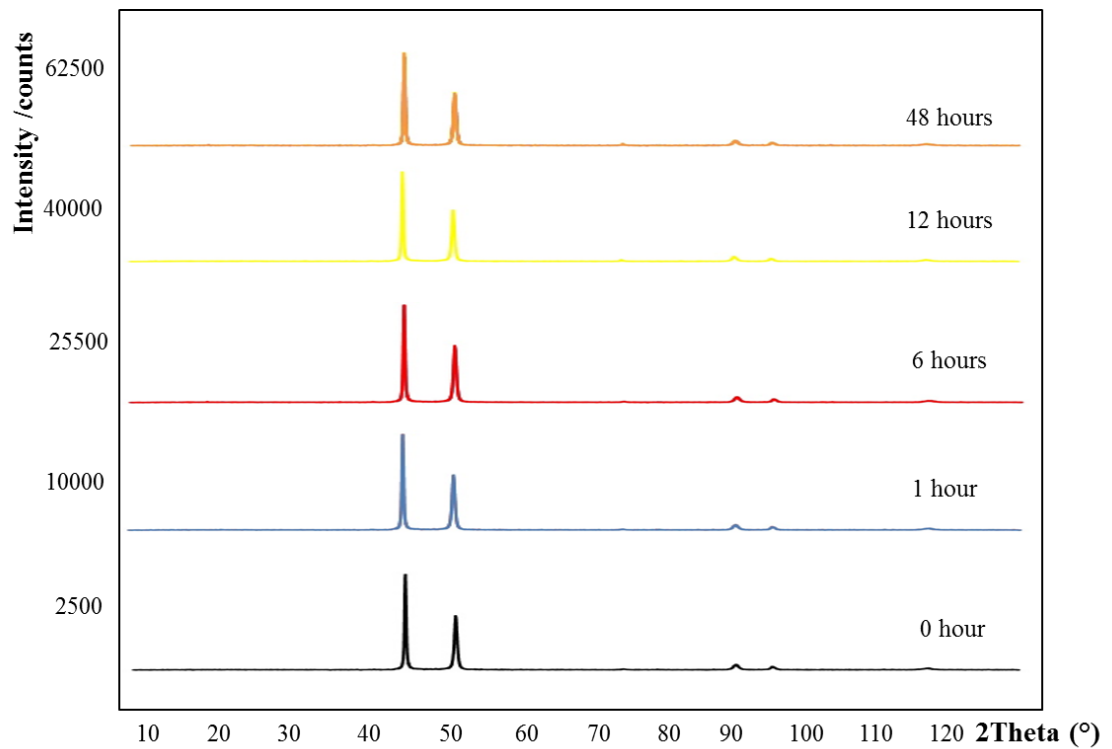
Figure 6.10 XRD scans for EP-100 copper films at 0, 1, 6, 12 and 48 hours after deposition time. The intensity of the peaks was not adjusted to reveal the true intensity. There was no significant difference in the peak width of the diffraction patterns from 0 up to 48 hours.

To test this hypothesis, the copper deposit from the E-100 electrolyte was subjected to XRD analysis at different time intervals after plating: 0, 1, 6, 12 and 48 hours. The XRD analysis results are shown in Fig. 6.10. The results clearly indicated that there was no appreciable change in the peak width of the diffraction patterns from the initial time of deposition (0 hour) to over a period of 48 hours. This implies that the grain structure of the deposits was stable; and that grain growth, which was earlier hypothesised from the ρ data, probably did not occur. Therefore, the decrease in ρ may have been caused by a phenomenon other than self-annealing. One study suggested that minor reduction in deposit resistivity might be due to a recovery process similar to those observed during annealing of

metals [6.24]. This recovery process involves lattice relaxation caused by the annihilation of opposite dislocations in subgrain boundaries. Alternatively, Stangl *et al*. [6.25] observed a stage of significant stress relaxation in the deposit prior to grain growth of self-annealed copper. The phenomenon was due to the diffusion of impurities out of the deposit, and causes only a modest decrease in ρ. It is likely that only stress relaxation occurred in the current samples, and that the energy state in the deposit after stress relaxation was not enough to fuel grain growth.

The deposits from the standard electrolytes displayed the lowest ρ's; while the deposits of the EnFACE electrolyte registered relatively higher sheet resistances. Even the product of the additive-free EnFACE electrolyte (E-0) already had greater ρ than the product of the additive-containing (S) electrolyte. The use of addition agents further increased the ρ of both standard and EnFACE copper, which is due to the observed additive-induced grain refinement in the deposits. The inherently high ρ found in the product of the additive-free EnFACE electrolyte may have been caused by the unconventional nature of the electrolyte composition; specifically, by two factors in the electrolyte: (i) the absence of sulfuric acid or (ii) the low copper salt composition of the electrolyte. Considering the first factor, none of the published works mentioned the influence of sulfuric acid on ρ. Furthermore, Landau [6.26] even suggested the use of acid-free electrolyte to counter the electrical resistance effect in the Damascene process. This means that the acid probably has no significant impact on the conductivity of electroplated films; and that copper plated from an acid-free electrolyte will have no issues when used in interconnect applications. Having eliminated the

contribution of the acid, then it is strongly suspected that the low concentration of copper ions in the electrolyte caused the high ρ in the EnFACE deposit. Anderson [6.27] reported that at low copper ion concentrations and at relatively high current densities, the deposit tends to be fine-grained and consequently resistive. The fine-grained structure resulted from the rapid reduction of metal ions reaching the cathode due to the excess in applied energy or overpotential. Conversely, it is hypothesised that a lower ρ would be obtained from the products of the EnFACE electrolyte if adjustments in the applied current density are done.

6.4. Tensile properties

Table 6.4 presents the measured yield strength (σ_y), tensile strength (σ_f) and ductility (e_f) of the plated copper from the different EnFACE and standard copper electrolytes. The 0.2% offset yield stress was necessary to use, as the stress-strain plot did not show a clear yield plateau. Figure 6.11 shows the plot of mechanical properties of the plated copper as a function of additive concentration. These results reveal the strong effect of additive concentration on mechanical properties. Both σ_y and σ_f increased while e_f decreased with increasing additive concentrations. The percent increase in σ_y and σ_f, and the % decrease in e_f are almost similar; a ~40% change in value from the lowest to the highest additive concentration. Copper plated from the standard electrolyte showed marginally better σ_y and σ_f and lower e_f than the product of the EnFACE electrolyte.

Table 6.4 Mechanical properties of copper plated from the different EnFACE and standard electrolytes.

Sample designation	σ_y (MPa)	σ_f (MPa)	e_f (%)
E-0	126 ± 2.8	132 ± 2.5	2.48 ± 0.07
E-17	154 ± 2.4	171 ± 2.9	2.25 ± 0.04
E-33	159 ± 2.9	185 ± 4.6	2.20 ± 0.07
E-50	167 ± 2.9	213 ± 2.5	2.08 ± 0.08
E-100	206 ± 2.9	238 ± 4.3	2.04 ± 0.04
E-200	227 ± 3.4	288 ± 7.4	1.65 ± 0.03
S-100	218 ± 3.2	255 ± 4.5	1.70 ± 0.02
S-0	136 ± 2.5	145 ± 2.5	2.76 ± 0.01
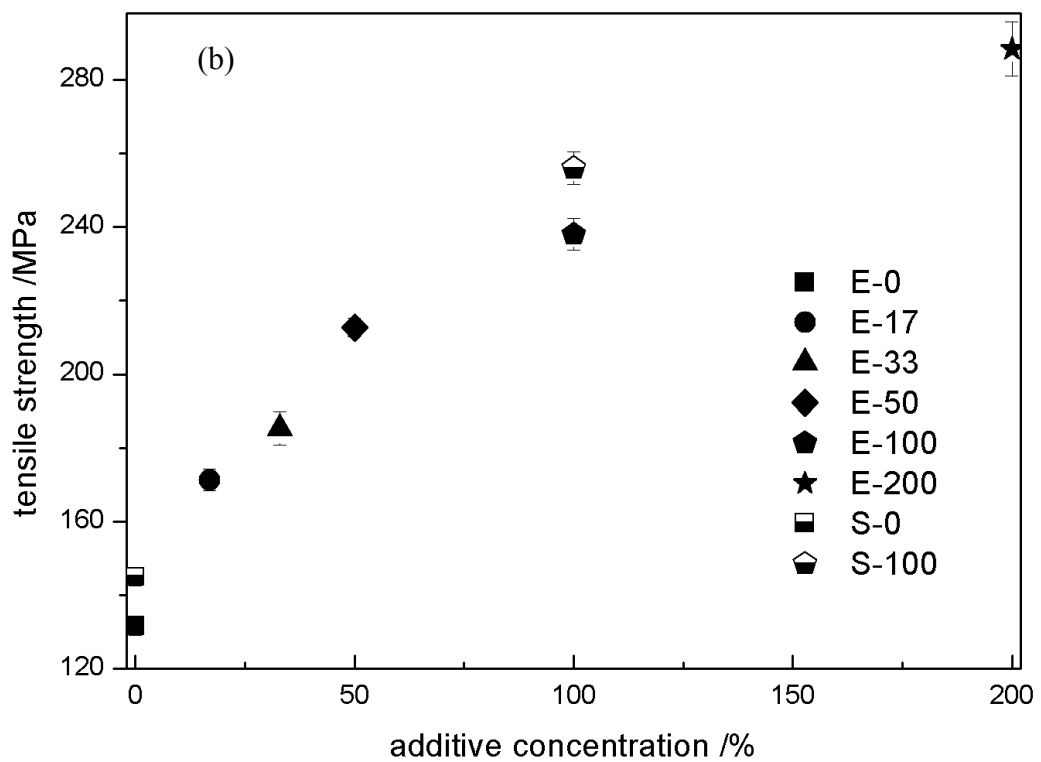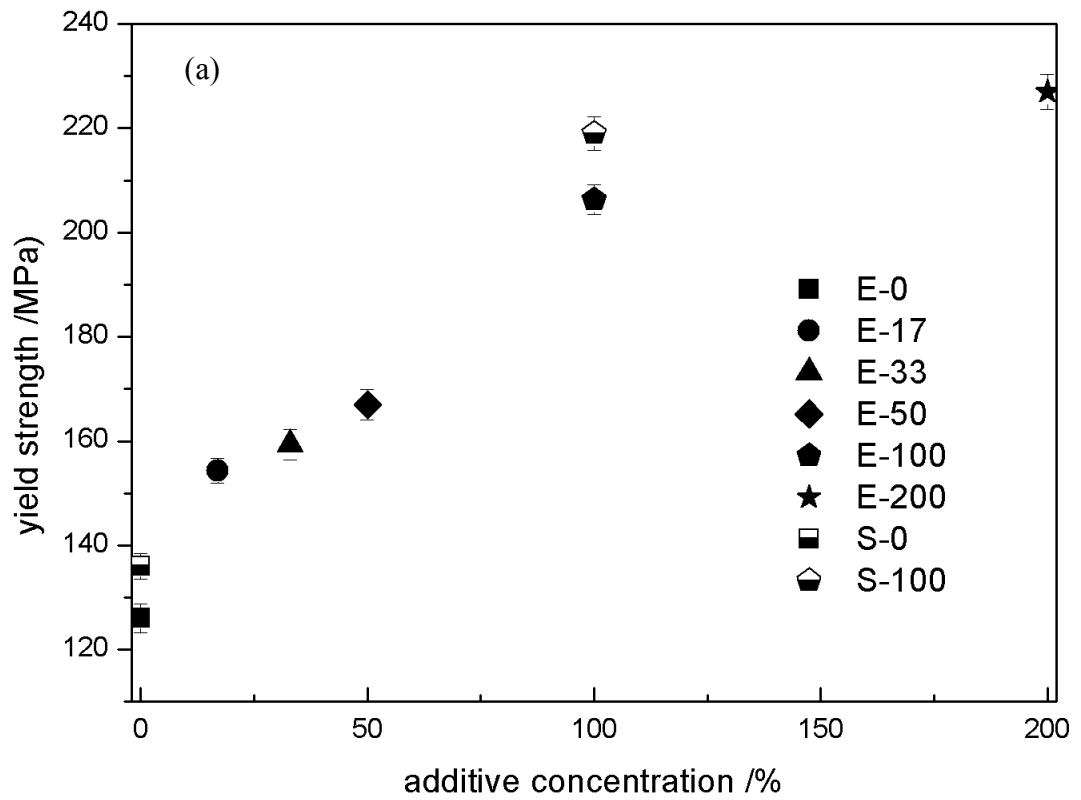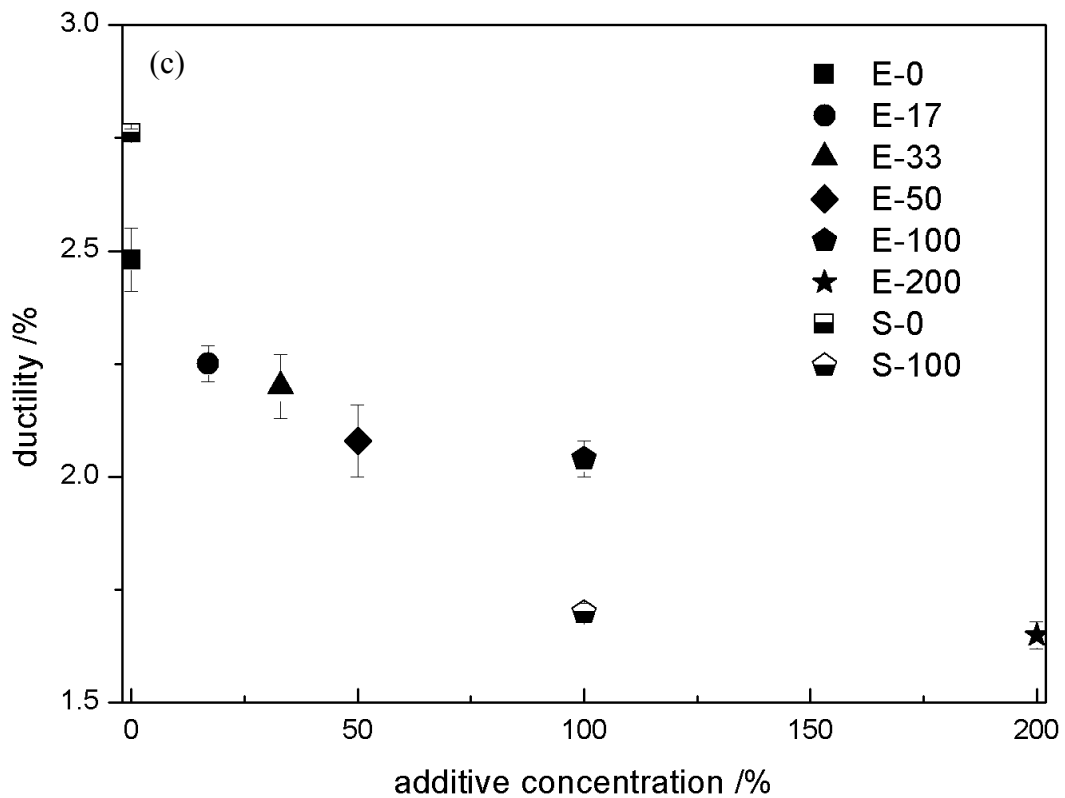
Figure 6.11 Mechanical properties: (a) yield strength, (b) tensile strength, and (c) ductility, of copper films of the EnFACE electrolyte with different additive concentrations.

The observed trends in the standard and EnFACE deposits are consistent with the well-known mechanical behavior of metals. Typically, an increase in the metal's strength will be accompanied by a loss in ductility. The results also indicate a clear improvement in the mechanical strength of the plated copper when additives are used with the electrolyte. To explain how additive concentration affects mechanical properties, one needs to consider the inherent microstructural features of the plated metal. Important microstructural features include dislocations, grain boundaries and voids [6.7].

It is reasonable to assume that the observed grain size refinement directly caused the changes in the metal's σ_y and ductility; a statement consistent with published work [6.28, 6.39, 6.30]. Classical theories on slip and plastic yielding explain how grain boundaries can serve as dislocation barriers, thereby lowering dislocation mobility and preventing easy plastic deformation to occur. Consequently, such an action increases σ_y and lowers ductility. Tensile strength, on the other hand, is strongly affected by the amount of voids, and an inverse relation exists between the two.

A quantitative correlation between the measured grain size and yield strength, σ_y, is possible by using the Hall-Petch equation (see section 2.5.2):

$$\sigma_y = \sigma_o + \frac{k_y}{\sqrt{d}} \qquad \text{Equation (6.2)}$$

where σ_o is the initial stress to cause dislocation motion, and k_y is the strengthening coefficient. These two parameters are constants specific to each material. The equation predicts a linear relationship between σ_y and $1/\sqrt{\text{grain}}$ diameter, $d^{-1/2}$.

Figure 6.12 shows the plot of σ_y versus $d^{-1/2}$, where deposit grain sizes were obtained from the EBSD analysis. Another plot is superimposed which shows the Hall-Petch predicted values for copper ($\sigma_o = 25$ MPa and $k_y = 0.14$ MPa.m$^{1/2}$) [6.31].

The plot of experimental data shows poor linearity; further indicated by the low value of R^2 (i.e. 0.69). Consequently, the derived material constants for the DC-plated copper were significantly different from the theoretical value. This

deviation from Hall-Petch linearity may be due to factors that affect the mechanical strength of copper such as solute atoms, dislocations, voids and pores. The inherently low ductility of the DC-plated specimens is a good indication of the presence of voids in the plated copper. Voids, and other so-called stress concentrators, in the deposit can cause mechanical weakness, especially when void density is above a critical value [6.32]. Voids lead to reliability problems in copper metallisation [6.33]. The study by Feng *et al.* [6.34] suggests that void formation favors high current densities as well as aged electrolytes. Alternatively, a non-uniform plating thickness may also cause considerable mechanical weakness. Non-uniform deposit thickness occurs when some plating areas, particularly the edges, possess higher current densities and experience faster deposition rate. In the case of non-uniform thickness, the thinner regions will possess a lower load-bearing cross-sectional area. Consequently, these areas will be the first to break under a load. Future studies may then focus on reducing void density in the EnFACE plating, as well as improving deposit thickness to minimise inaccuracies in the results of the mechanical tests.
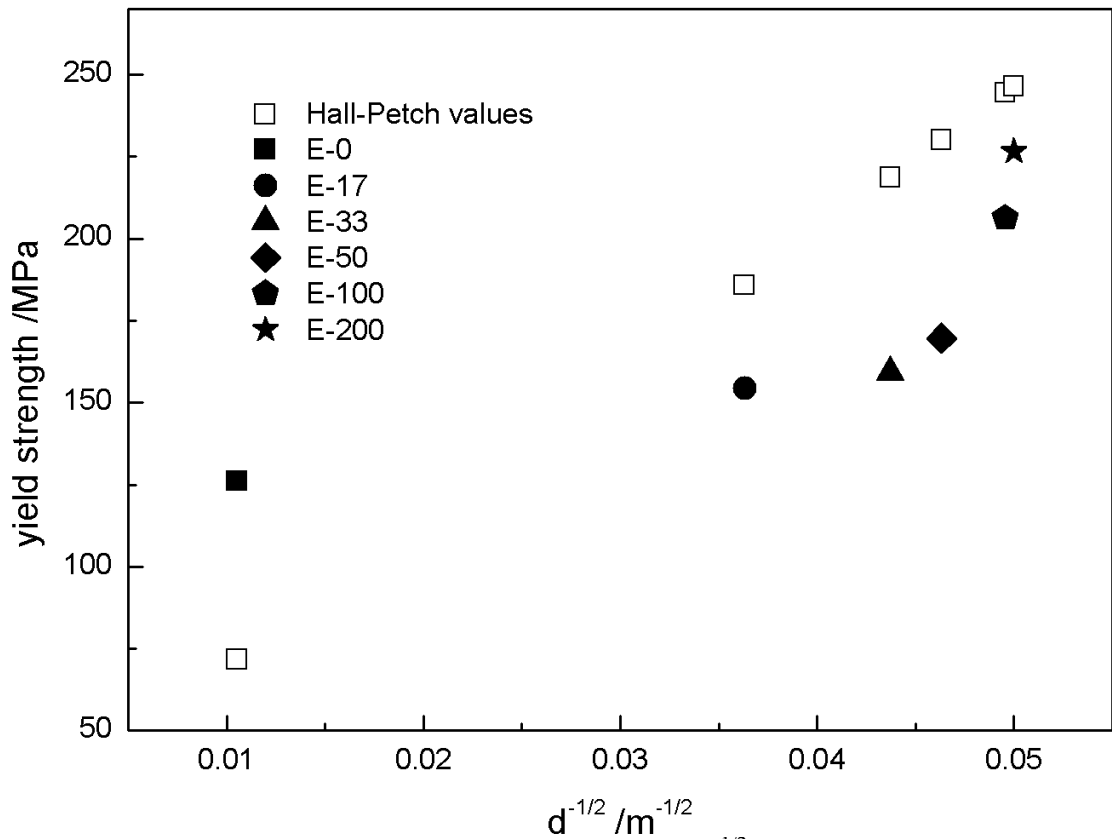
Figure 6.12 Plot of yield strength versus grain diameter$^{-1/2}$ for the DC-plated copper compared against the Hall-Petch predicted values.

6.5 Through-Hole Plating

Figure 6.13 is a magnified image of a cross section of the plated through hole. The deposit thickness was not always uniform and plating overhangs can also be present that made measurements difficult. Figure 6.14 presents a comparison of the deposit thickness measured at three locations: at the exposed area or at the top (T) of the through-hole; at the hole corner or edge (E), and at the center (C) of the hole.

The results indicated that the thickest deposit was formed at the top (T) of the through-hole, followed by the hole corner or edge (E), then at the center (C) of the hole. Also, the measured thickness at C appears to be constant, regardless of

additive concentration and hole diameter. Lastly, the measured thickness at T and E significantly increase with additive concentration; but was not significantly affected by the size of the through-hole.
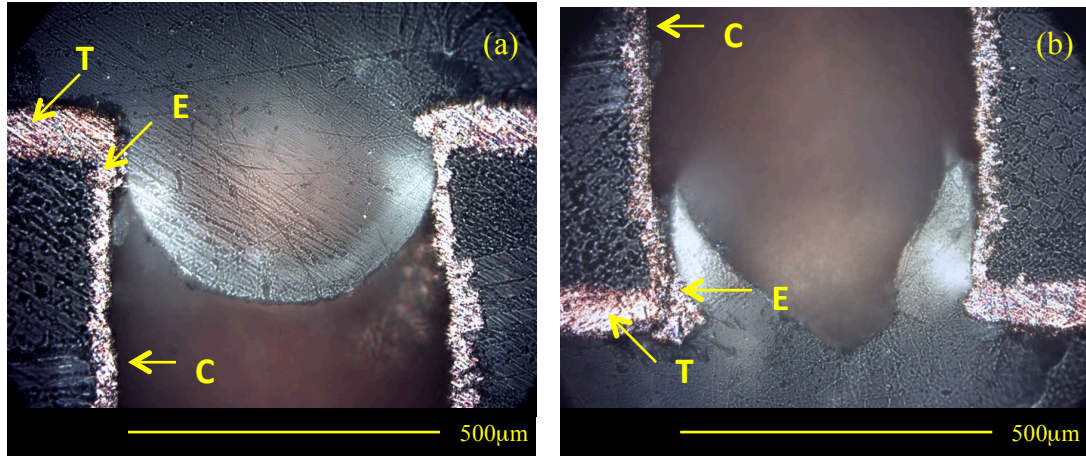
Figure 6.13 Light microscope image of a cross-section of the plated through-hole: (a) top and (b) bottom section. The sections where thickness measurements were taken are also indicated: (i) T - top; (ii) E – edge; (iii) C - center of hole.
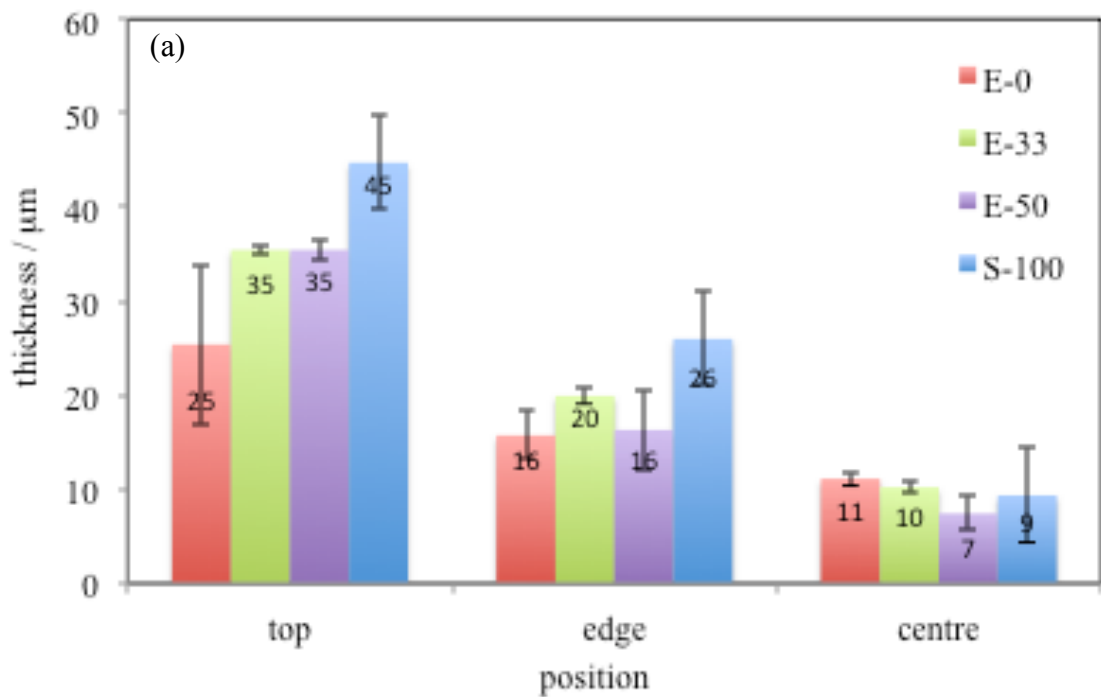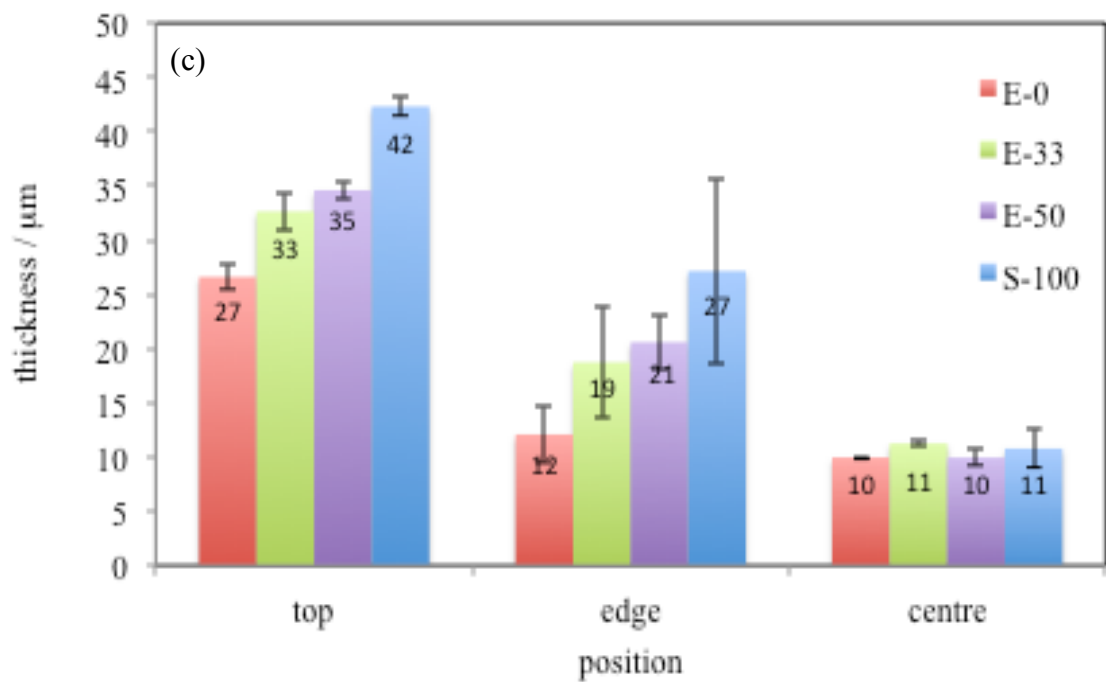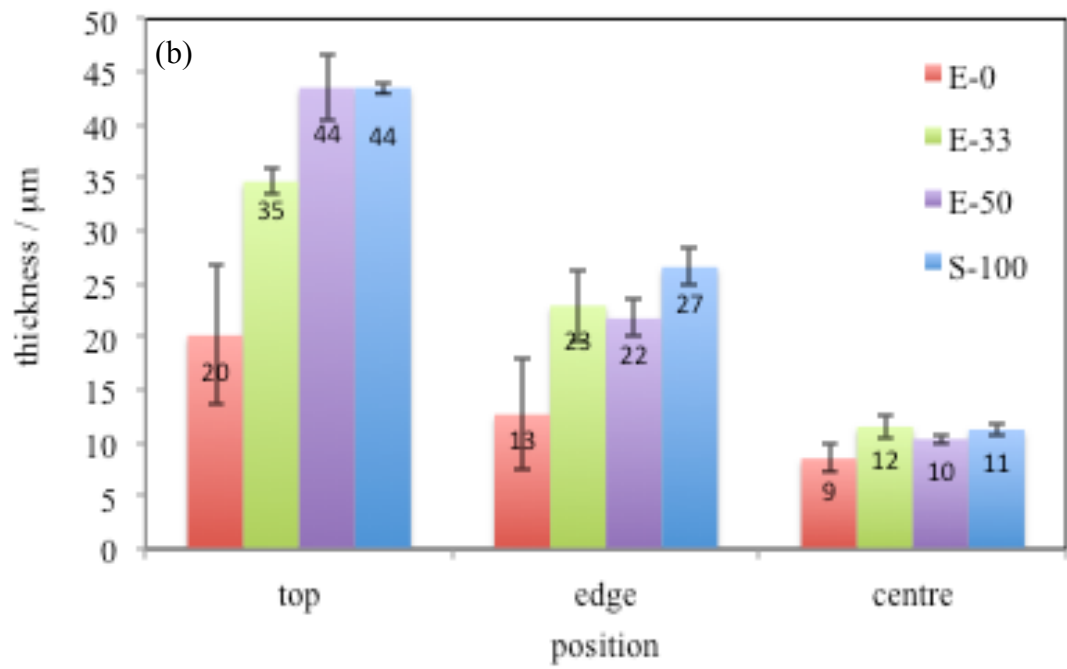
Figure 6.14 Thickness measurement at the top, edge and center of hole of the plated through-hole for the different hole diameters: (a) 200 μm; (b) 350 μm and (c) 500 μm.
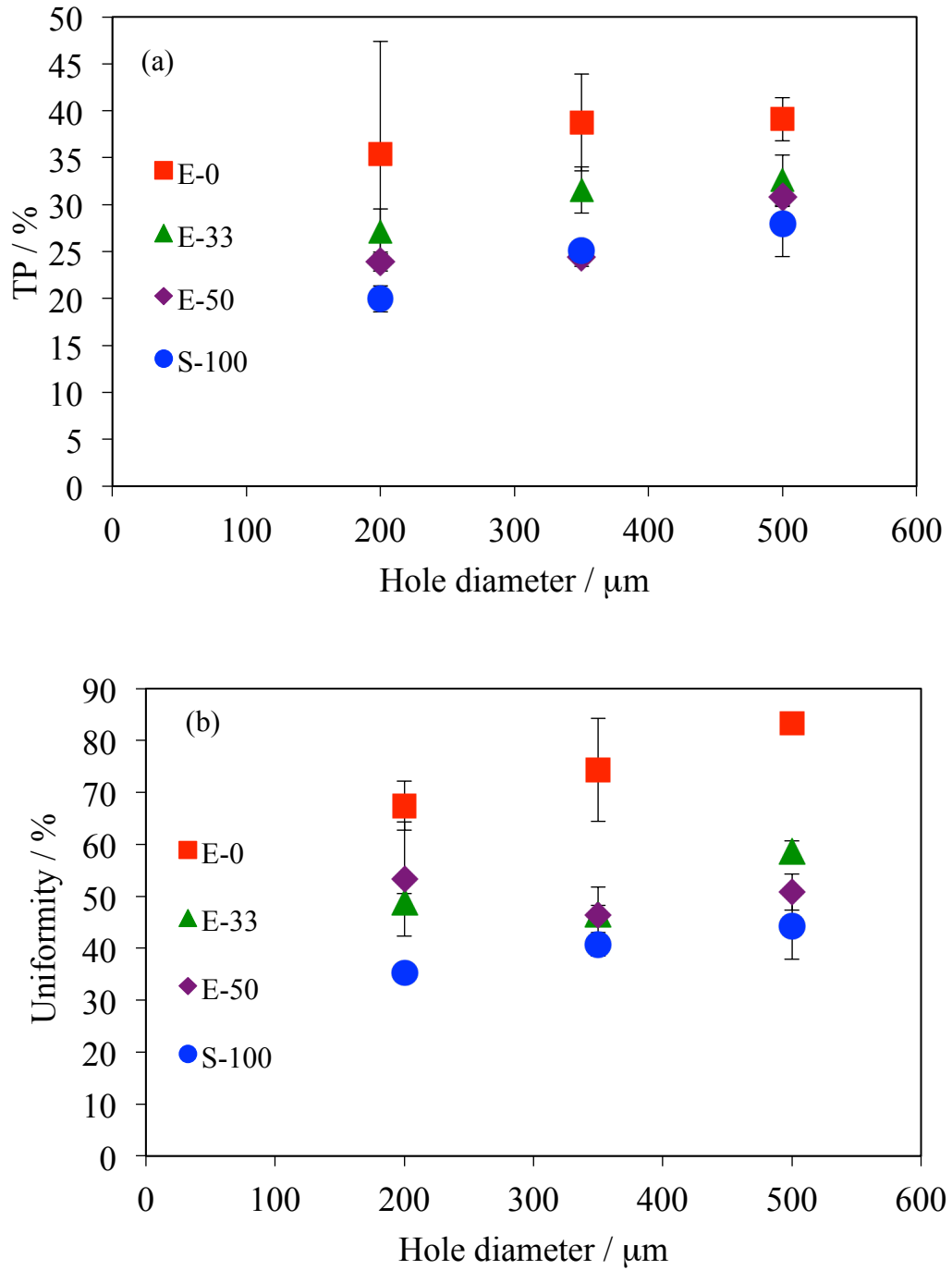
Figure 6.15 Plot of (a) throwing power and (b) uniformity versus hole diameter for the through-hole plated features using the different electrolytes.

Throwing power (TP) and uniformity was measured to assess the uniformity of plating thickness in the plated through-holes. Figure 6.15a and b shows TP and uniformity, respectively, as a function of hole diameter for the different electrolytes. Since the T and E plating thicknesses were significantly increasing with increasing additive concentration, while the C thickness remained unchanged, then both TP and uniformity decreased with increasing additive amounts. On the other hand, while it is expected that TP and uniformity should increase with increasing hole diameter, no clear relationship between these parameters was observed.

The results indicated that additives created poor plating thickness uniformity in the through holes. Interestingly, additives are known to improve throwing power of different plating systems [6.31]. The contrast in the current result may be the result of the absence of stirring or mechanical agitation during through-hole plating. The fact that the hole center thickness remained the same regardless of changes in hole diameter and the presence of additives is proof that the conditions in the holes during plating were fairly constant. Also, the observation that only the deposit thickness in the exposed region was affected by the presence of additives is another proof that the additives were not uniformly distributed. By stirring the plating solution, the additives would have reached different areas of the through-hole and create the expected changes in plating kinetics. Stirring would have also added more contrast and thus reveal the true effect of hole diameter on TP.

While the additive-free EnFACE electrolyte had some shortcomings in terms of through-hole plating (THP) performance, the performance of the E-50

electrolyte was comparable to the standard copper (S-100) electrolyte. This is welcome news as this increases the possibility of employing the additive-containing EnFACE electrolyte for PCB application.

In this chapter, the influence of additives on the morphological, mechanical and electrical properties of DC-plated copper from the EnFACE solution was discussed. The primary effect of additives on the copper deposit is grain refinement. Such reduction in the grain size resulted to an increase in the mechanical strength, and a reduction in the ductility and conductivity of the copper deposits.

References

6.1   Liebreich E (1935) The Effects of Film Formation on the Structure of Electrodeposited Metallic Coatings. Downloaded by Newcastle University on 24/10/2013 21:20:09,1188-1194]

6.2   Oniciu L, Muresan L (1991) Some Fundamental Aspects of Levelling and Brightening in Metal Electrodeposition. J. Appl. Electrochem. 21; 565-574

6.3   Dela Pena EM, Roy S (2015) Effect of additive concentration during copper deposition using EnFACE electrolyte. IMF 93(6); 288-293

6.4   Schönenberger I, Roy S (2005) Microscale pattern transfer without photolithography of substrates. Electrochim. Acta 51; 809-819

6.5   Hansal EGW, Roy S (2012) Pulse plating. 1st edition, Eugen G. Lueze Verglag KK. Germany; pp. 100-118

6.6   Paunovic M, Arndt R (1983) Surface Preparation and Finishes for Metals. J. Electrochem. Soc. 130; 794-799

6.7   Dini D, Snyder D (2010) Modern Electroplating: 5th Edition" Edited by Mordechay Schlesinger, Milan Paunovic, John Wiley and Sons, NY

6.8   Tan M, Guymon C, Wheeler D, Harb J (2007) The Role of SPS, MPSA, and Chloride in Additive Systems for Copper Electrodeposition. J. Electrochem. Soc. 154 (2); D78-D81

6.9   Kim MJ, Cho SK, Koo H-C, Lim T, Park KJ, Kim JJ (2010) J. Electrochem. Soc. 157; D564-D569

6.10   Fisher, G.L. 1978. Power Savings Using Sulfur-Activated Nickel Anode Materials. Plat. Surf. Finish. 65; 46-53

6.11   Darken J (1979) Recent Progress in Bright Plating from Zincate

Electrolyte. Trans IMF 57; 145-145

6.12   Paunovic M, Schlesinger M (1998) Fundamentals of Electrochemical

Deposition. John Wiley & Sons Inc

6.13   Manu R, Jayakrishnan S (2010) Influence of polymer additive molecular

weight on surface and microstructural characteristics of electrodeposited

copper. Bull. Mater. Sci. 32(2); 347-356

6.14   Cullity BD, Stock SR (2001) Elements of X-Ray Diffraction (2001) 3rd

Ed. Prentice-Hall Inc; 167-171

6.15   Marechal N, Quesnel E, Pauleau Y (1994) Characterization of silver

films deposited by radio frequency magnetron sputtering. J. Vac. Sci.

and technol. 12; 707-714

6.16   Knorr DB, Tracy DP (1995) A review of microstructure in vapor

deposited copper thin films. Materials Chemistry and Physics 41(3); 206

− 216

6.17   Gupta T (2009) Copper Interconnect Technology. Springer-Verlag New

York Ed. 1; 423-465

6.18   Mayadas A, Shatzkes M (1970) Electrical-Resistivity Model for

Polycrystalline Films: the Case of Arbitrary Reflection of External

Surfaces. Phys. Rev. B 1; 1382-1389

6.19   Harper J, Cabral C, Andricacos P, Gignac L, Noyan I, Rodbell K, Hu C

(1999) J. Appl. Phys. 86; 2516–2525

6.20   Moffat TP, Bonevich JE, Huber WH, Stanishevsky A, Kelly DR,

Stafford GR and Josell D (2000) Superconformal Electrodeposition of

Copper in 500-90 nm Features. J. Electrochem. Soc. 147(12); 4524-4535

6.21   Brongersma SH, Richard E, Vervoort I, Bender H, Vandervorst W, Lagrange S, Beyer G, Maex K (1999) J. Appl. Phys. 86; 3642-3645

6.22   Moffat TP, Wheeler D, Witt C, Josell D (2002) Superconformal Electrodepositon Using Derivatized Substrates. Electrochem and Solid-State Lett. 5; C110-C112

6.23   Nishi Y, Doerin R (2008) Handbook of Semiconductor Manufacturing Technology, Second Edition. CRC Press, FL, USA, 11-79

6.24   Alshwawreh N, Militzer M, Bizzotto D, Kuo JC (2012) Resistivity-microstructure correlation of self-annealed electrodeposited copper thin films. Microelectronic Engineering 95; 26-33

6.25   Stangl M, Acker J, Dittel V, Gruner W, Hoffmann V, Wetzig K (2005) Characterization of electroplated copper self-annealing with investigations focused on incorporated impurities. Microelect. Eng. 82; 189–195

6.26   Landau U (1982) Plating New Prospect for an Old Art, Electrochemistry in Industry, New Directions, Plenum Press New York

6.27   Anderson D, Haak R, Ogden C, Tench D, White J (1985) Tensile Properties of Acid Copper Electrodeposits. J. Appl. Electrochem. 15; 631-637

6.28   Hofer EM, Hintermann HE (1965) The Structure of Electrodeposited Copper Examined by X-Ray Diffraction Techniques. J. Electrochem. Soc. 112(2); 167-173

6.29   Michailova E, Vitanova I, Stoychev D, Milchev A (1993) Initial Stages

of Copper Electrodepostion in the Presence of Organic Additives. Electrochim. Acta 38(16); 2455-2458

6.30 Rusli E, Xue F, Drews T, Vereecken P, Andricacos P, Deligianni H, Braatz R, Alkire R (2007) Effect of Additives on Shape Evolution during Electrodeposition. J. Electrochem. Soc. 154(11); D584 – D597

6.31 Davis JR (2001) ASM Specialty Handbook: Copper and Copper alloys. Edited by JR Davis, Davis and Associates. ASM International Materials Park, OH USA 44073-0002

6.32 Romankiw LT, Sullivan O (1997) Plating Techniques. Handbook of Microlithography, Micromachining, and Microfabrication. Vol 2 SPIE Press Bellingham Washington DC

6.33 Datta M, Romankiw LT (1989) Application of Chemical and Electrochemical Micromachining in Electronics Industry. J. Electrochem. Soc. 136(6); 285C-292C

6.34 Feng H.P, Cheng MY, Weng YL, Chang SC, Wang YY, Wan CC (2006) Mechanism for Cu Void Defect on Various Electroplated Film Conditions. Thin Solid Films 488; 56-59

Chapter 7

Results and Discussion: Structures and Properties of Pulsed Current plated Copper from EnFACE Electrolyte with Additives

The use of pulsed current is known to improve the properties of electroplated deposits. The current chapter presents the results of characterisation on PC-plated copper from the EnFACE electrolyte with additives. Whenever possible, these results will be compared with the results of the DC-plating experiments presented in Chapter 6. This will give us a better perspective on the data obtained and allow us to draw more meaningful conclusions.

Some of the supplementary objectives of the study were: (i) to determine if the properties of the DC and PC-plated copper from the EnfACE electrolyte can meet the property requirements of the industry on electronic copper described in IPC-TM-650; and (ii) determine an optimum additive concentration for the EnFACE electrolyte. The pulse plating parameters used in the electroplating experiments were listed in table 4.11. The results of these investigations are presented in a latter section.

7.1 Morphology and grain size

The SEM images (planar view) of the PC plated deposits using EnFACE electrolyte with different additive concentration and the standard electrolyte are presented in Fig.7.1. Similar to the DC-plated copper, the additive-free electrolytes (i.e. EP-0 and SP-0) gave the coarsest deposits. On the other hand, with the use of increasing amounts of additive, the deposits became smoother and featureless. The

product of the electrolytes with 100% (EP-100) and 200% (EP-200) additive concentrations appeared the smoothest.

These results indicated that even low concentration of additives can (i) produce smooth deposits and (ii) continue to influence deposit properties during PC deposition. As mentioned in the previous chapter, low surface roughness points to a fine-grained structure, and such would have implications on deposit properties.

a) EP-0   b) EP-17   c) EP-33

d) EP-50   e) EP-100   f) EP-200

g) SP-0   h) SP-100
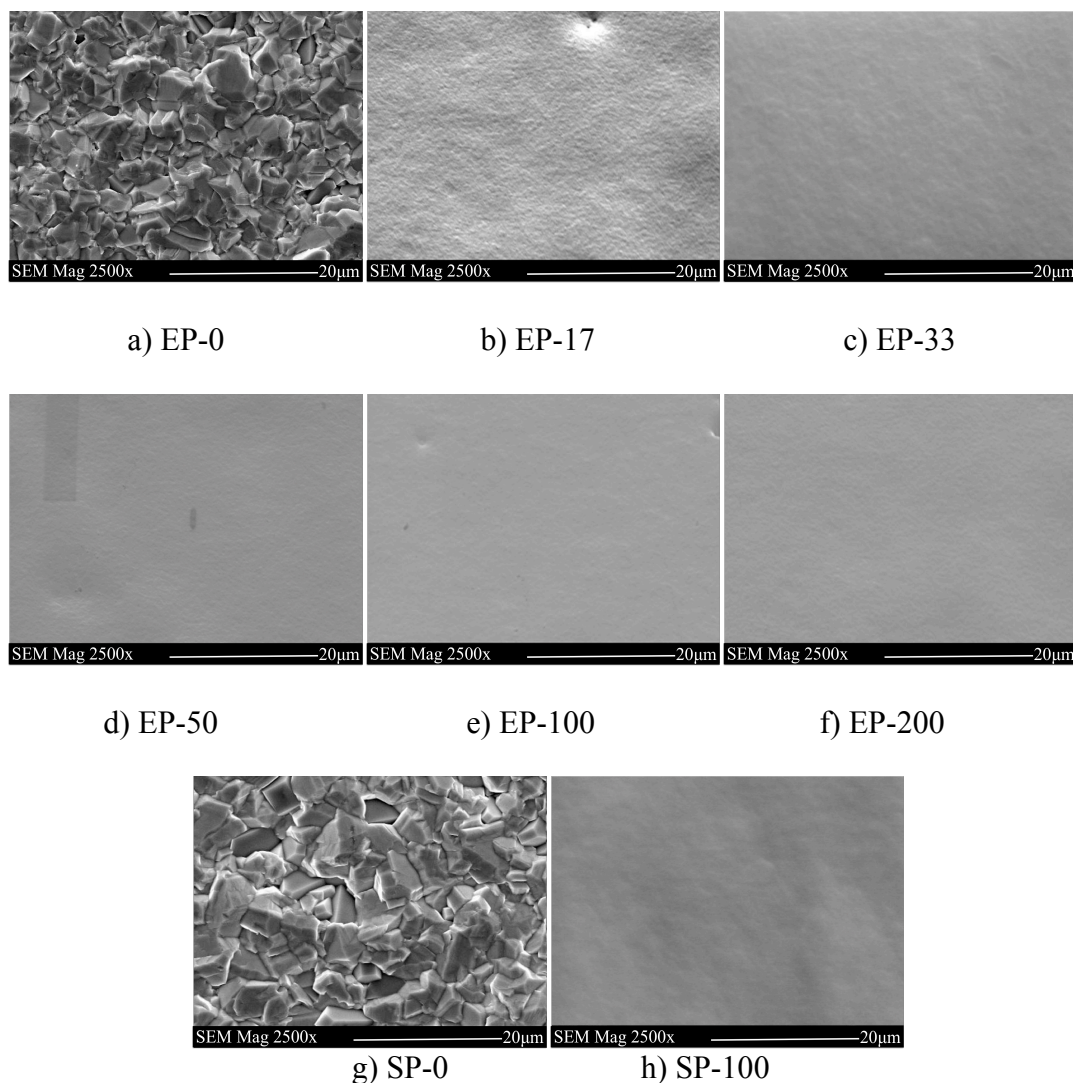
Figure 7.1 SEM images of PC–plated copper deposits from EnFACE electrolyte with different additive concentration: a) EP-0 with no additive, b) EP-17 with 17% additive concentration, c) EP-33 with 33% additive concentration, d) EP-50 with 50% additive concentration, e) EP-100 with 100% additive concentration and f) EP-200 with 200% additive concentration; and standard electrolyte g) SP-0 with no additive and h) SP-100 with 100% additive. These percentages are relative to the industry recommended additive concentration of 10 ml/L Copper Gleam B, 0.5 ml/L Copper Gleam A, and 70 ppm Cl$^-$.

Figure 7.2 shows the corresponding EBSD maps for the products of the PC-plated Cu using the EnFACE electrolytes with different additive concentrations. No EBSD data was obtained for the deposits of the additive-free electrolytes. The rough

surface of these deposits made it difficult to obtain quality EBSD patterns. Table 7.1 gives a summary of the calculated grain size of the PC-plated deposits, while Fig. 7.3 shows a comparison of the grain size of the DC and PC-plated Cu at different additive concentrations in the EnFACE electrolyte. Again, since the large grain size scale range used in Fig. 7.3a does not immediately reveal the effect of additives and pulsed current modulation on grain size, a plot of grain size in the additive concentration range of 17% to 200% is shown in Fig. 7.3b.

a) EP-17   b) EP-33   c) EP-50

d) EP-100   e) EP-200   f) SP-100

g) inverse pole legend
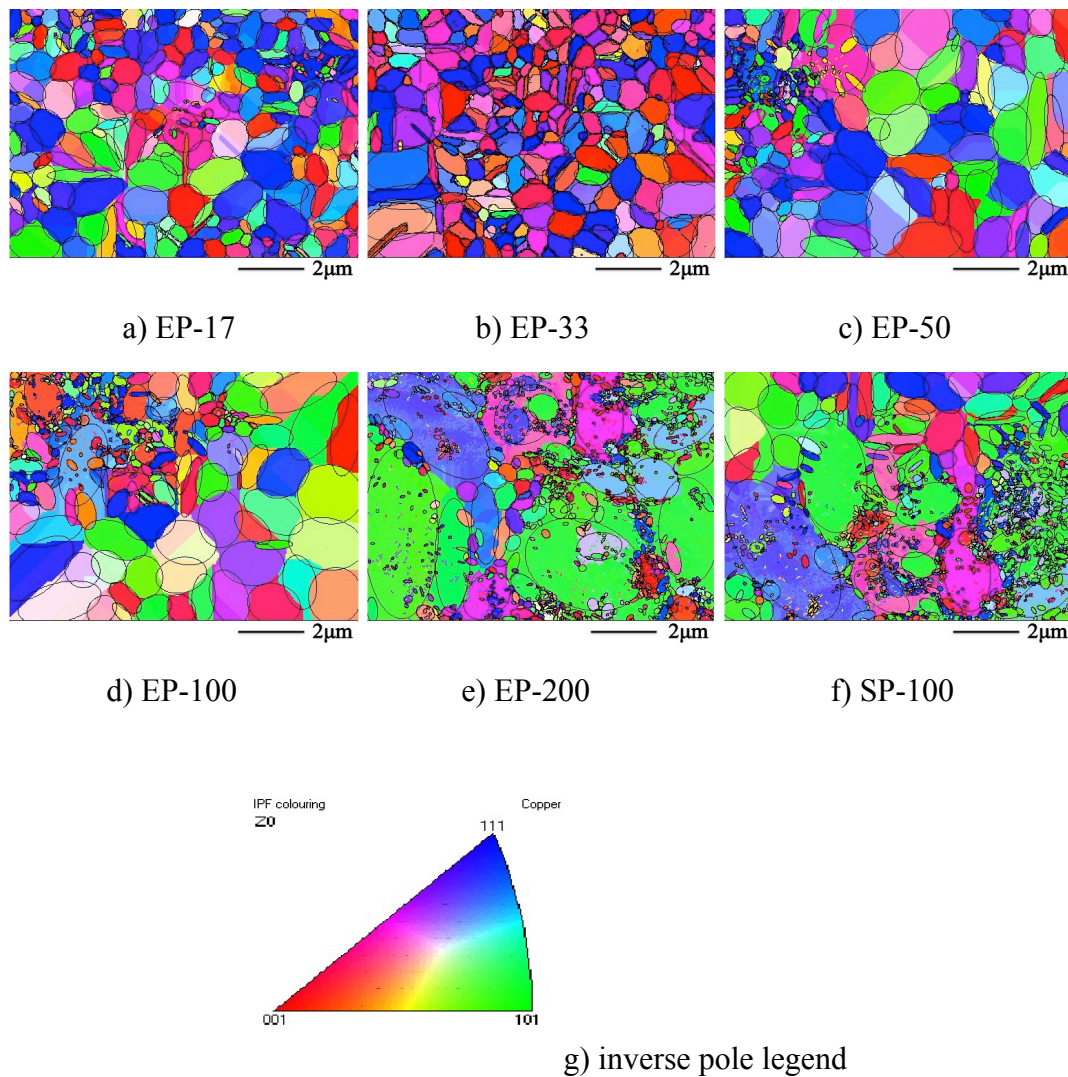
Figure 7.2 EBSD images of pulse deposited copper from EnFACE electrolyte with different additive concentration: a) 17% (EP-17), b) 33% (EP-33), c) 50% (EP-50), d) 100% (EP-100), e) 200% (EP-200), and f) standard electrolyte (SP-100). These percentages are relative to the industry recommended additive concentration of 10 ml/L Copper Gleam B, 0.5 ml/L Copper Gleam A, and 70 ppm Cl⁻. The calibration bar represents a length of 2 μm. The different colours in the EBSD map represent different crystals planes as described by the g) inverse pole legend.

Table 7.1 Grain size of PC-plated deposits from the standard and EnFACE electrolyteswith different additive concentration.

Specimen designation	PC-plated Cugrain size (nm)
EP-0	2459±35
EP-17	659±38
EP-33	465±29
EP-50	335±25
EP-100	303±12
EP-200	235±24
SP-0	8941± 117
SP-100	290±26
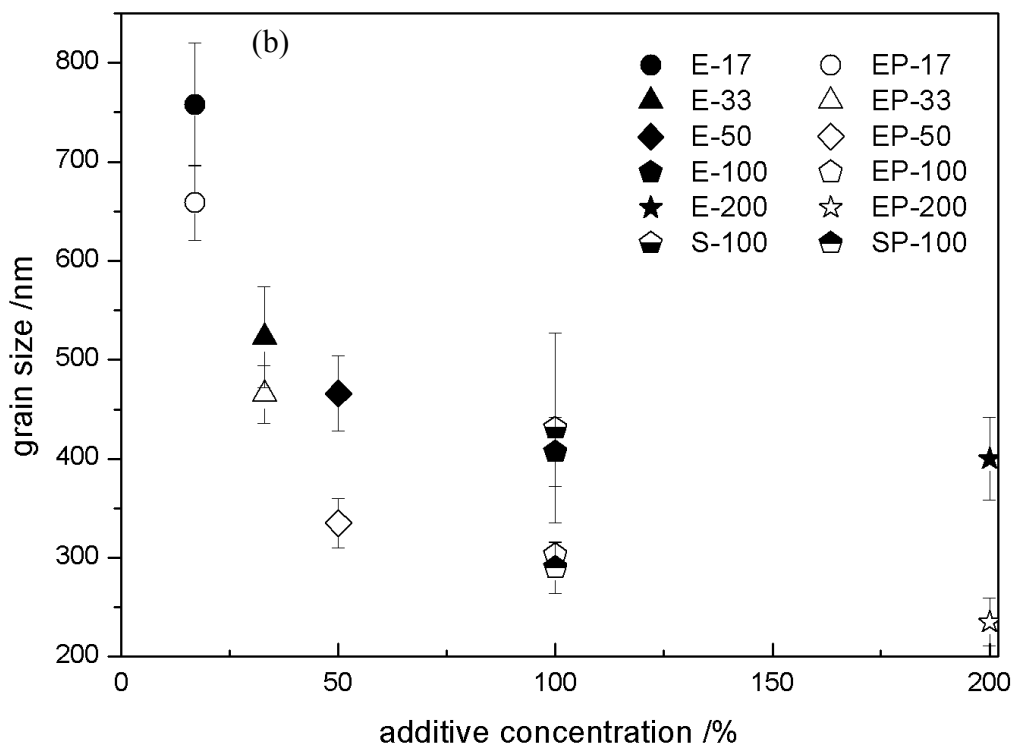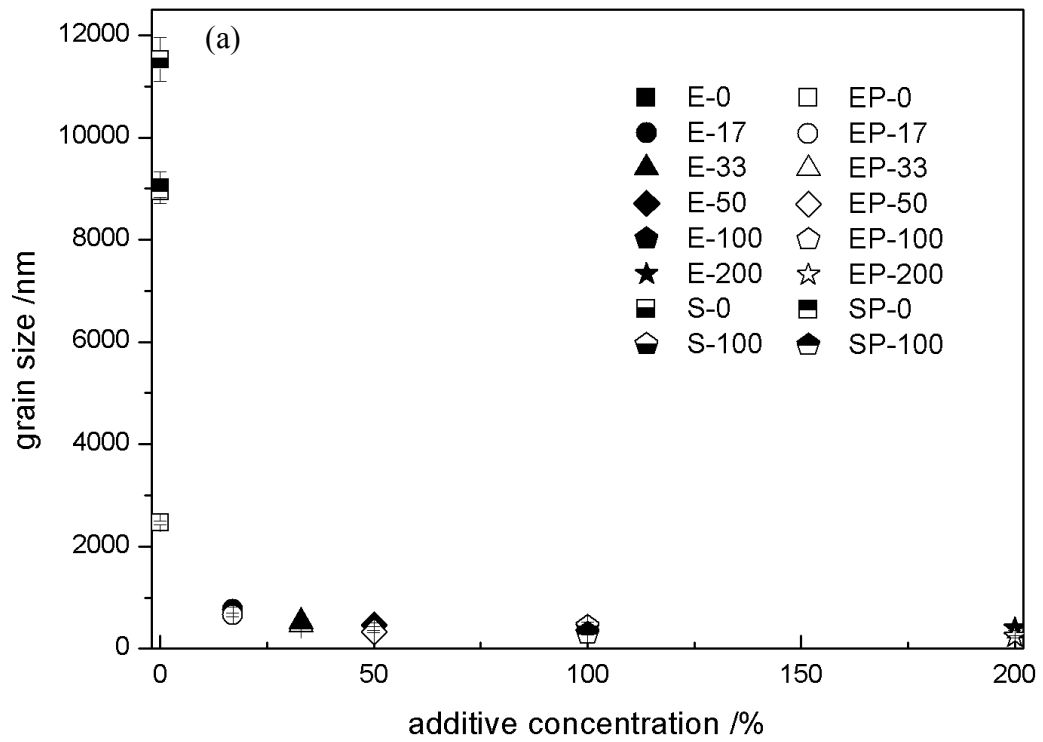
Figure 7.3 (a) Grain size of DC and PC-plated Cu using the EnFACE electrolyte at different additive concentrations. (b) Plot zoomed in at the additive concentration range 17 to 200%.

The EBSD images showed that the grain structure was predominantly equiaxed. The coarsest grains were found in the deposits from the additive-free electrolytes; and the grain size became smaller as additive concentration increased. In both EnFACE and standard electrolytes, the PC-plated deposit had finer grains than their DC-plated counterparts.

Both the SEM and EBSD results indicated that additives created a finer grain structure in the deposit in PC plating modes; and validated the grain-refining action of additives on the Cu deposits. This is consistent with past studies that reported the benefits of additives in PC [7.1, 7.2, 7.3, 7.4] plating using the conventional acid-copper sulphate baths. The grain refining effect of additives in the acid-free, low metal ion concentration electrolyte appears to be more pronounced than in the standard electrolyte, as seen with the finer grain size observed in the deposits of the EnFACE electrolyte compared to the standard at the same additive concentration. Figure 7.3 also shows that the degree of grain refinement is proportional to the amount of additives. However, as was also seen in the DC-plated copper films, the decrease in grain size was marginal beyond the 100% concentration, consistent with the polarisation plateau.

The appearance of small grains scattered on larger grains suggest the nucleation of new grains on top of the initial Cu deposit. The propensity for grain nucleation appears to be dependent on additive concentration, since this phenomenon was seen in electrolytes having at least 50% additive concentration (i.e. EP-50, EP-100 and EP-200).

Figure 7.3a indicated that the reduction in grain size caused by using pulsed current in the additive-free EnFACE electrolyte is significantly greater than in the additive-free standard electrolyte. To illustrate, the decrease in grain size from DC to PC plating is 72% for the deposit from the EnFACE electrolyte and only 22% for the deposit from the standard electrolyte. This difference may be traced to the difference in the composition of the two electrolytes. The absence of the acid and the low Cu salt concentration makes the EnFACE electrolyte sensitive to mass transport effects. Pulse plating is known to positively influence mass transport especially in the vicinity of the electrode [7.5].

Results indicated that pulsed current caused additional grain refinement in the deposits from the additive-containing EnFACE electrolyte, as seen in Fig. 7.3b. Such result agrees well with published studies [7.4, 7.5, 7.6, 7.7], which suggest that pulsed current can increase nucleation while limiting grain growth in deposits [7.3, 7.4, 7.8].

Additional insights on the interaction of pulsed current and additives are gained by comparing the grain size of the PC-plated and DC-plated Cu using the EnFACE and the standard electrolyte at additive concentrations of 0% and 100%, as shown in Fig. 7.3. At zero concentration, the disparity between the grain sizes of DC- and PC-plated Cu films is significant and quite evident, indicating the strong influence of pulsed current. However, at 100% additive concentration (EP-100), the difference between grain size of the deposits becomes minimal, indicating that size became independent of the plating mode (i.e. DC or PC plating). This implies that (i) the grain-refining effect of pulse plating is more pronounced when additives are not present; and that (ii) the influence of additives dominates over pulsed current when

these two factors are present. The strong influence of additives may be related to the effect of additives on both diffusional and non-diffusional mechanisms of plating [7.5, 7.9, 7.10, 7.11].

7.2 Microstrain and Crystallographic texture

Figure 7.4 shows the XRD patterns of the PC deposited Cu. Five prominent peaks were again present in the XRD plots: (111), (200), and (220), (311) and (222). Figure 7.5gives a magnified view of the peaks corresponding to these five diffraction planes. In the PC-plated deposit, the diffraction peak intensity increased up to the EP-33 electrolyte, then became steady beyond the 33% additive concentration. Peak broadening in the (111), (200), and (220) steadily increased with increasing additive concentration.
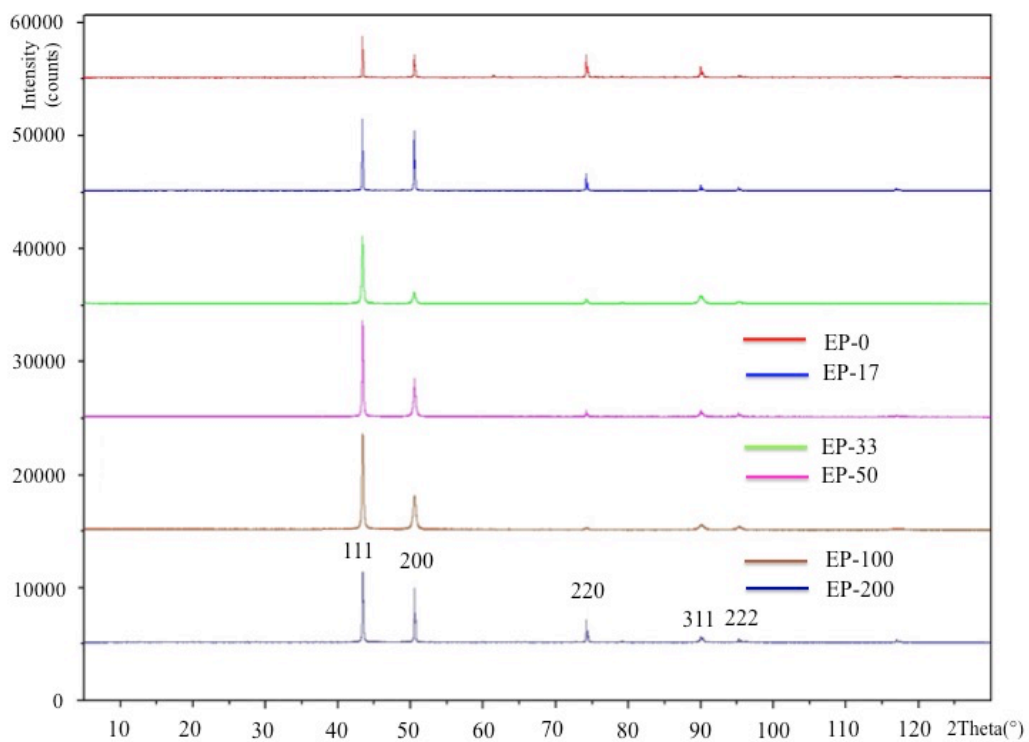
Figure 7.4 XRD scans of (a) pulse deposited copper films at different additive concentration. The scans were shifted along the intensity axis except the high concentration setting. However, the intensity of the peaks was not adjusted to reveal the true intensity.

(a)

(b)
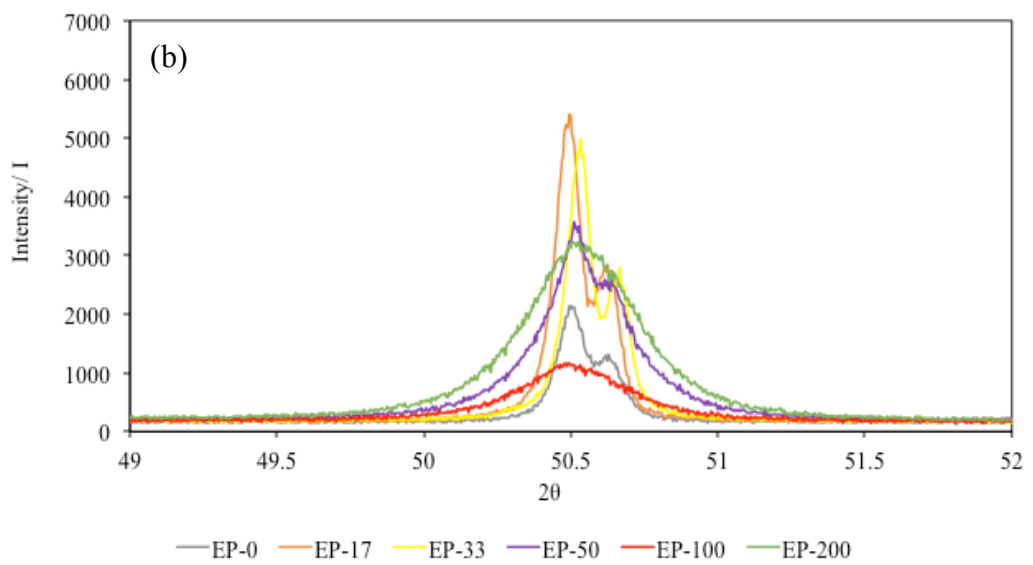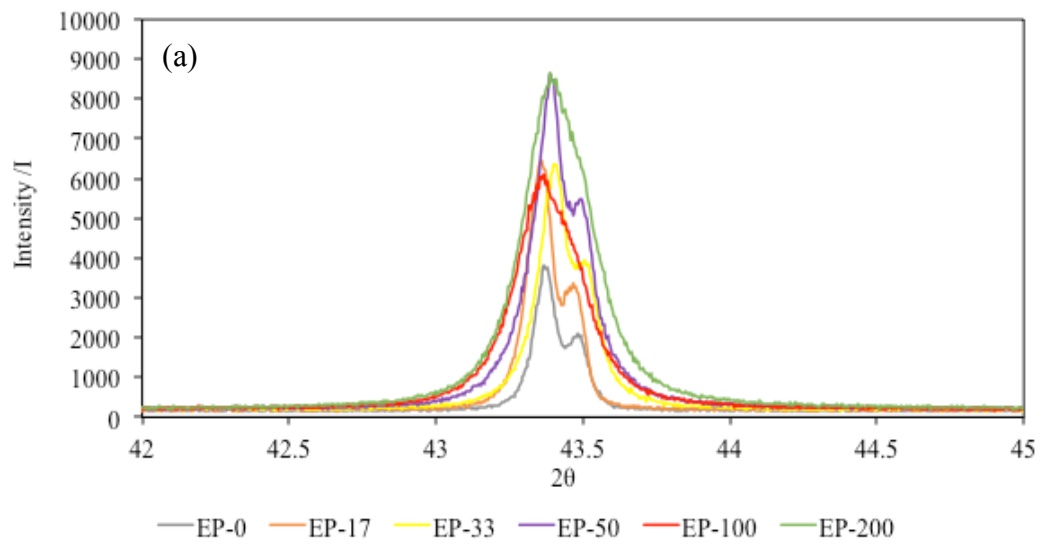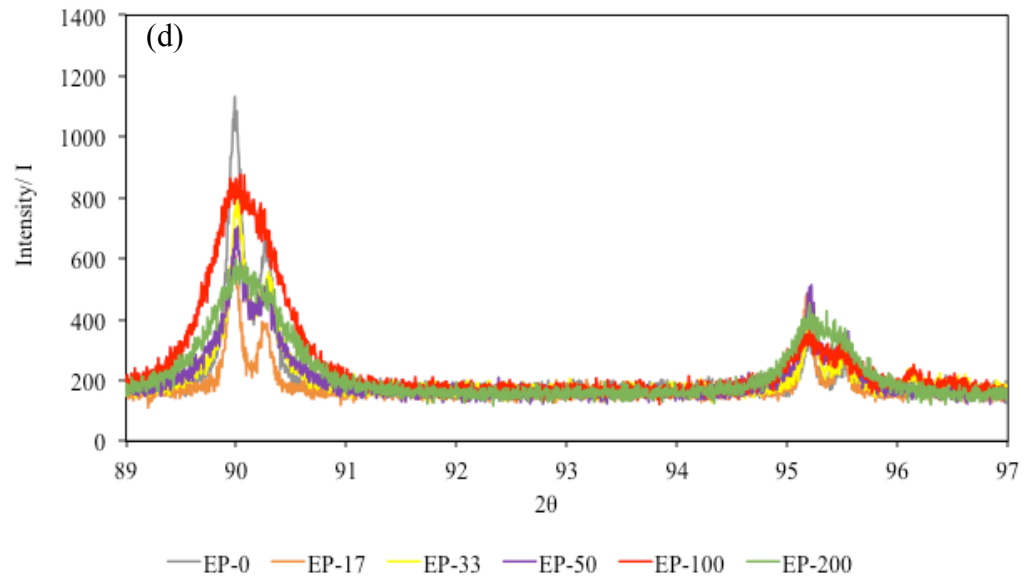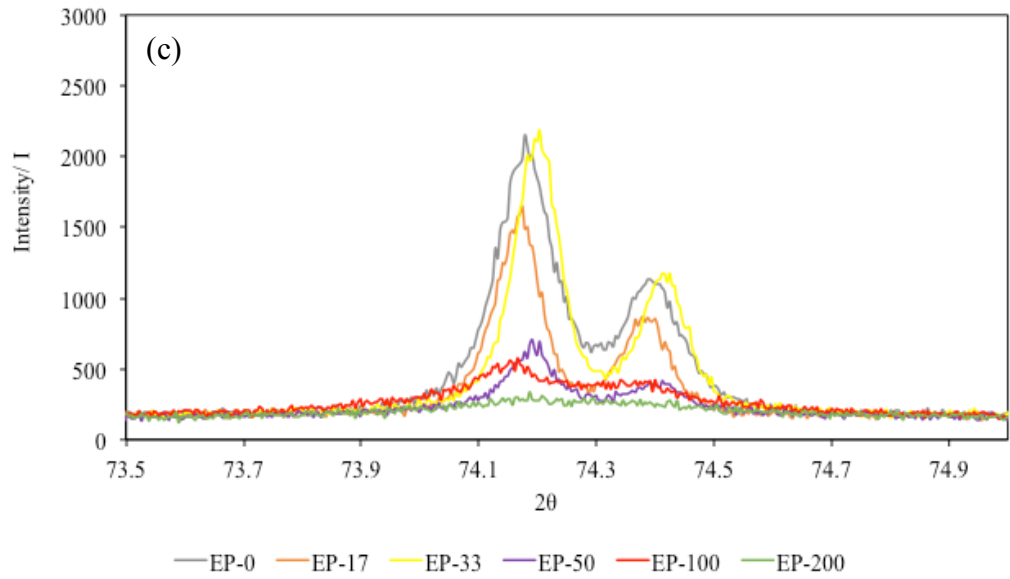
Figure 7.5 XRD plots zoomed in at (a) 111 (b) 200 (c) 220 and (d) 311 and 222 diffraction peaks.

As mentioned in Chapter 6.2, peak broadening may be related to a decrease in crystallite size, or an increase in microstrain. Table 7.2 shows the (i) crystallite size, derived using Scherrer's equation, and the (ii) microstrain, calculated using the

Williamson-Hall technique, in the deposits from the additive-containing EnFACE electrolyte. Figure 7.6 compares the microstrain present in the PC- and DC-plated deposits from the additive-containing EnFACE electrolytes.

Table 7.2 Calculated crystallite size (Scherrer's equation) and microstrain (Williamson–Hall technique) of the PC-plated copper from the EnFACE electrolyte with different additive concentration.

Additive concentration	Crystallite size (nm)	Microstrain (%)
EP-0	868 ± 316	0.066 ± 0.025
EP-17	857 ± 33	0.043 ± 0.002
EP-33	550 ± 22	0.040± 0.004
EP-50	210 ± 10	0.035 ± 0.003
EP-100	158 ± 52	0.024 ± 0.004
EP-200	109 ± 46	0.020± 0.001
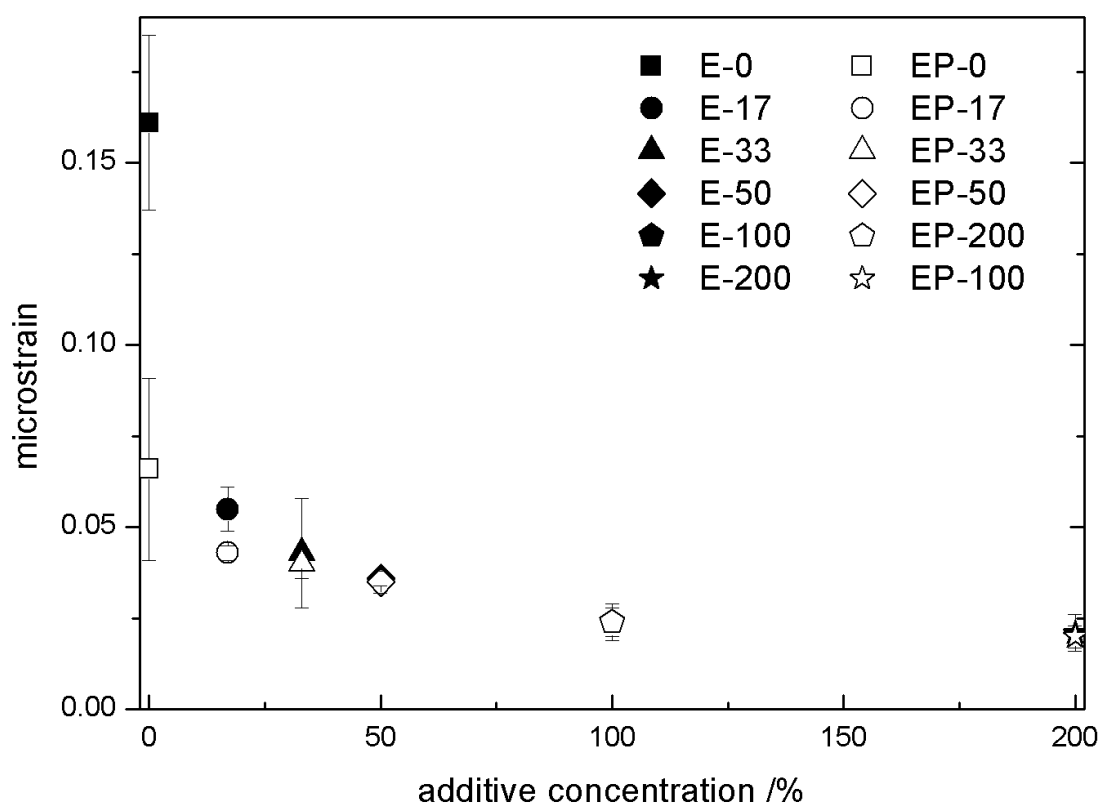
Figure 7.6 Plot of microstrain in the PC and DC-plated copper films from the EnFACE electrolyte with different additive concentration.

The results of the XRD analysis agree with that of the EBSD and SEM; i.e. crystallite size decreased with increasing additive amounts. Furthermore, similar to what was observed in the DC-plated copper films, the amount of microstrainin the PC-plated deposits decreased with increasing additives. This indicates that additives, when used in both DC and PC plating, created a less strainedcrystal lattice probably due to the low defect density in the deposit.

At low additive concentrations(i.e. less than 50%), the PC-plated deposits possessed lower microstrain than their DC-plated counterparts. The highest difference in microstrainwas seen between the deposits of the additive-free baths. At high additive concentrations, there was no appreciable difference between the two types of deposits. A pulsed current could reduce microstrain by controlling the crystal growth process [7.12]. However, the results clearly indicated that pulsed current is most effective in reducing microstrain in the absence of additives. At high additive concentrations, the effect of current modulation on microstrain becomes negligible while the influence of additive begins to dominate.
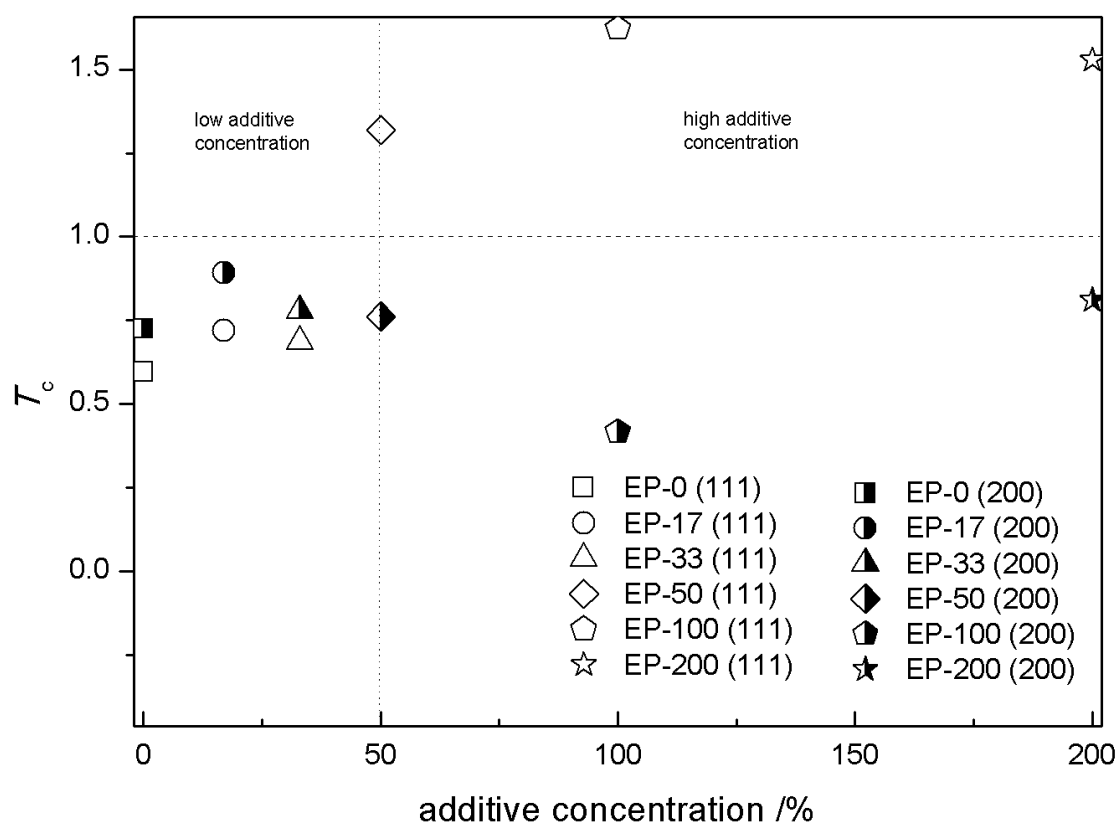
Figure 7.7 Plot of texture coefficient for the (111) and (200) in the PC-plated deposits of the different EnFACE electrolytes. A T_c value above 1.0 (dotted line) indicates the occurrence of texture.

Texture in the PC- plated films were assessed using the texture coefficient, T_c(hkl), of the (111) and (200) plane, as shown in Fig. 7.7. For the PC-plated Cu, the (111) texture was observed only at high additive concentrations (at least 50%), in agreement with previous reports [7.13]. In contrast, such was not found in the DC-plated Cu films as there was no definite trend in the occurrence of the (111) texture with respect to additive concentration. Similarly, there was no preferential orientation for (200) in the PC-plated deposits.

As explained previously, the (111) plane is dominant in all the Cu deposits since microstructure evolution in thin films is governed by surface energy

minimisation [7.13]. In electronic application, a (111) crystalline texture is preferred due to improved electromigration resistance [7.14]. Since pulsed current and the use of additives can contribute to creating the (111) texture, then this may be important for interconnect applications.

7.3 Film resistivity and self-annealing

Figure 7.8 Electrical resistivity of the PC and DC-plated copper films using the EnFACE and standard electrolytes.

Figure 7.8 show the electrical resistivity, ρ of the DC- and PC-deposited copper films from both the standard copper (S) and EnFACE (E) electrolytes containing different levels of additives.

The deposit of the PC-plated standard electrolyte possessed lower resistivity than the PC-plated deposit of the EnFACE electrolyte. To illustrate, the ρ ranged from 2.0 to 2.12μohm·cm for the additive-free (EP-0) and 100%EnFACEelectrolyte (EP-100), respectively. In contrast, the ρ were 1.54 and 1.60μohm·cm for the additive-free (SP-0) and additive-containing S electrolyte (SP-100), respectively. This may be due to the low concentration of Cu ions in the EnFACE electrolyte. At low Cu ion concentrations and at relatively high current densities, deposit tends to be fine-grained and consequently resistive [7.15].

The ρ of the copper films from the EnFACE electrolyte increased with increasing additive concentration. Beyond 100% additive concentration, marginal increase in resistivity was observed. As was previously mentioned in Chapter 6.3, the increase in the resistivity of the Cu film can be explained by the significant reduction of grain size brought about by additive use. The plateau in resistivity at additive concentrations above 100% is consistent with the observed plateau in grain size reduction and the polarisation plateau.

Figure 7.8further indicated that the PC-plated copper from the EnFACE electrolyte displayed better conductivity than their DC-plated counterparts. This is quite unexpected since the additional PC-induced grain refinement should have made the PC-plated deposits more resistive. This improvement in conductivity may be due to the presence of a compact deposit with fewer defects (i.e. other than grain boundaries) created during pulse plating. A reduction in defect density is known to improve thin film conductivity [7.3]. The presence of lower microstrain could also

have contributed to better conductivity in the in the PC-plated deposits, though this would only be true at the low additive concentration levels.

In Chapter 6.3, it was stated that the phenomenon of self-annealing was not detected in the DC-plated films. Since a finer grain structure was observed in the PC-plated deposits, then the possibility of self-annealing occurring in these films is higher. Therefore, self-annealing studies were conducted on the PC-plated deposits by monitoring changes in the electrical resistivity of the copper films over a period of 168 hours, as shown in Fig. 7.9. Table 7.3 compares the starting and final ρ'sof the PC-plated copper deposits.
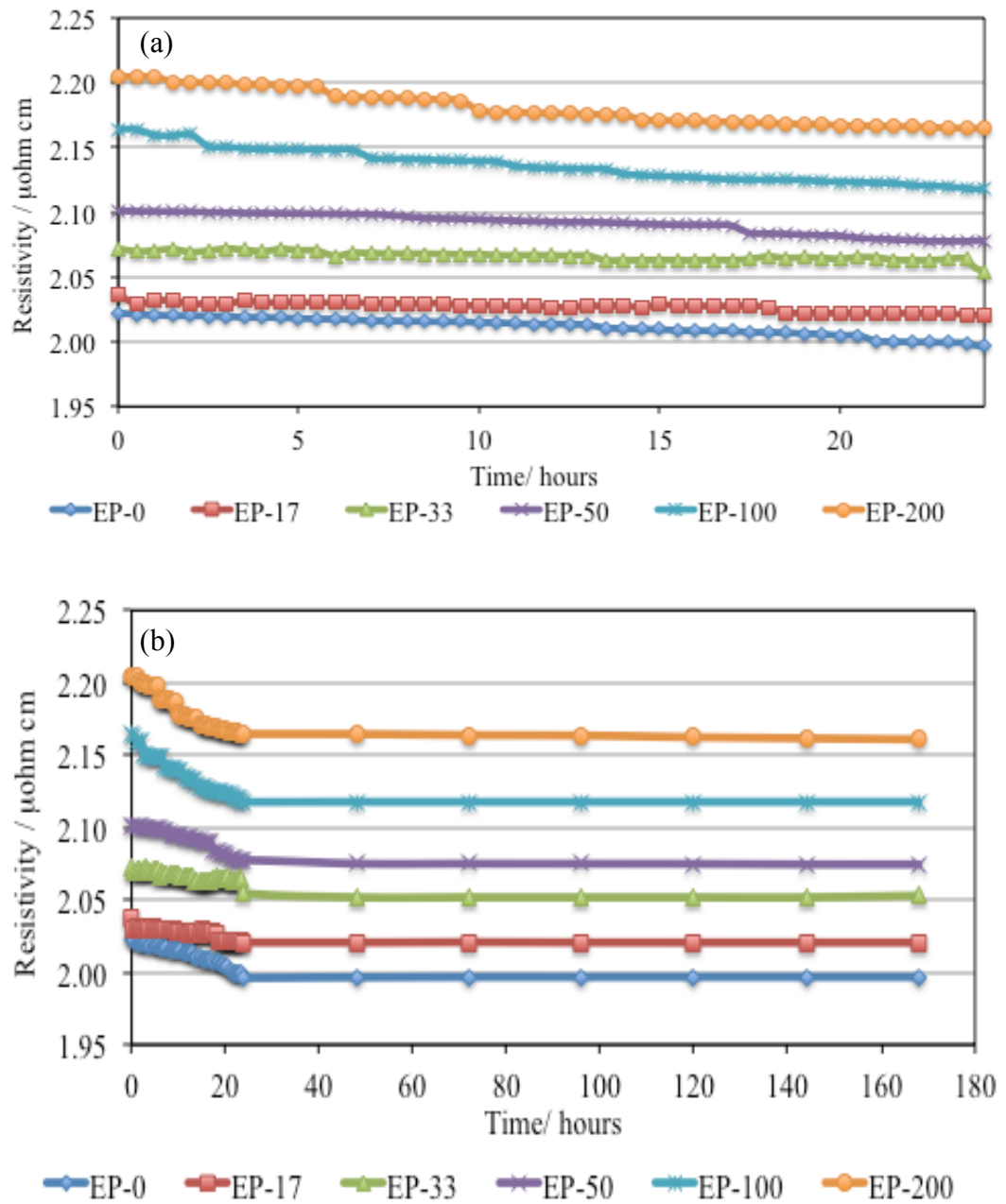
Figure 7.9 Resistivity of the copper films of the EnFACEwith different additives measured in the first a) 24 hours and over a period of b) 168 hours after deposition.

Table 7.3 Summary of the starting (peak) and final electrical resistivity of the PC-plated copper deposits of the EnFACE and standard electrolytes.

Sample designation	Peak ρ (μohm·cm)	Final ρ (μohm·cm)	Difference (μohm·cm)	Change (%)
EP-0	2.01	2.00± 0.006	0.01	-0.5
EP-17	2.04	2.02± 0.006	0.02	-0.99
EP-33	2.07	2.05± 0.006	0.02	-0.98
EP-50	2.10	2.07± 0.006	0.03	-1.4
EP-100	2.16	2.12± 0.005	0.04	-1.88
EP-200	2.20	2.16± 0.006	0.04	-1.85
SP-100	1.75	1.60± 0.006	0.95	-9.38
SP-0	1.67	1.54± 0.006	1.03	-8.44

While the results indicate that there was again a reduction of ρ over time, the drop in resistivity values is not enough to attribute this phenomenon to self-annealing. Confirmatory runs to detect self-annealing were performed using the XRD; and Fig. 7.10 shows the results of XRD analysis conducted at different times for the deposit of the EP-100 electrolyte. Again, there was no noticeable difference in the diffraction patterns of the copper film over time. Both resistivity and XRD tests indicated that self-annealing is not occurring in the PC-plated deposits from the EnFACE electrolyte, and the slight reduction in ρ could be attributed to a lattice relaxation mechanism [7.16].

Past studies on self-annealing of copper films observed dynamic recrystallisation occurring at grain sizes less than 100 nm [7.16,7.17]. These studies confirm that self-annealing is largely driven by the initial energy of grain boundaries; but is also influenced by impurities and residual stress. Thus, the absence of self-annealing in both the PC and the DC-plated copper was likely due to the relatively

large grains of the deposits. The grain sizes measured in the deposits of the additive-containing electrolytes vary from 200 to 800 nm. In this size range, the deposit did not possess the necessary energy to drive the self-annealing process.
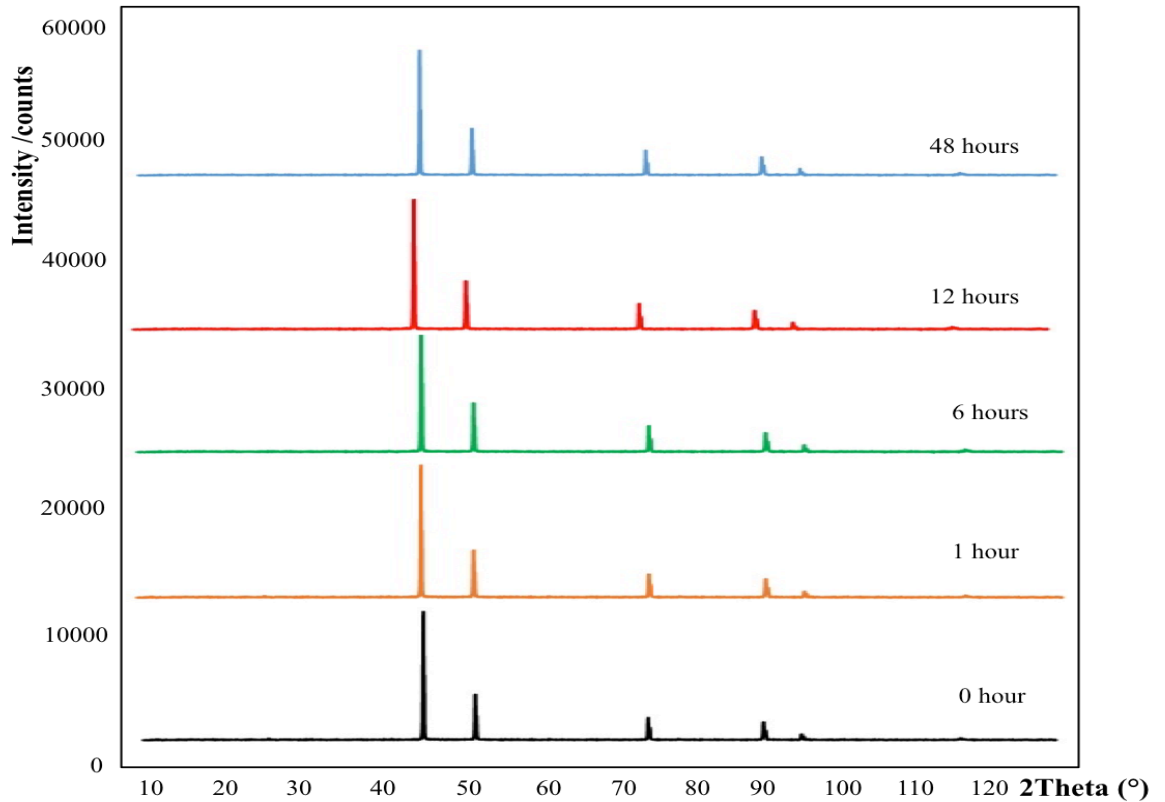
Figure 7.10 XRD scans for EP-100 copper films at 0,1, 6, 12 and 48 hours after deposition time.The intensity of the peaks was not adjusted to reveal the true intensity.No significant difference in the diffraction patterns was observed.

7.4 Tensile properties

Table 7.4 shows the measured; (i) 0.2% offset yield strength (σ_y), (ii) ultimate tensile strength (σ_f), and (iii) ductility (ε_f) of the PC-plated copper from varying additive concentration of the EnFACE and standard electrolyte; while Fig.7.11 compares the mechanical properties of the PC and DC-plated Cu films. The mechanical properties of the deposit from the EnFACE electrolyte were comparable

to the deposit of the standard electrolyte at the same additive concentration. The PC-plated deposits showed higher σ_y, σ_f and ε_f than the DC-plated deposits. Figure 7.11 also shows that increasing additive concentration increased the mechanical strength (i.e σ_y and σ_f) but reduced the ductility of copper, in both DC and PC mode.

Table 7.4 Mechanical properties of PC-plated copper from the different EnFACE and standard electrolytes.

Sample designation	σ_y (MPa)	σ_f (MPa)	e_f (%)
EP-0	135±1.8	168± 1.4	3.84±0.06
EP-17	206±2.0	281±2.8	3.37± 0.02
EP-33	225±2.7	309±2.9	3.08± 0.05
EP-50	261±2.9	329±2.8	2.94± 0.04
EP-100	278±2.2	378±3.8	2.57± 0.01
EP-200	297±2.3	417±4.2	2.30±0.01
SP-100	269±2.5	397±3.4	3.31± 0.02
SP-0	175±1.3	252±2.3	5.61± 0.02

(a)

(b)
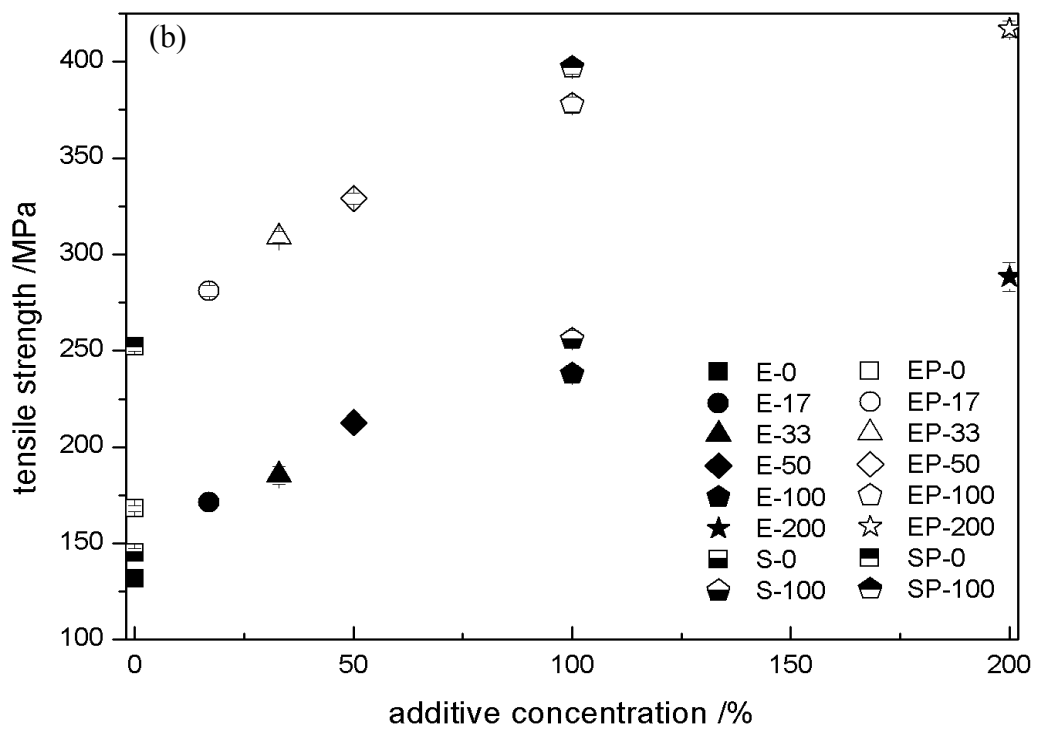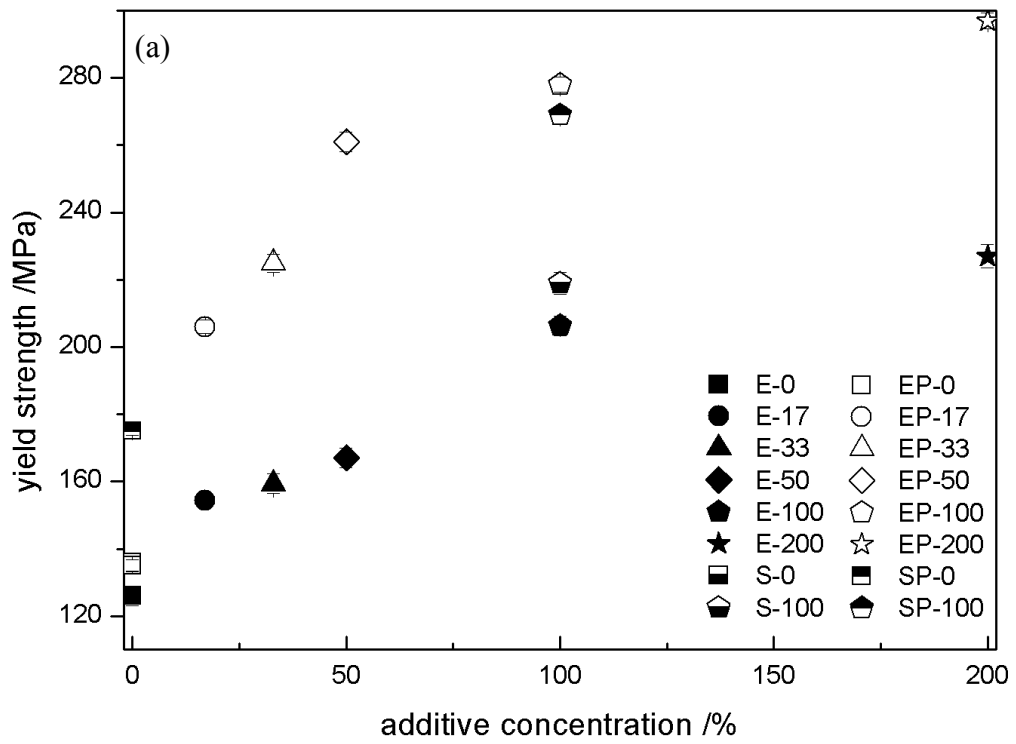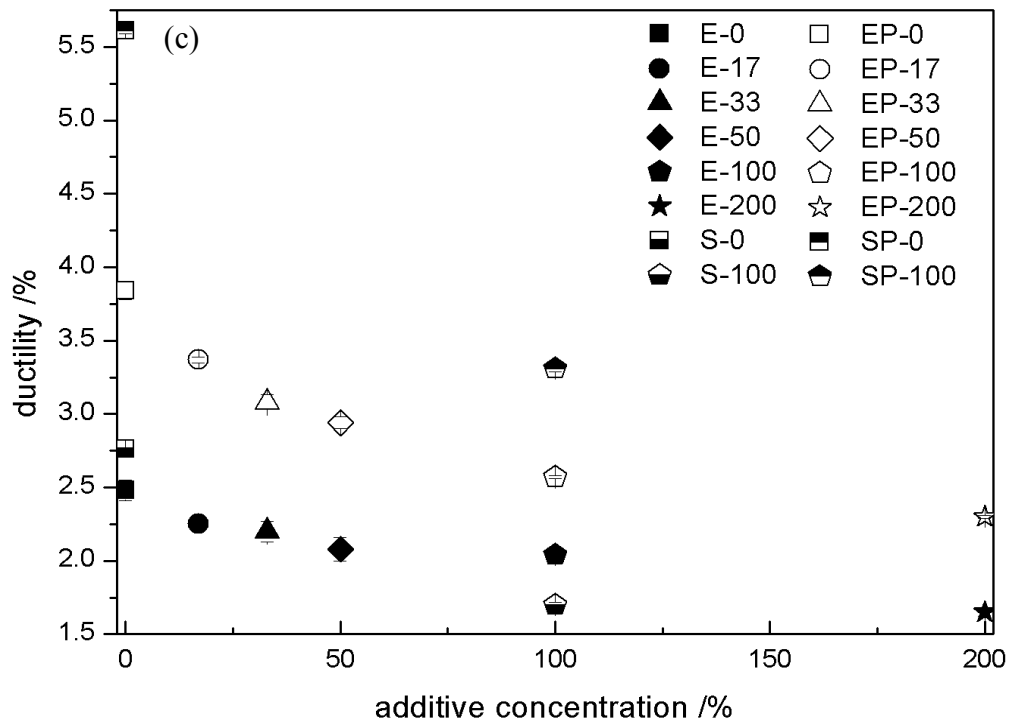
Figure 7.11 a) Yield strength, b) tensile strength and c) ductility of DC and PC-plated Cu using the EnFACE and standard electrolytes.

The observed changes in mechanical properties in the PC-plated copper films can be similarly traced to the reduction in grain size caused by (i) additives and the (ii) action of the pulsed current; which is in good agreement with past works [7.18, 7.19, 7.20, 7.21].Finer structures are stronger due to the high grain boundary area that effectively impedes dislocation motion.

The PC-plated deposits have higher σ_y and σ_f than the DC-plated, which is again due to the additional grain refinement induced by the pulsed current. Figure 7.12compares the observed yield strength of the PC-plated deposits using the additive-containing EnFACE electrolyte against the theoretical yield strength as predicted by the Hall-Petch equation ($\sigma_i = 25$ MPa, $k_y = 0.14$ MPa m$^{-1/2}$, [7.22]).

In Chapter 6.4, it was stated that the measured strength of the DC-plated deposits was lower than the theoretical value, and did not follow the expected linear relationship between σ_y and $d^{-1/2}$ predicted by the Hall-Petch equation. On the other hand, as can be seen from Fig. 7.12, the actual strength of the PC-plated deposits approximated the Hall-Petch prediction, and showed a fairly linear relationship between σ_y and $d^{-1/2}$. The good strength of the PC-plated Cu and its adherence to the Hall-Petch relation may be traced to the presence of a compact deposit structure that possessed fewer defects. The high nucleation rate achieved during PC plating is known to reduce void formation and create compact deposits [7.2, 7.3, 7.5]. The fact that the PC-plated deposits had better ductility than the DC-plated Cu further confirmed the benefits of the compact structure created by pulsed plating. Good ductility in strong deposits is typically unexpected, since an increase in strength is often accompanied by a reduction in ductility. However, by possessing a compact structure, the PC-plated deposits had fewer volume defects that are known to cause brittle fracture of electroplated films [7.23].
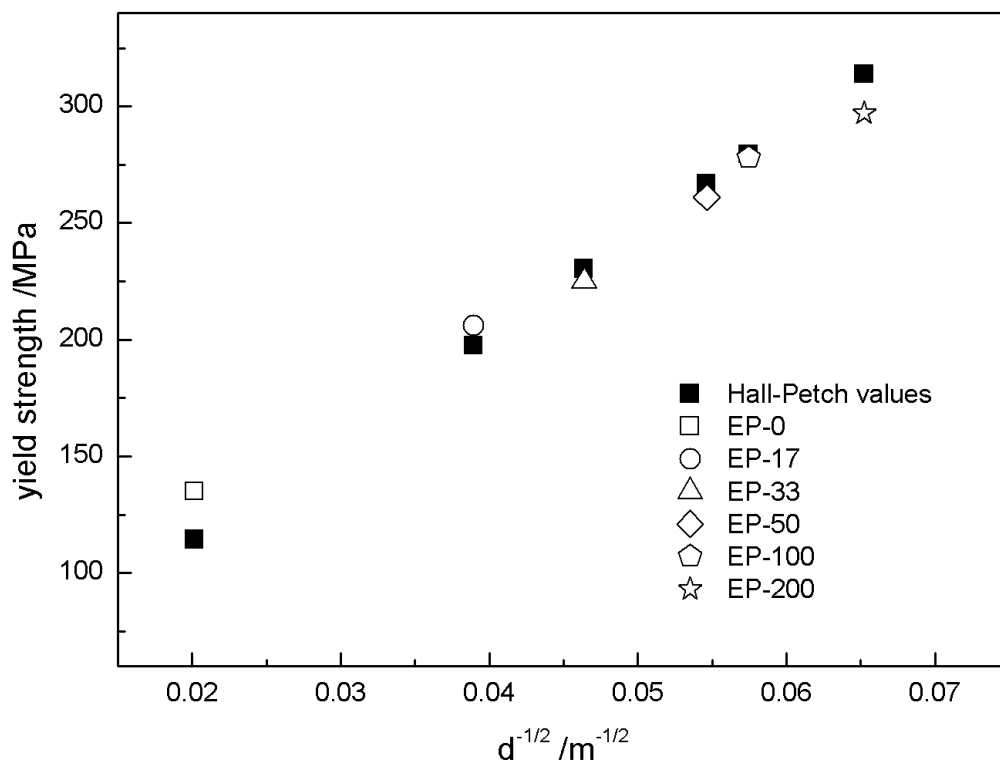
Figure 7.12 Comparison of the theoretical (using Hall-Petch equation) and actual yield strength of the PC-plated Cu from the EnFACE electrolyte with different additive concentration.

7.5 Comparison to IPC Standard and Optimum Additive Concentration

One of the objectives of this study is to determine if the properties of the DC- and PC-plated copper films can meet the product requirements of the electronics industry. Table 7.5 shows the properties of some of the DC and PC-plated Cu that approximate the IPC-TM-650 standards. For DC-plating, the E-50 electrolyte was chosen. For PC-plating, two electrolytes, EP-33 and EP-50, were considered. Although the properties of the E-50 deposit are slightly different from the standard values specified, further improvements in deposit properties could be obtained by optimising plating conditions. On the other hand, although both EP-33 and EP-50

deposits surpass the standard, EP-33 would be the better choice since it uses fewer additives.

Table 7.5 Comparison of the properties obtained from DC and PC plated copper deposit versus IPC standards.

Sample designation	Resistivity (μohm·cm)	Tensile strength (MPa)	Ductility (%)
IPC standard	2.00	207	3.00
E-50	2.39	213	2.09
EP-33	2.05	309	3.08
EP-50	2.07	329	2.94

Another significance of choosing E-50 and EP-33is that these concentrations represent the optimum additive concentrations for the EnFACE electrolyte under DC and PC plating, respectively. This implies that the EnFACE process requires fewer additives than the standard process. Again, the use of PC plating is the more attractive alternative since it requires up to 67% lower additive concentration than the standard; as compared to 50% for the DC plating process. Such benefit, aside from the positive effects on strength, ductility, and resistivity of the Cu deposit, increased the attractiveness of using pulse plating on the additive-containing EnFACE electrolyte.

Notably, the EnFACE electrolyte has a low metal ion concentration, which can limit plating rates (c.f. Table 4.5; Table 4.11).In PCB manufacturing, plating rates are important and a current density of 1.5-2.0 ASD (15 - 20 mA·cm^{-2}) are advised. In the current study, it was observed that the plating rate of the standard electrolyte was nearly four times higher than the best EnFACE electrolyte (i.e. E-50 or EP-33).The use of pulsed current further reduced efficiency and plating rates.

Such implies that plating rates need to be improved; for example, by employing agitation during plating. Nevertheless, all of the EnFACE electrolytes exceededthe plating rate requirement of the industry, indicating thatEnFACE could be used in real application. On the other hand, by employing electrolytes that have low metal and additive concentration, savings and sustainability can be achieved.

In this chapter, the influence of additives on the morphological, mechanical and electrical properties of PC-plated copper from the EnFACE solution was presented. Similar to what was observed in DC-plated deposits, the primary effect of additives on the PC-plated copper deposit is grain refinement. Consequently, such resulted to the increase in the mechanical strength, and the reduction in the ductility and conductivity of the copper deposits. PC-plated deposits were generally found to possess better properties than their DC-plated counterparts, probably due to improvements in deposit morphology brought about by the action of the pulsed current.

References

7.1 Kalantary MR, Gabe DR, Goodenough MR (1993) Unipolar and Bipolar Pulsed Current Electrodeposition for PCB Production. J. Appl.Electrochem. 23(3); 231-240

7.2 Chandrasekar MS, Pushpavanam M (2008) Pulse and pulse reverse plating—Conceptual, advantages and applications.ElectrochimicaActa 53(8); 3313–3322

7.3 Osero N (1986) An Overview of Pulse Plating. Plat.and Surf. Finish. 73(3); 20-22

7.4 Renzai-Kalantary M (1990) Pulse electroplating of copper for printed circuit technology. PhD thesis Loughborough University UK

7.5 Hansal EGW, Roy S (2012) Pulse plating. 1st edition Eugen G LuezeVerglag KK Germany

7.6 Devaraj G, Guruviah S (1999) Pulse plating. Materials Chemistry and Physics. 25(5), 439 - 461

7.7 Chène O, Landolt D (1989) The influence of mass transport on the deposit morphology and current efficiency in pulse plating of copper. J. Appl. Electrochem.19(2); 188-194.

7.8 Balasubramanian A, Srikumar DS, Raja G, Mohan S (2009) Effect of pulse parameter on pulsed electrodeposition of copper on stainless steel. Surf. Engg. 25(5); 389-392

7.9 Yin KM, Jan SL, Lee CC (1997) Current Pulse with Reverse Plating of Nickel –Iron Alloys in Sulphate Bath. Surf. and Coat. Technol. 88(1); 219-225

7.10 Oniciu L, Muresan L (1991) Some Fundamental Aspects of Levelling and Brightening in Metal Electrodeposition.J. Appl.Electrochem. 21; 565-574

7.11 L Muresan, S Varvara: Leveling and brightening mechanisms in metal electrodeposition. In Metal Electrodeposition (2005). Nunez M edtr. Nova Science Publishers. New York, USA, 2-45.

7.12 Bicelli LP, Bozzini B, Mele C, D'Urzo L (2008) A review on Nanostructural Aspects of Metal Electrodeposition. Int. J. Electrochem. Sci. 3; 356-408

7.13 Marechal N, Quesnel E, Pauleau Y (1994) Characterization of silver films deposited by radio frequency magnetron sputtering. J. Vac. Sci. and technol. 12; 707-714

7.14 Gupta T (2009) Copper Interconnect Technology. Springer-Verlag New York 1; 423-465

7.15 Anderson D, Haak R, Ogden C, Tench D, White J(1985) Tensile Properties of Acid Copper Electrodeposits. J. Appl. Electrochem. 15; 631-637

7.16 Stangl M, Acker J,Dittel V, Gruner W, Hoffmann V, Wetzig K(2005) Characterization of electroplated copper self-annealing with investigations focused on incorporated impurities. Microelect. Eng. 82; 189–195

7.17 Lagrange S, Brongersma SH, Judelewicz M, Saerens A, Vervoort I, Richard E, Palmans R, Maex K (2000) Self-annealing characterization of electroplated copper films. Microelectronic Engineering 50; 449-457

7.18 Michailova E, Vitanova I, Stoychev D, Milchev A(1993) Initial Stages of

Copper Electrodepostion in the Presence of Organic Additives. Electrochim. Acta 38(16); 2455-2458

7.19 Hofer EM, Hintermann HE(1965) The Structure of Electrodeposited Copper Examined by X-Ray Diffraction Techniques. J. Electrochem. Soc. 112(2); 167-173

7.20 Melnicki LS(1998) Electrochemical Technology in Electronics' in L Romankiw and T Osaka (Eds) (1988) PV 88–23 ECS Proceedings Series Pennington NJ; 95–103

7.21 Rusli E, Xue F, Drews T, Vereecken P, Andricacos P, Deligianni H, Braatz R, Alkire R(2007) Effect of Additives on Shape Evolution during Electrodeposition. J. Electrochem. Soc. 154(11); D584 – D597

7.22 Lugo N, Llorca N, Cabrera JM,Horita Z (2008)Microstructures and mechanical properties of pure copper deformed severely by equal-channel angular pressing and high pressure torsion. Matls. Sci. and Engg. 477(1-2); 366-371

7.23 Callister WD, Rethwisch DG (2014) Materials science and engineering: an introduction. John Wiley and Sons, Inc. Hoboken, NJ, USA

Chapter 8

Conclusions

The EnFACE process offers some unique possibilities to industries using the copper electroplating process; and its true potential will only be revealed with continuous research. At its core, this study was an opportunity to learn more about the effects of using additives and different current modulation on the deposits of the EnFACE process. The following conclusions were drawn from the different results obtained from the present study:

1. The potentiodynamic cathode polarisation curve of the additive-free EnFACE electrolyte possessed the typical S-shape showing different polarisation regions; namely (i) charge transfer, (ii) mixed mechanism, (iii) limiting current and (iv) hydrogen evolution regions.

2. The EnFACE electrolyte showed higher polarisation than a standard electrolyte due to its high resistivity. This was seen in the limiting current of the additive-free EnFACE electrolyte that is about 5 times lower compared to the limiting current of the standard copper electrolyte. This low limiting current could limit actual plating rates in the EnFACE electrolyte.

3. Copper Gleam A, Copper Gleam B and Cl⁻, when used separately, induced a concentration-dependent polarisation of the cathode in the EnFACE electrolyte. The increase in polarisation indicated plating inhibition. Plating inhibition was probably due to the adsorption of additives at the cathode

surface. The adsorbed additives had a two-fold effect on plating: i) adversely influenced the interfacial charge-transfer rate of Cu^{2+} and ii) prevented Cu^{2+} from reaching the cathode by covering active surfaces.

4. A synergistic effect on plating inhibition, especially in the mass-transport limited regions, occurred when a mixture of Copper Gleam B and Cl^- was used. Using a suppressor action model based on the PEG molecule, it is believed that $PEG-Cu^{2+}-Cl^-$ complex is formed and covered the cathode surface that inhibited copper plating.

5. The accelerating effect of Copper Gleam A was revealed when added to the Copper Gleam B-Cl^- containing EnFACE electrolyte. Using a suppressor action model based on the SPS molecule, it is believed that SPS either weakened the bond of PEG to the $PEG-Cu^{2+}-Cl^-$ complex or prevented PEG from attaching to Cl^- ions.

6. In the presence of additives, the EnFACE electrolyte showed similar electrochemical behaviour as the standard electrolyte, suggesting the possibility of the electrolyte giving similar results when used in actual service.

7. A polarisation plateau occurred at the 100% additive concentration for the EnFACE electrolyte (E-100). At this concentration maximum polarisation

occurred, and further increase in additive concentration only resulted in marginal increase in polarisation.

8. Copper was successfully plated on stainless steel coupons using both direct current (DC) and pulsed current (PC) mode on EnFACE electrolyte containing different concentrations of additives. The deposits were characterised and compared to the properties of deposits from the standard copper electrolyte.

9. The main morphological effect of additives is the refinement of the grain structure of deposits, as proven by SEM, EBSD and XRD analysis. The degree of grain refinement was proportional to additive concentration, but grain size reduction levels off beyond the 100% additive concentration corresponding to the polarisation plateau. Additives can cause grain refinement by altering the different mechanisms (e.g. charge transfers or diffusion-based mechanisms) involved in electroplating.

10. XRD analysis showed that deposit microstrain decreased with increasing additive concentration. The application of pulsed current also reduced microstrain, although its effect was strongest in the absence of additives.

11. Results of four-point probe analysis showed that the additive-induced grain refinement increased resistivity of the deposits of the EnFACE electrolyte.

Grain boundaries can reduce electron mobility by acting as electron scattering centers.

12. While a slight reduction in the electrical resistivity of the copper films over time was observed, self-annealing was not evident in both the DC and PC-plated copper films from the additive-containing EnFACE electrolyte, as proven by resistivity and XRD analysis. The observed reduction in resistivity over time may be attributed to a lattice relaxation mechanism.

13. Results of tensile tests on the copper films indicated that grain refinement increased the yield and tensile strength, and reduced the ductility of the plated copper. These changes in tensile behaviour may be traced to the ability of grain boundaries to impede dislocation motion and prevent crystal slip.

14. The primary effect of pulsed current on deposit morphology is grain refinement. This change in morphology is linked to the ability of pulsed current to affect the charge transfer mechanism and influence mass transport in the electrolyte during plating.

15. The ability of pulsed current to induce grain refinement is most evident in the absence of additives.

16. The positive benefits of pulsed current over direct current modulation include improvements in properties such as: (i) yield strength, (ii) tensile strength,

(iii) ductility and (iv) conductivity. This is believed to be due to the formation of a compact and fine-grained structure having a low defect population.

17. A comparison of the properties of the direct and pulse-deposited EnFACE Cu films with IPC standards indicated that properties meet the required specifications; even at 50% additive concentrations for DC plating and 33% additive concentrations for PC plating using the EnFACE electrolyte. These concentrations are also considered as the optimum additive concentrations for the corresponding processes. The reduction in the required additive translates to huge savings in operation expenses. This increased the appeal of using pulse current plating on the additive-containing EnFACE electrolyte, and contributes to the sustainability of the EnFACE process in future applications.

Chapter 9

Future Work

The current study is just the first step to understanding the effects of additives on the EnFACE process and its products. Some parameters, e.g. mechanical stirring or temperature, were not included in the study to remove complications in analysis and reveal the very basic function of the additives in the EnFACE process. The next logical step therefore is to look at the effect of these parameters, in particular, that of mechanical agitation, on the additive-containing EnFACE electrolyte. The results of such study will be particularly relevant since an important element of the EnFACE process is the control of electrolyte flow in the reactor.

Another relevant study that may be done is to use the additive-containing EnFACE electrolyte in the actual EnFACE reactor. The study can investigate the effect of additives on the properties of a patterned deposit produced in the reactor. Optimisation runs can also be done to see the operating parameters affected by additive use in the EnFACE process.

It has been determined that an optimum additive concentration exists for the EnFACE electrolyte; and this concentration is much lower than the conventional dosage used in the industry. Further optimisation runs may be done, especially in agitated electrolytes, to precisely determine the exact optimum value. This study could potentially yield an optimum concentration that is lower than what was currently obtained.

So far, only the Copper Gleam additives were tested with the EnFACE electrolytes. Future studies can look at the possibility of using other commercially available formulations, or creating unique additive mixtures by using basic additive ingredients such as PEG and SPS, to create deposits with better properties.

The EnFACE process was successfully applied not only to electroplating copper, but also to plating nickel [9.1, 9.2]. The effect of additives on nickel plating using the EnFACE process has not been investigated. The use of additives could potentially address the problems due to hydrogen evolution encountered in the study by Widayatno *et al.* [9.1, 9.2] In the current study, additives increased the hydrogen evolution overpotential in the EnFACE electrolyte.

Reference

9.1 Widayatno T, Roy S (2013) Micropattern Transfer Without Photolithography of Substrate: Ni Electrodeposition using EnFACE Technology. PhD Thesis School of Chemical and Process Engineering Newcastle University UK

9.2 Widayatno T, Roy S (2014) Nickel Electrodeposition using EnFACE. J. of Appl. Electrochem. 44(4); DOI: 10.1007/s10800-014-0686-y

Appendix 1

Manufacturer's Description of Copper Gleam Additives

Copper Gleam HS-200 is a full bright acid copper plating process specifically formulated for use in vertical in line plating equipment. Formulated for high current density plating, the process is capable of producing uniform, bright deposits of high ductility and tensile strength in accelerated plating times. In addition to productivity, this technology exhibit exceptional metal distribution that can be utilised in the manufacture of high density product. Simple analytical procedures are available for all components allowing for the use of cyclic voltammetry techniques.

Advantages

- Suitable for insoluble anode

- High throwing power, in vertical plating applications, at accelerated plating rates (>35ASF)

- Capable of producing bright, uniform deposits

- Excellent through-hole microlevelling

- Superior plating distribution (less than 10% variation over the usable surface)

- Deposits exhibit unsurpassed physical properties, typically >15%elongation and tensile strength of 44 kpsi, 2300 N/mm^2

- Thermal shock resistance exceeds MIL-P-55110E

- Complete analytical control

Bath make-up

Component	Metric	(U.S.)
Deionized water	650 ml/l	65% v/v
Electronic grade copper sulphate $CuSO_4 \cdot 5H_2O$	100 g/l	13 oz./gal.
Sulfur free carbon powder	6g/l	0.8 oz./gal.
Norit 211 Granular or Norit RO 0.8	9 g/l	1.2 oz./gal.
C.P. Grade concentrated sulphuric acid	200 g/l	25 oz./gal.
C.P. Grade concentrated Hydrochloric acid	0.163 ml/l	0.0163% v/v
Copper Gleam HS-200 A	0.5 ml/l	0.05% v/v
Copper Gleam HS-200 B	10 ml/l	1.0% v/v

Reference: Rohm and Haas. 2007. Copper Gleam HS-200 vertical acid copper for PWB metallization application. Electronic Materials Circuit board technologies, CB07N009, Rev.1.

Appendix 2

List of Publications

1. Dela Pena EM, Bains N, Hussain A, Cobley A, Roy S: (2015) Effect of additive concentration during copper deposition using EnFACE electrolyte. IMF 93(6); 288-293

2. Dela Pena EM, Roy S: Electrochemical Effect of Copper Gleam Additives during Copper Electrodeposition, *in press*

3. Dela Pena EM, Roy S: The Properties of Pulse-plated Copper using the Additive-containing EnFACE Electrolyte, *in preparation*

4. Dela Pena EM, Roy S: The Role of Additives in the Modern Copper Electroplating; *in revision*

Appendix 3

List of Conferences attended

- **COST – Electrochemical Processing Methodologies and Corrosion Protection for Device and Systems Miniaturization**
  Athens Greece
  October 14 – 16, 2016

- **Electrochem 2016**
  University of Liecester, United Kingdom
  August 17 – 19, 2016 (Oral Presentation)

- **Research Presentation Day 2016**
  University of Strathclyde, United Kingdom
  June 23, 2016 (Oral Presentation)

- **Nanomaterials for Technology Workshop**
  Technology and Inovation Centre,
  University of Strathclyde United Kingdom
  June 20 – 21, 2016 (Oral and Poster Presentation)

- **2016 Scotland and North England Electrochemistry Symposium (Butler meeting)**
  University of Glasgow, United Kingdom
  April 20, 2016 (Poster Presentation)

- **Chemical and Process Engineering Presentation Day 2016**
  University of Strathclyde, United Kingdom
  April 12, 2016 (Oral Presentation)

- **Hardness Testing Seminar**
  The Advanced Materials Research Laboratory (AMRL)
  University of Strathclyde, United Kingdom
  November 18, 2015

- **Electrochem 2015**
  Calman Learning Center
  Durham University, United Kingdom

September 13 – 15, 2015 (Oral Presentation)

- **European Academy of Surface Technology Conference**

  Lund, Sweden

  June 25 – 26, 2015 (Oral Presentation)

- **7th European Summer School for Electrochemical Engineering**

  Leeuwarden, Netherlands

  June 22 – 26, 2015 (Poster Presentation)

- **Postgraduate Conference 2015**

  Newcastle University

  May 29, 2015 (Oral Presentation)

- **Inovative electronics Manufacturing Research Centre (IeMRC) – 9th Annual Conference**

  Holywell Park, Loughborough United Kingdom

  February 17, 2015 (Poster Presentation)

- **Electrochem 2014**

  Loughborough University

  September 7 – 9, 2014 (Oral Presentation)

- **Introduction to Learning and Teaching in Higher Education (ILTHE)**

  Newcastle University

  September 22 – 23, 2014

- **EPSRC meeting**

  Devonshire Building, Newcastle University

  December 2014 (Poster Presentation)

- **Electrochemical Deposition for Electronics**

  The University of Edinburgh, Kings Building Campus

  April 30, 2014 (Poster Presentation)

- **Postgraduate Conference 2014**

  Research Beehive, Newcastle University

  March 2014 (Poster Presentation)

Effect of additive concentration during copper deposition using EnFACE electrolyte[†]

E. M. Dela Pena[1,3,4], N. Bains[2], A. Hussain[2], A. Cobley[2] and S. Roy[1,3]*

Copper deposition from solutions using high concentration of acid, metal ions and polyethylene glycol (PEG), and bis-(3-sulphopropyl) disulphide (SPS) and chloride ions (Cl⁻) is well known. A recent maskless micropatterning technology, which has the potential to replace the traditional photolithographic process, called EnFACE, proposed using an acid-free, low metal ion solution which is in direct contrast to those used in standard plating technology. In this work copper has been deposited using both standard electroplating solutions and those used in the EnFACE process. In the standard electrolyte 0.63 M CuSO$_4$ and 2.04 M H$_2$SO$_4$ has been used, along with Gleam additives supplied by Dow Chemicals. For the Enface electrolyte, copper deposition has been carried out without any acid, and with different concentrations of additives between 17% - 200% of those recommended by suppliers. 25 μm of metal has been plated on stainless steel coupons as suggested by ASTM, peeled off and subjected to ductility and resistance measurements. Scanning electron microscopy and electron back scatter diffraction have been carried out to determine the deposit morphology. It was found that copper deposits obtained from acid-free solutions containing low concentration of metal ion and additives produced copper deposits with properties which are comparable to those obtained from standard electrolytes. The optimum additive concentration for the EnFACE electrolyte was 50% of the supplier recommended value.

Keywords: EnFACE process, Copper film, Additives, Electrodeposition, Electroplating

1. Introduction

Copper is the standard metal used in wiring printed circuit boards[1] and interconnects in electronic devices.[2] The standard manufacturing process for both these technologies uses electrodeposition. It is well established that the electrodeposition processes employ electrolyte chemistry of high metal and acid concentrations and employ additives, which impart desirable properties to the plated copper.[3] Numerous studies aimed at understanding the role of additives in electroplating have concluded that these chemicals are essential to obtaining metal deposits of high quality.[4–9]

Recently a new mask-less process, called EnFACE, has been proposed to deposit microscale copper features.[10] As opposed to the standard electrolytes used for PCB and electronic manufacturing, EnFACE proposed a solution using 0.1 M CuSO$_4$ and no acid.[10–15] Since most of the current literature is focused on understanding the role of additives in the established processes,[16–19] the effect on this new chemistry on deposited copper is still unknown. In addition, it is unclear how much additive is required to change deposit properties and what effect they would have on the deposit.

This work examines the effect of additives on deposit properties when copper is deposited from EnFACE electrolyte and when additives are added to the bath. The additives used were Gleam A and B (Dow Chemical) which are used in printed circuit board manufacturing. The EnFACE electrolyte consisted of a 0.1 M CuSO$_4$ solution without addition of acid. Additive levels of 17%, 33%, 50%, 100% and 200% of that recommended by the supplier were added to the solution. In addition, a solution of 0.63 M CuSO$_4$ with 2.04 M H$_2$SO$_4$ with additives as per supplier recommendations was also used in plating experiments.

Copper films of 25 μm have been electroplated on polished steel coupons in a beaker without agitation. Deposits were plated from the different electrolytes and subjected to ductility and resistivity tests. Deposit morphology was examined by scanning electron microscopy and electron back scatter diffraction. Yield strength and sheet resistance were measured to compare deposit properties against those recommended by the Institute of Interconnecting and Packaging Electronic Circuits. Deposit properties are interpreted in terms of additive concentration in the bath. The effectiveness of using low concentrations of metal ions and additives in influencing deposit properties has been assessed.

2. Experimental

2.1. Apparatus

Electrodeposition experiments were carried out using a traditional two-electrode plating set-up. The working electrode was a dog-bone shaped stainless steel coupon with an area of 31.92 cm^2. The counter electrode was a copper rod with an exposed area of 58.1 cm^2. Plating was done in a 2-litre cell using the appropriate plating solution, and the current source was a Thurlby Thundar PL-310 power unit.

Morphological analysis (SEM and EBSD) was done using the JEOL JSM-5300LV. Resistivity of the plated films was measured using the Signatone Pro4 (four point probe) system in the Electronics and Electrical Engineering Department, Newcastle University, UK. Mechanical properties were characterised using a Tinius Olsen H50KS with Horizon software for data recording. All tensile tests followed ASTM E-345,[20] a standard for determining tensile properties of metallic films. Morphological and mechanical characterisations were conducted in the Advanced Chemical and Materials

Table 1 Bath compositions and nomenclature

Designation	Setting description	Cu$_2$SO$_4$ /M	H$_2$SO$_4$ /M	Gleam B /mL L^{-1}	Gleam A /mL L^{-1}	HCl/ ppm
S	Standard bath	0.63	2.04	10	0.5	70
S-0	Standard bath without additives	0.63	2.04	X	X	X
E-0	EnFACE bath without additives	0.1	X	X	X	X
E-17	17% of the recommended additive concentration	0.1	X	1.7	0.08	12
E-33	33% of the recommended additive concentration	0.1	X	3.3	0.17	23
E-50	50% of the recommended additive concentration	0.1	X	5.0	0.25	35
E-100	Recommended additive concentration	0.1	X	10.0	0.50	70
E-200	High concentration (double of the recommended additive)	0.1	X	20.0	1.0	140

'S' stands for 'standard' electrolytes based on supplier recommendation and 'E' stands for 'Enface' baths. The number following the 'S' and 'E' stands for the percent of additive concentration added to the electrolyte

Analysis (ACMA) Laboratory, Newcastle University.

2.2. Chemicals and electrolytes

Steel coupons (308 stainless) were manufactured to the specifications of IPC-TM-650 (IPC-TM is the Institute for Interconnecting and Packaging Electronic Circuits Testing Methods) standard. Technical grade CuSO$_4$ and H$_2$SO$_4$ (Sigma-Aldrich) were used to prepare the plating electrolyte. The additives used were commercially available Copper Gleam series (Rohm Haas). Copper Gleam HS – 200 A served as the accelerator (SPS), while Copper Gleam B was the inhibitor (PEG). The Cl$^-$ ions were sourced from concentrated HCl (37%, Sigma Aldrich). Chemicals for pretreatment of the coupons include concentrated HNO$_3$ and ethanol (Sigma Aldrich). The PRP200 photoresist (Electrolube) was used to insulate the backside of the coupons. Table 1 lists the composition of the different plating baths used for copper deposition.

2.3. Procedure

Prior to actual plating, the stainless steel coupons were cleaned with concentrated HNO$_3$, and then rinsed with water for 1 min. The coupons

were mechanically polished using silicon carbide sheets, starting at grit #220 and progressing to grit #4000. One side of the coupon was coated with the photoresist, and left to dry. The exposed side of the coupon was swabbed with ethanol for 30 seconds and again allowed to dry.

Electrodeposition was carried out in direct current (DC) mode. The counter and working electrodes were set-up parallel in the plating cell containing different electrolytes. Table 2 shows the plating parameters used for the different experiments. These parameters were derived from polarisation experiments that yielded limiting current regarding each bath type. Since the deposits become rougher as they approach the limiting current,[21] the current was set at a fraction of this value to ensure that dendritic copper was not electrodeposited. The total plating time was calculated to obtain a copper film with thickness of 25 μm.

After the allotted deposition time was reached, the coupons were removed from the solution and washed with deionised water for 1 min. The surface was dried using a lint free cloth and left to dry in air. The electrodeposited copper films were then carefully peeled off from the stainless steel substrate, and were prepared for subsequent characterisation. Each experiment

was repeated three times to check for reproducibility.

For SEM and EBSD analysis, a 2×2 cm^2 area was cut out from the central portion of the copper coupon. For mechanical and resistivity testing, the whole coupon was used. Necessary care was taken to prevent damage on the coupons, particularly during handling and specimen mounting in the UTM that would compromise the quality of results of the mechanical tests. The values reported in this manuscript are the average of measurements from three different films.

## 3. Results and discussion

3.1. Morphology and grain size measurements

Figure 1 shows the SEM images (planar view) of the products of the EnFACE bath with different additive concentration and the standard bath. It can be observed that as the amount of additive increased, the surface roughness of the deposit from the EnFACE bath noticeably decreased. In fact, the product of the bath with 100% and 200% additive concentrations appeared the smoothest and most compact among all the samples. On the other hand, in terms of appearance, the deposit from the standard copper bath is similar to that of the E-33 and E-50 EnFACE bath, which showed that even at low concentrations the influence of additives is substantial.

The observed reduction in surface roughness may indicate the occurrence of a fine-grained structure in the deposit. However, attempts to quantify the grain size of the copper films proved difficult since the grain structures were not easily discernible, even when viewed at high

Table 2 Plating parameters

Electrolyte	Plating current /mA (40% from I_{LIM})	Plating time /min	Grain size From EBSD /nm
S	245	146	431
S-0	255	152	11524
E-0	68	615	9016
E-17	68	623	758
E-33	63	623	523
E-50	58	669	466
E-100	54	705	407
E-200	53	708	400
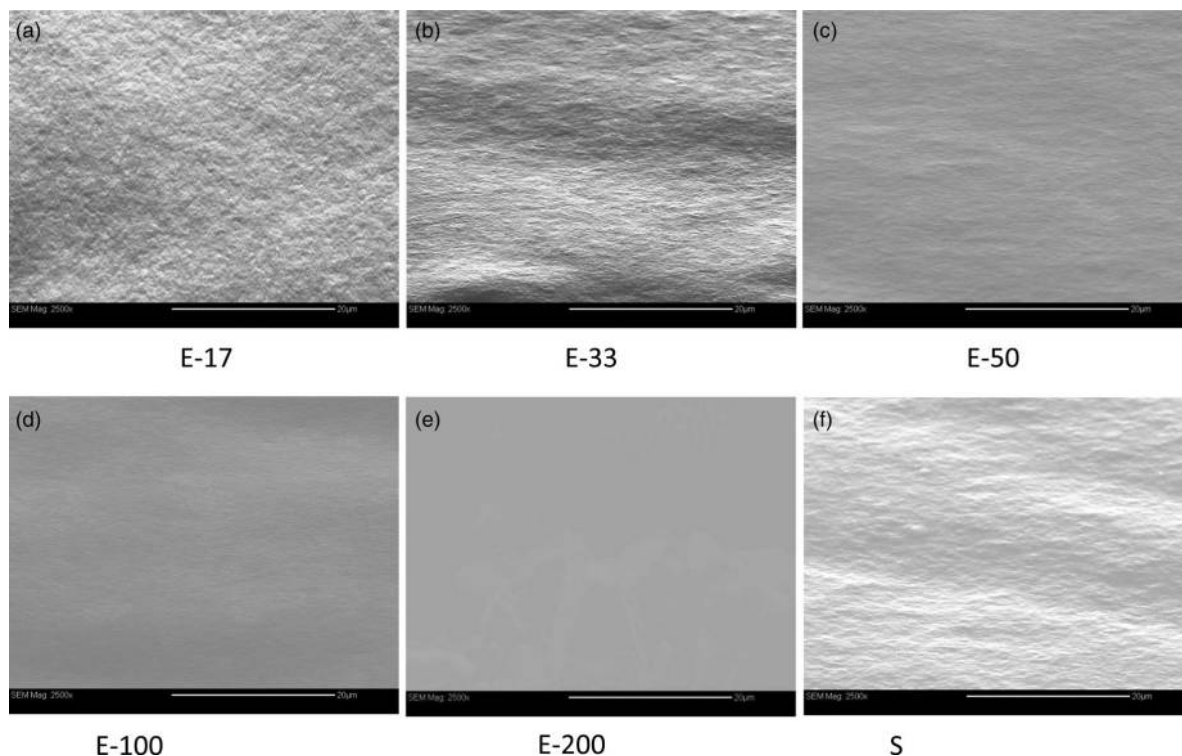
1 SEM images of copper deposits from EnFACE bath with different additive concentration: a) E-17 with 17% additive concentration, b) E-33 with 33% additive concentration, c) E-50 with 50% additive concentration, d) E-100 with 100% additive concentration and e) E-200 with 200% additive concentration, and f) S - standard bath. These percentages are relative to the industry recommended additive concentration of 10 mL L^{-1} Copper Gleam B, 0.5 mL L^{-1} Copper Gleam A, and 70 ppm Cl$^-$.

magnifications. Therefore, it became necessary to use another imaging technique that allowed accurate visualisation of grain morphology. Electron back-scatter diffraction (EBSD) was chosen because the technique allows grain size and grain orientation analysis without the need to alter the surface condition of the metal.

Figure 2 shows the corresponding EBSD maps for the products of the EnFACE bath with different levels of additive concentration, and of the standard copper bath. The EBSD images revealed the grain structure, which was predominantly equiaxed for the electrolyte without additives, and becomes smaller as additive concentration is increased. The EBSD data allowed measurement of the grain size of deposits.

The right hand column in Table 2 gives a summary of the calculated grain size of deposits measured using the EBSD image analysing software TANGO (HKL Technology A/S, 2001). The grain structure map produced in EBSD was processed by performing noise reduction and wild spikes extrapolation. The band contrast was adjusted to clearly see the grains. The grain size

parameter used is the major and minor axis of the fitted ellipse and the software automatically measures the grain size based on the delineation of all of the grain boundaries.

Similar to the conclusions made from SEM analysis, the EBSD results indicated that additives created a finer grain structure in the deposit, and that the decrease in grain size was proportional to the concentration of additives used. The appearance of small grains inside the larger ones was further analysed, and these small grains were identified as sub-grains brought about by recrystallisation. Dynamic recrystallisation or self-annealing is a recognised phenomenon that exclusively occurs in copper plated from additive-containing electrolytes.[22]

The SEM and EBSD results validate the grain-refining action of additives on the copper deposits. While numerous studies have reported similar observations in conventional copper baths,[18,23,24] these observations may be the first report on the effect of additives used for super-filling on the products of the EnFACE bath. It is also observed that the grain refining effect of

additives on the EnFACE bath is more pronounced than in the standard bath. This was seen with the finer grain size obtained in the EnFACE copper compared to the standard copper at the same additive concentration.

Grain refinement is one of the most important morphological and structural effects of additives.[23] It is known that additives affect the mechanisms of nucleation and growth during plating.[25] For example, brighteners enhance nucleation rates, while levelling agents inhibit dendritic growth. Both these actions can contribute to creating the fine-grained structure seen in the deposits. The effect could even be synergistic when different types of additives are present in the electrolyte. Since, grain refinement would affect the mechanical and electrical properties, these properties were measured and are reported below.

3.2. Mechanical and resistance measurements

Figure 3 shows the resistivity measurements for deposits from different additive concentration
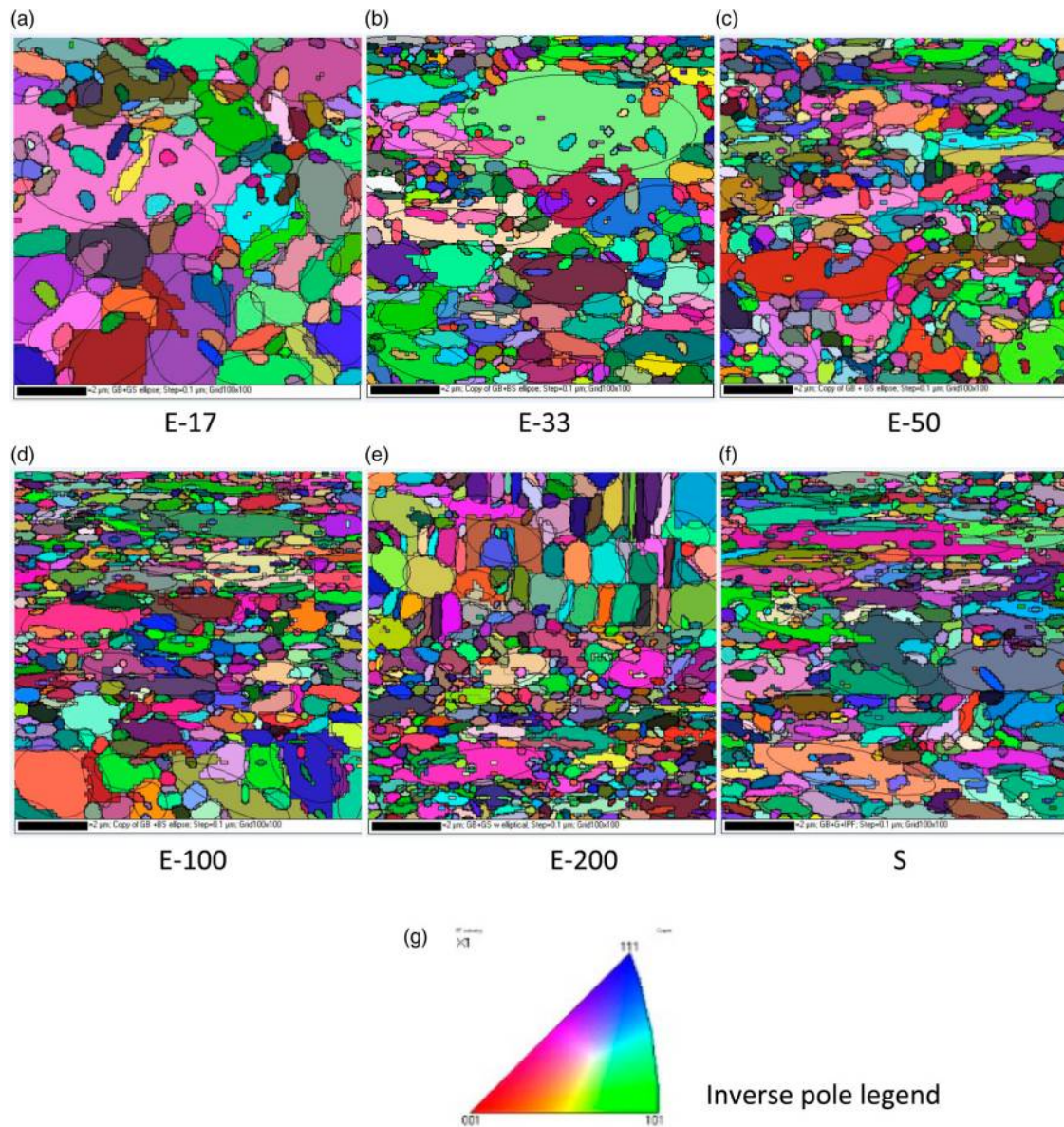
2 EBSD images of copper deposits from EnFACE bath with different additive concentration: a) E-17 with 17% additive concentration, b) E-33 with 33% additive concentration, c) E-50 with 50% additive concentration, d) E-100 with 100% additive concentration and e) E-200 with 200% additive concentration, and f) S - standard bath. These percentages are relative to the industry recommended additive concentration of 10 mL L^{-1} Copper Gleam B, 0.5 mL L^{-1} Copper Gleam A, and 70 ppm Cl^{-}. The calibration bar is for 2 μm length. The different colours in the EBSD map represent different crystals planes as described by the g) inverse pole legend.

using EnFACE electrolyte. Clearly, the progressive addition of additives created a more resistive copper deposit. Furthermore, the resistivity of some of the EnFACE copper deposits is similar in value to copper deposited from a standard electrolyte; i.e. the resistivity is 2.27 μohm-cm when copper is plated from a standard bath, and 2.30 and 2.31 μohm-cm when deposited from E-33 and E-50, respectively.

The increase in the resistivity of the copper film is explained by the significant reduction of grain size brought about by additive use. Morphological analysis presented earlier

has already confirmed a change in grain size. Grain boundaries, together with other defects, act as electron scattering centres and reduce the effective displacement of the free electrons during electronic conduction.[26] Thus, the increase in grain boundary area during grain refinement caused the increase in resistivity of the deposited film.

Figure 4 shows the plot of mechanical properties; namely, 0.2% offset yield strength (YS), ultimate tensile strength (UTS), and the ductility of the electrodeposited copper films, as a function of additive concentration. The results reveal the

strong effect of additive concentration on mechanical properties. Both YS and TS increased while ductility decreased with increasing additive concentrations. The percent increase in YS and TS, and the % decrease in ductility are almost similar; a ~40% change in value from the lowest to the highest additive concentration.

Table 3 summarises the mechanical properties of copper plated from a standard bath. The Institute for Interconnecting and Packaging Electronic Circuits advises that copper for interconnects should have a minimum tensile strength of 207
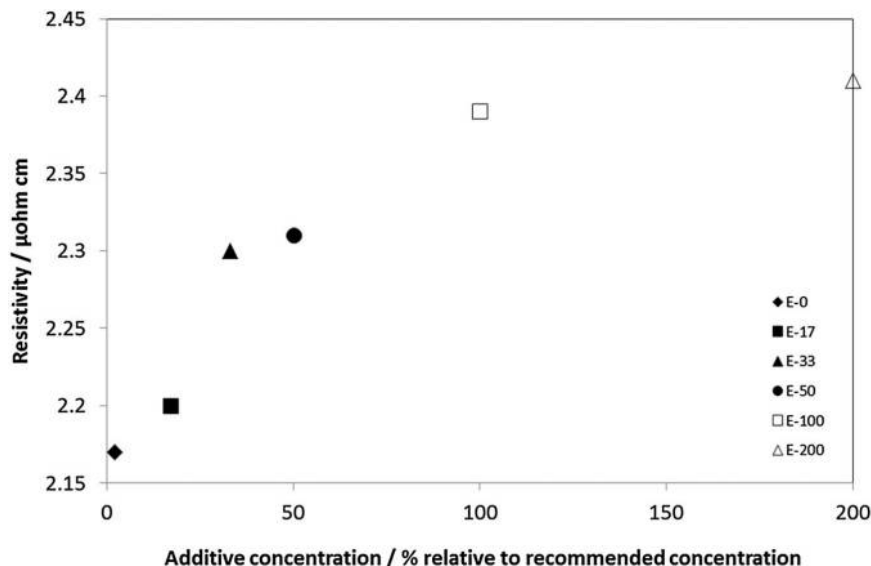
3 Resistivity measurements of electrodeposited copper films using EnFACE electrolyte with varying additive concentrations.
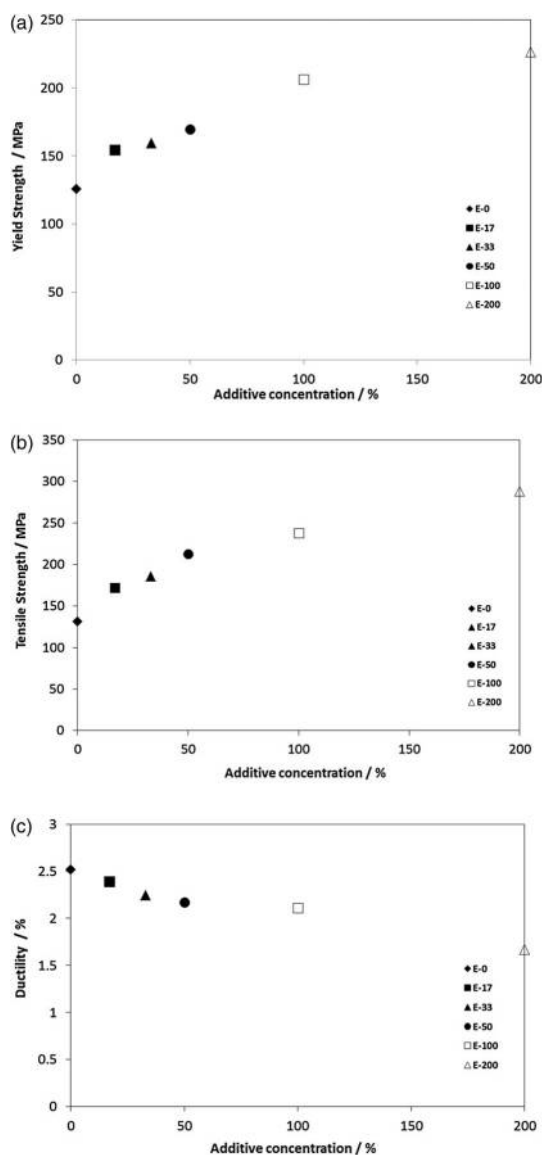
4 The a) yield strength, b) tensile strength and c) ductility of plated copper films using EnFACE electrolyte with varying additive concentrations.

MPa and ductility of 3%.[27] Using these values, it can be seen that plated films from EnFACE electrolytes are closer to the specification of the Institution than those obtained from the standard electrolyte. It is envisaged that by optimising bath and plating conditions, the specifications for interconnections and packaging can be achieved.

The observed trends in the plated copper are consistent with the well-known mechanical behaviour of metals. Typically, an increase in the metal's strength will be accompanied by a loss in ductility. The results also indicate a clear improvement in the mechanical strength of the plated copper when additives are used with the bath. To explain how additive concentration affects mechanical properties, the plated metal's inherent microstructural features need to be considered. Important microstructural features include dislocations, grain boundaries and voids.[24]

It is reasonable to assume that the observed grain size refinement directly caused the changes in the metal's yield strength and ductility; a statement consistent with published work.[28–30] Classical theories on slip and plastic yielding explain how grain boundaries can serve as dislocation barriers, thereby lowering dislocation mobility and preventing easy plastic deformation to occur. Consequently, such an action increases YS and lowers ductility. Tensile strength, on the other hand, is strongly affected by the amount

Table 3   Mechanical properties of copper plated from S, S-0 and E-50 baths

Bath	$YS_{0.2\%}$ /MPa	TS /MPa	Ductility /%
S	219	256	1.69
S-0	136	145	2.77
E-50	170	213	2.17

of voids, and an inverse relation exists between the two.

3.3. Optimum additive concentration

By inspecting the properties of the copper plated from EnFACE electrolytes containing different concentration of additives, it was found that at an additive concentration of 50%, the plated copper has properties close to the specifications stated by IPC. Though the properties of the E-50 electrolyte are slightly different from the values specified, they are closer than those obtained from a standard electrolyte. It can be envisaged that further improvements in deposit properties could be obtained by optimising plating conditions.

Notably, the EnFACE electrolyte has a low metal ion concentration, which can limit plating rates (cf. Table 2). In fact, the plating rate of the standard electrolyte is nearly four times higher than the best EnFACE electrolyte (E-50). This means that the rate of plating needs to be increased by improving agitation. In many industries, such as circuit board manufacturing, plating rates of 1.5–2.0 A dm^{-2} (ASD) or 15 - 20 mA cm^{-2} are advised. Since all of the EnFACE electrolytes exceed this plating rate, it should not affect plating rates in an industrial environment. On the other hand, by operating baths which have low metal and additive concentration, savings and sustainability can be achieved.

4. Conclusions

Copper was successfully electroplated from the additive-containing EnFACE bath, and its properties were characterised and compared to that achieved using a standard electrolyte. Stainless steel coupons were plated with 25 μm copper films using electrolytes of different additive concentrations. Additives caused the refinement of the grain structure of deposits, and the decrease in grain size was proportional to the concentration of additive used. This grain refinement consequently increased resistivity, yield and tensile strength, and reduced the ductility of plated copper. The EnFACE bath required a lower amount of additive to obtain a product that has comparable properties to that obtained from a standard electrolyte. The optimum additive concentration appears to be about 50% lower than the industry recommended dosage.

Funding

References

1. P. C. Andricacos, C. Uzoh, J. C. Dukovic, J. Horkans and H. Deligiani: *IBM J. Res. Dev.*, 1998, **42**, 567.
2. S. Franssila: 2nd Edition; 2010, John Wiley & Sons Ltd, West Sussex, United Kingdom.
3. A. Brenner: '*Electrodeposition of alloys. Principles and practice*', 1962, New York, Academic Press.
4. S. S. Kruglikov, N. T. Kudriavtsev, G. F. Vorobiova and A. Ya. Antonov: *Electrochimica Acta*, 1965, **10**, 253–261.
5. G. Fabricus and G. Sundholm: *J. Appl. Electrochem.*, 1985, **15**, 797–801.
6. T. C. Franklin: *Surf. Coat. Technol.*, 1987, **30**, 415–428.
7. L. Oniciu and L. Muresan: *J. Appl. Electrochem.*, 1991, 565–574.
8. E. Michailova, I. Vitanova, D. Stoychev and A. Milchev: *Electrochimica Acta*, 1993, **38**, (16), 2455–2458.
9. J. J. Kelly, C. Tian and A. C. West: *J. Electrochem. Soc.*, 1998, **146**, (7), 2540–2545.
10. S. Nouraei and S. Roy: *Electrochimica Acta*, 2009, 54, 2444–2449.
11. S. Roy: *J. Phys. D: Appl. Phys.*, 2007, **40**, (22), R413–R426.
12. Q. Wu, T. A. Green and S. Roy: *Electrochem. Commun.*, 2011, **13**, 1229–1232.
13. S. Coleman and S. Roy: *Chem. Eng. Sci.*, 2014, **113**, 35–44.
14. S. Coleman and S. Roy: *J. Appl. Electrochem.*, 2015, **45**, (8), 889–898.
15. I. Schönenberger and S. Roy: *Electrochimica Acta*, 2005, **51**, 809–19.
16. U. Landau: 1982, New York, *Plenum Press*.
17. L. N. Schoenberg: *J. Electrochem. Soc.*, 1971, **118**, (70), 1571–1576.
18. M. Paunovic and R. Arndt: *J. Electrochem. Soc.*, 1983, **130**, 794–799.
19. T. P. Moffat, D. Wheeler and D. Josell: 'The electrochemical society interface', *Winter*, 2004.
20. ASTM E-345 Standard Test Methods of Tension Testing of Metallic Foil.
21. T. P. Moffat, D. Wheeler, C. Witt and D. Josell: *Electrochem. and Solid-State Lett.*, 2002, **5**, C110–C112.
22. C. Cabral Jr., C. Andricacos, L. Gignac, I. C. Noyan, K. P. Rodbel, T. M. Shaw, R. Rosenberg, and J. M. E. Harper: Abstracts of the Advanced Metallization Conference (AMC), October 6–8; 1998, Colorado Springs, Colorado.
23. L. Oniciu and L. Muresan: *J. Appl. Electrochem.*, 1991, **21**, 565–574.
24. D. Dini and D. Snyder: in '*Modern electroplating: 5th edition*', (ed. M. Schlesinger and ?M. Paunovic); 2010, NY, John Wiley and Sons.
25. M. Tan, C. Guymon, D. Wheeler, and J. Harb: *J. Electrochem. Soc.*, 2007, **154**, (2), D78–D81.
26. W. Callister: in '*Materials science and engineering: An introduction*', 7th edn, 2007, Hoboken, NJ, John Wiley & Sons.
27. IPC-TM-650 test methods manual. Number 2.4.18. The Institute for Interconnecting and Packaging Electronic Circuits, 2215 Sanders Road, Northbrook, IL.
28. E. M. Hofer and H. E. Hintermann: *J. Electrochem. Soc.*, 1965, **112**, 167–173.
29. E. Michailova, I. Vitanova, D. Stoychev and A. Milchev: *Electrochimica Acta*, 1993, **38**, (16), 2455–2458.
30. E. Rusli, F. Xue, T. Drews, P. Vereecken, P. Andricacos, H. Deligianni, R. Braatz and R. Alkire: *J. Electrochem. Soc.*, 2007, **154**, (11), D584–D597.